



UNIVERSITÉ DE STRASBOURG

ÉCOLE DOCTORALE PHYSIQUE ET CHIMIE PHYSIQUE (ED 182)

Institut Charles Sadron (UPR-22 CNRS)

THÈSE présentée par :

Andreas WEINBERGER

soutenue le : **30 septembre 2013**

pour obtenir le grade de : **Docteur de l'université de Strasbourg**

Discipline/ Spécialité : **Physique**

**Systemes Modèles de Membranes et
Potentiel de Pénétration de
Polypeptides**

THÈSE dirigée par :

M. MARQUES Carlos

Professeur, Université de Strasbourg

RAPPORTEURS :

Mme. CLAESSENS Mireille

Professeur, University of Twente

M. LECOMMANDOUX Sébastien

Professeur, Université de Bordeaux

AUTRES MEMBRES DU JURY :

M. BAGATOLLI Luis

Professeur, University of Southern Denmark

M. BASCHNAGEL Jörg

Professeur, Université de Strasbourg



Subject: Physics

Model lipid systems and their interactions with polypeptides

Dissertation by

Andreas Weinberger

September 30, 2013

PhD committee:

President:	M.	Jörg BASCHNAGEL
Rapporteur:	M.	Sébastien LECOMMANDOUX
Rapporteur:	Ms.	Mireille CLAESSENS
Examiner:	M.	Luis BAGATOLLI
Supervisor:	M.	Carlos MARQUES

Acknowledgments

I would like to express my gratitude to all that helped and supported me throughout the three years of my PhD.

This PhD work was performed within the framework of the International Research Training Group (IRTG): “Soft Matter Science - Concepts for the Design of Functional Materials”, which is an international research program between universities of the Rhine valley. I am very thankful that the organizers of the IRTG gave me the opportunity to be part of an excellent graduate program, from which I will certainly benefit in my future career. Many of the collaborative projects and exchanges during my PhD thesis were due to contacts within the IRTG. Especially I would like to thank Jörg Baschnagel as the IRTG spokesperson in Strasbourg and the respective IRTG coordinators Christelle Vergnat, Amandine Henckel and Birgitta Zovko for being of a great help. Besides I gratefully acknowledge the Région Alsace for funding this work.

Working on several projects in the field of Soft Matter involves collaborations with numerous great people. I would like to thank Stefan Schiller and Nehrukumar Mathaiyan for synthesis of the glycolipids and Wolfgang Meier for providing block copolymers within the common IRTG project. Many thanks to Ashutosch Chilkoti and Sarah MacEwan for the opportunity to work with elastin-like polypeptides. They always rapidly provided peptides after special requests from our side. I very much appreciated the work with Gijsje Koenderink and Feng-Ching Tsai, who inspired me to start working on the PVA-assisted swelling method and Thais Schmidt for testing our method with cardiolipin. I also want to thank Andreas Zumbuehl and Radu Tanasescu, who introduced me to the new exciting field of lipidology and amide-bearing phospholipids.

I want to thank the jury members for the interest in my work and accepting to play important roles during my PhD defense: Jörg Baschnagel who presided over my jury, Mireille Claessens and Sébastien Lecommandoux who accepted to write a report after reading the manuscript and Luis Bagatolli for his helpful comments.

First and foremost I would like to thank my PhD supervisor, Carlos Marques for supervision and guidance throughout the 3 years. I greatly appreciate the time spent on discussions, where he certainly showed me the importance of my work at times I did not see them. Special thanks also to André Schröder and Tatiana Schmatko who helped me a lot learning the experimental techniques and their co-supervision of my thesis. Thanks also to all other colleagues from the M-cube team and people from the ICS I had the pleasure to meet. It was a unique experience I would not want to miss.

I am really glad for the new friendships gained during my PhD: especially Georges, Laure, Arnaud, Constantin, Martin and Philippe, who showed and introduced me to the French aspects (life, food, culture, language,...) and suffered with me during their PhD thesis.

Special thanks to Lydie and her support and motivation during the last year and of course my parents, which transformed my PhD celebration into a memorable finish of the doctorate.

Table of contents

List of figures	viii
List of tables	ix
Abbreviations	xi
Preface	1
1 Introduction	3
1.1 The membrane, a protective skin	3
1.2 Amphiphiles do self-assemble	4
1.3 Lipids, a major molecular class in membranes	7
1.4 Model systems for the biophysicist	11
1.4.1 Monolayers and the Langmuir-Blodgett technique	12
1.4.2 Bilayers on a substrate	12
1.4.3 Vesicles as cell-mimicking compartments	14
1.4.4 Vesicles decorated with polymers are sturdier	15
1.5 Membrane permeability - a passive process	16
1.6 All roads lead to GUVs	19
1.6.1 Vesicles are formed spontaneously	20
1.6.2 Emulsions for better defined vesicles	22
1.6.3 Energy can assist GUV formation	26
2 Materials & Methods	31
2.1 Chemicals	31
2.1.1 Lipids	31
2.1.2 Proteins for encapsulation	33
2.1.3 Polyvinyl alcohol and fluorescent PVA	33
2.1.4 Synthesis of functionalized elastin-like polypeptides	34

2.2	Preparation of vesicles	35
2.2.1	Small unilamellar vesicles	35
2.2.2	Large unilamellar vesicles	36
2.2.3	Giant unilamellar vesicles	37
2.3	Optical microscopy	40
2.3.1	Principle	40
2.3.2	Contrast enhancing methods	41
2.3.3	Reflection interference contrast microscopy	44
2.3.4	Experimental setup	46
2.4	Confocal microscopy	46
2.4.1	Basics of fluorescence	46
2.4.2	Confocal laser scanning microscopy	48
2.4.3	Experimental setup	49
2.5	Quartz crystal microbalance	49
2.6	Isothermal titration calorimetry	51
3	Elastin-like polypeptides	53
3.1	Transport through cell membranes	53
3.2	Cell penetrating peptides	54
3.3	Elastin-like polypeptides	56
3.4	ELPs for studying interactions with GUVs	58
3.5	Evaluation of ELP _{BC} -membrane interactions	60
3.6	Less than six arginine residues	62
3.7	Six or more arginine residues	64
3.7.1	Interactions between ELP micelles and the membrane	65
3.7.2	Quantification of the adsorbed ELP amount	66
3.7.3	Stability of micelles during interaction	68
3.8	Complementary studies	72
3.8.1	Quartz crystal microbalance	72
3.8.2	Isothermal titration calorimetry	74
3.9	Discussion and Conclusions	75
4	PVA-assisted GUV formation	79
4.1	Introduction	79
4.2	A PVA film below a lipid bilayer promotes GUV formation	81

4.3	Optical properties of DTAF-labeled PVA films	84
4.4	Lipid distribution	85
4.5	GUV formation: dealing with the hard cases	89
4.6	Encapsulation of proteins	95
4.7	A growth scenario	97
4.8	Summary: GUV formation on PVA-gel	100
4.9	Conclusions	101
5	Artificial lipids	103
5.1	Synthetic glycolipids	103
5.1.1	Introduction	103
5.1.2	Experimental methods	106
5.1.3	Results	107
5.1.4	Conclusions	111
5.2	Amide-bearing phospholipids	112
5.2.1	Introduction	112
5.2.2	Results	113
5.2.3	Conclusions	118
	Conclusions & Perspectives	119
	Appendix	123
	Bibliography	139

List of figures

1.1	Schematic illustration of a cell membrane	4
1.2	Optimal surface area per amphiphile	5
1.3	Critical packing parameter	5
1.4	Structures formed by amphiphiles	6
1.5	General structure of phospholipids and headgroup names	9
1.6	Phase transitions in lipid bilayers	10
1.7	Structure of cholesterol	11
1.8	Langmuir trough and Langmuir isotherms	13
1.9	Langmuir-Blodgett deposition	14
1.10	Unilamellar vesicles of all sizes	15
1.11	Physical properties vs. molecular weight	16
1.12	Permeability of the lipid bilayer	17
1.13	Permeability coefficients of different molecules	18
1.14	Modifications of GUVs as model systems	19
1.15	Stages of spontaneous swelling	21
1.16	Osmotic flow causes bilayer repulsion	21
1.17	Inverted emulsion technique	23
1.18	GUV formation via microfluidic jetting	24
1.19	Illustration of the cDICE method	25
1.20	Illustration of the double emulsion method	25
1.21	Free energy of phospholipid aggregates	27
1.22	Illustration of an electroformation chamber	28
1.23	Illustration of the inverse phase precursor method	29
1.24	Localized IR heating forms GUVs	30
2.1	Absorbance spectra of DTAF solutions	34
2.2	Hydrodynamic radius of LUVs prepared by extrusion	37
2.3	Heating cell for microscopy	40

2.4	Amplitude and phase specimens	41
2.5	GUVs in phase contrast and DIC mode	42
2.6	Phase contrast technique	43
2.7	Differential interference contrast technique	43
2.8	RICM technique	45
2.9	Vesicle “states” and RICM images	45
2.10	Simplified Jablonski diagram for fluorescence and Stokes’ shift	47
2.11	Setup for confocal microscopy	48
2.12	Isothermal titration calorimeter	51
2.13	Typical ITC curves	52
3.1	Types of endocytosis	54
3.2	Chemical structure of elastin-like polypeptides	56
3.3	ELPs possess an inverse phase transition temperature	57
3.4	Block copolymers of elastin-like polypeptides	58
3.5	ELP _{BC} form micelles above the T _t	59
3.6	Radial profile across a GUV dispersed in fluorescent ELP _{BC} solution	60
3.7	Linear behavior of fluorescence intensity with concentration	61
3.8	Peptide sequence of non-functionalized and Arg ₅ -functionalized ELP _{BC}	62
3.9	No change of partition coefficient is observed within one hour	63
3.10	Histogram obtained from evaluation of confocal images	64
3.11	Peptide sequence of Arg ₈ and TAT-functionalized ELP _{BC}	64
3.12	Accumulation of Arg ₈ -ELP _{BC} on the membrane	65
3.13	RICM images of adhered GUVs in ELP _{BC} solution	66
3.14	Radial profile of GUVs with adhered ELP _{BC}	66
3.15	Number of ELPs per 1000 lipids	68
3.16	Quenching of BODIPY-labeled ELP _{BC}	69
3.17	N _{PTL} values for samples with different amounts of fluorophores	70
3.18	Evolution of N _{PTL} over time	71
3.19	Reversibility of ELP _{BC} adsorption	72
3.20	QCM-D plot for a supported bilayer incubated with Arg ₈ -ELP _{BC}	73
3.21	ITC curves for titration of ELP _{BC} solution with LUVs	74
3.22	ITC curves for dilution of micellar or unimer ELP _{BC} solutions	74
3.23	Adhesion of ELPs as micelles	76

4.1	GUVs formed with EF and PVA swelling	81
4.2	GUVs during growing on a PVA substrate	82
4.3	Evolution of vesicle diameter and merging events	83
4.4	GUVs grown on fluorescently labeled PVA	84
4.5	Emission spectra of free DTAF and in presence of PVA	85
4.6	CLSM z-profiles of DTAF-labeled PVA with and without lipids	85
4.7	CLSM images of labeled lipid grown on unlabeled PVA	86
4.8	3D reconstruction of GUVs grown on PVA gel	87
4.9	Lipid distribution on PVA gel	88
4.10	Mixture of small multilamellar vesicles with PVA after swelling	89
4.11	DOTAP vesicles obtained by PVA-assisted formation	90
4.12	PVA additives assist in the formation process	90
4.13	Comparison of different lipid headgroups during GUV formation on PVA	91
4.14	Tube formation during swelling of a DOPS bilayer stack	92
4.15	Chemical structure of cardiolipin	92
4.16	Growing of cardiolipin vesicles with different techniques	93
4.17	Multilamellar structures with PVA-PAA substrate	94
4.18	Encapsulation of actin filaments and bundles	95
4.19	Encapsulation of neutravidin and biotin and membrane decoration	96
4.20	Water penetration pathways	97
4.21	Self-quenching of fluorescein	98
4.22	Swelling in presence of fluorescein	99
5.1	Chemical structure of DPhPC	104
5.2	3D model of concanavalin A	105
5.3	Glycolipids used in this work	105
5.4	Glycolipids form GUVs	108
5.5	Binding of ConA to glycolipids	108
5.6	GUVs containing glycolipids with cholesterol as lipid tail	109
5.7	Influence of the linker length on ConA binding	109
5.8	Possible confirmations of ConA bound to glycolipids in membranes	110
5.9	Lipids per ConA sub-unit	111
5.10	Chemical structure of Pad-PC-Pad	113
5.11	Pad-PC-Pad GUVs formed by electroformation and PVA-assisted swelling	114
5.12	Domain formation in Pad-PC-Pad GUVs	114

5.13 3D reconstruction of a RhodB- and NBD-labeled Pad-PC-Pad vesicle .	115
5.14 Faceted GUVs are obtained by rapid cooling	116
5.15 Apparatus for shearing of GUVs	117
5.16 Shearing of Pad-PC-Pad GUVs	117
5.17 Sheared GUVs of Pad-PC-Pad show increased permeability	118

List of tables

1.1	Classification system for lipids	7
1.2	Trivial names of fatty acids	8
1.3	Phospholipid composition of the human erythrocyte membrane	10
1.4	Transition temperatures of phospholipids	11
1.5	Gentle hydration method	22
1.6	Emulsion based methods	26
1.7	Energy-assisted methods	30
2.1	Abbreviations of chemicals	32
2.2	Chemical suppliers	32
2.3	Buffer solutions	33
2.4	Preparation of unilamellar vesicles	35
2.5	Physical properties of sugar solutions	43
2.6	Fluorophores and their characteristics	49
3.1	ELP _{BC} used in this work	59
3.2	Partition coefficients for different samples	62
4.1	GUVs formed by PVA-assisted swelling	100
5.1	Nomenclature of glycolipids used in this work	106
5.2	CLSM settings	107
5.3	Properties of artificial 1,3-diamidophospholipids	112

Abbreviations

Common abbreviations used in this thesis are listed below. Abbreviations of chemicals are listed in chapter 2.

CLSM	confocal laser scanning microscopy
CMC	critical micelle concentration
CMT	critical micellar temperature
CPP	cell penetrating peptide
DIC	differential interference contrast
DLS	dynamic light scattering
ELP	elastin-like polypeptide
ELP _{BC}	block copolymers of elastin-like polypeptides
GUV	giant unilamellar vesicle
ITC	isothermal titration calorimetry
ITO	indium tin oxide
LUV	large unilamellar vesicle
MLV	multilamellar vesicle
QCM-D	quartz crystal microbalance with dissipation monitoring
RICM	reflection interference contrast microscopy
SLS	static light scattering
SUV	small unilamellar vesicle
T _m	phase transition temperature of lipids
T _t	ELP _{BC} transition temperature for ELP _{BC}

Preface

The efficient delivery of a drug across the plasma membrane of the cell is a crucial element of modern strategies for developing treatment of cancer and other diseases. Drug delivery systems such as stealth liposomes, nanoparticles and also a whole variety of other drug carriers can be functionalized by cell penetrating peptides, such as arginine rich polypeptides, which promote transport across the membrane. Current trends in biomedical research attempt to reduce treatment side effects by targeting delivery to specific body areas or tissue types. For cell penetrating peptides, this can be achieved, with a new class of self-assembling elastin-like polypeptides that can be activated by a thermal trigger.

The interaction with the plasma membrane is the first key step for assisted translocation of cell penetrating peptides. Although cell penetrating peptides are universally attracted to zwitterionic and anionic ions, attachment of cargo molecules can compromise the attraction, either due to size-exclusion or electrostatic effects of the cargo. Therefore the rational design of efficient delivery systems requires a fundamental understanding of the interplay between self-assembly and membrane interactions for the polypeptide-cargo constructs. For such studies, biomimetic models of the plasma membrane allow to considerably reduce the complexity of the system, while retaining most of its key features.

Giant unilamellar vesicles are a valuable platform for studying peptide-membrane interactions. These large objects of cell-like dimensions can be prepared from different lipid compositions and studied by optical microscopy techniques, thus allowing direct visualization of phenomena such as adsorption of peptides on membranes or transport across the model bilayers. While original methods for giant unilamellar vesicle formation were optimized for single-component, often neutral bilayers, the need to mimic plasma cell behavior called for the development of methods that enable giant vesicle formation from complex mixtures. Despite the emergence of a variety of new

methods for giant vesicle formation, growing vesicles in physiological buffers or from lipid mixtures containing charged lipids is still a challenging task.

During this PhD-work, we contributed to the study of peptide-lipid interactions and developed new gentle methods for the formation of model membrane systems from new lipids. In the first chapter, we introduce basic concepts of amphiphile self-assembly, properties of lipid bilayers and methods to form model membrane systems. The second chapter describes materials and methods relevant for this work.

In chapter 3, we investigate lipid-peptide interactions for a new class of cell penetrating peptides, based on functionalized elastin-like polypeptides. These arginine rich peptides can be thermally switched between an active and non-active state and are synthesized by Sarah MacEwan in the group of Ashutosh Chilkoti at the Duke university in North Carolina. We investigate the interaction of these arginine rich elastin-like polypeptides with giant unilamellar vesicles composed of neutral lipids.

In chapter 4, we develop a new method to efficiently form giant unilamellar vesicles, which is the model system for all of our experiments. For some classes of lipids, such as charged lipids or new artificial lipids, the typical pathways to obtain GUVs are inefficient. Our method is based on gel-assisted swelling of lipid bilayer stacks. This project was performed in collaboration with Feng-Ching Tsai and Gijsje Koenderink from the AMOLF institute in Amsterdam.

In the last chapter, we apply our gel-assisted method for systems of new synthetic phospholipids and glycolipids, for which membrane assembly into GUVs is difficult or impossible with classic methods. These new lipids, important for applications that require sugar-based interactions or sensitivity to viscous stresses, were synthesized within the framework of the International Research Training Group (IRTG): "Soft Matter Science - Concepts for the Design of Functional Materials". Glycolipids are synthesized by Nehrukumar Mathaiyan in the group of Stefan Schiller in Freiburg in Germany and amide-bearing phospholipids in the group of Andreas Zumbuehl in Fribourg in Switzerland.

Introduction

In this chapter some of the fundamental terms and techniques are discussed. After introducing the reader to the basic concepts of amphiphile self-assembly of bilayers and membrane permeability, this chapter provides also an overview of the basic methods that lead to the formation of giant unilamellar vesicles.

1.1 The membrane, a protective skin

Cell membranes are ubiquitous in living organisms. Not only they separate the inner from the outer part of the cell, but also enclose many of the internal cell organelles: mitochondria, endoplasmic reticulum and the Golgi apparatus to only name a few. Cell membranes are bilayers, self-assembled from amphiphilic molecules, such as phospholipids and cholesterol.

These self-assembled structures define thus the external and the internal boundaries of the cell and regulate the transport of molecules across it. The functions performed by the membrane require a large variety of proteins, carbohydrates or other bio-molecules.

The nature of this composite structure was discussed by Singer and Nicolson [1] in the seventies. They proposed the so-called fluid mosaic model, where the membrane is considered as a two-dimensional liquid, composed from different lipids with various kinds of embedded proteins. A schematic representation of this model is shown in Figure 1.1. More recent descriptions of the cell membrane do not view the lipid matrix as a passive medium, but recognize the structuring roles of the many different kinds of saturated and unsaturated lipids that compose it. In particular the interaction of the lipids with the proteins, and the propensity of the saturated and unsaturated

lipids to induce lateral phase separation, has been discussed within the so-called raft hypothesis, as essential for membrane function [2].

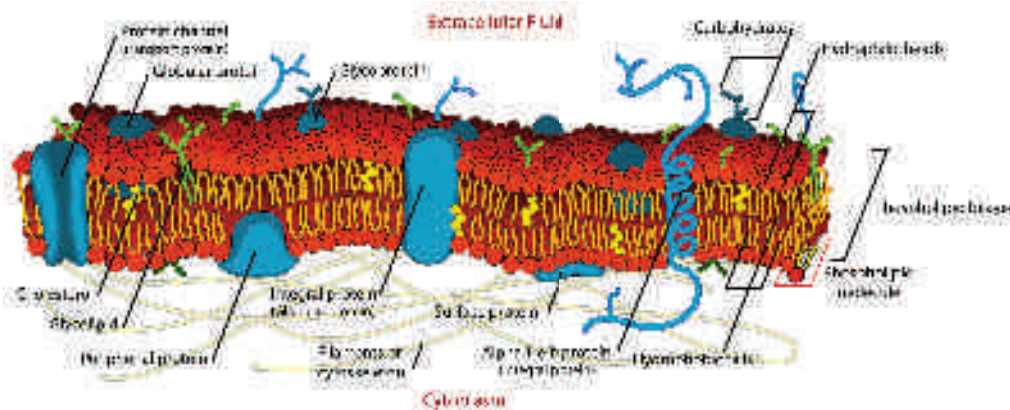


Figure 1.1: Schematic illustration of a cell membrane separating the cytoplasm from the exterior of the cell [3].

Biological membranes are of great interest in life sciences [4] and their complexity has prompted many studies in simpler model systems in physics, physical chemistry and mathematics. Of particular interest, for instance, is the ability of phospholipids to form self-assembled structures that we now describe.

1.2 Amphiphiles do self-assemble

Lipids, the main component of natural (biological) membranes, are amphiphiles. An amphiphile is a molecule possessing a hydrophilic and a hydrophobic (lipophilic) moiety. The lipophilic group is typically a large hydrocarbon moiety, whereas the hydrophilic group can be a charged group, for instance phosphates in phospholipids, or polar, uncharged groups such as alcohols. A key property of amphiphiles is their insolubility in water and their tendency to segregate to an air-water interface [5]. The segregation is driven by a competition between two forces: the attractive interaction between the carbon chains and the repulsion energy between the polar heads. In order to minimize their total energy, amphiphiles possess an optimal surface area a_0 where these two forces are balanced, see Figure 1.2 [6].

Depending on the geometrical properties, these molecules can assemble into diverse structures above the critical micelle concentration (CMC). The so called packing parameter P can help predict which structures a lipid or surfactant can assume and is defined as:

$$P = \frac{V}{a_0 L_c} \quad (1.1)$$

where L_c is the length of the lipid tail, V the volume that the lipid tail occupies and a_0 the head group area of the hydrophilic head group, see also Figure 1.3. If the packing parameter P is below $1/3$, spherical micelles can be formed. One common example of a surfactant forming spherical micelles is sodium dodecyl sulfate (SDS). For values of P between $1/2$ and 1 , vesicles or planar bilayers can be formed. Figure 1.4 shows possible structures which can be obtained depending on the geometrical properties of the amphiphile [6].

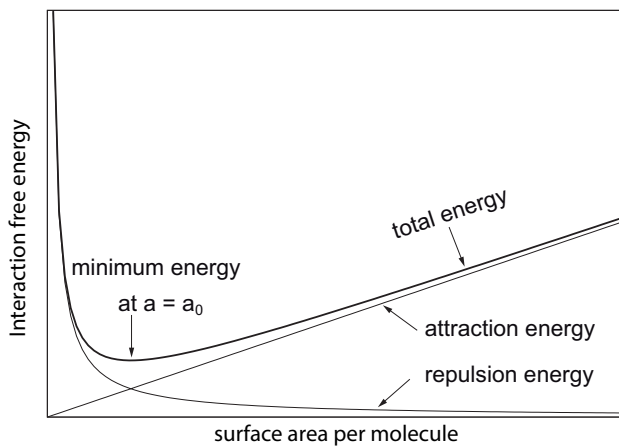


Figure 1.2: Optimal surface area a_0 derived from the minimum total energy, for balanced attractive and repulsive energy.

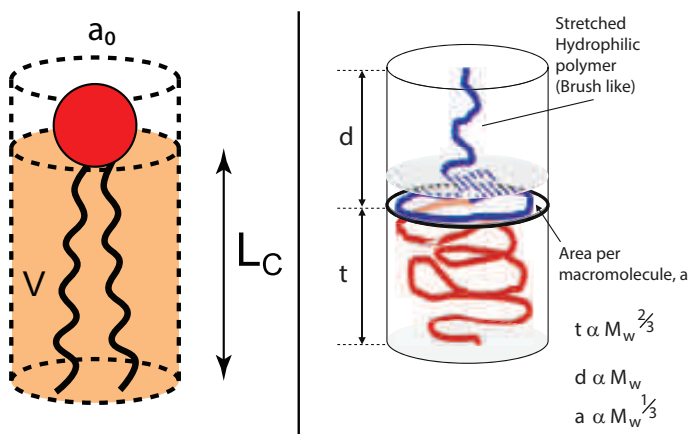


Figure 1.3: Geometrical parameters predicting possible structures of amphiphiles. (Left) variables defining the critical packing parameter P for surfactants and lipids. (Right) occupied area and bilayer thickness is directly proportional to the molecular weight, adapted from Massignani et al. [7].

This packing parameter is well established for surfactants and lipids, it can be generally applied to block copolymers as well, although it is more convenient to use the volume or weight fraction f of the hydrophilic block ($0 < f < 1$) to describe their shape [8]. It is expected to form vesicular structures, called polymersomes, if $f \approx 35 \pm 10\%$ [9]. For f -values $> 45\%$ spherical micelles are expected, whereas f -values $< 25\%$ lead

to inverted micelles. Additionally, the total molecular weight of the copolymer directly influences the thickness of the formed bilayer, see also Figure 1.3.


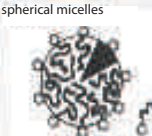



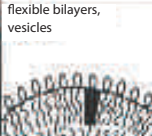



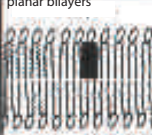
Lipid	Critical packing parameter P	Critical packing shape	Structures formed
Single-chained lipids (surfactants) with large head-group areas: SDS in low salt,....	$< 1/3$	cone 	spherical micelles 
Single-chained lipids with small head-group areas: SDS and CTAB in high salt, nonionic lipids,....	$1/3-1/2$	truncated cone 	cylindrical micelles 
Double-chained lipids with large head-group areas, fluid chains: Phosphatidyl choline, phosphatidyl serine, phosphatidyl glycerol, phosphatidyl inositol, phosphatidic acid, sphingomyelin, ...	$1/2-1$	truncated cone 	flexible bilayers, vesicles 
Double-chained lipids with small head-group areas, anionic lipids in high salt, saturated frozen chains: Phosphatidyl ethanolamine	~ 1	cylinder 	planar bilayers 
Double-chained lipids with small head-group areas, nonionic lipids, poly(cis) unsaturated chains, high temperature: Unsaturated phosphatidyl ethanolamine, ...	> 1	inverted truncated cone or wedge 	inverted micelles 

Figure 1.4: Possible structures obtained depending on the geometrical properties of the amphiphile [6].

1.3 Lipids, a major molecular class in membranes

The major structural lipids in eukaryotic membranes are glycerophospholipids [10]. Glycerophospholipids are based upon glycerol, a polyol, which acts as the lipid backbone. The lipids are formed by esterification of two of the hydroxyl moieties with fatty acids and the remaining one with phosphoric acid or an analog. Besides glycerophospholipids many other lipids are known. These other lipids contribute in a minor amount to cell membranes, but can be still of great importance.

Nomenclature of lipids Several systems exist to name lipids. Traditional phospholipid nomenclature used the C_n:m X notation, where n is the number of carbons in the chain, m the number of unsaturations and X the polar head group. For instance, 1,2-dioleoyl-sn-glycero-3-phosphocholine or DOPC has two oleoyl chains and a phosphatidylcholine (PC) head; therefore the notation is diC18:1 PC. This works well for the phospholipids but can be tedious for the other classes of lipids.

Category	Abbreviation	Example
Fatty acyls	FA	Arachidonic acid
Glycerolipids	GL	1,2-dipalmitoyl-sn-glycerol
Glycerophospholipids	GP	1,2-dioleoyl-sn-glycero-3-phosphocholine
Sphingolipids	SP	Sphingomyelin
Sterol Lipids	ST	Testosterone
Prenol Lipids	PR	Carotenoids
Saccharolipids	SL	Kdo2-lipid
Polyketides	PK	Doxycycline

Table 1.1: Classification system for lipids, after Fahy et al. [11].

Basically, all lipids can be named by applying the standard IUPAC nomenclature rules, which can be quite complicated for more complex lipids. In 2005 the International Lipid Classification and Nomenclature Committee suggested a classification system for lipids and the nomenclature of lipids, which follows existing IUPAC rules closely, but simplifies systematic naming by identifying core structures. This updated classification system organizes lipids into eight different categories that cover eukaryotic and prokaryotic sources. It has been adopted internationally and widely accepted by the lipidomics community. Table 1.1 lists the eight different categories together with one important example [11].

In this manuscript, we only focus on glycerophospholipids. By convention, glycerol is defined as the backbone of the lipid. The Fischer projection of glycerol is drawn in such a way that the hydroxyl group on C2 is oriented on the left (Figure 1.5, inset A).

The carbon atoms in the backbone are numbered by assigning the C3 to the position where the phosphoric acid is esterified with glycerol. Each natural glycerophospholipid is therefore a derivative of sn-glycero-3-phosphoric acid and the fatty acids are always at position C1 and C2. The headgroup at position C3 is named as suggested by the committee (compare Figure 1.5), while the trivial names for fatty acids are used for naming the lipid tails (compare Table 1.2).

Trivial name	Abbreviation	Chain length : Saturations
Lauric acid	L, Lau	12:0
Myristic acid	M, Myr	14:0
Palmitic acid	P, Pam	16:0
Stearic acid	S, Ste	18:0
Arachidic acid	Ach	20:0
Palmitoleic acid	Δ Pam	16:1
Oleic acid	O, Ole	18:1
Linoleic acid	Lin	18:2
α -Linolenic acid	α Lnn	18:3
Arachidonic acid	Δ_4 Ach	20:4

Table 1.2: Common fatty acids in natural phospholipids. Note that all mentioned phospholipids are natural occurring, thus the double bond is in a cis configuration. One letter code abbreviation for the fatty acid is the common used abbreviation, three letter code as suggested by IUPAC [12].

This classification and nomenclature system is very useful for natural lipids, but there is clearly a lack of a well defined nomenclature for synthetic lipids. With a continuous growing field of lipid synthesis some might argue that there is a need for developing a new nomenclature system to classify natural occurring and synthetic lipids.

Recently, Fedotenko et.al [13] proposed a nomenclature based on a two-letter code that unambiguously identifies the chemical linker. This code would follow the standard trivial abbreviation of fatty acids (Table 1.2) and head groups (Figure 1.5). Additionally, an abbreviation for the linker would be added to the one letter code of the fatty acid and the obtained abbreviations sorted by their position in the backbone. 1,2-dioleoyl-sn-glycero-3-phosphocholine (DOPC) would, for example, lead to Oes-Oes-PC. Besides “es” for ester, “ad” might stand for amide, “an” for amine, “et” for ether etc.

To facilitate naming of used lipids in this manuscript, the nomenclature suggested in Ref. Fahy et al. [11] is used for natural lipids. By combining the abbreviation for the fatty tails and the head group, POPC, for instance, is the abbreviation of 1-palmitoyl-2-oleoyl-sn-glycero-3-phosphocholine. For synthetic lipids the system proposed by Fedotenko et.al [13] will be used.

Lipid composition of membranes. The basic structure of biological membranes is provided by the lipid bilayer, typically 5 nm thick. Numerous different lipids can be assembled by the lipid tails and head groups summarized in Table 1.2 and Figure 1.5. In nature, thousands of different lipids exist, leading to different properties of the membrane. Additionally to the lipids, proteins are embedded in this lipid bilayer. The usual plasma membrane is composed in equal parts from proteins (50 wt%) and lipids. Phospholipids and cholesterol make up over 90 % of the involved lipids in biological membranes, but these amounts may vary depending on which type of membrane and functions are needed in the cell [14].

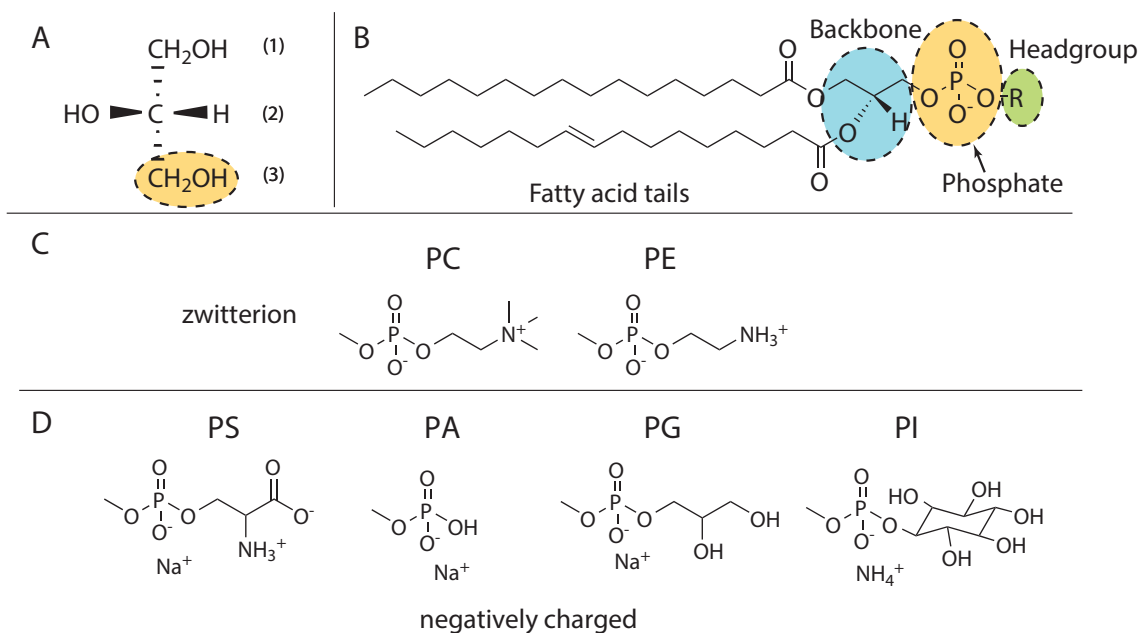


Figure 1.5: (A) Fischer projection of a glycerol. By convention the hydroxyl group on C2 is drawn on the left. (B) Characteristic chemical structure of a phospholipid, composed of two hydrophobic tails connected via ester bonds on C1 and C2 of the glycerol backbone and a hydrophilic head group, which is in turn composed from a phosphate group and a polar head group. (C and D) Polar head groups common in phospholipids: (C) Zwitterionic head groups: phosphatidylcholine (PC), phosphatidylethanolamine (PE). (D) Negatively charged head groups: phosphatidylserine (PS), phosphatidic acid (PA), phosphatidylglycerol (PG) and phosphatidylinositol (PI).

For instance, 86 wt% of the lipid composition of human red blood cells is composed by 20 wt% cholesterol, 48 wt% glycerophospholipids and 18 wt% sphingomyelin [15]. Among the glycerophospholipids the most abundant class is the phosphocholines. Table 1.3 lists the phospholipid composition of human erythrocytes. As mentioned, the composition of lipids varies depending on the organelles where the lipid bilayer is located. The glycolipids for example, a very important class for cellular recognition, amount to only 3 % of the lipid composition and reside almost exclusively in the

plasma membrane. Additionally, differences in the composition of the inner and outer leaflet of the membrane exist, leading to asymmetric membranes.

Phospholipid	mol% \pm SD
Phosphatidylcholine	29.3 \pm 1.5
Sphingomyelin	25.5 \pm 1.4
Lysophosphatidylcholine	1.0 \pm 0.8
Phosphatidylethanolamine	27.6 \pm 1.5
Phosphatidylserine	14.9 \pm 1.7
Phosphatidylinositol	0.6 \pm 0.5
Phosphatidic acid	1.1 \pm 0.5

Table 1.3: Phospholipid composition of the human erythrocyte membrane, adapted from Virtanen et al. [16].

Phase transitions and transition temperature. The fluidity of the lipid bilayer and thus the membrane permeability and stability depends on the lipid composition in the membrane. In red blood cells for instance, 60 mol% of the lipid tails are two kinds of saturated lipid tails (palmityl- and stearyl-tail) and two kinds of unsaturated tails (oleoyl- and arachidonyl-tails) [17]. A basic rule is that the main transition temperature T_m decreases with shorter carbon chains or with the number of unsaturations (Table 1.4). The head group choice can also influence the main transition temperature, but typically has a smaller effect for common phospholipids.

Bilayers show interesting phase behavior. For temperatures above the main transition temperature the bilayer is in a fluid state L_α . If the temperature is decreased below the subtransition temperature L_{sub} the membrane undergoes a transition to the crystalline phase L_C , where the highest degree of ordering is observed. Between both phases, transition into a gel phase $L_{\beta'}$ or the rippled phase $P_{\beta'}$ can be distinguished, separated by the pre-transition temperature T_p (see Figure 1.6).

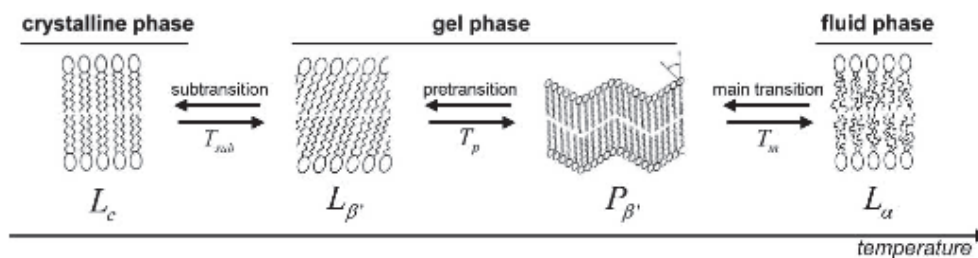


Figure 1.6: Bilayer undergoing different phase transitions.

Name	Abbreviation	T_m ($^{\circ}\text{C}$)
1,2-distearoyl-sn-glycero-3-phosphocholine	DSPC	55
1,2-dipalmitoyl-sn-glycero-3-phosphocholine	DPPC	41
1-palmitoyl-2-oleoyl-sn-glycero-3-phosphocholine	POPC	-2
1,2-dioleoyl-sn-glycero-3-phosphocholine	DOPC	-20
1,2-dioleoyl-sn-glycero-3-phosphoethanolamine	DOPE	-16
1-palmitoyl-2-oleoyl-sn-glycero-3-phosphoethanolamine	POPE	25

Table 1.4: Transition temperatures of common phospholipids, both head group and lipid tails influence transition temperature of the lipids.

The cell also controls membrane fluidity and permeability by adapting amount of cholesterol in the bilayer (Figure 1.7). Cholesterol increases membrane packing, which in turn reduces membrane fluidity. These fluid phases, liquid-disordered L_d and liquid-ordered L_o phase, occur in phosphatidylcholine/cholesterol mixtures under certain conditions [15].

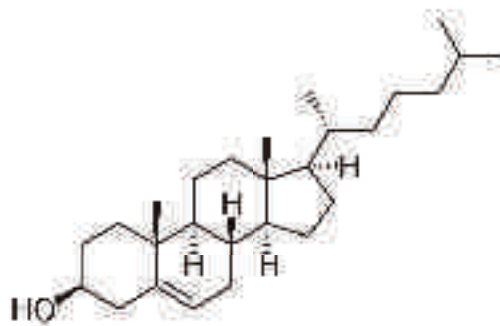


Figure 1.7: Cholesterol, an essential component to control membrane permeability and fluidity.

1.4 Model systems for the biophysicist

Due to the huge variety of bio-molecules building up the cell membrane, it is difficult to relate certain properties to certain lipids or proteins. In order to be able to investigate certain membrane properties and fundamental effects in life sciences, scientists perform research on model membrane systems obtained through self-assembly of amphiphiles. In this model systems the number of different components are limited to a small number.

In the last years, in addition to model membrane systems composed from natural ingredients such as lipids and proteins, various synthetic amphiphiles were synthesized,

able to self-assemble into membranes, thus leading to membranes which are difficult to classify as either biological and artificial membranes. Typical model systems used in biophysics are monolayers, planar (supported) bilayers and liposomes.

1.4.1 Monolayers and the Langmuir-Blodgett technique

Insoluble amphiphiles can assemble into mono-molecular layers, the so-called Langmuir monolayers, at the air-water interface. Caused by the presence of the amphiphiles, the surface tension of the pure water γ_0 is lowered and can be expressed by the surface pressure Π .

$$\Pi = \gamma_0 - \gamma \quad (1.2)$$

If a known amount of amphiphiles is spread on the air-water interface of a Langmuir-Blodgett (LB) trough with a known surface area, as in Figure 1.8, the monolayer can be compressed by movable barriers and allows decreasing the surface area per molecule. The surface pressure Π is determined using the so called Wilhelmy plate method, which measures the force on a plate due to wetting [18].

In this technique the surface pressure Π vs. the area per molecule is recorded. As the Langmuir monolayer at low surface pressure behaves similarly to a gas, phase transitions can be observed during compression of the monolayer: a gaseous (G), a liquid-expanded (LE) and a liquid-condensed (LC) phase are crossed one after the other. The lipid tails can be either tilted or untilted, which separates the liquid-condensed from a solid-like phase [19]. At very high surface pressures the monolayer can eventually collapse.

The main drawback of these Langmuir monolayers is the effective comparability with bilayer membranes. As the bilayer membranes of vesicles have zero surface tension and the surface tension of hydrocarbons at the air/water interface is 30 mN/m, it is difficult to directly compare LB results to real membranes [21].

1.4.2 Bilayers on a substrate

With the Langmuir Blodgett technique, compressed monolayers can be deposited onto a substrate to form a supported bilayer. The substrate is pulled out of the subphase while compressing the monolayer to keep the surface pressure constant. The substrate crosses the air/water interface and a monolayer is deposited on it, depending on the hydrophilicity of the substrate. When a hydrophilic substrate is used, it is withdrawn from the aqueous subphase and the hydrophilic head groups are in direct

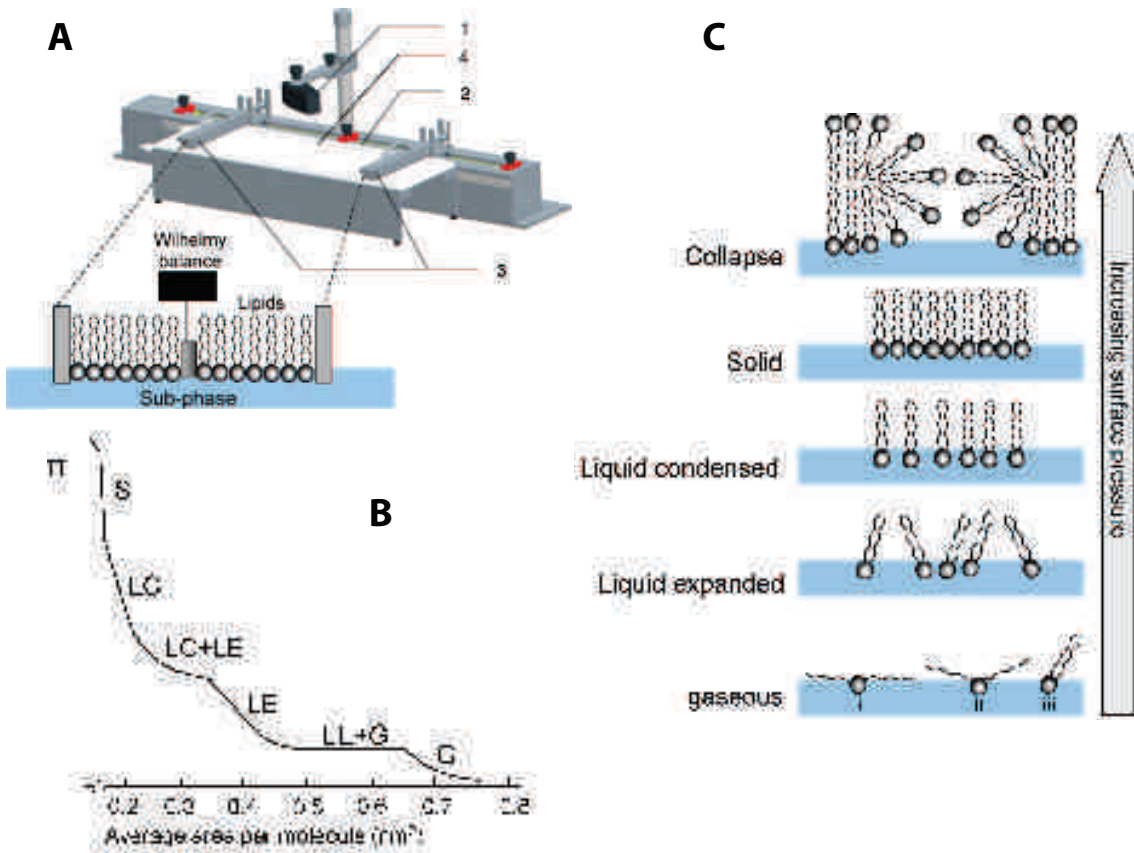


Figure 1.8: (A) Schematic illustration of a Langmuir trough with the balance (1) and the Wilhelmy plate (4), the trough filled with the subphase (2) and the movable barriers (3). (B) Generalized Langmuir Isotherm, showing different phases from low to high compressions: a gaseous (G), a liquid-expanded (LE), a liquid condensed (LC) and a solid-like phase (S). (C) Schematic representation of lipid packaging at the monolayer interface. At very high surface pressure the monolayer can collapse, adapted from Moghaddam et al. [20].

contact with the substrate, see Figure 1.9. By re-immersion of the monolayer-covered substrate, a supported bilayer can be formed. By reversing the order, first immersion and then withdrawing of a hydrophobic substrate, an inverted bilayer is formed (the head groups of the two monolayers are in direct contact), in order to obtain a complete bilayer the process has to be repeated.

This common technique allows even the preparation of asymmetric bilayers consisting of different amphiphiles per monolayer. The density of molecules in a monolayer is adjusted by the surface pressure in such a way that planar bilayers without defects can be obtained. Supported bilayers can also be formed by adsorption of small unilamellar vesicles on a hydrophilic substrate and subsequent bursting on the surface, leading to the formation of a bilayer [22].

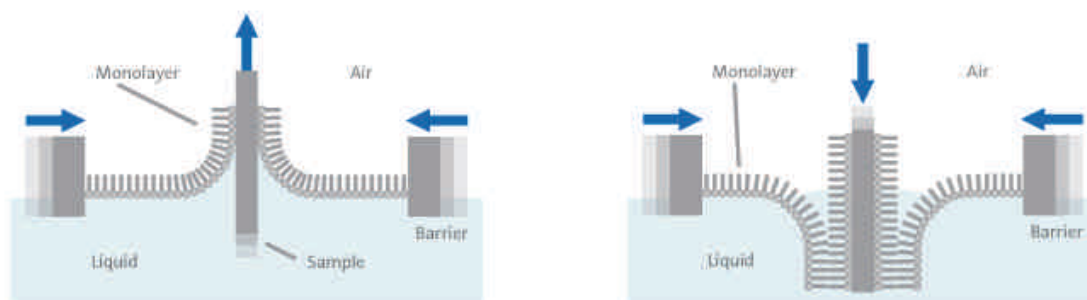


Figure 1.9: Schematic illustration of Langmuir-Blodgett deposition on a hydrophilic substrate. Left: First layer of amphiphiles is deposited on the substrate by withdrawing from the subphase and keeping the surface pressure constant. Right: By passing a second time through the air-water interface with a compressed monolayer of amphiphiles a bilayer can be obtained. Image from KSV NIMA (<http://www.ksvnima.com/>).

Such supported bilayers are very stable and thus allow them to be studied by techniques like Atomic Force Microscopy (AFM), fluorescence-based techniques [23] and scattering experiments [24, 25].

1.4.3 Vesicles as cell-mimicking compartments

Besides flat supported bilayers, membranes can close into spherical vesicles. These energetically more favorable structures can be unilamellar or multilamellar. Multilamellar vesicles (MLV) form spontaneously when dry phospholipid films swell in aqueous solution [26]. For making unilamellar vesicles some energy must be dissipated into the system in order to produce them [27].

Unilamellar vesicles can be divided in different classes according to their size: Small Unilamellar Vesicles (SUVs; 20 to 100 nm), Large Unilamellar Vesicles (LUVs; 100 to 500 nm) and Giant Unilamellar Vesicles (GUVs; 0.5 to 100 μm), see also Figure 1.10. The size of unilamellar vesicles can be controlled by choosing a suitable preparation technique. SUVs are typically obtained by sonication and LUVs by extrusion [28]. Different methods leading to GUVs are described in detail in section 1.6.

Due to their biocompatibility, and to their ability to entrap water-soluble components inside the vesicle and/or water-insoluble components into the membrane, liposomes (SUVs and LUVs) are widely used for drug-delivery [29]. Furthermore, they also can be used as models for cellular organelles or to stabilize suspensions in the cosmetic industry. GUVs, for instance, can be used as cell mimicking compartments. The big advantage of GUVs is that due to their large size, they can directly be observed by optical microscopy.

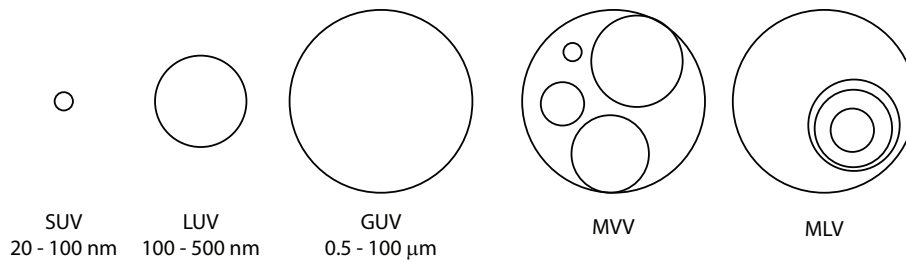


Figure 1.10: Unilamellar vesicles of different sizes used in research: SUVs, LUVs, GUVs. Multilamellar vesicles (MLV) and multivesicular vesicles (MVV) are typically formed spontaneously.

1.4.4 Vesicles decorated with polymers are sturdier

The first attempts to deliver drugs with liposomes were made in the 1950s [30]. However, it appeared that liposomes based on natural lipids were detected by the immune system and destroyed within a few hours. By modifying liposomes with short polyethylene glycol (PEG) chains (around 2000 Dalton in length) and creating the so-called “stealth liposomes”, the detection by the body’s immune system is avoided and the circulation time in blood can be greatly improved [31, 32]. This allows for example improving the cellular uptake of doxorubicin, a drug used in cancer therapy [33].

However, these PEGylated liposomes are limited in their ability to integrate high molar ratios of PEG–lipids, while keeping their ability to form stable liposomes because of their high curvature. Liposomes based on polymers, the so-called polymersomes, are vesicles composed entirely from a diblock copolymer. These polymersomes have shown in-vivo up to two fold longer circulation times than PEGylated liposomes [34]. One of the best known example of a diblock copolymer able to form polymersomes is PEO-PBD with polyethylene oxide (PEO) as the hydrophilic block and polybutadiene (PBD) as the hydrophobic block [35]. Another common example for the hydrophilic block is poly(2-methyloxazoline) (PMOXA) [36]. Examples of polymers used for the hydrophobic block are polydimethylsiloxane [36], poly(caprolactone) (PCL) and poly(lactide) (PLA) [37].

Besides their circulation time, the electromechanical stability increases as well with membrane thickness, which in turn depends on the molecular weight (M) of the polymer. Equation 1.3 shows how copolymer membrane thickness d scales with the molecular weight M of the hydrophobic block [38].

$$d \approx M^{0.55} \quad (1.3)$$

The typical range of membrane thickness of liposomes is between 3–5 nm, whereas the one of polymersomes is typically between 8–21 nm [9]. Furthermore, lateral diffusivity [39] and apparent membrane viscosity [40] decrease, showing that membrane fluidity generally decreases with increasing molecular weight.

One drawback of polymersomes is the reduced water permeation of polymersome membranes compared to phospholipid membranes. For instance, the water permeability of DOPC is circa $160 \mu\text{m s}^{-1}$ [41], while the water permeability for typical polymersomes was reported to be of the order of $2.5 \mu\text{m s}^{-1}$ [35].

Figure 1.11 shows the change of electromechanical stability, lateral mobility and permeability of a membrane composed from amphiphiles with different molecular weights.

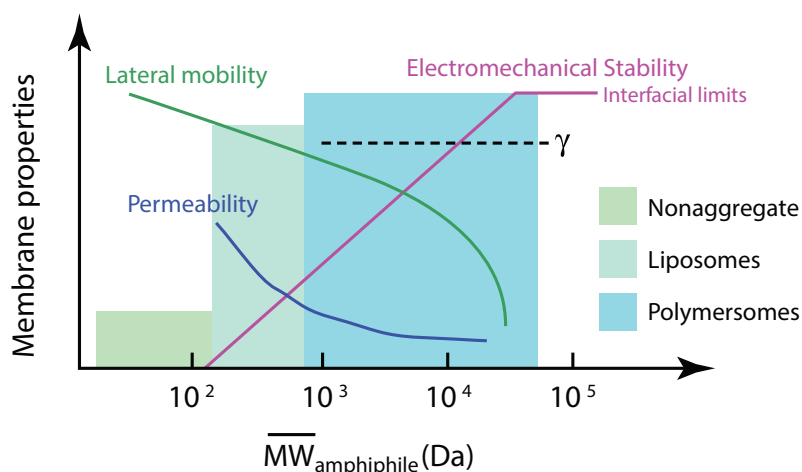
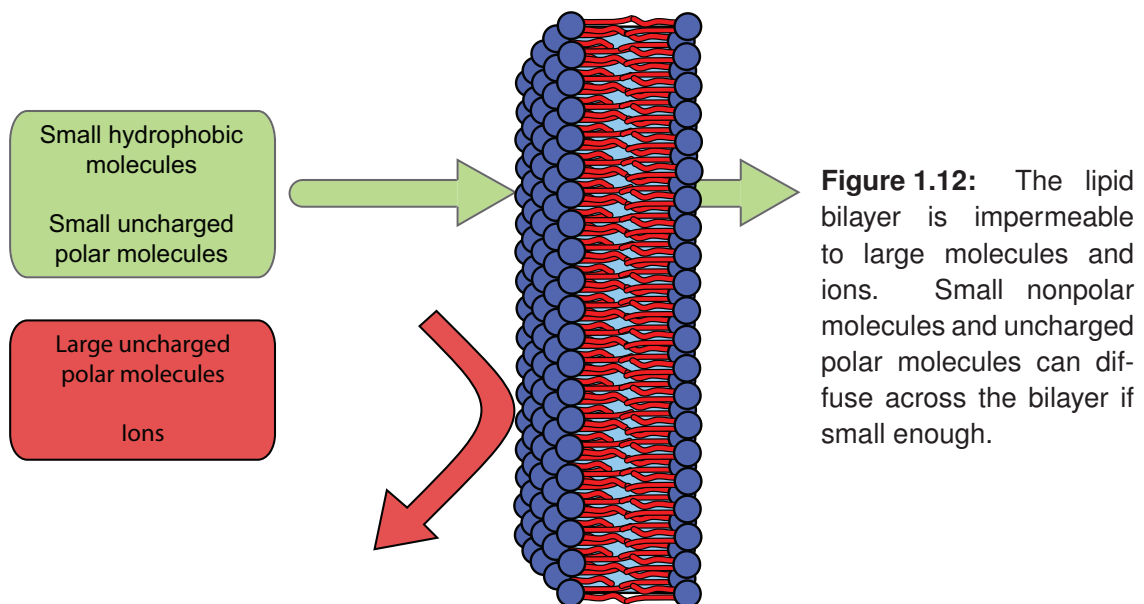


Figure 1.11: Typical physical properties of membranes depending on the molecular weight of the constituent amphiphiles [9].

1.5 Membrane permeability - a passive process

The cell membrane of living cells is a semi-permeable membrane, which acts as a protective skin and mediates the permeability. The underlying bilayer is practically impermeable to large uncharged polar molecules, such as glucose and sucrose, and ions, such as Ca^{2+} , Na^+ , K^+ . To cross the membrane these molecules require typically an active transport process, for example aided by transport proteins. Small hydrophobic molecules, such as O_2 and CO_2 , and small uncharged polar molecules, such as water and urea, can diffuse through the bilayer [14] (Figure 1.12). The ability of water to cross the lipid bilayer and the inability of sugars to do the same is also used when dealing with giant unilamellar vesicles (see below).

Water permeability. Large unilamellar vesicles can be used as model systems to test the water permeability of the membrane. The water permeability coefficient, typically given in $\mu\text{m s}^{-1}$, can be used to characterize the membrane permeability. This is very important in living cells, as in various cell compartments, a concentration gradient on the two sides of the membrane exists, which in turn leads to an osmotic flow of the water across the membrane. From measurements a characteristic value, the osmotic water permeability, can be determined. Besides osmotic water permeability, diffusive permeability can be observed; typically osmotic water permeability is higher than diffusive permeability. Water permeability in lipid bilayers is only weakly influenced by the thickness of the hydrophobic region; therefore a variation of the lipid tail length leads only to minor changes in the values.



However, the permeability to water is strongly influenced by the choice of different head groups and hydrogen bonding between them, which in case of charged phospholipids is influenced by changes in the ionic strength of the surrounding media [42]. Additionally a decrease in water permeability is seen for lipids below the transition temperature, in the gel phase [43]. In a region around T_m , a maximum for water permeability can be observed [44]. Moreover, it was found that with increasing number of unsaturations in the lipid chain the water permeability increases [45].

Typical experiments allow the measurement of water permeability by preparation of LUVs entrapping a fluorophore and monitoring the self-quenching on a stopped-flow fluorimeter upon exposing to an osmotic shock [46]. Another example is to follow exchange of water by monitoring the ^{17}O signal of water by NMR spectroscopy [47]. By combining osmotic shocks and the micropipette aspiration method on GUVs, bilayer

water permeability can be measured directly under the microscope [45].

Permeability to other molecules. Some indication of the permeability coefficients of other molecules through a lipid bilayer in the fluid phase is given in Figure 1.13. Depending on the molecules, the permeation process can involve a transient pore formation or changes to a solubility-diffusion controlled process, where the permeability coefficient is proportional to the product of its partition coefficient and diffusion coefficient in the membrane but inversely proportional to the thickness of the membrane [41]. For ions with a sufficiently thin membrane the pore formation process dominates. Neutral molecules cross exclusively by solubility-diffusion mechanisms [48].

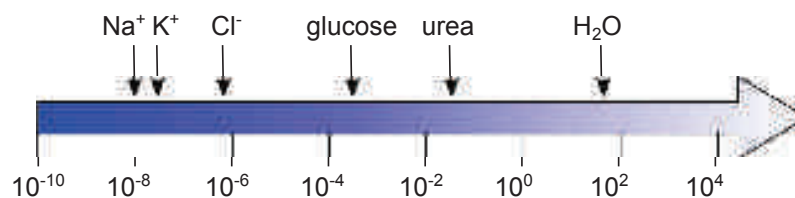


Figure 1.13: Permeability coefficients of different molecules through a lipid bilayer in the fluid phase, values are in $\mu\text{m s}^{-1}$, adapted from Lodish et al. [49].

The majority of lipids in a cell is made of tails with 16 carbons or longer where the permeation is solubility-diffusion controlled, thus making it more difficult for large and/or charged molecules to permeate a bilayer. The permeability of ions, such as sodium, potassium and calcium ions, across the membrane is by a factor of 10^9 lower than for water, which can be explained by a change in the permeation process. Furthermore, the permeability of ions is directly related with the membrane thickness. The proton permeability increases with decreasing membrane thickness. For larger ions, such as potassium, it was found that the permeability decreases with increasing number of carbon atoms up to a certain chain length, where higher membrane thickness has only minor influence [48]. Even though there is some finite permeability for ions and sugars, in practice, the lipid bilayer is often considered as impermeable for molecules with permeability coefficients below $10^{-2} \mu\text{m s}^{-1}$.

In binary mixtures of lipids and cholesterol an increase of the passive permeability in the transition region can be observed for low amounts of cholesterol, whereas for high cholesterol concentration the permeability is suppressed [50, 51].

1.6 All roads lead to GUVs

As already further described in section 1.3, the cell membrane is a complex entity, where both active and passive phenomena take place, calling for simpler model systems [52].

Giant unilamellar vesicles (GUVs) are appropriate tools for studying membrane properties, due not only to their relative simplicity, but also because they can be prepared in a size range similar to that of cells. GUVs allow investigation of membrane properties, like membrane permeability, investigation of bilayer interactions and determination of mechanical and rheological properties [53]. Recent examples for the application of GUVs include the use as microreactors [54] or microscopic vessels for protein crystallization [55].

Several methods exist for the formation of giant unilamellar vesicles (GUVs). Each of these methods is typically designed for a peculiar purpose, as schematically shown in Figure 1.14, that gives a basic overview of possible modifications of GUVs.

In the following chapters, a non-exhaustive overview of the basic methods is given. For a better and more complete review, the reader is referred to Walde et al. [28].

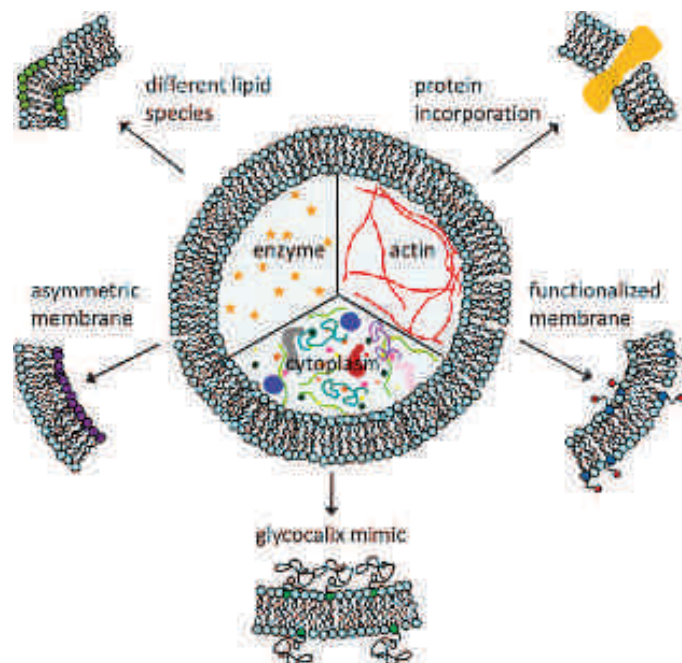


Figure 1.14: A schematic representation of possible modifications of GUVs achieved by various methods. The composition of the membrane can be varied as well as the different structures to be encapsulated in the interior, after Fenz and Sengupta [52].

In this manuscript, the formation methods are conveniently grouped into three different classes. Each class contains one of the major methods used to form GUVs. The basic method will be explained and some of the advantages and drawbacks further described:

1. Methods based on spontaneous swelling (Section 1.6.1)
2. Solvent or emulsion based methods (Section 1.6.2)
3. Energy-assisted methods (Section 1.6.3)

All of the mentioned methods can be used to prepare liposomes as well as polymer-somes.

1.6.1 Vesicles are formed spontaneously

Methods based on spontaneous swelling are the oldest of the existing methods. They can be traced back to 1969 when Reeves and Dowben [56] described that controlled hydration of a thin dry film of egg yolk phosphatidylcholines on a glass surface leads to the formation of giant unilamellar vesicles. An important observation was that even slight agitation can cause the formation of undesired MLVs. The swelling process proceeds in three stages. First the water molecules penetrate the lipid bilayers of the pre-assembled stack and causes them to swell. Second the bilayer peels off from the stack and in a last step the outermost bilayer is unbound due to thermal fluctuations, which can only happen in the liquid state [57]. Therefore, it is important to perform the hydration at temperatures above T_m . This method is commonly known as spontaneous swelling or gentle hydration method. In Figure 1.15 the different stages of spontaneous swelling are shown.

During the last 40 years several improvements and modifications of the gently hydration methods have been reported. An important feature, already mentioned in the paper of Reeves and Dowben is the pre-hydration of the pre-assembled lipid stack with water-saturated nitrogen gas [56, 59]. Gentle hydration in physiological salt solutions typically requires mixed lipid films containing 10-20 mol% of a charged lipid, such as PG or PS. The negatively charged lipids provide electrostatic repulsion between bilayers, which facilitates the GUV formation [60].

The use of PEGylated lipids with short PEG moieties of around 2000 Da has a similar effect as negatively charged lipids [55]. Furthermore, it was observed that doping of dry lipid films with monosaccharides (glucose, mannose, fructose) leads to efficient formation of giant liposomes. The dissolving sugar molecules cause a high osmotic pressure between the lamellae of the bilayer stack leading to repulsive interactions forming GUVs [61], see Figure 1.16.

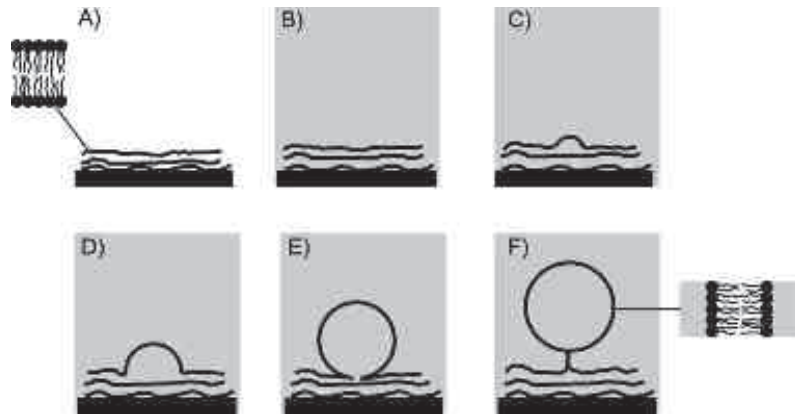


Figure 1.15: Illustration representing the stages of spontaneous swelling, adapted from Shi-manouchi et al. [58], taken from Ref. [28]. (A) Pre-assembled bilayer stack. (B) Water penetration into the bilayer stack. (C–E) Budding and vesicle formation. (F) Detaching of the formed GUV from the bilayer stack.

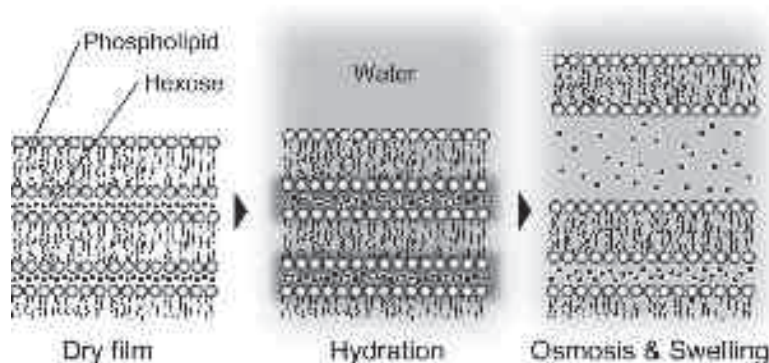


Figure 1.16: Penetrating water dissolves sugar molecules leading to an osmotic flow and repulsion of the bilayer lamellae [61].

Within the method of spontaneous swelling a broad range of vesicle sizes (1–150 μm) is obtained. Some control over the vesicle size distribution could be successfully achieved by the use of patterned surfaces as substrate [62]. As previously mentioned, it is of interest to encapsulate macromolecules. However, encapsulation efficiencies during GUV formation with film hydration based methods are generally low. It was shown, that the use of polymeric crowding agents, for instance 10 wt% PEG₂₀₀₀ can increase the yield [63].

All these methods require swelling times of a couple of hours, often over night, and elevated temperatures, which could lead to lipid breakdown [64]. A recent study showed that by hydration of hybrid lipid/agarose films with solutions of physiological ionic strength, GUVs can be rapidly formed within minutes. This method can be used with a wide range of lipid compositions and buffer conditions and showed promising

results in the efficient encapsulation of various biomolecules [65]. One drawback, however, is that the agarose gel dissolves partly upon swelling and remnants can afterwards be detected in or on the membrane.

In chapter 4, we will describe an improved method based on swelling of a gel beneath a stack of lipid bilayers.

Table 1.5 compares the mentioned modifications of the film hydration methods by listing of some of the advantages and disadvantages.

Methods based on spontaneous swelling are effective methods for GUV formation of different lipid species, as well as encapsulation of macromolecules. If one compares this method with Figure 1.14, it becomes clear that it is not possible to create vesicles with an asymmetric membrane. For achieving this one has to look at the solvent or emulsion based methods.

Modification	Advantage	Disadvantage
Charged lipids	Physiological conditions	Limitation in membrane composition Pre-hydration required
PEGylated lipids	For high salt concentrations	Requires special lipids
Doping with monosaccharides	For neutral lipids	Only for neutral lipids Low salt concentrations
Patterned surface	Narrow size distribution	Extensive sample preparation
Polymeric crowding agents	Improves encapsulation efficiency	Requires crowding agent
Lipid/agarose hybrid films	Fast	Contamination with agarose

Table 1.5: Advantages and disadvantages of the gentle hydration method.

1.6.2 Emulsions for better defined vesicles

Solvent or emulsion based methods are applicable to the formation of asymmetric bilayers, encapsulation of other molecules, they also allow controlling the vesicle size distribution.

Solvent evaporation. One of the first methods able to form GUVs in a high yield was developed by Moscho et al. [66]. Herein a two-phase system of oil and aqueous solution is prepared, where lipids accumulate at the oil/water interface in such a way that hydrophobic tails are directed inwards of the oil phase (a mixture of chloroform and methanol) with a higher density than water. Evaporation leads to formation of bubbles, which ruptures the phospholipid monolayer into fragments, ultimately leading to vesicles. This method is very simple and fast, but the obtained vesicles are not all unilamellar and the size distribution is very broad.

Inverted emulsion. A much better controlled method is the use of water-in-oil (W/O) emulsions. In a first step, W/O emulsions are prepared wherein the lipid acts as a surfactant stabilizing an inverted emulsion. The inverted emulsion is then transferred in a vial containing lipid-saturated oil on top of an aqueous solution. The monolayer at the oil-water interface completes the bilayer when the droplets from the first emulsion sediment and pass the monolayer [67]. A schematic illustration is shown in Figure 1.17. An improvement of this method uses a centrifuge to speed-up the sedimentation process [68]. This inverted emulsion technique is able to form asymmetric vesicles. A drawback is that the size of the formed vesicles is limited by the droplet size of the emulsion; GUVs are typically smaller than 1 μm .

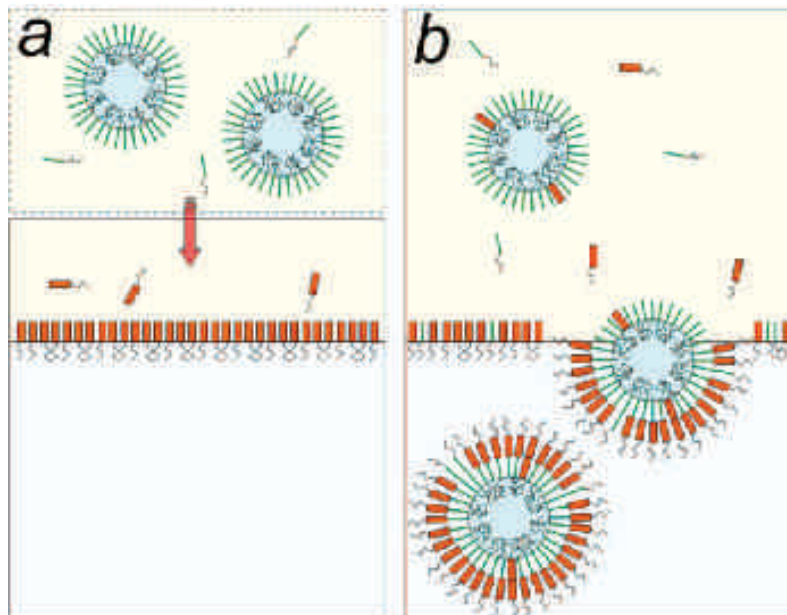


Figure 1.17: Schematic illustration of the inverted emulsion technique to produce asymmetric GUVs [69]. Here the method is used for the formation of asymmetric polymersomes. (a) Droplets of a water-in-oil emulsion are stabilized by the amphiphile building up the inner leaflet. (b) Upon centrifugation the water droplets are crossing the monolayer, composed of the amphiphiles destined for the outer leaflet and completing GUV formation [68].

Jet-blowing. A related method is the so-called jet-blowing. The basic principle is that a pulsed microfluidic jet is blown against a planar lipid bilayer and monodisperse GUVs are formed encapsulating the jet solution. Jetting velocity and volumes determine the GUV size [70, 71]. Figure 1.18 shows a schematic of the microfluidic jetting device.

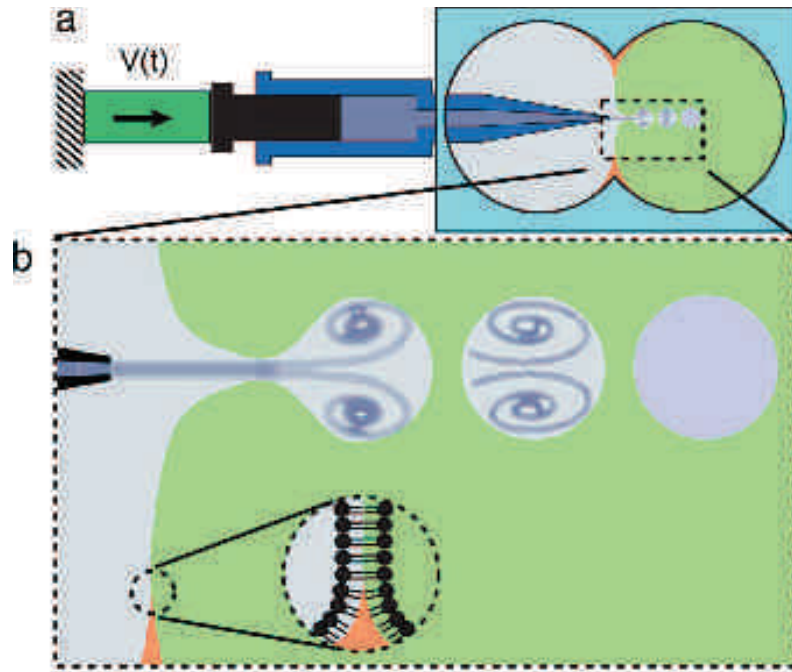


Figure 1.18: Illustration of GUV formation by microfluidic jetting. (a) A piezoelectric-driven microfluidic jetting device jets droplets against the lipid bilayer. (b) Zoom of the vesicle-formation process, adapted from Stachowiak et al. [71].

Continous droplet interface crossing encapsulation (cDICE). A somewhat easier method based on droplets crossing a lipid monolayer at a water-oil interface is the method developed by Abkarian et al. [72]. This so-called continous droplet interface crossing encapsulation (cDICE) method uses a rotating cylindrical chamber, in which first a dispersing aqueous solution (DAS), then a lower density lipid-in-oil solution (LOS) and finally decane with a lower viscosity are injected. The three fluids are immiscible between each other. At the interface of DAS and LOS a saturated lipid monolayer is formed. A capillary is inserted in the decane and the encapsulated aqueous solution (EAS) is injected at a constant pressure. Due to the shearing forces exerted by the rotating oil, droplets are detached from the capillary tip and centrifuged radially towards the LOS/DAS interface. During the movement of the EAS droplet through the LOS phase, lipids saturate the surface of the droplet, thus forming a lipid monolayer. When the droplet crosses the LOS/DAS monolayer the final bilayer is formed. Droplet size is determined by the capillary diameter and approximately equal to three times the capillary size, which in turn defines the final vesicles size [72]. Figure 1.19 shows an illustration of the cDICE method.

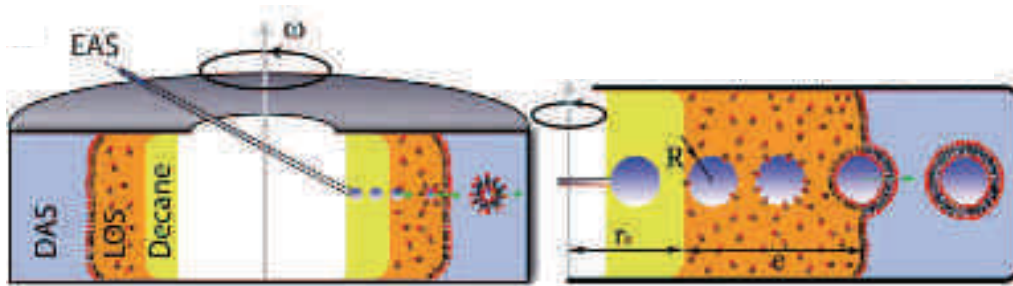


Figure 1.19: Schematic illustration of the cDICE method. The capillary is fixed and the chamber is rotating at a speed ω . Encapsulated aqueous solution (EAS) droplets are driven by the centrifugal force to the outside. The droplets saturate with lipids in the lipid-in-oil solution (LOS) and form GUVs when passing the LOS/DAS interface, adapted from Abkarian et al. [72].

Double emulsion. In another microfluidic based method, developed by Shum et al. [73], GUVs are formed with the help of a W/O/W double emulsion formed via a microcapillary device. An inner aqueous solution is “wrapped” by a middle phase, containing lipids in a volatile organic solvent, is injected into an aqueous solution of poly(vinyl alcohol) (PVA) and glycerol. The lipid double emulsion is stabilized by the used lipids. Afterwards, the middle organic phase is evaporated. The double emulsion droplets act as a template and help to form the GUVs, compare Figure 1.20.

All these methods are typically very fast and produce GUVs within minutes. Encapsulation is almost always more efficient in methods based on spontaneous swelling. Some methods allow a controlled GUV size. A big disadvantage is that traces of oil or organic solvent can be left in the obtained GUVs. Also higher amounts are used than in gentle hydration. For microfluidic based methods, special equipment and expertise are required [28].

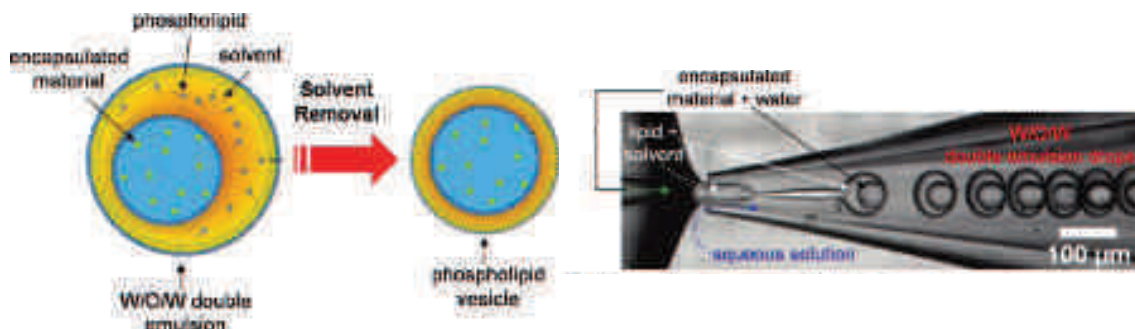


Figure 1.20: Left: Schematic illustration of the preparation of phospholipid vesicles using double emulsion as templates. Right: Formation of phospholipid-stabilized W/O/W double emulsion in a glass microcapillary device, adapted from Shum et al. [73].

Table 1.6 lists some of the advantages and disadvantages encountered when using these emulsion or solvent based methods.

Method	Advantage	Disadvantage
Solvent evaporation	Simple equipment Broad composition range	MLVs Low encapsulation efficiency No size control Oil remnants
Inverted emulsion	Simple equipment Asymmetric bilayers	Upper size limit Difficult size control Oil remnants
Jet-blowing	High encapsulation yield Size control High throughput	Special equipment Oil remnants
cDICE	Efficient encapsulation Size control High throughput	Special equipment Oil remnants
Double emulsion	High encapsulation efficiency Size control High throughput	Special equipment Oil remnants

Table 1.6: Advantages and disadvantages of the emulsion based methods.

1.6.3 Energy can assist GU formation

Spontaneous vesicle formation occurs when a stack of lipid bilayers is hydrated by an aqueous solution. Without or almost no energy-input into the system typically MLVs are formed [26]. Figure 1.21 shows an approximate energy diagram of uncharged phospholipid aggregates at low concentrations in water [27]. It can be observed that the free energy of unilamellar vesicles, such as SUVs and LUVs, is higher than for phospholipid aggregates and MLVs. Therefore, energy must be dissipated into the system for the formation of unilamellar vesicles.

For the formation of SUVs, the highest amount of energy has to be put into the system. This is typically done with the help of sonication [74]. All unilamellar vesicles are in a kinetically trapped state and fuse into LUVs and MLVs to decrease their free energy. SUVs typically can fuse into LUVs after a couple of days. A freeze-thawing procedure can be applied, to help crossing the energy barrier and speeding up the fusion of vesicles [75]. Extrusion, a common method nowadays, leads to the formation of LUVs by forcing MLVs through polycarbonate membranes with a pore size of 100 nm

[76]. LUVs are typically much more stable than SUVs. These methods for LUV formation are also more gentle, which can be explained by the lower free energy of LUVs, therefore lower energy is needed for the transition into unilamellar vesicles.

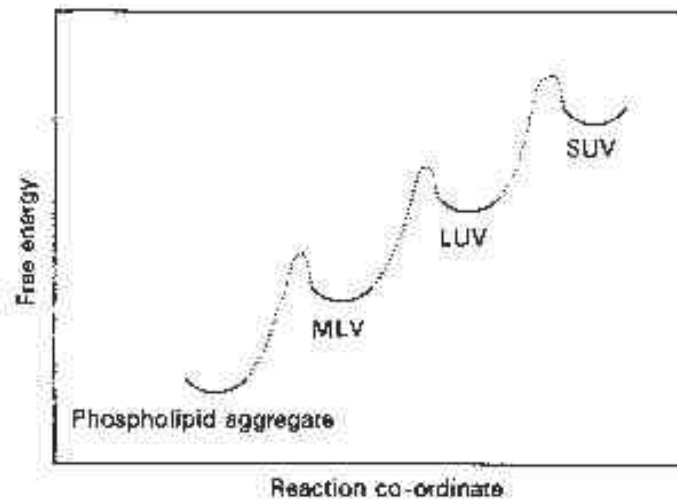


Figure 1.21: Energy diagram of different phospholipid aggregates [27].

GUVs are somewhat comparable to LUVs. Besides the spontaneous swelling described in section 1.6.1, some methods are described also in this chapter, which lead to GUV formation by input of energy. In this manuscript these methods are classified as energy-assisted methods.

The two basic existing methods are electroformation and localized IR heating. All other described methods are variations of the well-known electroformation method.

Electroformation. In 1986, Angelova and Dimitrov, published a paper describing the hydration of a pre-assembled bilayer stack in presence of an oscillatory electric field [77]. Known as the electroformation method or electroswelling, it became one of the most common methods to prepare GUVs in a simple and fast manner. Mechanical stress induced by the electric field on the bilayer can rupture the lipid bilayers, which then close into liposomes and lead to formation of spherical GUVs of different sizes. The electroosmotic effect is the driving force behind the electroformation [78]. Membrane fluidity and stiffness influence the size of the formed GUVs [58], that are still connected to the residual lipid film by long thin membrane threads[79].

A typical electroformation chamber is assembled from two indium tin oxide (ITO) coated glass slides separated by some spacer, on which a lipid film is spread. The chamber is then filled with a sucrose solution and an alternating field of 1 V with a frequency of 10 Hz is typically applied across the chamber. Alternatively, instead of ITO

coated glass slides, Pt wires are also used as electrodes. GUVs are formed within a couple of hours. This method can also be used for the formation of polymersomes. Figure 1.22 shows a cross section of an electroformation chamber.

Electroswelling shows some restrictions in regard of buffer composition and lipid compositions, as well as encapsulation of molecules. It works well for GUV formation in aqueous solution or buffer solutions of low ionic strength. GUV formation in physiological conditions or lipid mixtures with a high amount of charges do not form giant vesicles [80]. Encapsulation yield is generally also low.

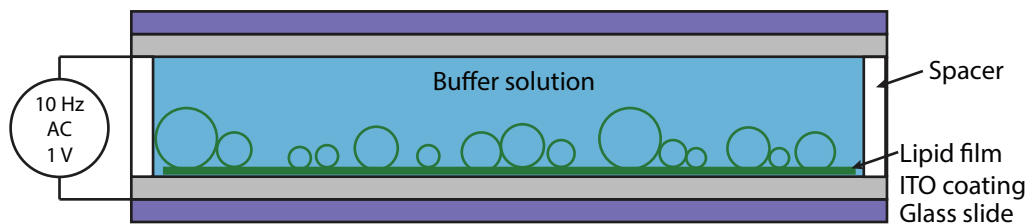


Figure 1.22: Schematic illustration of an electroformation chamber. The lipid is spread upon ITO coated glass slides. An alternating field is applied across the buffer filled chamber.

Some modifications to the electroformation method allow a the better controlled formation of GUVs with high charges and/or in physiological buffers.

Variation of electric field. Applying a step-wise electroformation protocol, starting with an electrical field with low frequency and amplitude and then applying a higher frequency and voltage allows GUV formation at physiological relevant conditions [81, 82].

Flow chamber. A flow chamber can be used to obtain GUVs in high ionic strength. Surface-attached giant liposomes in solutions with low ionic strength containing glycerol are formed in a flow chamber and then exchanged against solutions of high ionic strength (up to 2 M KCl). Furthermore it is possible to encapsulate large biomolecules [83].

Spin-coating. Spin-coating of lipid solutions on an ITO coated glass slides generates uniform lipid films. If electroformation is performed with this homogeneous precursor lipid film, GUVs in a higher number and significantly larger can be obtained. Spin-coating improves also to some amount GUV formation with lipid mixtures purely composed from charged lipids, such as DOPS [84].

Inverse phase precursor. Mertins et al. [85] reported a method using an inverted emulsion prepared from a volatile water-immiscible organic solvent deposited on ITO glass slides. After evaporation of the solvent, the normal electroswelling leads to GUV formation. This method allows encapsulation and decoration of the membrane with hydrophilic macromolecules. Fig 1.23 shows a schematic illustration of the inverse phase precursor method.

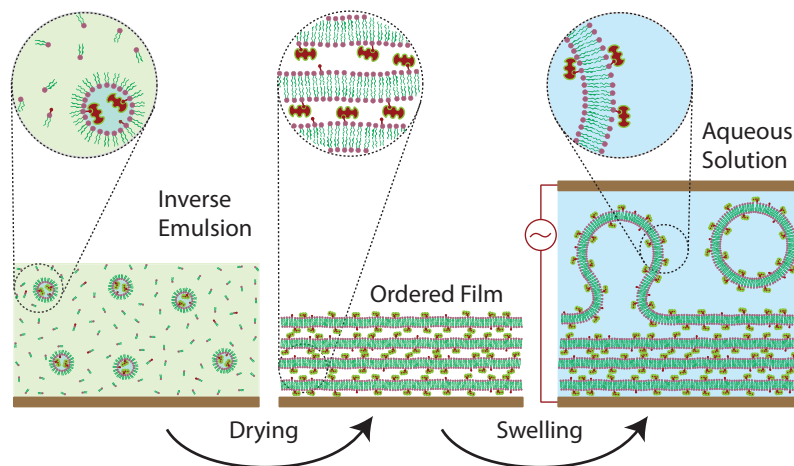


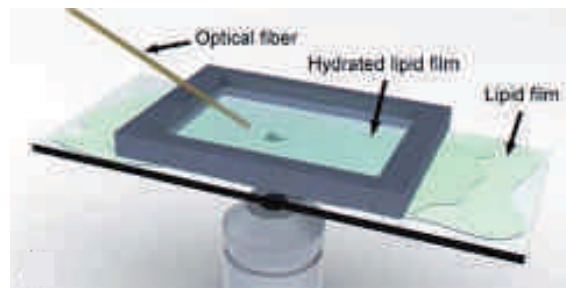
Figure 1.23: Schematic illustration of the inverse phase precursor method. An inverse emulsion is prepared and spread on an ITO coated glass slide. After drying the pre-ordered film, electroformation leads to GUVs. In this sketch the membrane is decorated with fluorescent streptavidin which recognizes the biotinylated lipids of the membrane [85].

Non-electroconductive substrate. The lipid film is normally spread directly on the electrodes of the electroformation chamber. It was reported by Okumura et al. [86] that direct contact of the lipid is not necessary. This allows eliminating one of the disadvantages of the electroformation method: lipids possessing one or more unsaturations can degrade due to peroxidation of the lipids through the applied electrical field [87]. It was also reported that the commonly used ITO electrodes can lead to an increased liquid-ordered/liquid-disordered area in tertiary mixtures of DOPC, sphingomyelin and cholesterol [64, 88].

Localized IR heating. Recently, a novel method for the generation of GUVs from spin-coated lipid films was reported [89]. An IR-B laser locally heats a planar lipid film, causes it to rapidly form GUVs within minutes. This technique allows GUV formation from charged and neutral lipids and mixtures in various ionic strength conditions. Additionally, encapsulation is possible. An advantage is that the spin-coated lipid films can be prepared in advance and stored in the freezer. Disadvantages are that not

only unilamellar vesicles are obtained and that the temperature locally reaches up to 90 °C, which is problematic for encapsulation of proteins.

Figure 1.24: Schematic diagram of the localized IR heating method. GUVs are generated from a deposited lipid film, by heating with an IR-B laser through an optical fiber, adapted from Billerit et al. [89].



All electroformation-based methods allow the fast and facile production of GUVs without the need for special equipment. Contrary to the gentle hydration method, here most of the vesicles are unilamellar. Even with the mentioned modifications, there are still limitations, when it comes to GUVs containing a high amount of charges or when growing in physiological conditions is performed. Moreover, encapsulation efficiencies for large water-soluble molecules or charged compounds are generally low.

Table 1.7 lists some of the advantages and disadvantages for energy-assisted methods.

Method	Advantage	Disadvantage
Electroformation	Rapid GUV formation Easy setup	Low encapsulation yield Ionic strength of buffer Low amount of charged lipids
Variation of electric field	High ionic strength High amount of charges	Low encapsulation yield
Flow chamber	High ionic strength Encapsulation possible	
Spin-coating	Charged lipids	Encapsulation yield
Inverse phase precursor	Encapsulation possible	Charged lipids High ionic strength
Localized IR heating	High encapsulation yield Rapid Storage of samples	Lamellarity distribution High local temperature

Table 1.7: Some advantages and disadvantages of the energy-assisted methods.

Materials & Methods

In this chapter the methods and materials used for this work are described. The chapter lists also chemicals and describes sample preparation (e.g. fluorescent labeling). The various preparation methods for unilamellar vesicles are described, as well as different optical microscopy techniques. The chapter closes with a brief description of complementary techniques such as spectroscopy and calorimetry.

2.1 Chemicals

In order to ensure comprehensibility and legibility throughout the text, abbreviations have been introduced for some compounds which are specified in Table 2.1.

The supplier of the chemicals and solvents are listed in Table 2.2. Table 2.3 lists the composition of the buffer solutions. All chemicals were purchased as analytical grade and used without further purification unless specified otherwise.

In some experiments we formed polymersomes from the triblock copolymer PMOXA₁₀-PDMS₈₇-PMOXA₁₀. Its synthesis is described in reference [90].

2.1.1 Lipids

Lipids were purchased as a powder and dissolved in chloroform. Stock solutions were prepared with a concentration of 10 mg mL⁻¹. The stock solutions were stored at -20 °C in glass vials closed with teflon caps. To protect the stock solutions from loss of solvent, caps were additionally wrapped with teflon tape and covered with parafilm. Before use, the stock solutions were mixed and diluted with chloroform to obtain the desired concentrations and lipid mixtures. As a fluorescent marker we used rhod-PE in a 0.2–0.5 mol% mixture with other lipids.

Abbreviation	Name of the molecule
DOPC	1,2-dioleoyl-sn-glycero-3-phosphocholine
DOPG	1,2-dioleoyl-sn-glycero-3-phospho-(1'-rac-glycerol) (sodium salt)
DOPS	1,2-dioleoyl-sn-glycero-3-phospho-L-serine (sodium salt)
DOTAP	1,2-dioleoyl-3-trimethylammonium-propane (chloride salt)
DPPC	1,2-dipalmitoyl-sn-glycero-3-phosphocholine
DPhPC	1,2-diphytanoyl-sn-glycero-3-phosphocholine
cardiolipin	1,1',2,2'-tetramyristoyl cardiolipin
rhod-PE	1,2-dioleoyl-sn-glycero-3-phosphoethanolamine-N-(lissamine rhodamine B sulfonyl)
biotin-PE	1,2-dipalmitoyl-sn-glycero-3-phosphoethanolamine-N-(cap biotiny)
PEG-PE	1,2-dipalmitoyl-sn-glycero-3-phosphoethanolamine-N-[methoxy(polyethyleneglycol)-2000]
PMOXA	Poly(2-methyl-2-oxazoline)
PDMS	Polydimethylsiloxane
DTAF	[5-(4,6-Dichlorotriazinyl)-aminofluorescein]
PVA	Polyvinyl alcohol
PBS	Phosphate buffered saline
AF350	Alexa Fluor 350
AF488	Alexa Fluor 488
DTT	dithiothreitol
CaCl ₂	calcium chloride
Na ₂ ATP	Adenosine 5'-triphosphate disodium salt hydrate
Tris-HCl	Tris(hydroxymethyl)aminomethane hydrochloride
BODIPY	boron-dipyrrromethene
ConA	Concanavalin A
ConA-FITC	FITC labeled ConA

Table 2.1: Abbreviations for certain chemicals.

Supplier		Name
Sigma Aldrich	St. Louis, MO, USA	DOPC, DPPC, DOPG, DTAF, PBS tablets chloroform, sucrose, glucose, glutaraldehyde
Avanti Polar Lipids	Alabaster, AL, USA	DOPS, DOTAP, DPhPC, Cardiolipin rhod-PE, biotin-PE, PEG-PE
Invitrogen	Breda, The Netherlands	Neutravidin, AF350-Neutravidin, AF488-actin AF488 carboxylic acid succinimidyl ester
Thermo Scientific	Breda, The Netherlands	Streptavidin
Tebu-bio	Heerhugowaard, The Netherlands	G-actin, biotinylated G-actin
Laboratory	ICS, Strasbourg, France	Millipore water (18 MΩcm)
VWR International	Fontenay-sous-Bois, France	PVA 145,000 g mol ⁻¹ (Merck KGaA, Darmstadt, Germany)
Wolfgang Meier Laboratory	Basel, Switzerland	PMOXA ₁₀ -PDMS ₈₇ -PMOXA ₁₀ (MW 8154, PDI 2.2)

Table 2.2: Supplier of used chemicals.

2.1.2 Proteins for encapsulation

Neutravidin, AF350 labeled neutravidin and streptavidin were purchased from the supplier as described in Table 2.2. Rabbit skeletal muscle G-actin was purified by standard procedures including a gel filtration on a Sephacryl S-200 high-resolution column (GE Healthcare, Muenich, Germany) [91] or purchased from Tebu-bio. Fluorescent actin with a dye/protein molar ratio of 0.6 was prepared by labeling amine groups with AF488 carboxylic acid succinimidyl ester [92] or purchased from Invitrogen. G-actin labeled with biotin was purchased from Tebu-bio. G-actin was stored at $-80\text{ }^{\circ}\text{C}$ in G-buffer. Before use, G-actin solutions were thawed, treated with 5 mM DTT to reduce potential oxidized sulfhydryl groups, centrifuged at 120,000 g for 30 min to remove potential protein aggregates, and finally bath-sonicated for 5 min to disrupt potential actin dimers [93].

Name	pH	Components
PBS	7.4	PBS tablets to dissolve in 200 mL, contain: 0.01 M phosphate buffer, 0.0027 M KCl and 0.137 M NaCl
G-buffer	7.8	2 mM Tris-HCl, 0.2 mM Na_2ATP 0.2 mM CaCl_2 , 2 mM DTT
I-buffer	7.4	25 mM imidazole-HCl, 1 mM DTT, 0.1 mM MgATP, 50 mM KCl 2 mM MgCl_2 , 280 mM sucrose, 0.5 % (v/v) glycerol, 2 mM trolox 2 mM protocatechuic acid and 0.1 μM protocatechuate 3,4-dioxygenase
O-Buffer	7.4	glucose solution or PBS buffer

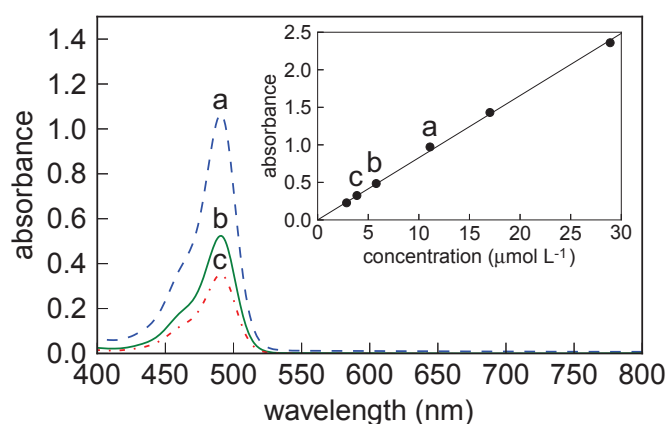
Table 2.3: Composition of used buffer solutions.

2.1.3 Polyvinyl alcohol and fluorescent PVA

For fluorescent studies, we labeled PVA with DTAF by elimination of hydrochloride using previously described protocols [94, 95]. DTAF covalently couples to the alcohol groups of PVA at pH levels above 9. DTAF-labeled PVA was separated from free DTAF by extensive dialysis against MilliQ water using a regenerated cellulose membrane with a molecular weight cut-off of 4000-6000 Da. The average labeling stoichiometry was determined by spectrophotometric measurements of the light absorbance of the dialysed PVA-DTAF solution at a wavelength of 495 nm, corresponding to the excitation maximum. The emission maximum of DTAF is at 516 nm. We first determined the extinction coefficient of aqueous solutions of DTAF at different concentrations by recording absorbance spectra between wavelengths of 400 to 800 nm with a scan rate

of 600 nm min^{-1} on a UV/Vis Cary 500 Spectrometer (Figure 2.1). These measurements were performed using pH adjusted solutions, because of the pH dependence of the fluorescence properties of fluorescein analogs. We determined an extinction coefficient of $82900 \text{ L mol}^{-1} \text{ cm}^{-1}$ (inset in Figure 2.1) and measured a DTAF concentration of $8.72 \times 10^{-5} \text{ mol L}^{-1}$ in the solution of DTAF-labeled PVA. A polymer concentration of $2.97 \pm 0.07 \%$ (w/w) was determined by drying 1 g of the PVA-DTAF solution. Thus, the degree of labeling was 0.43 mol DTAF per mol of PVA chain, or $1.30 \times 10^{-4} \text{ mol DTAF per mol of repeating unit}$, implying that approximately every second PVA chain bears one fluorescent label. Both labeled and unlabeled polymers can be dissolved when exposed at temperatures higher than $50 \text{ }^\circ\text{C}$ for longer than 30 min.

Figure 2.1: Absorbance spectra of DTAF standard solutions and standard curve for DTAF solutions in water (inset). For the inset the absorbance at 495 nm, the absorption maximum of DTAF, was used to draw the standard curve. Points a, b, c on the standard curve correspond to the spectra marked as a, b, c.



To estimate the amount of residual free fluorophore, PVA-DTAF coated glass slides, chemically crosslinked with glutaraldehyde, were immersed in water for 1 hour and the absorbance of the solution measured after adjusting the pH. From the standard curve, a maximum amount of 10 mol% free fluorophore in the labeled PVA was determined, providing an estimation for the uncertainty in fluorescence measurements.

2.1.4 Synthesis of functionalized elastin-like polypeptides

ELP block copolymers (ELP_{BC}) were synthesized by Sarah MacEwan in the lab of Ashutosh Chilkoti at the Duke university in North Carolina, USA. ELP_{BC} were named by their functionalization of the cell-penetrating peptide (CPP) on the C-terminal of the ELP-BC: $\text{Arg}_5\text{-ELP}_{\text{BC}}$, $\text{Arg}_8\text{-ELP}_{\text{BC}}$, $\text{TAT-ELP}_{\text{BC}}$ (47YGRKKRRQRRR57) and non-functionalized control ELP_{BC} . $\text{Arg}_5\text{-ELP}_{\text{BC}}$ and its respective non-functionalized control ELP_{BC} were genetically designed by Recursive Directional Ligation (RDL) as described elsewhere [96].

$\text{Arg}_8\text{-ELP}_{\text{BC}}$, $\text{TAT-ELP}_{\text{BC}}$ and their respective control ELP_{BC} were genetically designed by RDL by plasmid reconstruction (PRe-RDL) as described in [97]. All of the ELP_{BC}

possess a 'leader' sequence (GCGWPG), the Arg₅-ELP_{BC} was composed by the following peptide sequence (VPGVG)₆₀-(VPGXG)[X=V:G:A,1:7:8]₉₆ and the rest of the ELP_{BC} by (VPGVG)₆₀-(VPGAGVPGGG)₃₀.

E.Coli cells containing the ELP genes were grown 24 hours at 37 °C while shaking in the presence of kanamycin. E.Coli cells were collected by centrifugation and cells were lysed by sonication. ELPs were purified by their thermal properties by inverse transition cycling as described in [98]. For fluorescent labeling AF488 C5-maleimide was conjugated to a cysteine residue on the N-terminus of the ELP_{BC} in the presence of 3 mM TCEP-HCl and 10 mM NaH₂PO₄ at a pH of 7 for 2 hours. Aggregation of ELP_{BC} was induced by addition of NaCl, the labeled ELPs collected by centrifugation and the supernatant was discarded. Afterwards the ELP_{BC} were resuspended in PBS buffer solution and remaining free fluorophore was removed with a desalting column. Dialysis was performed against water and the ELP_{BC} were lyophilized. The lyophilized ELP_{BC} were stored at -20 °C and resuspended in PBS solution at concentrations between 16–25 µM before use.

2.2 Preparation of vesicles

In the following chapter, the methods used to prepare unilamellar vesicles of all sizes are described. The following table shows an overview of the methods used:

Vesicle type	Preparation method
SUV	Sonication with a titanium microtip
LUV	Extrusion through 100 nm polycarbonate membranes
GUV	Electroformation with ITO glass slides Gel-assisted formation with PVA as substrate

Table 2.4: Techniques to prepare unilamellar vesicles in this work.

2.2.1 Small unilamellar vesicles

Small unilamellar vesicles (SUV) were prepared by sonication with a 500 W Vibra-Cell Ultrasonic Processor and a 1/8" tapered microtip (Sonics, Newton, CT, USA) of a vesicle suspension containing large, multilamellar vesicles. By this method SUVs with diameters in the range of 15–50 nm are produced. SUVs are usually used immediately after preparation; they are metastable and spontaneously fuse into larger vesicles due to their high membrane curvature.

In a first step, the desired lipids were typically dissolved in chloroform at the desired concentration (between 1 and 10 mg mL⁻¹). An aliquot of this sample containing the

desired amount of lipids was pipetted in a glass vial. The solvent was evaporated by a gentle nitrogen stream in a fume hood, and placed in a desiccator for 30 min when dry, to ensure a complete removal of the solvent. Then the lipid sample was hydrated with sucrose or PBS buffer for 1 hour at room temperature (above the transition temperature of the lipid), which lead to formation of large, multilamellar vesicles. The vial was vortexed vigorously for 1 min to ensure complete re-suspension of the lipids, which resulted in a milky suspension.

The titanium tip sonicator was then inserted and sonication performed during cooling in an ice bath to prevent degradation from overheating. Sonication was done in pulses of 50 s with a 20 s pause in between them. The standard setting for the power was 20 % at a fixed frequency of 20 kHz and the sonication time between 2–5 min, if not stated otherwise. The lipid suspension should begin to clarify to yield a slightly hazy transparent solution. If necessary, titanium particles from the microtip in the sample, were removed by centrifugation at 13000 g for 10 minutes. However, TEM images still show a small amount of multilamellar vesicles, which can be neglected for the experiments for which LUVs are used in this work.

The prepared SUVs are immediately used after sonication.

2.2.2 Large unilamellar vesicles

Large unilamellar vesicles (LUVs) were prepared by extrusion of multilamellar vesicles through polycarbonate membranes. LUVs obtained by this method exhibit a narrow size distribution. If the hydrated lipid suspension is subjected to freeze/thaw cycles before extrusion, the average vesicle size and the encapsulation efficiency of water-soluble molecules can be further increased [76]. The obtained LUVs are typically bigger than the pore size of the polycarbonate membrane [99].

The desired lipid(s) were dissolved in chloroform at concentrations between 1 and 10 mg mL⁻¹. An aliquot with the desired lipid amount was evaporated in a glass vial with the help of a nitrogen stream. After placing the dry lipid film in a desiccator for 30 min to ensure complete removal of the solvent, the film was hydrated in sucrose or PBS buffer for 1 hour above the transition temperature of the lipid(s). The resulting multilamellar vesicle suspension was subjected to 6 freeze/thaw cycles in dry ice or warm water.

The resulting opalescent solution containing MLVs was extruded 11 times through a 100 nm pore diameter polycarbonate membrane on a Mini-extruder (Avanti Lipids, USA) above T_m . The LUV containing solution was studied with dynamic light scattering and showed a narrow hydrodynamic radius of around 70 nm, see Figure 2.2.

The obtained LUVs are stable in the fridge for a couple of days.

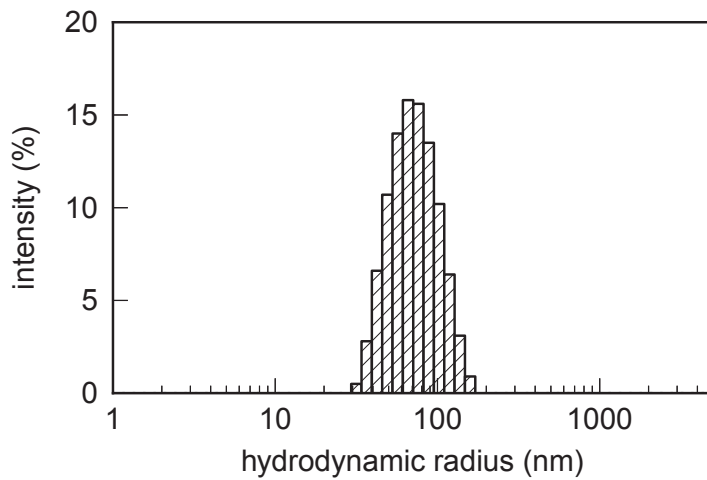


Figure 2.2: Typical graph obtained by dynamic light scattering measurement of the hydrodynamic radius of LUVs prepared by extrusion. The average radius is 64 nm.

2.2.3 Giant unilamellar vesicles

Electroformation and gel-assisted swelling were used in this work to prepare GUVs.

In some cases encapsulation of biomolecules inside of GUVs was achieved by combining these methods with spin-coating and preparing an inverse emulsion as precursor, as described below.

GUVs by electroformation

Electroformation was performed following the method of Angelova et al. [77]. Briefly, 10 μL of a lipid solution (1 mg mL^{-1} in chloroform) containing 0.5 mol% rhodB-PE as fluorescent label were spread on an indium tin oxide (ITO) coated glass slide. After drying of the lipid film under vacuum for 30 min, a chamber was formed with a second ITO slide and Sigillum wax (Vitrex, Copenhagen, Denmark) as a sealing agent. This chamber was filled with sucrose solution for neutral lipids and with a PBS buffer solution for lipid mixtures containing charged lipids. The osmolarity of the buffer was measured with an osmometer (Osmomat030, Gonotec, Berlin, Germany) and adjusted to 280 mOsm kg^{-1} . An alternating electric field was applied across the chamber for 3–12 hours at a temperature above T_m of the lipid mixture. The amplitude and the frequency of the field were 1 V and 10 Hz for neutral lipids and up to 5 V and 500 Hz for charged lipids. Successful formation was checked by observing the growing chamber by phase contrast microscopy. The obtained GUVs were transferred to an Eppendorf tube, diluted 5-times with isoosmotic glucose or PBS solution, and left undisturbed for 15 min before observation.

Gel-assisted swelling

A 5 % (w/w) solution of PVA was prepared by stirring PVA in water or in a 280 mM sucrose solution while heating at 90 °C. For fluorescent PVA substrates, one part of the DTAF labeled PVA solution from section 2.1.3 was mixed with 140 volume parts of unlabeled PVA. PVA-coated substrates were prepared by spreading 100–300 μL of PVA solution on a microscope cover slip (30 mm in diameter, Menzel-Gläser), which was then dried for 30 min in an oven at 50 °C. 10–20 μL of lipids dissolved in chloroform (1 mg mL^{-1}) were spread on the dried PVA film and placed under vacuum for 30 min to evaporate the solvent. Prior to use, the cover slips were cleaned with UV/Ozone for 15 min in order to prevent dewetting of the PVA film. A chamber was formed with Vitrex and filled with sucrose for neutral lipids or PBS buffer for charged lipids as described for the electroformation method. GUV formation was followed using phase contrast microscopy. When the desired vesicle sizes were reached, typically in less than 1 hour, GUVs were transferred into an Eppendorf tube using a pipette. The solution was diluted 5-times with isoosmotic glucose or PBS buffer and left undisturbed for 15 min before use.

Encapsulation of proteins

For encapsulation of proteins a similar protocol was used. Instead of spreading the PVA and lipid solutions (3.75 mg mL^{-1}) by hand, PVA was spin-coated on the cover slips at 1200 rpm for 30 s (DELTA 10BM, SUSS MicroTec). A typical lipid mixture was composed of 94.8:0.2:5.0 DOPC/RhodB-PE/PEG-PE. In experiments containing biotinylated lipids 1 % of DOPC was substituted by biotin-PE. 150 μL of lipid mixture were spin-coated on the dried PVA-coated slide at 1200 rpm for 300 sec. We used either open-top formation chambers, assembled by placing a 0.12 mm thick spacer (secure-seal spacer, Invitrogen) on the coated slide, or closed chambers, assembled by placing a 0.5 mm thick spacer (Coverwell, 13 mm in diameter, Invitrogen) and another cover slide on the coated slide. Lipid swelling was initiated by introducing a (inner) buffer containing the proteins to be encapsulated (I-buffer, compare Table 2.3). This I-buffer contains all necessary elements for the polymerization of actin, sucrose for osmotic pressure matching and oxygen-scavenging chemicals that minimize blinking and photobleaching [100].

The lipid film was allowed to swell for 45 min at a temperature of 4 °C, where actin polymerization is minimized. The GUVs were harvested by pipetting at least 2 chamber volumes of O-buffer (outer buffer) into the formation chamber, causing the GUVs to flow into the adjacent observation chamber or into an open-top observation chamber assembled by placing a 0.5 mm thicker spacer on a glass slide and closed by a

cover slide after GUVs harvest. The glass slides were passivated by a casein solution (2 mg mL^{-1}) to prevent liposome adhesion and rupture. Actin polymerization was initiated by bringing the observation chamber to room temperature. The O-buffer osmolarity was adjusted to be at least 20 mOsm kg^{-1} higher than the I-buffer osmolarity (Osmomat030, Gonotec GmbH) to prevent bursting of vesicles.

The actin concentration in all experiments was $23.8 \text{ }\mu\text{M}$ (equivalent to 1 mg mL^{-1}), including 20 mol% or 30 mol% of AF488 labeled actin and 0.25 mol% of biotinylated actin (1:400 molar ratio to actin). Streptavidin at a 1:25 molar ratio to the total actin concentration was included as a network crosslinker.

Inverse-phase precursor films for gel-assisted encapsulation

We adapted the inverse phase precursor method, which was previously combined with electroformation [85], to prepare lipid films containing biotinylated lipids complexed with neutravidin. By dispersing small water droplets containing hydrophilic moieties in the organic solvent containing the phospholipids, this method allows to prepare vesicles decorated with neutravidin or chitosan on their membrane. If neutravidin is used, it enables specific anchoring of encapsulated molecules to the membrane. An inverse emulsion was prepared from a mixture of lipids in chloroform and buffer. Briefly, a volume of $2 \text{ }\mu\text{L}$ neutravidin in PBS (48 mg mL^{-1}) was added to $60 \text{ }\mu\text{L}$ of a lipid solution as described above. In control experiments without biotin-PE lipids, pure PBS buffer was added. The mixture was pipetted up and down several times with a $500 \text{ }\mu\text{L}$ glass syringe in a vial until the mixture became opalescent, signifying that an inverted emulsion was formed. $40 \text{ }\mu\text{L}$ of this precursor emulsion was spin-coated on the PVA-coated slide (prepared as described above) at 100 rpm for 100 s. The slide was then dried under vacuum for 100 min at room temperature. The remaining steps were the same as in the PVA swelling method, except that the lipid swelling time was 90 min instead of 45 min.

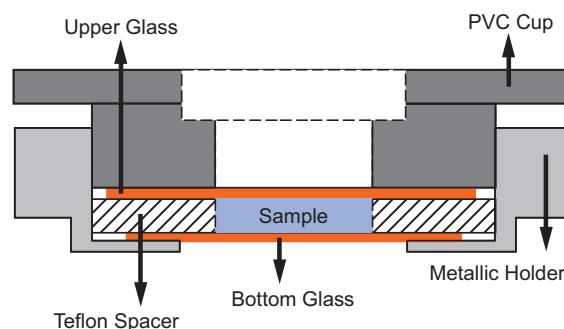
Interactions of cell-penetrating peptides with GUVs

GUVs were prepared by following the electroformation protocol, leading to a PBS buffer solution containing GUVs.

The ELP_{BC} were dissolved in a 280 mOsm kg^{-1} PBS solution in a concentration range of 16 to $25 \text{ }\mu\text{M}$. The solutions were adjusted such that around 0.5 % of the ELPs are fluorescently labeled with AF488. For a typical experiment three volume parts of the solution containing the ELPs were mixed with one volume of the previous prepared vesicle solution. Parallel samples were usually prepared and incubated at $25 \text{ }^\circ\text{C}$ and at $37 \text{ }^\circ\text{C}$ or $40 \text{ }^\circ\text{C}$. Samples were either incubated for 16 hours using Eppendorf tubes

at 37 °C and then observed at room temperature or continuously for 1.5–2 hours under the microscope. For the experiments at 40 °C under the microscope, a home made heating cell was used, as shown in Figure 2.3.

Figure 2.3: Home-made heating cell for observations under the microscope during heating.



2.3 Optical microscopy

2.3.1 Principle

The major technique used for this work was optical microscopy. Optical microscopy is easy to set-up and cheap compared to other techniques. The observation of giant unilamellar vesicles under the light microscope is easily possible due to their large size, above 1 μm . The limit of resolution of light microscopy, i.e. the ability to distinguish two separated objects from each other, can be estimated by Abbe's diffraction limit d :

$$d = \frac{\lambda}{2 \text{NA}} \quad \text{with} \quad \text{NA} = n \sin\theta \quad (2.1)$$

where n is the refractive index of the medium between object and objective, θ is half the angle of the light cone accepted by the objective and NA the numerical aperture. For our objectives NA is in the range of 0.45–1.25, where the high numerical apertures are only achieved by usage of immersion oil between sample and objective. The resolution limit is also set by the wavelength of visible light, which is in the range of 400–700 nm. Under the best conditions with violet light of a wavelength of 400 nm and a numerical aperture of 1.25, we are able to reach a resolution limit of 200 nm.

The observation of GUVs is not a trivial task, as these objects are transparent and have a poor contrast. Several contrast enhancing methods are available, which can be used to distinguish a vesicle from the background.

In general, when light passes through a colored or semitransparent sample, the sample can reduce the amplitude or intensity of the light. Samples causing this effect are called amplitude specimens. If transparent specimens are observed, which do not absorb light, a phase change of the light can be seen. These samples are called phase specimens. (Figure 2.4). Cells or unilamellar vesicles are typically phase specimens. The phase shift is approximately a quarter of a wavelength and too small to be observed by standard microscopy techniques. Contrast enhancing methods further increase this phase shift, leading to interference and ultimately better contrast.

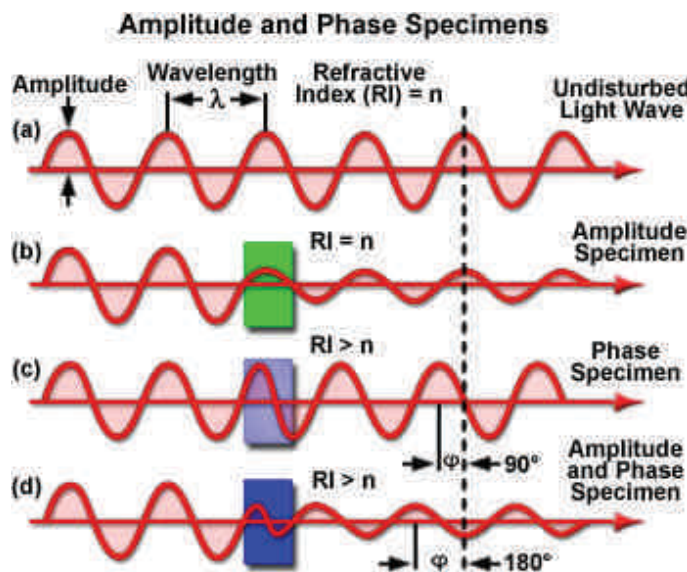


Figure 2.4: Differentiation of amplitude and phase specimens. (a) Undisturbed light wave emitted from a light source with a defined amplitude and wavelength. (b) Amplitude specimen cause a decrease in the amplitude after passing the sample. (c) Phase specimen do not decrease the intensity, but cause a phase shift ϕ . (d) In reality, the majority of samples cause a combination of both effects. Source: <http://www.microscopyu.com/>

Many techniques are available which modify the light path to generate an improved contrast image from a sample; two methods were used in this work to achieve a better contrast: the phase contrast and the differential interference contrast (DIC) technique.

2.3.2 Contrast enhancing methods

Two common contrast enhancing methods used for observation of transparent samples in biology and biophysics are the phase contrast microscopy and the differential interference contrast microscopy (DIC). Figure 2.5 shows GUVs imaged by both techniques.

Phase contrast microscopy transforms refractive index differences in the sample in contrast differences. Besides the standard microscopy elements, such as Köhler Illumination, condenser and an objective, two additional elements are needed for

phase contrast microscopy. An annular phase ring for the condenser and a special phase contrast objective with a phase plate are needed. Figure 2.6 shows the setup of the optical path for phase contrast microscopy. Through this setup, direct light is attenuated and phase-shifted by another quarter of a wavelength, thus leading to destructive interference. A total phase shift of up to 180° is achieved and causes an image with increased contrast [101].

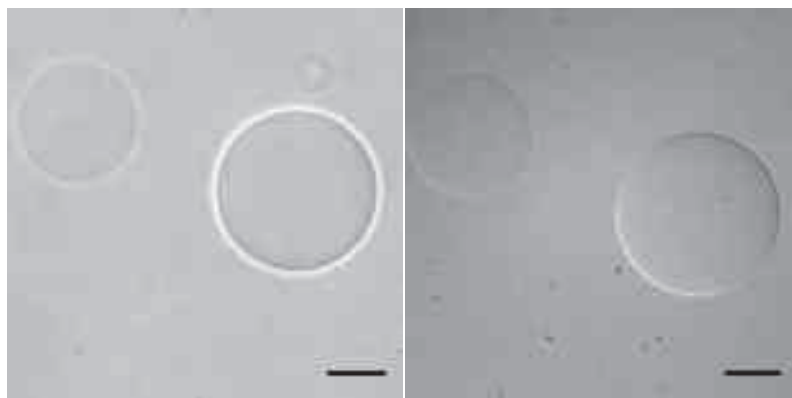


Figure 2.5: Images obtained by phase contrast microscopy (left) and DIC microscopy (right). DOPC-GUVs were obtained by electroformation in sucrose. Both images were recorded from the same GUVs after dispersion in glucose solution. Halo effect for phase contrast and 3D effect for DIC can be observed, as discussed below. Scale bars: 25 μm .

When giant unilamellar vesicles are observed, they are typically grown in sucrose and then immersed in a glucose solution. Due to the differences in the refractive index of these sugar solutions, the contrast is increased by the phase contrast technique; vesicles appear dark on a bright background (see Figure 2.5). This feature allows the observation of pore opening events. A suddenly decreasing contrast is a sign of the exchange from interior and exterior buffer solutions. In addition to enhancing the optical contrast, dilution helps to disperse and create isolated vesicles from the normally tube-connected GUVs. Moreover, differences in densities cause settling of the sucrose filled vesicles to the bottom of the observation chamber and observation of them under an inverted microscope is facilitated [53] (compare Table 2.5).

A characteristic feature of the phase contrast technique is the bright halo around the GUV. It enables to determine precisely the membrane position, by analyzing the very well defined contrast profile across the halo [102]. However, a disadvantage is that halos from out of plane objects are also visible. If several vesicles are on top of each other, halos of several objects can overlay and reduce the quality of the obtained image. This can be minimized by using a highly diluted sample. Phase contrast microscopy is used for very fine structures in very thin, non-stained specimens ($< 5 \mu\text{m}$). Images from thicker specimens can suffer from out-of-focus blur.

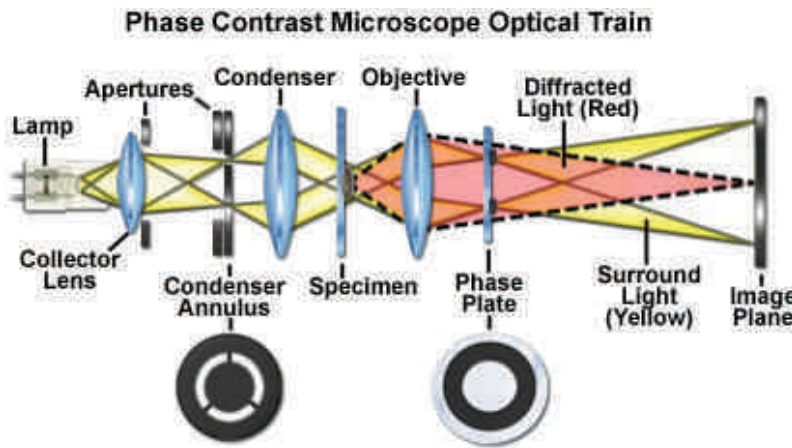


Figure 2.6: Concept of the phase contrast technique. Typical phase contrast objectives include the phase plate in the objective. Source: <http://www.microscopyu.com/>

Sugar	n_D at 20 °C	c (mol L ⁻¹)	ρ (g cm ⁻³)
Sucrose	1.3388	0.118	1.0139
Glucose	1.3358	0.112	1.0058

Table 2.5: Physical properties of sugar solutions at 20 °C used to enhance contrast and facilitate observation under an inverted microscope [103].

Differential interference contrast microscopy transforms optical path length gradients into contrast differences; the steeper the gradient in path length is, the better the contrast. Therefore, differences in the refractive indices between the bulk and the membrane are of greater importance than differences of the refractive indices of inside and outside solution. Images show a pseudo three-dimensional relief shading, which is characteristic of the DIC technique distinctively from phase contrast. Figure 2.5 shows a DIC image of a GUV.

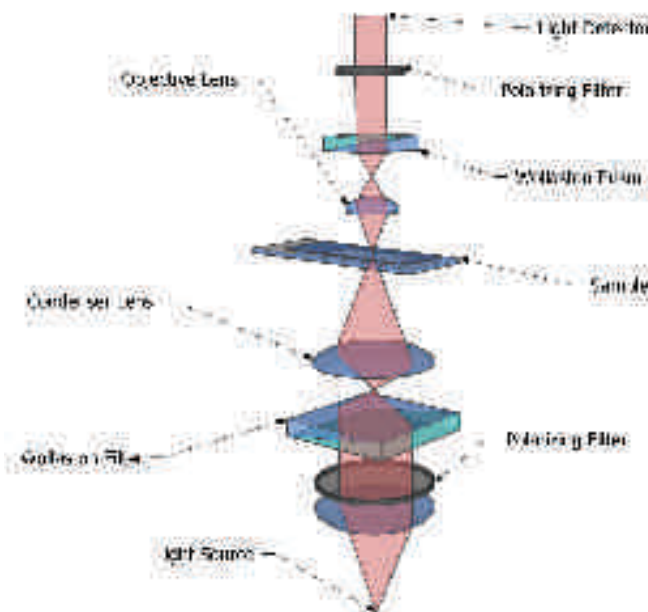


Figure 2.7: Schematic illustration of the differential interference contrast technique. The key elements are two polarizers and two Nomarski or Wollaston prisms, which split the polarised light into two rays and then recombine them. Optical path differences lead to interference and enhance the contrast. Image created by Richard Wheeler under GNU Free Documentation License.

For the DIC technique, two Nomarski (Wollaston) prisms, a polarizer and an analyzer (second polarizer) are necessary. The first polarizer and Nomarski prism lead to two linear light beams, which are retarded by a quarter wavelength plate. When they illuminate the sample, optical gradients in the object introduce a difference in the optical path. This results in a phase difference after the two beams interfere and are recombined by the second Nomarski prism, which leads to improved contrast. The contrast of the DIC image can typically be adjusted by the polarizer able to rotate relative to a quarter wave plate. Figure 2.7 shows the necessary setup of the differential interference contrast technique. DIC microscopy is suited for thick, non-stained specimens ($> 5 \mu\text{m}$) and shows improved axial resolution, compared to normal brightfield techniques [101].

Basically every existing objective can be used for DIC, provided that the insertion of the prisms and polarizers is possible, contrary to phase contrast microscopy, where only a phase contrast dedicated objective can be used.

2.3.3 Reflection interference contrast microscopy

Reflection interference contrast microscopy (RICM) is a method which can be used to measure the proximity of the object to the glass surface. Since it was first applied to study adhesion of cells to glass [104], it has also been applied to Giant Unilamellar Vesicles by Rädler and Sackmann [105]. This now widely used technique allows to measure distances with nano-meter precision in vertical direction [53]. The basic principle of the RICM technique can be seen in Figure 2.8. Monochromatic light of 546 nm (I_0) is partly reflected at the glass/medium interface; the transmitted light (I_1) is again reflected at the surface of the membrane (I_2). Both reflected rays interfere and lead to intensity I , as calculated by the following formula:

$$I = I_1 + I_2 + 2\sqrt{I_1 I_2} \cos[2kh(x, y) + \phi] \quad (2.2)$$

where the wave number $k = 2\pi n_1 \lambda^{-1}$, ϕ is the phase shift (typically π), $h(x, y)$ is the distance from the surface and $I_1 = r_{01}^2 I_0$ and $I_2 = (1 - r_{01}^2) r_{12}^2 I_0$, with r_{ij} the Fresnel reflection coefficient: $r_{ij} = (n_i - n_j) / (n_i + n_j)$ ($i, j = 0, 1, 2$). For a lipid vesicle, the intensities I_1 and I_2 depend on the refractive indices of glass ($n_0 = 1.525$), of the aqueous buffer solution ($n_1 = 1.333$) and of the lipid membrane ($n_2 = 1.486$). The immersion oil has the same refractive index as glass to avoid reflection at the glass/oil interface. Thus, for homogeneous samples, intensity (gray level) variations correspond to variations in the distance from the object to the substrate [106].

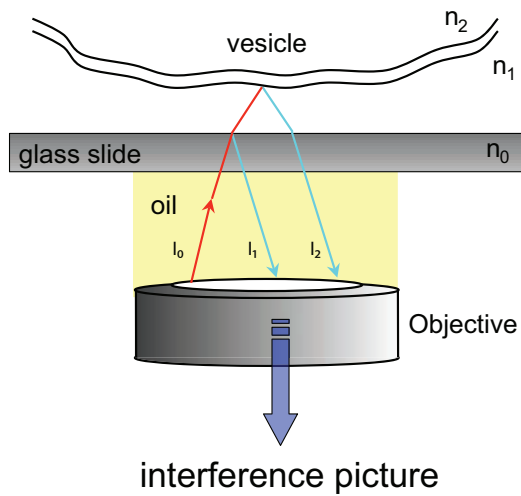


Figure 2.8: Schematic illustration of the RICM technique. Light with a wavelength of 546 nm is used to illuminate the sample. An interference picture is obtained from the light reflected at the different interfaces.

RICM imaging requires a polarizer, an analyzer and an oil immersion objective with a built-in quarter wave plate. This so-called antireflect method is used to reduce the stray light contribution, thus improving the resulting image. The antireflect objective with the quarter-wave plate is optimized for monochromatic light of a wavelength of 546 nm. The incident monochromatic light is linearly polarized by the polarizer and reflected at the sample surface. The reflected ray from the sample again passes through the quarter-wave plate and is linearly polarized with a $\pi/2$ orientation shift. It can cross the analyzer unperturbed, whereas the reflected stray light that did not come out of the objective is blocked by the crossed analyzer, oriented at 90° with respect to the polarizer.

Additionally to the determination of the distance from the substrate, the RICM technique can be used to distinguish between tense and floppy vesicles and is able to reveal GUVs adhered to the substrate. Figure 2.9 shows examples of a stretched vesicle, a floppy vesicle and an adhered GUV. In this work RICM was used for the investigation of GUV/cell penetrating peptide interactions.

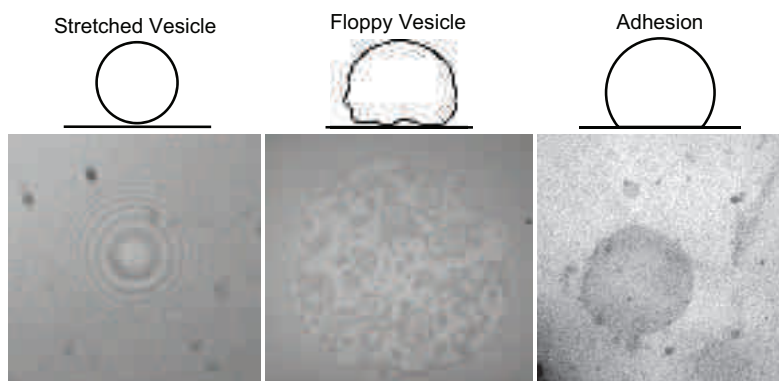


Figure 2.9: Top row: Illustration of different vesicle "states" on and above a substrate. Vesicles can be either stretched or floppy. If there is some attractive force between substrate and vesicle, the GUVs can adhere. Bottom row: Corresponding RICM images.

2.3.4 Experimental setup

Vesicle contours were imaged on an inverted TE 2000 or TE 200 microscope (Nikon, Japan) equipped with a 40x Ph2/NA 0.60 Plan Fluor objective for phase contrast microscopy or with a 60x WI/1.2 NA Plan Apo DIC objective for differential interference contrast microscopy. The reflection interference contrast microscopy technique (RICM) was used with a 100x NA 1.3 Plan Apo oil immersion objective (Leica, Germany) for locating tense or adhered vesicles. Images were recorded with a digital camera with a pixel depth of sixteen bits (Hamamatsu EM-CCD, Japan) or a pixel depth of eight bits (NDIAG 1800, Diagnostic Instruments, Sterling Heights, MI) with a home-written software. Saved images were opened and processed with ImageJ.

2.4 Confocal microscopy

Besides phase contrast microscopy, differential interference contrast microscopy and reflective interference contrast microscopy, confocal microscopy was used in this work. To obtain confocal images fluorophores are added to the sample, which allow recording of a confocal image. Fluorescent images can reveal defects not visible in light microscopy.

2.4.1 Basics of fluorescence

When a fluorophore containing sample is illuminated, a photon with a certain energy is absorbed, causing excitation of an electron in an orbital from a ground state (S_0) to an orbital with a higher energy (S_1). There are several ways to return to the ground state of a molecule. One way is by Fluorescence; by emission of a photon the molecule can return to its ground state. Due to molecular vibrations, a loss of energy occurs. A smaller energy amount is emitted than absorbed, thus a shift to longer wavelengths and lower intensity of the emitted light occurs. This phenomenon is known as Stokes' shift (compare Figure 2.10).

Two important effects have to be kept in mind when working with fluorophores and fluorescence microscopy: self-quenching and photobleaching.

Self-quenching refers to the decrease of fluorescence intensity of a fluorophore. Energy loss through energy transfer is an alternative relaxation process to fluorescence, it results in a reduced overall fluorescence intensity. Rather than the emission of a photon, energy can be transferred to other molecules. Common chemical quenchers are for instance molecular oxygen or iodide ions. Besides the transfer to

other molecules, the acceptor molecules can be the originating species. This process is called self-quenching and is typically observed at high fluorophore concentrations.

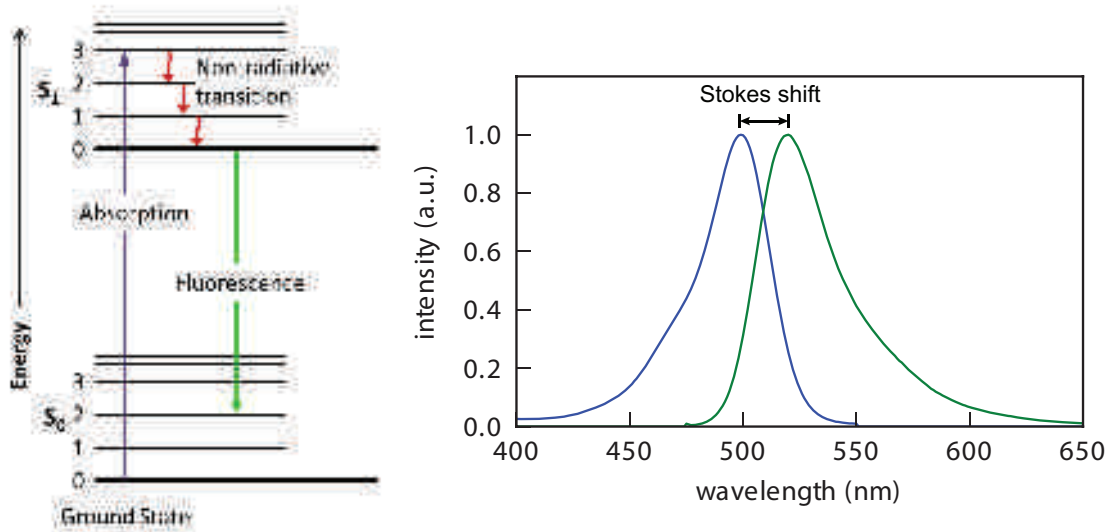


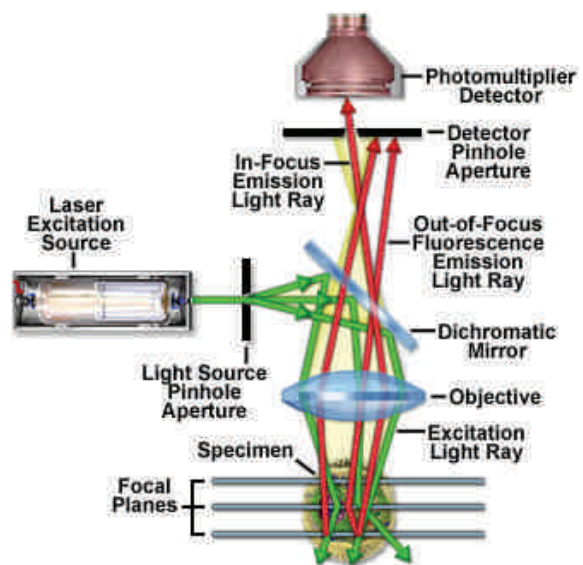
Figure 2.10: **Left:** Simplified Jablonski diagram for fluorescence. Emitted light has lower energy than the absorbed light, therefore a shift to a higher wavelength occurs, known as Stokes' shift. **Right:** Absorption and emission spectra of Alexa Fluor 488. Data obtained from Invitrogen.

Photobleaching can occur and complicates the observation of fluorescent molecules. Photobleaching is the degradation of fluorophores under illumination. Unnecessary exposure, such as long exposure times or higher intensities, should be avoided to minimize degradation of the fluorophores. This disadvantage can be used in techniques as Fluorescence Recovery After Photobleaching (FRAP) to observe lateral diffusion in a lipid bilayer and determine diffusion coefficients. Photobleaching can be minimized by the choice of a suitable technique and a more photostable fluorophore. Alexa Fluor 488, for instance, is a fluorophore showing higher photostability than its fluorescein counterpart.

2.4.2 Confocal laser scanning microscopy

Confocal laser scanning microscopy (CLSM) or confocal microscopy is an improved microscopy technique based on fluorescence. In standard fluorescence microscopy, the sample is illuminated with light filtered with an excitation filter and then reflected with a dichroic mirror towards the sample. The emitted fluorescence is radiated in all directions and partly passes through the microscope objective. It passes again the dichroic mirror, it is filtered by an emission filter and the signal is recorded by a camera. The disadvantage of this method is the complete illumination of the sample, leading to a big amount of out-of-focus light.

Figure 2.11: Schematic representation of a confocal microscopy setup and light pathways. A laser emits light of a defined wavelength through a pinhole and is reflected by a dichromatic mirror through the objective on the specimen. Emitted light in-focus is reaching the detector, whereas out-of-focus light is eliminated.



Confocal microscopy uses point illumination and a spatial pinhole to eliminate (or minimize) out-of-focus light. The excitation of the sample is achieved by a laser with a defined wavelength. Additionally the axial and lateral resolution are improved, due to point-like excitation and detection. The emitted light is typically detected pixel by pixel using a photomultiplier. The sample is scanned line by line and a two-dimensional image is reconstructed. Confocal microscopy allows also to construct a three-dimensional image of the sample from a stack of individual XY slices. Due to this recording technique image acquisition is rather long, requiring nearly immobile samples.

2.4.3 Experimental setup

Fluorescent imaging was performed using confocal laser scanning microscopy (CLSM) with a Nikon C1 scanhead on an inverted TE 2000 microscope (Nikon, Japan) equipped with a 60x WI/1.2 NA Plan Apo DIC objective. Images were captured using EZ-C1 software (Nikon, version 3.50).

Fluorophores were excited using a diode laser at 408 nm, an argon-ion laser at 488 nm or a helium-neon laser at 543 nm from Melles-Griot. Table 2.6 lists all fluorophores used in this work. Depending on the fluorophore a suitable excitation laser was chosen.

Fluorophor	Excitation (nm)	Emission (nm)	MW (g mol ⁻¹)	ϵ (L mol ⁻¹ cm ⁻¹)
AF350	346	442	410	19,000
Fluoresceine	494	521	332	93,000
DTAF	495	516	532	83,000
AF488	495	519	643	71,000
BODIPY FL	504	513	389	68,000
rhod-PE	557	571	479	106,000

Table 2.6: Used fluorophores and their characteristics, data from Invitrogen.

Quantitative analysis of fluorescent intensities in the confocal images was performed using ImageJ, with appropriate rescaling of the acquired signals to the same standard levels. In all measurements the background noise measured from blank samples containing no fluorophores was subtracted.

2.5 Quartz crystal microbalance

When an alternating current is applied to a quartz crystal, it causes the crystal to oscillate at a defined resonant frequency. This effect is known as the piezoelectric effect. When molecules are adsorbed on the crystal, thus a mass change of the quartz occurs, a frequency shift is observed. This behavior is well known and applied in the quartz crystal microbalance (QCM) technique. By monitoring the dissipation (ΔD) the viscoelastic properties of the adhered layers can be obtained and provide further information about the adsorbed molecules and the rigidity of the film [107]. The quartz crystal microbalance with dissipation (QCM-D) allows the measurement for mass densities below 10^{-2} mg m⁻² with high sensitivity. A standard QCM-D sensor is a quartz crystal of 14 mm diameter, coated with gold as electrode material.

The Sauerbrey equation is used to relate the frequency shift to the mass change on the quartz crystal [108]:

$$\Delta f = -\frac{2f_0^2}{A\sqrt{\rho_q\mu_q}}\Delta m = -C \Delta m \quad (2.3)$$

The mass sensitivity constant C , a fundamental property of the QCM crystal, is defined by the resonant frequency f_0 , the electrode area A , the quartz density ρ_q and shear modulus μ_q . For a standard QCM sensor this value is $C = 17.7 \text{ ng cm}^{-2} \text{ Hz}^{-1}$ at a resonant frequency of 5 MHz. The frequency shift Δf is typically the normalized frequency shift ($\Delta f/n$), where n is the overtone number $n = 1,3,5,7,9,11,13$. Monitoring at several overtones is useful to increase sensitivity and signal-to-noise ratio compared to the fundamental frequency.

Common applications for this technique are for example the investigation of interactions between a surface and biomolecules, such as proteins or lipids. In this work QCM-D was used to investigate ELP interactions with supported bilayers.

Experimental setup. All experiments were performed using quartz crystal microbalance with dissipation monitoring (QCM-D) Q-Sense E4 system equipped with three axial flow chambers (Q-Sense, Sweden). Quartz crystals with a thin SiO_2 layer were used as the sensors (Q-sense, Göteborg, Sweden). Measurements were performed at the resonance frequency of 5 MHz and data for Δf and D were recorded simultaneously at several harmonics (15, 25, and 35 MHz). Adsorbed masses were calculated with the Sauerbrey equation, which is valid for thin, rigid films coupled without friction to the sensor surface and is valid for lipid bilayers on surfaces [109]. If not stated otherwise, changes in dissipation and normalized frequency ($\Delta f_n = \Delta f/n$) with n being the overtone number are presented in this work.

Solutions were injected at a speed of $300 \mu\text{L min}^{-1}$ at a temperature of 37°C . Supported bilayers were prepared by injection of SUVs into a QCM cell. The injected SUVs adhere on a SiO_2 surface and form a stable supported bilayer within seconds [109]. SUVs were prepared by sonication of a PBS buffer solution containing DOPC-MLVs at a concentration of 1 mg mL^{-1} , as described in section 2.2.1. After stabilization of the measured frequency shift, PBS buffer was injected into the QCM chamber to rinse the supported bilayer and remove excess vesicles.

After formation of a stable supported bilayer, two injections of $600 \mu\text{L}$ of ELP_{BC} solution at a concentration of 1 mg mL^{-1} in PBS were done at 37°C . Between each injection, ELP_{BC} were allowed to interact for 90 min with the supported bilayer. The

three flow chambers of the QCM cell allow the parallel investigation of TAT, Arg₈ and non-functionalized ELP_{BC}. After the last ELP_{BC} injection the cell was rinsed with PBS buffer.

2.6 Isothermal titration calorimetry

Isothermal titration calorimetry (ITC) is a technique, which records heat changes caused by interactions between molecules, during titration of a sample with a reactant containing solution. It is often used to study binding affinities of small molecules (ligands) to larger bio-molecules, such as proteins, DNA or lipids. This quantitative technique allows for determination of binding affinities, enthalpy changes and binding stoichiometry. Figure 2.12 shows a schematic illustration of an isothermal titration calorimeter. A reference and a sample cell are surrounded by an adiabatic jacket and maintained at the sample temperature.

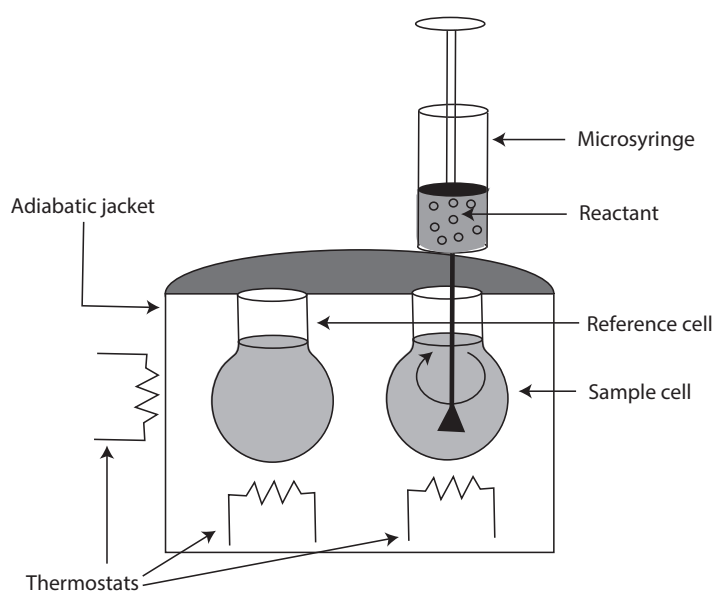


Figure 2.12: Schematic illustration of an isothermal titration calorimeter. Two identical cells are surrounded by an adiabatic jacket and kept at the same temperature with a constant power input. Upon addition of titrant, reaction between molecules occurs, causing a temperature change of the sample cell. Power consumption has to be regulated to maintain isothermal conditions and is recorded vs. time, adapted from Billot [110].

Upon addition of titrant in a stirred sample cell, interaction between two or more molecules in the sample occurs and exothermic or endothermic reactions cause a change of the sample cell temperature. The power input has to be regulated to maintain isothermal conditions. The heat flow is recorded with time. The left graph in Figure 2.13 shows an example of a heat flow curve. The peaks can be integrated and

a graph as in Figure 2.13 on the right side is obtained. The data can then be fitted to a model. In a standard experiment, the inflection point gives the stoichiometry of interacting molecules, the slope the binding constant K_a and the enthalpy change ΔH can be obtained from this graph.

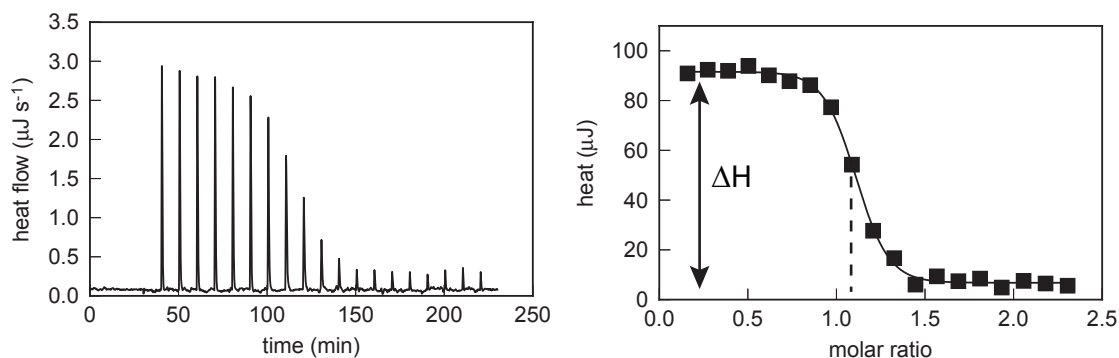


Figure 2.13: Exemplary curves obtained by Isothermal Titration Calorimetry for formation of double stranded DNA from single stranded DNA (12 basepairs). Left image: Raw curve as recorded by ITC. Right image: Integrated heat obtained from the raw data. The data can be fitted by some model and the binding constant, total enthalpy and stoichiometry can be determined.

Experimental setup. In this work ITC measurements were performed for measuring the heat of interaction between LUVs and functionalized ELP_{BC} with TA instruments Nano ITC 2G microcalorimeter. First, the dissociation energy of ELPs was determined. One aliquot of 2 μL followed by 19 aliquots of 5 μL of ELP solution (50 μM) in a 100 μL syringe were injected in 500 s intervals into the PBS filled working cell (1.5 mL) at 25 and 37 °C. For measuring the interaction energy of the ELPs with liposomes, 100 nm DOPC liposomes (100 μL of a 10 mg mL⁻¹ solution) were injected into ELP solution with the same injection steps at 25 and 37 °C.

The corresponding reference blank experiments were also performed, namely titration of PBS buffer into buffer and liposomes into PBS buffer. All samples were degassed for 10 min shortly before starting the measurements. The sample cell was constantly stirred at a rate of 250 rpm. Data analysis was performed with a software developed in-house.

Chapter 3

Elastin-like polypeptides

In this chapter, a short introduction into intracellular transport is first given. Then, cell penetrating peptides (CPPs) and CPP functionalized elastin-like polypeptides are described.

In this study, performed in close collaboration with Sarah MacEwan from the group of Ashutosh Chilkoti at Duke University in North Carolina, we investigated the interaction of elastin-like polypeptides with neutral lipid membranes. We evaluated the importance of the number of arginine units in these peptides and the influence of micellar assembly, which can, in these systems, be triggered by temperature.

3.1 Transport through cell membranes

We discussed in the introducing chapter, how gases and small hydrophobic molecules can be transported by diffusion across the bilayer. Hydrophilic or larger-sized molecules, such as ions, sugars or amino acids require other means of cellular uptake, such as integral membrane proteins. For even larger molecules, the cell deploys a large spectrum of internalization processes. These are based on endocytotic pathways, wherein a small portion of the membrane invaginates, pinches off to form an intracellular vesicle that can transport the wrapped substances into the cell.

Phagocytosis, also named cellular eating, is an actin-mediated process, where cells envelop bacteria and other large particles, via phagosomes, vesicles larger than 250 nm in diameter. This is relatively rare amongst different cell types [14].

A more common way in eucaryotic cells is the formation of small endocytic vesicles, smaller than 150 nm in diameter by receptor-mediated endocytosis. Here a specific

receptor on the cell surface binds tightly to the extracellular macromolecule, the ligand. Clathrin-mediated endocytosis utilizes specialized regions, called clathrin-coated pits, where extracellular substance can bind and form clathrin-coated vesicles that transport cargo inside the cell. Caveolae are another important small invaginations, a special type of lipid raft is formed from a bilayer containing the protein caveolin, cholesterol and glycolipids. Both pathways are specific uptake pathways [49].

Macropinocytosis is a non-specific uptake pathway where vesicle invaginations of 0.5–5 μm in diameter are formed. This process is an actin-mediated process requiring ATP consumption.

Figure 3.1 shows a schematic illustration of these three classes of endocytosis: phagocytosis, macropinocytosis (non-specific endocytosis) and receptor-mediated endocytosis. The terms endocytosis and pinocytosis are occasionally considered to be synonymous [111].

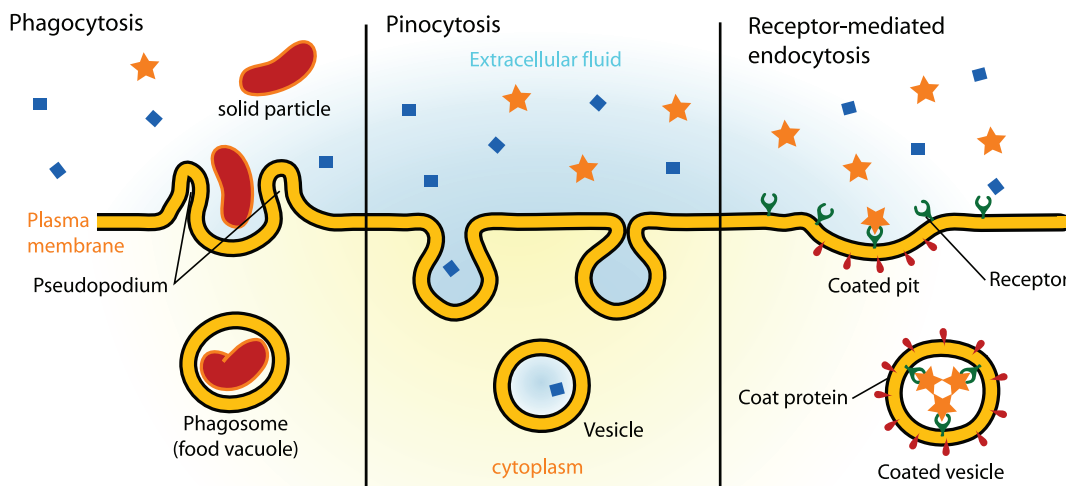


Figure 3.1: Schematic illustration of the three most important types of endocytosis. Phagocytosis, non-specific pinocytosis and receptor-mediated endocytosis. Image created by Mariana Ruiz Villarrea and published in the Wikimedia Commons database.

3.2 Cell penetrating peptides

Cell penetrating peptides (CPPs) are short peptides which facilitate the cellular uptake of a cargo in diverse cell types, making them desirable for delivery of anticancer drugs to solid tumors [112].

One of the best studied CPPs is the transactivator of transcription (TAT) protein of the Human Immunodeficiency Virus, that was discovered in 1988 independently by two different groups [113, 114]. This TAT protein was found to efficiently enter cells.

The TAT peptides contain six arginine and two lysine residues. From this the highly cationic, arginine rich polypeptides emerged.

Several mechanisms of membrane translocation were suggested as possible uptake pathways for CPPs.

Widely accepted pathways are:

- Energy-independent cell penetration or direct penetration
- Clathrin-mediated endocytosis
- Caveolin-mediated endocytosis
- Macropinocytosis

Early studies indicated a direct translocation mechanism, independent of endocytosis. Rapid translocation was observed even at 4 °C and/or by adding inhibitors to suppress endocytotic pathways. Most of these early studies were conducted using microscopy. Richard et al. [115] showed that fixation of cells can increase the apparent intracellular distribution of the TAT peptide. Reevaluation of cell penetration on living cells suggest, nonetheless, direct translocation [116]. Different mechanisms have been proposed enabling direct penetration of CPPs: the inverted micelle formation, pore formation and the carpet-like model to only name a few [117].

While there are discussions about the importance of the direct penetration, the importance of translocation due to receptor-mediated endocytosis or macropinocytosis is widely accepted. Recently, it was observed that all three penetration pathways, clathrin- and caveolin-mediated endocytosis and macropinocytosis can be used by one given CPP, but may also use nonendocytic entry routes, depending on the concentration of CPPs [118].

CPPs can be divided into three classes based on the peptide sequence and binding property to lipids: primary amphiphatic, secondary amphiphatic and nonamphiphatic CPPs are distinguished. Primary amphiphatic CPPs, such as transportan, typically contain more than 20 amino acid residues. Hydrophobic and cationic domains are sequentially part of the primary structure. Secondary amphiphatic CPPs, such as penetratin, are shorter and show a secondary structure upon interaction with lipids. Non-amphiphatic peptides are the shortest CPPs and are almost exclusively composed of cationic amino acids [119]. Arginine-rich polypeptides and TAT belong to this last group.

For primary amphiphatic CPPs, additional to endocytosis, direct membrane transduction is proposed, via the above mentioned mechanisms. Secondary amphiphatic

CPPs, can form an α -helix or a β -sheet structure upon interaction with lipids; they typically do bind to model membranes with a certain fraction of anionic lipids. Non-amphiphatic peptides bind strongly to lipid membranes with a high amount of anionic lipids [117].

3.3 Elastin-like polypeptides

A disadvantage of CPPs, if used for cancer treatment is the non-specific interaction with cancer and healthy cells. Unfortunately, the complete lack of cellular specificity causes that CPPs can be taken up in a number of organs within the body [120].

Macewan and Chilkoti [112] developed a new strategy to control the active state of a CPP by coupling arginine residues to elastin-like polypeptides. Elastin-like polypeptides (ELPs) are artificial polypeptides, composed from VPGXG pentapeptide units, with the guest residue X being valine (V), glycine (G) or alanine (A). Figure 3.2 shows the typical amino acids in ELPs, as well as one pentapeptide unit.

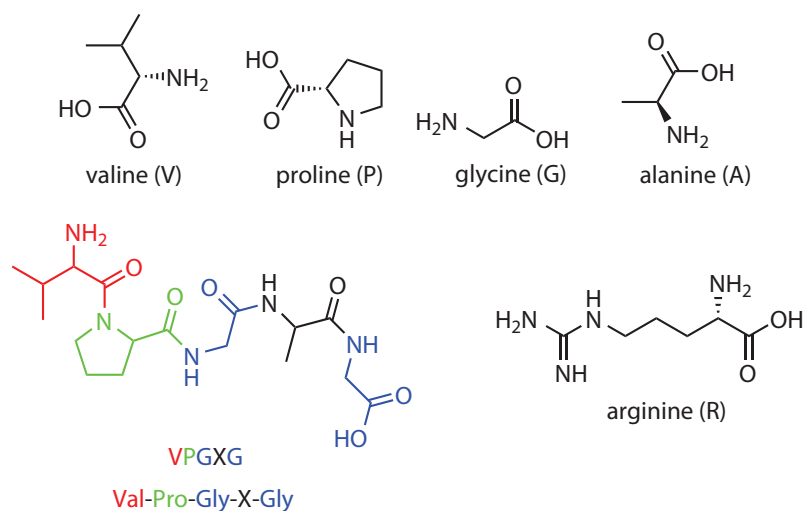


Figure 3.2: ELPs are composed of repetitive pentapeptide blocks. Here the amino acids which typically build up ELPs are shown.

ELPs display an inverse phase transition temperature; they are soluble in aqueous solution below their inverse transition temperature T_i and become insoluble above this temperature [121], see Figure 3.3.

By coupling two blocks of ELPs with different transition temperatures to each other, one obtains diblock copolymers ELP_{BC} which a “hydrophilic “ and a “hydrophobic” block, which are capable of temperature-triggered micelle assembly.

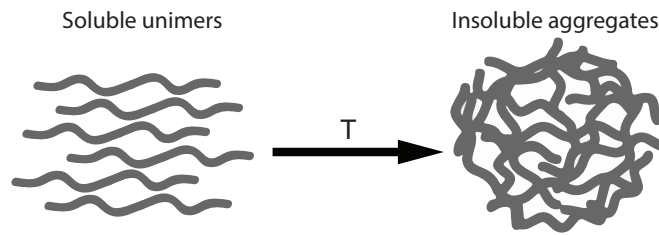


Figure 3.3: ELPs possess an inverse phase transition temperature; they are soluble unimers below their phase transition temperature and become insoluble aggregates above it.

This strategy builds upon the observation that arginine-rich CPPs display a strong cutoff effect in their cell penetration ability. Crucial for cell penetration is the number of arginine units in the moiety providing cell-penetrating properties. Above a critical threshold of six arginine units efficient cellular uptake of this class of molecules can be observed, whereas below this critical number no uptake occurs [122].

Macewan and Chilkoti [112] hypothesized that it is not the absolute number of Arg residues, but instead the local Arg density that is responsible for this threshold effect in cell uptake. A new class of cell penetrating peptides is obtained by coupling arginine residues to diblock copolymers of elastin-like polypeptides. Temperature-triggered micelle assembly of these diblock copolymer elastin-like polypeptides (ELP_{BC}) occurs if the critical micellar temperature (CMT) of these ELP_{BC} is exceeded.

This hypothesis then suggests that triggered micelle assembly of a diblock copolymer, with less than six arginine residues on its hydrophilic terminus, should provide a switchable CPP with on (micellar state) and off (unimer state) conditions (Figure 3.4).

Chilkoti's group tested this hypothesis by coupling Arg_5 residues to the ELP_{BC} and incubating with living cells. Upon incubation below the transition temperature, in the micellar state, no significant uptake was observed. In their micellar state, if these ELP_{BC} are functionalized with arginine rich moieties, a significant increase in cell uptake in living cells was demonstrated [112].

By inhibition of clathrin-mediated and caveolae-mediated pathways and non-specific macropinocytosis, they could show that macropinocytosis is the predominant mechanism of cellular uptake for arginine functionalized ELP_{BC} . As a secondary mechanism for cellular uptake of Arg_5 - ELP_{BC} caveolae-mediated endocytosis was determined.

In this thesis, we wanted to investigate the non-specific interaction of functionalized ELP_{BC} with lipid bilayers by utilizing giant unilamellar vesicles as model systems. In a first step, CPPs have to associate to the plasma membrane [123], independently

of the translocation pathway. By forming well-defined GUVs from zwitterionic lipids, we can ensure that receptor-mediated endocytotic processes and actin-mediated processes are excluded. Moreover, it allows the investigation of possible direct translocation.

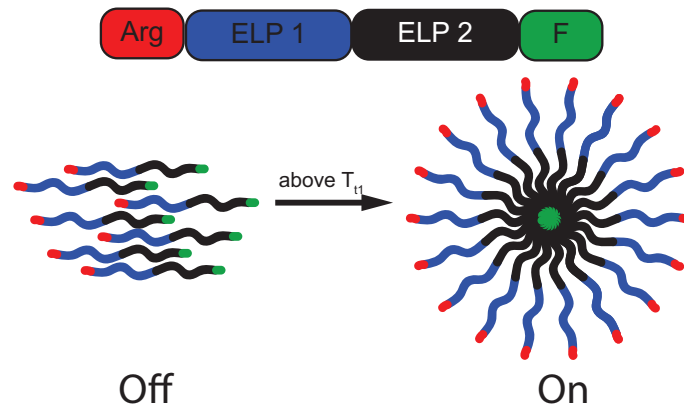


Figure 3.4: ELP block copolymers assemble into micelles above the transition temperature of the ELP1 block. Below T_{t1} ELP_{BC} are soluble unimers. ELP_{BC} are functionalized on the hydrophilic (ELP1) end with arginine rich CPPs. On the hydrophobic (ELP2) end a fluorophore is attached for confocal microscopy.

3.4 ELPs for studying interactions with GUVs

To investigate the importance of direct translocation of this new class of arginine-rich elastin-like polypeptides through a lipid bilayer, we used Giant Unilamellar Vesicles (GUVs) as a model system. Using DOPC-GUVs with no receptors or active cytoskeletons, other penetration pathways can be excluded. We investigated the importance of the number of arginine units for direct translocation and membrane-peptide interactions by using of Arg₅-, Arg₈- and TAT functionalized ELP_{BC} which are unimers at 25 °C and micelles above 34 °C. A non-functionalized control ELP_{BC} was used to ensure that observed effects were due to the functionality of the ELP_{BC}. The nomenclature and the synthesis of the ELP_{BC}, as well as the experimental setup for investigation of peptide-lipid interactions, are further described in the Materials & Methods chapter.

Table 3.1 lists all the used ELP_{BC} and their characteristic parameters, such as critical micellar temperature, molecular weight and hydrodynamic radius measured by DLS.

ELP construct	C-terminal functionality	MW (kDa)	CMT °C	R _h (nm) 25 °C	R _h (nm) 37 °C
ELP-BC (60/96)	none	61.8	33	6.8 ± 0.1	27.1 ± 0.9
Arg ₅ -ELP-BC (60/96)	Arg ₅	62.6	33	6.8 ± 0.2	28.6 ± 0.6
ELP-BC (60/60)	none	48.0	34	5.9 ± 0.8	24.1 ± 1.1
Arg ₈ -ELP-BC (60/60)	Arg ₈	49.3	31	7.5 ± 0.2	26.4 ± 0.3
TAT-ELP-BC (60/60)	TAT	49.6	32	6.0 ± 0.7	25.8 ± 1.4

Table 3.1: Characterization of used ELP_{BC}. ELP_{BC} at 20 μM in PBS. Data represents the average of 3 replicates ± standard error of measurement.

A typical graph obtained by DLS is plotted in Figure 3.5. DLS were recorded in the range between 25 °C and 50 °C and the hydrodynamic radius determined. Figure 3.5 shows an example of a recorded temperature dependant DLS. The temperature dependent self-assembly of ELP_{BC} at 25 μM in PBS buffer was monitored with dynamic light scattering and the critical micelle temperature determined.

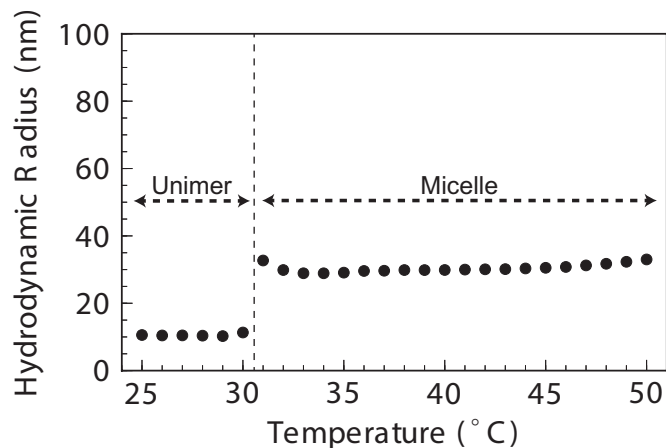


Figure 3.5: Hydrodynamic radius R_h was determined by DLS. Soluble unimers of Arg₈-ELP_{BC} existed with a R_h of approximately 10 nm up to 31 °C. At 31 °C self-assembly into micelles occurred. Micelles with a R_h of approximately 30 nm were formed. At temperatures above 50 °C micrometer size aggregates were formed.

All of the ELP_{BC} listed in Table 3.1 exist in a fluorescently labeled and non-labeled version. If not mentioned otherwise in the text, the conjugated fluorophor was Alexa Fluor 488 (AF488).

In a typical experiment, a 20 μM ELP_{BC} solution with a small amount of fluorescently labeled ELPS, typically between 0.5–1 %, was incubated with GUVs in vials in a heating bath or under the microscope in a heating cell, as further described in chapter 2.

3.5 Evaluation of ELP_{BC}-membrane interactions

To evaluate the interactions of functionalized and non-functionalized ELP_{BC}, GUVs of DOPC were incubated in a ELP solution containing AF488-labeled ELP_{BC}. In later experiments (see below) in some cases BODIPY was used as a fluorophore.

For quantitative analysis of fluorescent intensities in the confocal images, we defined the partition coefficient P , which is characteristic for the penetration potential of the ELPs. This coefficient was defined as the ratio of the average fluorescence intensity inside the vesicle I_{in} and the average fluorescence intensity of the bulk I_b :

$$P(\%) = \frac{I_{in}}{I_b} \times 100 \quad (3.1)$$

We obtained the partition coefficient by evaluating the radial profile of vesicles from recorded confocal images at the equatorial plane in ImageJ. Briefly, a circle bigger than the vesicle is drawn on the image in ImageJ and the radial profile, by drawing a line from the center of the vesicle to a distance larger than the vesicle diameter and averaging over 360°, is determined with the radial profile plugin for ImageJ. The points obtained from the plugin can be fitted to a sigmoidal curve.

Figure 3.6 shows an example of such a radial profile, the intensity is normalized by the bulk intensity and the radius by the vesicle radius. By doing this the partition coefficient can be directly determined from the radial profiles.

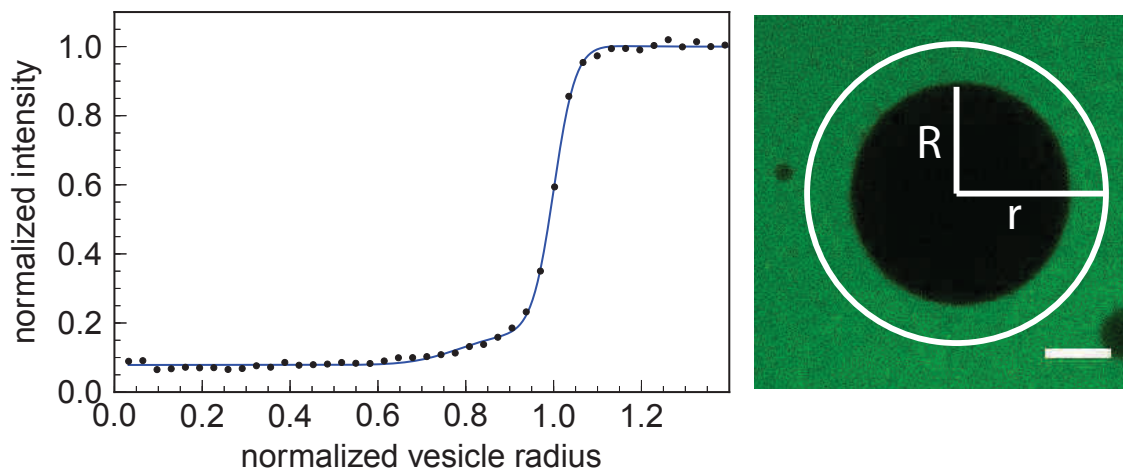


Figure 3.6: Example of a radial profile obtained from GUVs dispersed in ELP_{BC} containing PBS solution. Fluorescence intensity is normalized by the bulk intensity. Vesicle radius (R) is taken at the inflection point of the sigmoidal curve. Scale bar 20 μm .

To ensure that the measured fluorescence intensity of the AF488 labeled ELP_{BC} be-

has linearly with the concentration of the fluorophores and that the position within the observation chamber does not influence the measured intensities, a calibration curve was recorded with the confocal microscope at different heights from the glass slides (Figure 3.7).

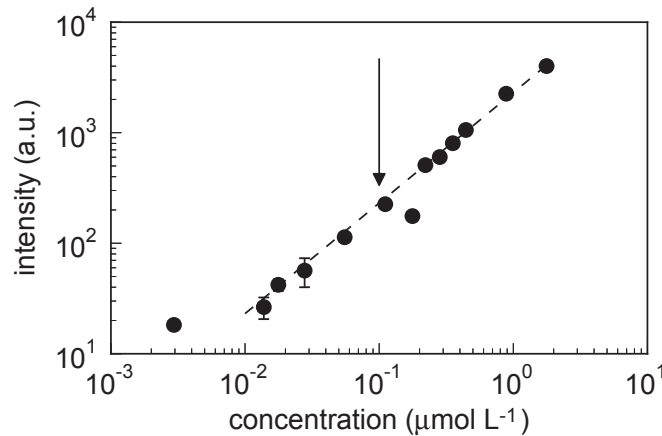


Figure 3.7: Fluorescence calibration curve for a solution of a control elastin-like polypeptide labeled with AF488 at room temperature. The arrow represents the typical working conditions. The values were measured at 20 μm, 50 μm, 80 μm and 130 μm from the glass surface. Points represent the mean value of the four different positions and errorbars the standard deviation.

In a first set of experiments, GUVs were mixed with the ELP_{BC} buffer solutions and incubated in vials in a heating bath set to 25 °C for ELP unimers or at 37 °C for ELP micelles.

In a second set of experiments, samples of a GUV containing buffer solution and the ELP containing PBS solution were preheated separately, GUVs dispersed in the preheated ELP_{BC} solution and incubated directly under the confocal microscope in a heating chamber at 40 °C ± 3 °C. Due to heat loss the temperature of the heating bath had to be set at higher temperatures, typically to 45 °C, to ensure appropriate temperatures in the chamber within the micellar range of the ELP_{BC}. The evolution of the partition coefficient was directly followed under the microscope. Per sample a minimum of 30 vesicles was evaluated. Out of focus light was minimized by imaging the GUV at the equator of the vesicle.

The results are grouped in two different classes. The first group describes the behavior of Arg₅ functionalized ELP_{BC}. This class is characteristic for ELPs with a total arginine number below the critical value of six. The second class contains experiments performed with ELPs with a high number of arginine units, such as Arg₈ and TAT.

Within each class the behavior of the respective ELPs is investigated in the unimer

state, below the transition temperature, and in micellar state above the transition temperature. Table 3.2 summarizes the obtained partition coefficients; the results are discussed more detailed in their corresponding groups below. In some (special) cases BODIPY was used as a fluorescent label, see paragraph 3.7.3.

ELP-Type	Fluorophore	25 °C		37 °C	
		Mean	SD	Mean	SD
Arg ₅	AlexaFluor	7.12	2.79	8.86	4.26
Arg ₈		9.00	2.16	16.22	8.59
TAT		8.18	1.33	20.53	13.33
No function		5.79	2.37	8.26	3.34
Arg ₈	BODIPY	6.93	1.52	19.42	9.89
No function				21.07	5.9

Table 3.2: Partition coefficient in % for different types of ELPs incubated with GUVs of DOPC at 25 °C and 37 °C.

3.6 Less than six arginine residues

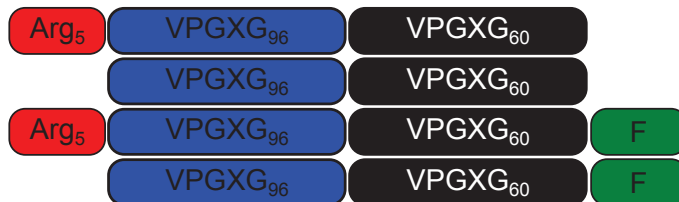


Figure 3.8: Peptide sequence of non-functionalized and Arg₅-functionalized ELP_{BC} with and without a fluorescent label.

As expected for GUVs incubated with non-functionalized and Arg₅ functionalized ELP_{BC} (Figure 3.8) at 25 °C, below the critical micellar temperature of the ELPs, in their unimer state, no significant permeability was observed after an incubation time of one hour.

In all experiments, independent from the used ELP_{BC}, an average partition coefficient of maximum 10 % was obtained. After one hour of incubation image recording of tens to hundreds of GUVs within the sample was started and usually finished after a maximum of two hours for the whole experiment.

By tracking of a single vesicle during an incubation time of 1 hour after mixing, it could be shown that the partition coefficient did not increase with incubation time. A value of 10 % is likely to be related to the mixing process during sample preparation and

occurred in all cases. Longer incubation times of up to 16 hours in a temperature controlled water bath did also not lead to a further increase of partition coefficients.

For incubation of GUVs with ELP_{BC} in their micellar state at 37 °C (incubation in vials) or 40 °C (incubation in the heating cell), similar values were obtained. No filled vesicles could be found within the sample even after an incubation time of 16 hours. All of the incubated GUVs seem to be stable. Stability is apparently not influenced by the presence of the ELP_{BC}.

Figure 3.9 shows the partition coefficient obtained for GUVs dispersed in the non-functionalized and functionalized (Arg₅, Arg₈ and TAT) ELP_{BC} PBS solutions at 25 °C and 40 °C. Each symbol stands for one single GUV per sample. It can be seen that all of the values for the partition coefficient for these experiments are around 10 %. Images for the first 30 minutes are not shown, but are in the same range.

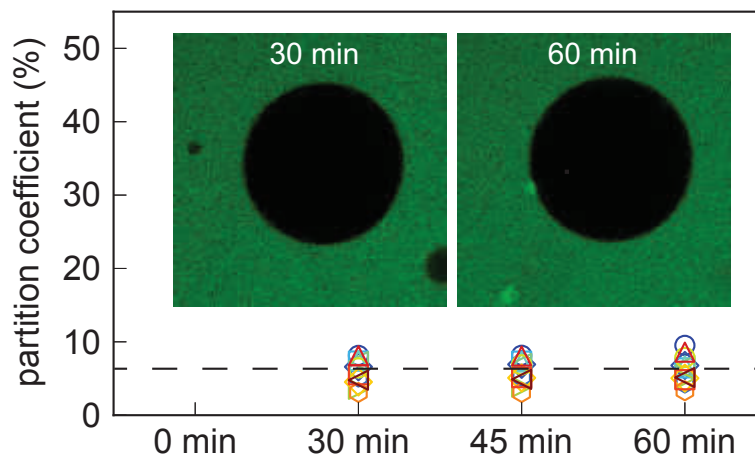


Figure 3.9: No change of partition coefficient within one hour. After 30 min of stabilization, recording was started. Here, the confocal pictures show one DOPC vesicle surrounded by a PBS buffer solution containing TAT functionalized ELPs at 40 °C. No change in partition coefficient can be observed. Each symbol stands for one single GUV per sample. Different symbols signify different functionalities and incubation temperatures. Scale bars 20 μ m.

The values of the partition coefficient obtained for several GUVs in one sample follow a distribution. Figure 3.10 shows an example of an obtained histogram for a sample incubated at 25 °C and 37 °C.

Table 3.2 lists the partition coefficients obtained for these experiments. Values obtained for unimers and micelles are comparable, as well as values obtained for GUVs incubated in vials at 37 °C and in the heating chamber at 40 °C, showing that the membrane is not permeable to ELPs with less than six arginine residues for any of the explored conditions.

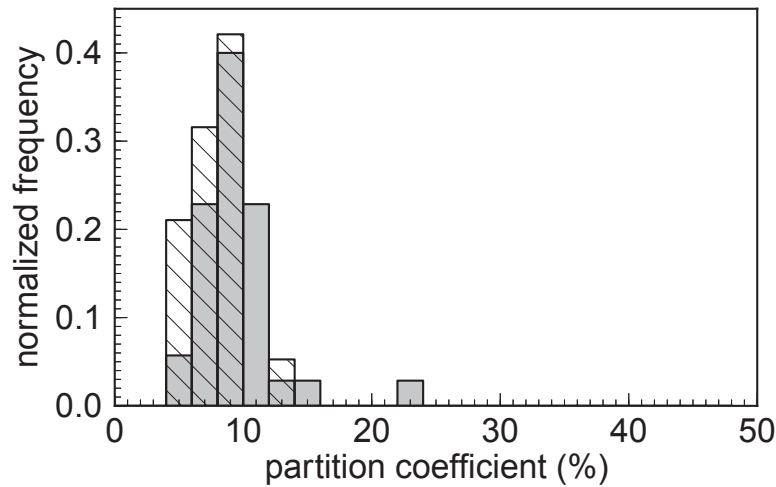


Figure 3.10: Example of a histogram obtained from evaluation of confocal images. DOPC-GUVs were dispersed and incubated for 1 hour in Arg₅-ELP_{BC} solution at 25 °C (hatched bars) and 40 °C (gray bars).

3.7 Six or more arginine residues



Figure 3.11: Peptide sequence of Arg₈ and TAT-functionalized ELP_{BC} with and without a fluorescent label. Non-functionalized ELP_{BC} was used to compare interactions of ELP_{BC} without a CPP residue.

For Arg₈ and TAT functionalized ELP_{BC} (Figure 3.11) again similar values for the partition coefficient were found below the CMT at 25 °C. For experiments performed in the micellar state of the ELP_{BC}, 37 °C for incubation in vials and 40 °C for incubation in the heating chamber under the microscope, a small increase of the partition coefficient up to 20 % could be observed. The values found were somewhat higher than the ones for the control and Arg₅ functionalized ELP. In the same time an increased dispersion of the values could be observed for all of them.

However, like in section 3.6, no time evolution could be observed. The higher initial partition is likely to be determined during mixing. Longer incubation times of up to

16 hours did not lead to an increased partition coefficient. Fully equilibrated GUVs could never be observed. All of the observed GUVs were stable in the ELP containing solution upon incubation.

The partition coefficients obtained for experiments with ELP_{BC} with six or more arginine residues are also summarized in Table 3.2. For these cases, the membrane also did not display any permeability.

3.7.1 Interactions between ELP micelles and the membrane

GUVs incubated at higher temperatures with the micellar forms of ELP_{BC} containing six or more arginine residues, display attractive interactions with the lipid bilayers, as evidenced by a fluorescent corona around the GUV membrane.

Figure 3.12 shows a typical confocal image of a GUV incubated for one hour with micellar ELP-BCs containing six or more arginine residues. Although the kinetics of corona building was sample dependent, all the GUVs displayed a fluorescent corona.

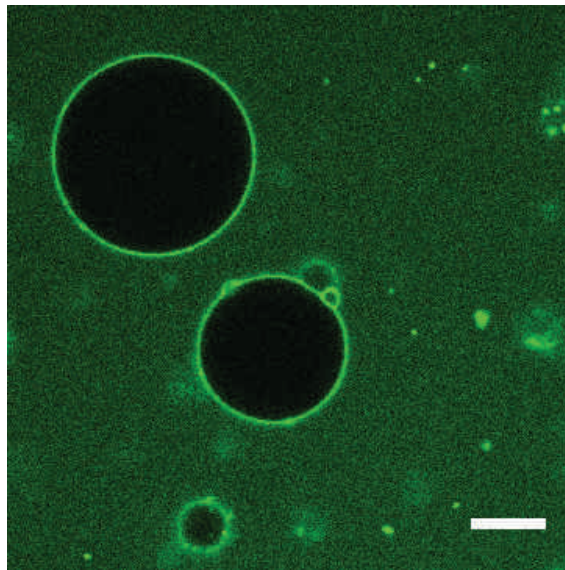


Figure 3.12: Corona appearing around the GUV, immediately after dispersing them in a solution of Arg₈-ELP_{BC} in PBS. Scale bars 20 μm .

The observation of a corona on GUVs composed from zwitterionic lipid membranes, was reproduceable in all cases for the Arg₈ and TAT functionalized ELPs at temperatures above the CMT. This is in stark contrast to the DOPC vesicles incubated with non-functionalized or Arg₅-functionalized ELP_{BC}, where no corona can be seen.

Additionally to the appearance of the corona, GUVs started to adhere on the glass surface of the heating cell, as observed by RICM (see Figure 3.13). The adhesion is

partly responsible for the higher observed partition coefficient due to out of focus light, as well as from some ELPs adhered on the glass.

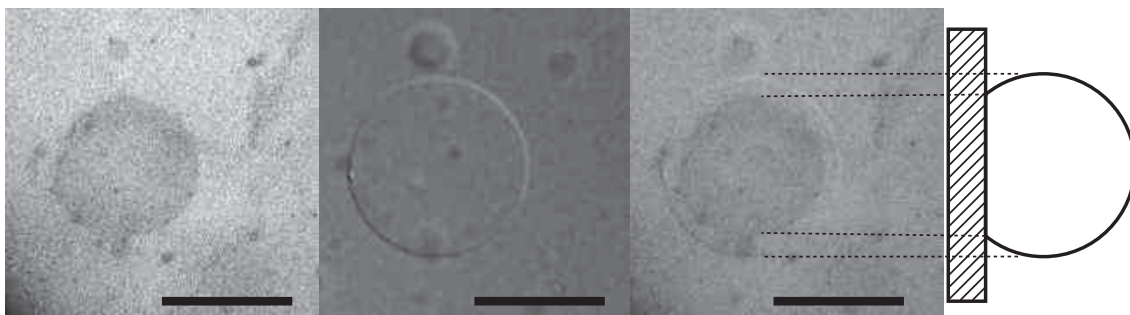


Figure 3.13: RICM images of the adhered vesicles, occurred in the samples containing TAT and Arg₈ functionalized ELPs, at elevated temperatures. Scale bars 20 μm.

When the mixture of GUVs and ELP_{BC} was cooled down rapidly within 10 min to 25 °C, a decrease of the fluorescence in the corona could be observed, indicating some degree of reversibility of the interactions. The same conclusion can be drawn from experiments involving incubation in vials, where the incubation was performed at 37 °C for one hour, but the observation was performed at 25 °C. In none of these cases, a corona could be seen, indicating reversibility of the process.

3.7.2 Quantification of the adsorbed ELP amount

Figure 3.14 shows a typical radial fluorescence profile for GUVs with a light corona.

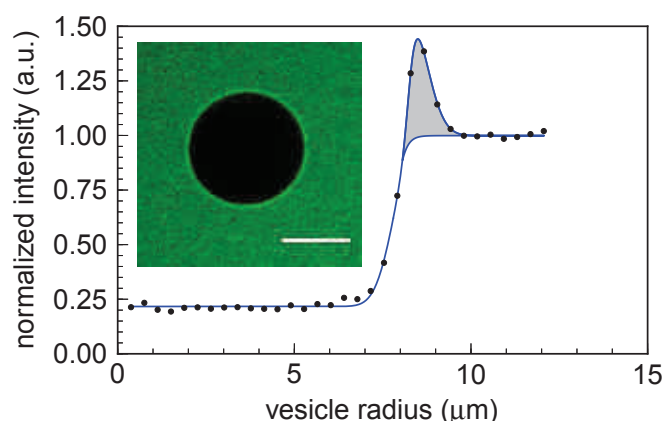


Figure 3.14: Example of a radial profile across a vesicle after incubation with Arg₈ and TAT-functionalized ELPs in micellar state. The (gray) area below the peak is integrated, accounting for the spherical geometry of the vesicles. Scale bars 20 μm.

The excess fluorescence above the level of sigmoidal profile for non decorated membranes, such as that in Figure 3.6, is due to a higher concentration of ELPs on the membrane or in the membrane vicinity. Although the fluorescent excess does not reveal the molecular detail of the interactions between the polypeptides and the membrane, it not only demonstrates that the interaction is attractive, but it also provides a quantitative measure of the number of ELPs per unit membrane surface Γ . Γ is given by

$$\Gamma = \frac{c_b}{R} \int dr r \frac{I_r - I_b}{I_b} \quad (3.2)$$

where I_r is the radial profile intensity, I_b the bulk intensity, c_b the bulk number concentration of the ELPs and R the radius of the vesicle.

This can be converted into a number of peptides per 1000 lipids N_{PTL} according to

$$N_{PTL} = \frac{1000}{\Gamma A_H} \quad (3.3)$$

where A_H is the lipid headgroup area of DOPC.

Figure 3.15 shows histograms drawn from the obtained peptide-lipid ratios for the TAT and Arg₈ functionalized ELP_{BC}. In average 10 ELPs per 1000 lipids are accumulated on the membrane. Values of Γ obtained for lipid-polypeptide interactions correspond also to adsorbed masses close to 1 mg m⁻², typical of many adsorbed polymer systems [124]. If the adsorbed peptide layer consists of ELP unimers, this would correspond to a full monolayer coverage. On the contrary, if the micelles do not disassemble upon adsorption, this would correspond to roughly a 35 % surface coverage with micelles. Note that the aggregation number for Arg₈ is 89 and 76 for TAT functionalized ELP_{BC} at 37 °C, as determined by SLS.

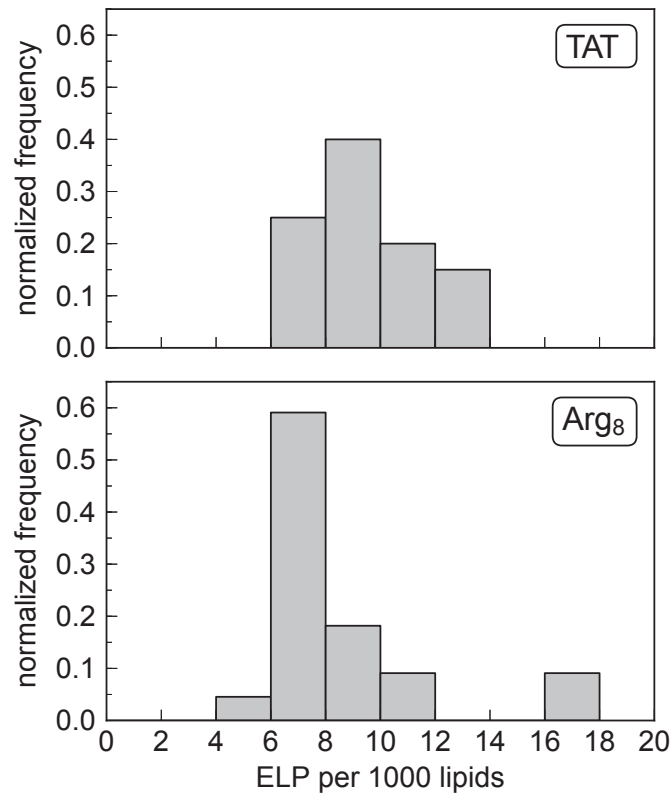


Figure 3.15: Estimation of the number of ELPs per 1000 lipids in the samples containing AF488 labeled TAT and Arg₈ functionalized ELPs.

3.7.3 Stability of micelles during interaction

For determining if the ELP_{BC} adsorb in their micellar state or disintegrate upon interaction with the lipid membrane, we used BODIPY as fluorophore instead of AF488. BODIPY is known to possess self-quenching behavior with increasing concentration, allowing clearly to distinguish between the unimer and micellar forms.

Indeed, self-quenching is observed upon assembly into micelles at 45 °C. Figure 3.16 shows an emission spectra recorded on a Spectrofluorimeter. A significant reduction of the intensity is observed in the micellar state for samples containing 50 % fluorescently labeled ELP_{BC}. For samples containing below 10 % of BODIPY-labeled ELP_{BC}, no quenching has been observed due to assembly into the micellar state at high temperature.

Note that the transition temperature and the hydrodynamic radius did not change for micelles containing as much fluorophore.

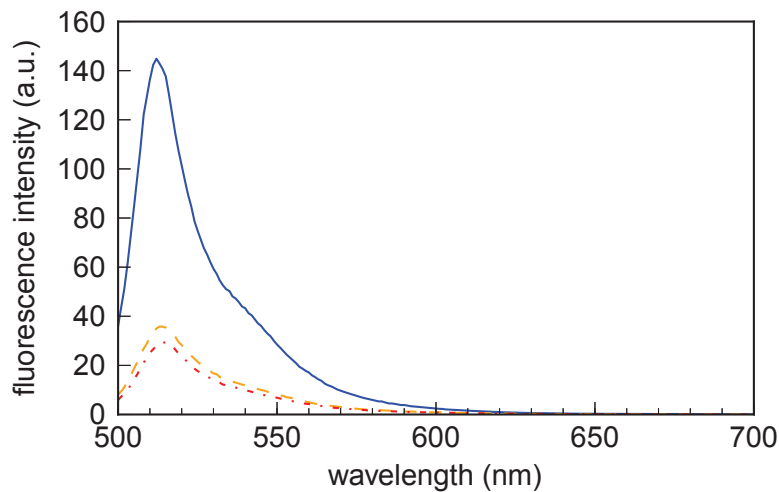


Figure 3.16: Spectrum of a 50 % BODIPY-labeled Arg₈-ELP_{BC} solution in the unimer state at 25 °C (blue solid line) recorded on a spectrofluorimeter. A total self-quenching of around 75 % is observed at 40 °C (orange dashed line) and 42 °C (red dashed dotted line).

We performed and analyzed experiments under conditions similar to those described in paragraph 3.7.2 above. Three different types of ELP_{BC} solutions were prepared: (i) Arg₈-ELP_{BC} with 1 % of BODIPY-labeled Arg₈-ELP_{BC} (ii) Arg₈-ELP_{BC} with 50 % of BODIPY-labeled Arg₈-ELP_{BC} (iii) Arg₈-ELP_{BC} with 1 % of AF488-labeled Arg₈-ELP_{BC}. Arg₈-ELP_{BC} and BODIPY-labeled Arg₈-ELP_{BC} were from a new batch synthesized roughly one month before the experiment.

Figure 3.17 shows histograms of N_{PTL} values obtained for the three types of samples described above. Average number of adsorbed ELPs per 1000 lipids are here for all samples close to 30, corresponding to about 3 mg m^{-2} . Differences between these values and those obtained for experiments in paragraph 3.7.2 above, might be due to either sample aging or to a few degrees difference in the observation chamber. Interestingly, these values correspond to a full coverage of the membrane surface by micelles.

That Arg₈-ELP_{BC} do adsorb in their micellar form is confirmed by the comparison between the first two histograms in Figure 3.17. Indeed, if breakage of the micelles occurred, samples with 50 % BODIPY-labeled ELP_{BC} should display significantly larger apparent values for N_{PTL} due to dequenching at the surface.

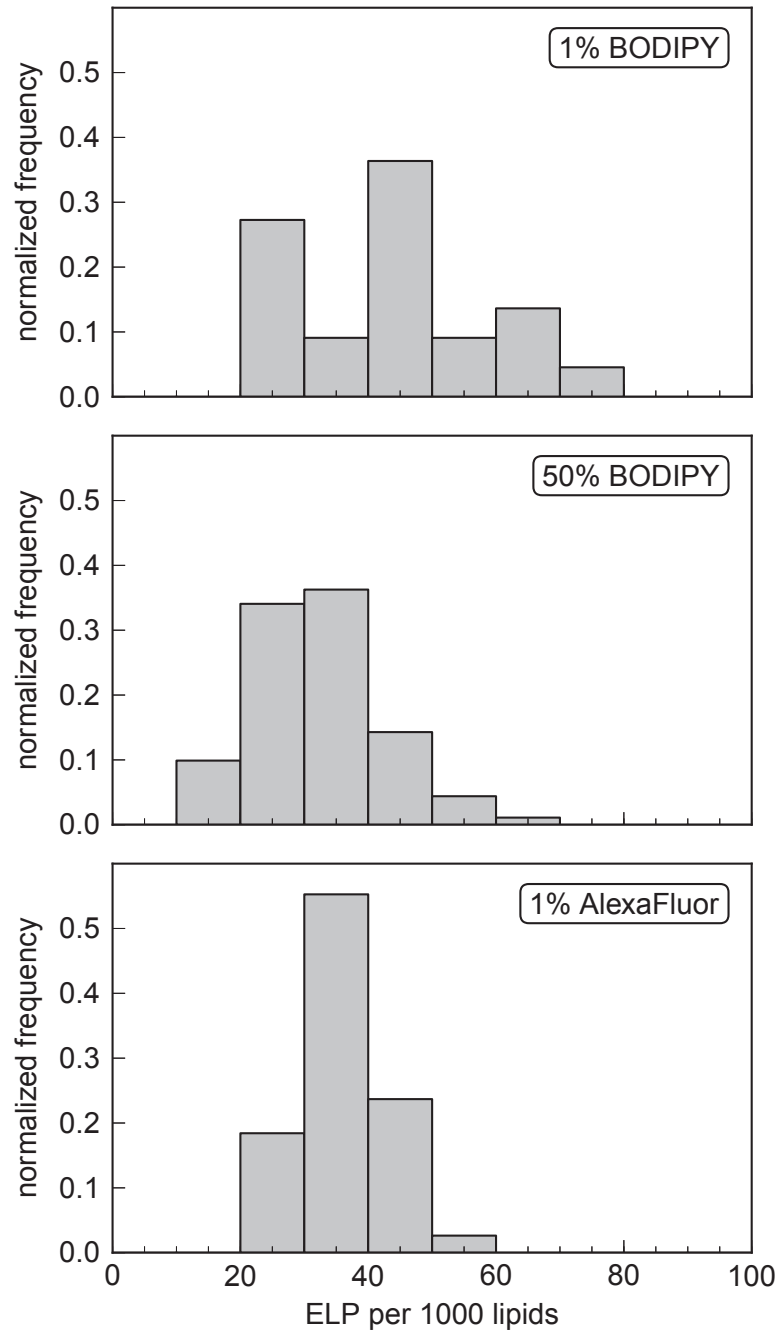


Figure 3.17: N_{PTL} values for samples containing Arg₈-ELP_{BC} with 1 % of BODIPY-labeled Arg₈-ELP_{BC}, with 50 % of BODIPY-labeled Arg₈-ELP_{BC} and with 1 % of AF488-labeled Arg₈-ELP_{BC}.

In these experiments, a light corona can be observed immediately after mixing of the GUVs with the ELPs. Evolution of the intensity of the corona and therefore of the associated N_{PTL} values, takes place over about one hour before reaching a plateau. Figure 3.18 shows the increase of the peptide-lipid ratio with time for a sample containing 50 % BODIPY-Arg₈-ELP_{BC}. This behavior is also observed with a low amount of fluorophore for BODIPY and AF488-labeled ELPs.

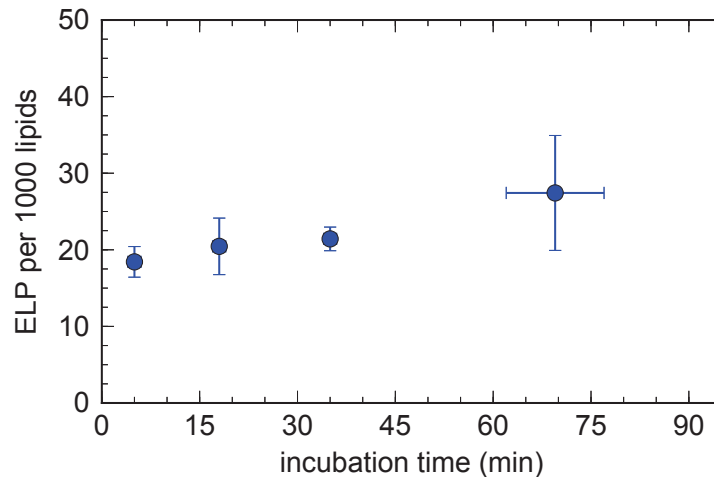


Figure 3.18: Evolution of the number of ELPs per 1000 Lipids with increasing incubation time at 40 °C for a 50 % BODIPY-Arg₈-ELP_{BC} sample. After one hour the value approaches a constant level. Error bars on the y-axis are the standard deviation from the mean value, error bars on the x-axis the incubation time window in which the confocal images were recorded.

The adsorption of ELP_{BC} micelles to the surface presents a strong degree of reversibility, as shown in Figure 3.19. After rapid cooling to 25 °C, the N_{PTL} values are reduced to one quarter of the original value within 60 minutes of incubation. The adsorption of ELP_{BC} micelles to the surface presents a strong degree of reversibility, as shown in Figure 3.19. After rapid cooling to 25 °C, the N_{PTL} values are reduced to one quarter of the original value within 60 minutes of incubation.

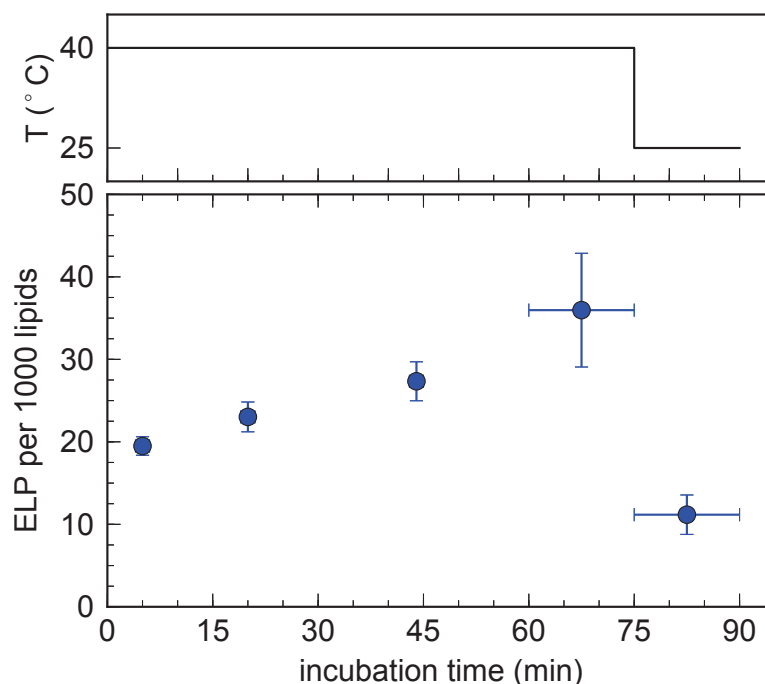


Figure 3.19: Evolution and reversibility of the adsorption of ELP micelles and decrease of the N_{PTL} values for a 1 % AF488-Arg₈-ELP_{BC} sample. After one hour of incubation at 40 °C, the value approaches a constant level. Error bars on the y-axis are the standard deviation from the mean value, error bars on the x-axis the incubation time window in which the confocal images were recorded. After 75 min the sample was rapidly cooled down (in an ice bath) to 25 °C. The peptide-lipid-ratio is reduced to one quarter of the original value.

3.8 Complementary studies

3.8.1 Quartz crystal microbalance

By using a quartz crystal microbalance we additionally tested, if the ELP_{BC} adsorb to a supported bilayer. A supported lipid bilayer can be prepared by adsorption of SUVs to a quartz surface [125], as described in the Materials & Methods section.

Upon injection of ELP_{BC}, no adsorption on the supported bilayer could be observed. Figure 3.20 shows the frequency shifts and dissipation recorded by QCM-D for cell with a supported bilayer of DOPC, after injection of a sample with Arg₈ functionalized ELP_{BC}. The supported bilayer was incubated two times with ELP_{BC} solution. After washing with PBS no frequency change, therefore no adsorption on the supported bilayer can be observed. Comparable graphs were obtained for TAT functionalized and non-functionalized ELP_{BC} (see Appendix)

As we do not see any frequency shifts, QCM-D allows only for qualitative observations and confirms that the bilayer is stable upon incubation with ELP_{BC} at 37 °C.

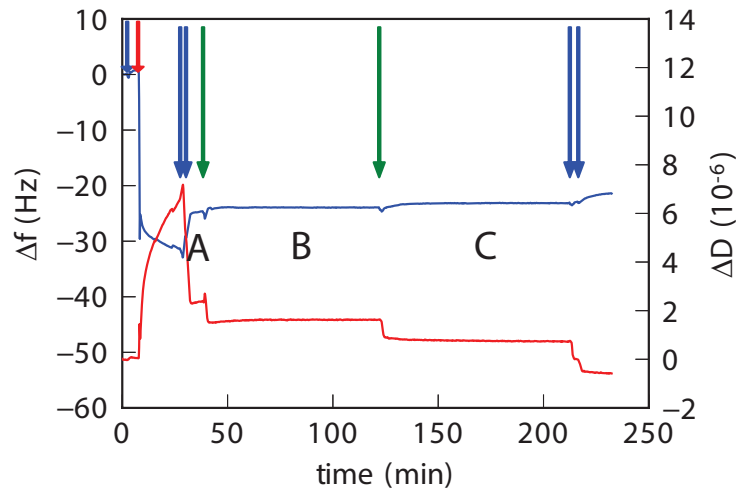


Figure 3.20: Frequency shift and dissipation recorded by QCM-D for Arg_8 sample. Plot shows the 7th overtone. Blue arrows indicate washing the cell with pure PBS buffer. The red arrow shows the injection of the SUVs to form a supported bilayer. The green arrows indicate injection of ELPs. Point A is the stable supported bilayer after washing with PBS. B and C are the incubation of the supported bilayer with ELPs.

In confocal microscopy experiments for these particular samples, values of 3 mg m^{-2} were obtained. This would correspond to frequency shifts of 17 Hz, easily detectable by QCM-D. Therefore, supported bilayers seem not to interact with ELP_{BC} .

3.8.2 Isothermal titration calorimetry

Isothermal titration calorimetry was used to investigate the enthalpy of interaction of LUVs dispersed in a cell containing ELP_{BC}. As expected for neutral lipids, the enthalpy change is very low for interaction of ELPs with LUVs. Figure 3.21 shows ITC curves for LUVs injected into a solution containing TAT- and Arg₈-functionalized ELP_{BC}.

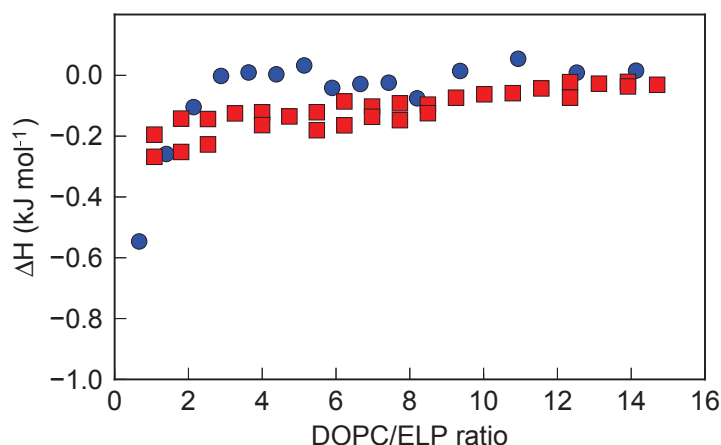


Figure 3.21: ITC curves obtained for injection of LUVs into a cell containing Arg₈-ELP_{BC} (blue circles) or TAT-ELP_{BC} (red squares) at 37 °C.

By injection of ELP_{BC} into PBS, we could determine that the CMC at 37 °C is below 1 μM for our ELP_{BC}, as shown in Figure 3.22 for Arg₈-ELP_{BC}. Comparable graphs were obtained for TAT and non-functionalized ELPs (see Appendix).

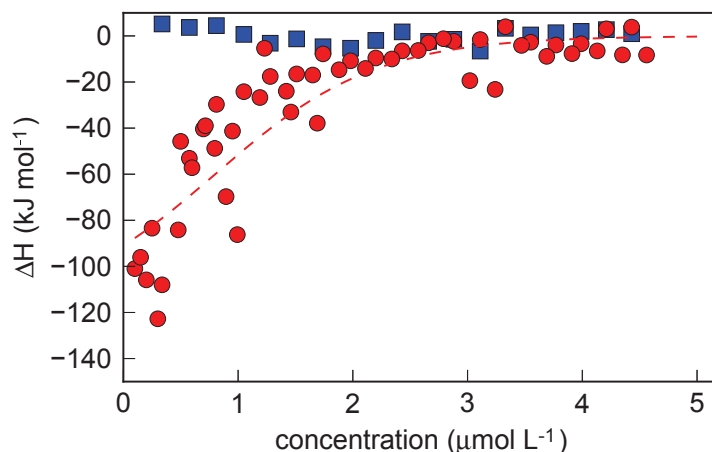


Figure 3.22: ITC curves obtained for dilution of Arg₈-ELP_{BC} solutions with PBS. Red circles signify the dilution of a micellar Arg₈-ELP_{BC} solution at 37 °C. Blue squares show dilution of a solution containing Arg₈-ELP_{BC} unimers at 25 °C.

3.9 Discussion and Conclusions

In this chapter, we showed that GUVs are well adapted systems for evaluating lipid membrane interactions with polypeptides. We defined a characteristic value, the partition coefficient, for evaluation of the penetration potential of ELP_{BC}.

Independent of the number of arginine units, no significant direct translocation across the membrane can be observed for the ELP_{BC} in the unimer or micellar state, excluding passive translocation pathways. In all performed experiments, partition coefficients of up to 20 % were obtained, which are likely to be related to the mixing process during sample preparation. By tracking single vesicles during incubation under the confocal microscope, we could also show that no increase of the partition coefficient occurs. No filled GUVs could be observed in any case; longer incubation times did not lead to a further increase of this value. Hence, bilayers of DOPC can be considered as impermeable to these ELP_{BC}. From our experiments, we estimate that permeability has to be lower than $10^{-4} \mu\text{m s}^{-1}$. In comparison, water permeability for DOPC bilayers is around $160 \mu\text{m s}^{-1}$ [41]. In all cases, the incubated vesicles seem stable, as also confirmed by QCM-D measurements of supported DOPC bilayers and injection of ELP_{BC} at 37 °C.

Ciobanasu et al. [126] reported that no translocation of fluorescently labeled TAT unimers for GUVs made from neutral lipids was observed. However, for experiments with GUVs containing around 40 % negative charges, equilibration of inside and outside was reported. The necessity of negative charges for accumulation could also be observed in other studies [127, 128]. Thorén et al. [127] observed that arginine rich CPPs can translocate into GUVs, but were less permeable than MLVs. Surprisingly, for LUVs CPPs were not able to translocate across the lipid bilayer [127], but bind to LUV membrane and cause aggregation of LUVs [129].

In living cells, different passive and active pathways are involved in the internalization of arginine rich polypeptides. For TAT for instance, insertion into the membrane is believed to lead to transient pore formation in membranes, enabling transportation into the cell. Indeed, simulations have confirmed pore formation in arginine rich polypeptides to be responsible for cellular uptake [130]. However, pore formation is aided by electrostatic interactions due to negative headgroups. Lipids with phosphoethanolamine headgroups with negative intrinsic curvature can assist in the pore formation process as well.

Besides direct translocation or pore formation, specific and/or non-specific endocytotic (energy dependent) pathways are believed to be involved, probably more than one pathway is involved in the translocation of one type of CPP. Translocation of non-amphiphatic CPPs through the plasma membrane by a non-endocytotic pathway pro-

ceeds in three elementary steps [123]. In a first step CPPs have to associate to the plasma membrane. This is followed by permeation through the membrane as the second step and finally release of these peptides in the cytoplasm as the last step. Cellular uptake of CPPs by endocytosis basically adds further intermediate steps between association and permeation.

Our experiments were designed to investigate membrane-peptide interactions between arginine rich CPPs and neutral lipids. The obtained results confirm the importance of this first step for later translocation for neutral lipids. By investigating membrane model systems composed only from zwitterionic lipids, we can exclude active translocation pathways and focus only on the membrane-peptide interactions. For GUVs incubated with micellar ELP_{BC} containing more than six arginine residues, a fluorescent corona on the GUV membrane was observed. These attractive interactions between the membrane and micellar ELPs was however not observed for ELP_{BC} with less than six arginine residues. The amount of ELPs per 1000 lipids (N_{PTL}) could be estimated by evaluation of the radial profile obtained from GUVs showing a corona. Values of around 30 ELPs per 1000 lipids, corresponding to adsorbed masses close to 30 mg m^{-2} were obtained from these profiles. By using BODIPY-labeled ELPs that show self-quenching behavior at high concentrations, we could show that ELP_{BC} adsorb in their micellar state. By taking into account the aggregation number for ELP_{BC} micelles, the average N_{PTL} values obtained for these experiments indicate a full coverage of the membrane. The accumulation of micelles on the membrane was shown to be reversible when the temperature was decreased below the CMT. Reversibility seems to further confirm that ELP_{BC} do not insert deeply in the membrane by disintegration of the micelles.

Figure 3.23 shows a schematic illustration for adsorption of micellar ELP_{BC} with more than six arginine residues, at temperatures above CMT with neutral lipids, as indicated by quenching experiments.

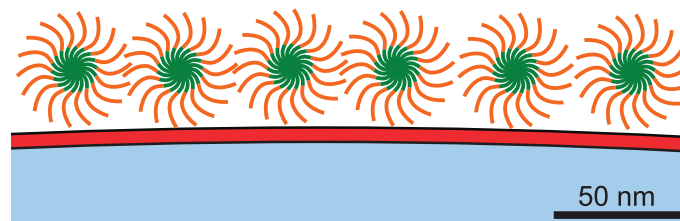


Figure 3.23: Schematic illustration of ELP micelles accumulated on the DOPC membrane.

In the past, several experiments were performed on the interaction of LUVs and GUVs with arginine-rich polypeptides. It was found that the total free energy of binding is only to $\approx 25 \%$ of electrostatic nature. 75 % are non-electrostatic interactions and corre-

spond to hydrogen bonding or hydrophobic interactions [131]. This is in contrast with previous ITC measurements performed with charged lipid vesicles and TAT, where around 77 % was believed to be of electrostatic origin [132]. It was suggested that the binding of charged proteins to oppositely charged vesicle membranes is a two step process. A first fast step involves electrostatic interactions, whereas in the slower second step (up to 60 times slower) non-electrostatic forces, such as hydrophobic interactions and hydrogen bonding are involved [131].

As we do not use charged lipids, hydrogen bonding and hydrophobic interactions are probably the major factors of binding to the membrane. Isothermal titration calorimetry (ITC) measurements show only very small values of interaction energy, indicating that hydrophobic interactions are involved.

Our experiments indicate that adhesion to the neutral lipids occurs without strong insertion. Indeed, it was observed that membrane-bound TAT unimers float on the membrane [133]. Additionally, a time dependence for accumulation on the membrane could be observed, longer incubation times lead to a brighter corona. We also confirmed this behavior for ELP_{BC}, a continuous increase of the N_{PTL} values until stabilization after an incubation time of 60 min was observed. The time dependence of the intensity of the corona seems also to indicate that non-electrostatic forces are the major driving force.

The corona effect can only be observed for micellar ELP_{BC} with a high number of charged peptides. In experiments under the microscope, no decoration of membranes with Arg₅ functionalized ELPs at high temperature was observed. For ELP_{BC} with more than six arginine residues at temperatures below CMT, no accumulation around the membrane can be observed, contrary to experiments performed with short arginine rich polypeptides and TAT. A cargo attached to the arginine rich CPPs apparently influences membrane-peptide interactions. Our results also confirm that local higher arginine density by self-assembly of ELP_{BC} helps to control membrane-peptide interactions, but that even in this case the number of arginine residues per peptide chain is crucial for interaction of micellar ELP_{BC} with neutral lipid bilayers.

In conclusion, our results indicate that the predominant mechanism for translocation of this new class of arginine rich ELP_{BC} has to be an energy-dependent non-specific endocytotic process. Indeed, in previous studies with live cells, macropinocytosis was suggested to be the primary endocytotic pathway [112]. Attachment of a cargo to CPPs also seems to decrease the ability of membrane-peptide interaction in the unimer state. Furthermore, we showed that triggered self-assembly into micelles can control lipid-peptide interactions of ELP_{BC} above a certain critical arginine number in the CPP residue, a strategy created by Professor Chilkoti. We believe that non-

electrostatic forces are very important for membrane-peptide interactions prior to the active cellular uptake process, which is likely to be regulated by ELP binding to the membrane. Our results show that not only receptor-mediated or electrostatic interactions are regulating membrane-peptide interactions, but also “simple” zwitterionic headgroups play a significant role, showing the complexity of translocation of a cargo across the plasma membrane in drug delivery.

PVA-assisted formation of GUVs

In this chapter a new method for the formation of Giant Unilamellar Vesicles by swelling of a polymer film under a stack of lipid bilayers will be presented. This method provides a facile and fast way to prepare vesicles with a wide range of lipid compositions. First the efficiency of GUV formation on a suitable gel is demonstrated and the growth process is studied by inspecting the distribution of lipids before and after growth. Next, the growing efficiencies for different ionic and non-ionic amphiphiles are compared and it is shown that the method allows the encapsulation of hydrophilic substances in the vesicles. The chapter concludes by proposing a mechanism for vesicle growth.

4.1 Introduction

As discussed in chapter 1, giant unilamellar vesicles (GUVs) have played a prominent role amongst model biomembranes [28]. Due to their large dimensions, in the range of typical cell sizes, GUVs can be easily observed and micro-manipulated under an optical microscope, thus allowing for the direct observation of relevant biophysical phenomena at a single membrane level [53].

The importance of GUVs has triggered a host of efforts seeking for GUV preparation methods that can provide a fast and easy route to form vesicles from a variety of lipid compositions and under different buffer conditions [28]. For all of the methods, as described in the general introduction, vesicle growth in physiological buffers or from lipid mixtures containing charged lipids is still challenging, in spite of the recent improvements. Another important difficulty of hydration based preparation methods is that encapsulation of proteins or other (bio)molecules, especially in buffers of physiological ionic strength, is generally inefficient and variable among liposomes.

There is currently a broad interest in the use of vesicles as a platform to build either protocells or artificial cells that mimic aspects of bacterial or mammalian cells [134]. Examples include the reconstitution of cytoskeletal protein networks [135–138], membrane-protein interactions [139, 140], cell adhesion [52] and gene transcription and translation [54]. In all these applications, biomolecules need to be encapsulated inside giant unilamellar vesicles in physiological buffers. This is still a challenging task due to the high salt levels present in physiological buffers and to the relatively low vesicle formation speed that hinders a precise control of the biological activity of the proteins. Recently several new strategies have been proposed which were designed to improve preparation speed, encapsulation efficiency, and/or applicability to charged lipids. An example, for instance, uses water-in-oil emulsion droplets as templates for bilayer vesicles and for reconstituting an actin shell inside a liposome[141].

Biomolecule encapsulation into emulsion droplets is highly efficient and reproducible even at physiological salt conditions. However, the emulsion-based methods generally require advanced equipment such as microfluidic devices. Moreover, traces of the oil phase can often be detected in the self-assembled membrane [28, 142]. Microfluidic inkjet encapsulation methods also improve biomolecule encapsulation and preparation speed compared to film hydration methods [71, 143], but again specialized equipment is needed and residual oil can be left in the membrane.

To minimize damage of the molecules of interest [64, 87], one is restricted so far to film hydration methods. Lipid film hydration methods have a strong potential for further development. It is important for instance to realize that membrane swelling from a pre-ordered bilayer film requires water penetration into the membrane stacks, a process that is partially hindered when the lipids are deposited on glass or other solid substrates. A larger exposure of the pre-ordered lipid films to hydration is achieved in a recently discovered agarose swelling method [65]. Here the organic solution containing the lipids is spread on a thin dried film of agarose, a naturally occurring polysaccharide. Upon addition of the buffer solution, GUVs are rapidly formed at the interface between the swollen agarose gel and the buffer. Vesicle formation is much faster than in classical electroformation or gentle swelling. Moreover, this method works with a wide range of lipid compositions and buffer conditions, and it is possible to efficiently encapsulate various biomolecules [65], including cellular proteins [142]. However, the vesicle formation efficiency is reduced because lipids are distributed over the whole gel thickness, which is several micrometers. Furthermore, the agarose gel dissolves partly upon swelling, and remnants can be detected in/on the membrane [65].

In this chapter we describe a new swelling method inspired by the earlier work on swelling from agarose gels, which provides a facile and fast way to prepare vesicles

with a wide range of lipid compositions. Instead of agarose, we use polyvinyl alcohol (PVA) gels. Our hypothesis was that PVA gels can optimize the lipid distribution at the interface between the substrate and the hydrating buffer. Moreover, PVA gels are expected to be much less prone to dissolution upon swelling at room temperature than other physical hydrophilic gels [144, 145]. Indeed, we find that vesicles formed by PVA-assisted swelling are not contaminated by polymer.

4.2 A PVA film below a lipid bilayer promotes GUV formation

Fully hydrolyzed high-molecular weight polyvinyl alcohol (PVA) was used to form a dry but swellable polymer film on a glass support. A thin film of lipids was then spread on the gel surface and the lipid-gel system was hydrated in an aqueous solution. Within two minutes, numerous unilamellar vesicles can be observed, as shown in Figure 4.1. This observation is in stark contrast with hydration of a lipid stack deposited directly on glass, where the majority of bilayer structures correspond to multilamellar vesicles or cylinders and only a minor fraction correspond to unilamellar vesicles. Compared to the standard electroformation method, vesicle formation from PVA-lipid films has the advantage that GUVs are formed much faster, as shown in Figure 4.1. Furthermore, the gel-assisted swelling method avoids the risk of lipid degradation, which may occur during electroformation [87, 88].

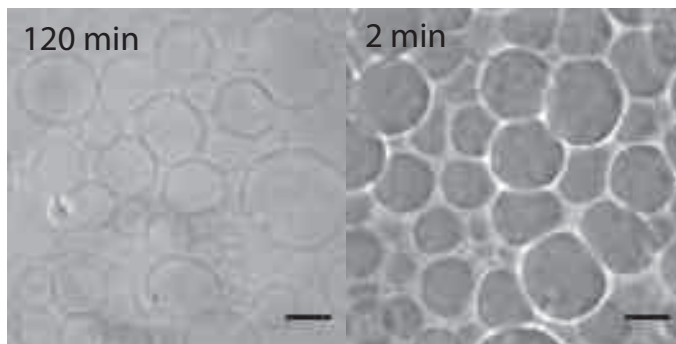


Figure 4.1: Phase contrast images of DOPC-GUVs, obtained by (A) electroformation and by (B) PVA-assisted swelling. Variations in contrast are due to differences in composition of inner and outer solutions. Scale bars 20 μm .

The kinetics of vesicle growth during gel-assisted formation displays initial diameter growth rates of order of tens of micrometers per minute, followed by a slower relaxation towards the final size. Growth occurs by transfer of the lipid membrane from the gel surface to the vesicle above, as evidenced from confocal microscopy where patches without membrane can be seen on the gel surface below each given vesicle (compare also section 4.4). Growth of vesicles and growth by merging two different vesicles can both be seen independently, as shown in Figure 4.2: an image sequence

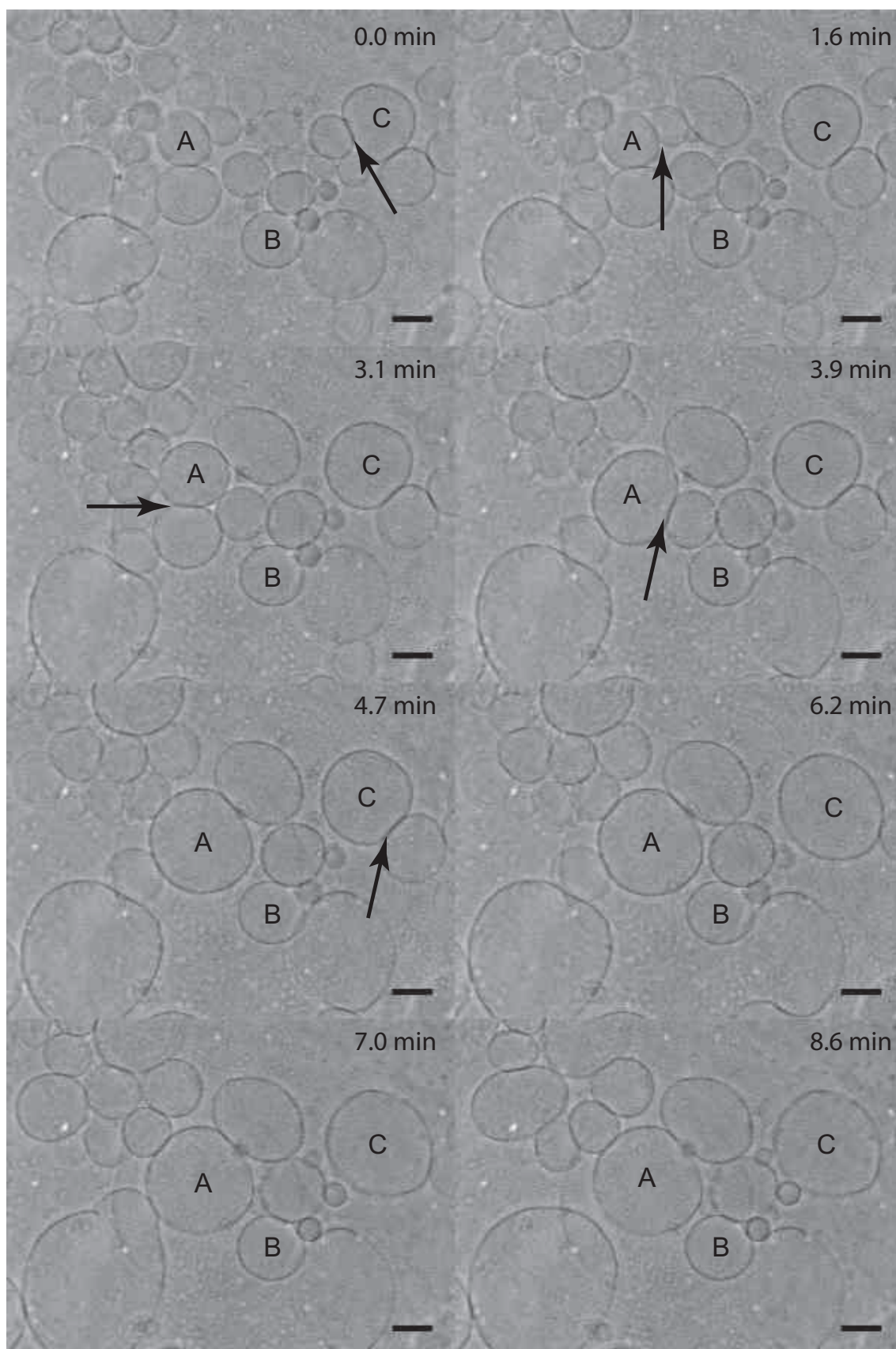


Figure 4.2: Image sequence of DOPC-GUVs growing on a PVA substrate. Arrows indicate fusion events before fusion. Vesicles A and C are GUVs where fusion was observed. For vesicle B, only growing was observed without detectable fusion events. Images were recorded in phase contrast mode. Time points are relative to the beginning of observation. Scale bars 20 μm .

of a patch of DOPC vesicles growing on a PVA substrate can be seen. Merging of GUVs and growth of GUVs can be observed.

The vesicles labeled as A and C in this image undergo merging events, whereas vesicle B grows independently. Figure 4.3 shows the evolution of the vesicle diameter with time for both cases. On the left plot of Figure 4.3, the arrows show the time when merging takes place.

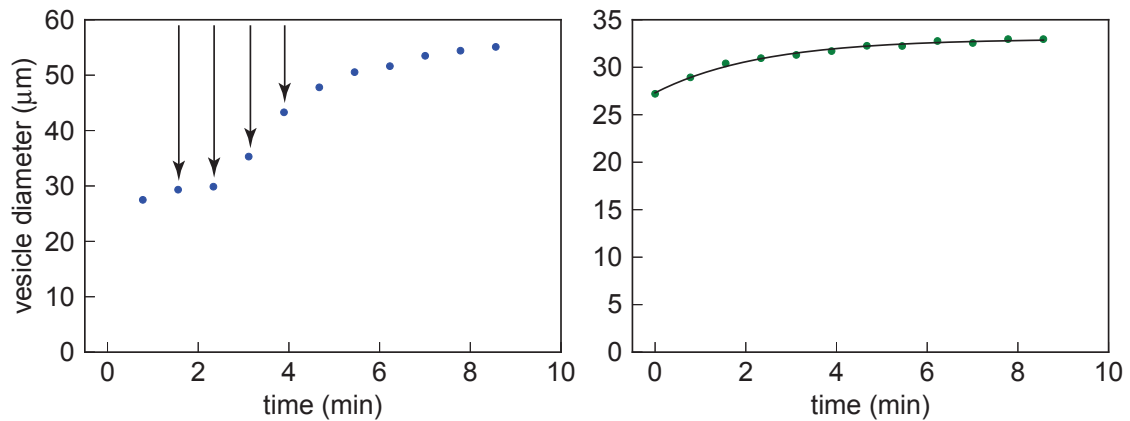


Figure 4.3: Evolution of vesicle A diameter (left image) and vesicle B (right image) from Figure 4.2. Arrows indicate merging with neighbor vesicles. For vesicle B a final exponential relaxation of the vesicle size can be observed.

The nature of the merging events remains to be studied. Indeed they could either correspond to the fusion of two neighboring vesicles or simply to a rearrangement of the membranes to which the vesicles are attached. On the right plot, the final relaxation of size growth is displayed.

By fitting with a curve for an exponential growth (decay) a time constant of $2 \mu\text{m min}^{-1}$ is obtained for such late stages of PVA swelling. Note the vesicle diameters are obtained by measurement of the projected vesicle area under the assumption that GUVs are round-shaped.

The speed of vesicle formation on swelling PVA gels is comparable to that observed previously on an agarose substrate [65]. However, the agarose-growing method leads to encapsulation of some agarose polymer, as well as to polymer decoration of the membrane [142]. To test whether PVA is present in the GUVs, we performed confocal microscopy of DOPC GUVs grown on fluorescently labeled PVA films.

As shown in Figure 4.4, no traces of fluorescent PVA can be found either on the vesicle membranes or inside the vesicles. This visual observation is confirmed by quantitative image analysis, weak fluorescence in the green channel is due to some free DTAF, as

discussed in chapter 2. The absence of vesicle contamination by PVA can be primarily traced to the PVA gel structure, which is much less prone to dissolution upon swelling at room temperature than other physical hydrophilic gels [144, 145]. Moreover, the lipid distribution in the PVA film prevents contamination of the vesicles by PVA, as discussed below.

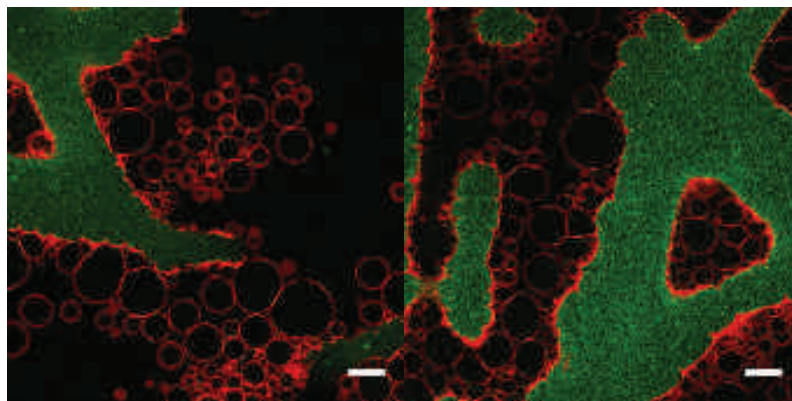


Figure 4.4: Confocal laser scanning microscopy (CLSM) images of DOPC-GUVs labeled with 0.5 mol% RhodB-PE, grown on a fluorescently (DTAF) labeled PVA film. Scale bars 20 μm .

4.3 Optical properties of DTAF-labeled PVA films

For dried DTAF-PVA films, some bleaching of the fluorophores was observed when recording confocal z-stacks, as seen in the left panel of Figure 4.6. Hence, typical confocal scans were performed by starting above the PVA gel and finishing on the glass surface. Hydration of the films caused an increase of the fluorescence intensity of both the DTAF-PVA and rhodamine lipids. This intensity increase can be explained by the change in refractive indices of the films upon hydration. In solution, the fluorescence of DTAF increases in the presence of PVA, as determined by fluorescence spectrophotometry using a Horiba Jobin Yvon FluoroMax-4 spectrofluorometer (see Figure 4.5), a comparable increase is found when DTAF is directly coupled to PVA.

Additionally, in the swollen DTAF-PVA films, the fluorescence spectrum of DTAF was broadened compared to free DTAF in solution (dashed line in Figure 4.5), as measured by CSLM. As a result, some emission bleeding of the green channel into the red channel occurred.

We checked that this did not influence the qualitative measurements of the lipid distribution by performing additional scans of labeled GUVs grown on unlabeled PVA and also compared the bleeding profile of labeled PVA with our samples, which is exactly the same up to experimental errors (Figure 4.6).

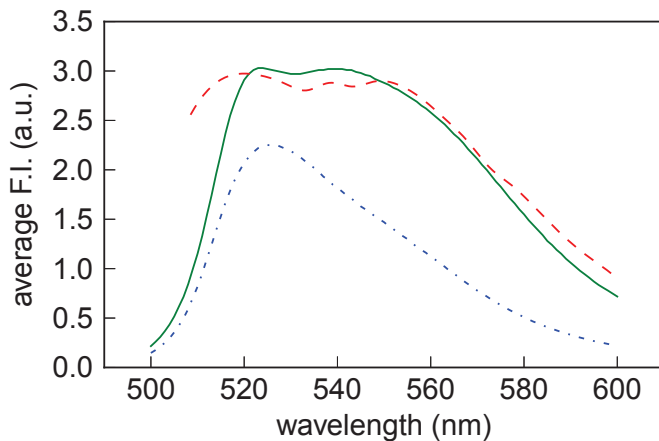


Figure 4.5: Fluorescence emission spectra of DTAF free in PBS solution (dash-dotted) and in the presence of PVA (solid line) obtained by excitation at 488 nm with a fluorescence spectrophotometer. Spectra of the DTAF labeled PVA obtained by CLSM at 488 nm after swelling with PBS (dashed line).

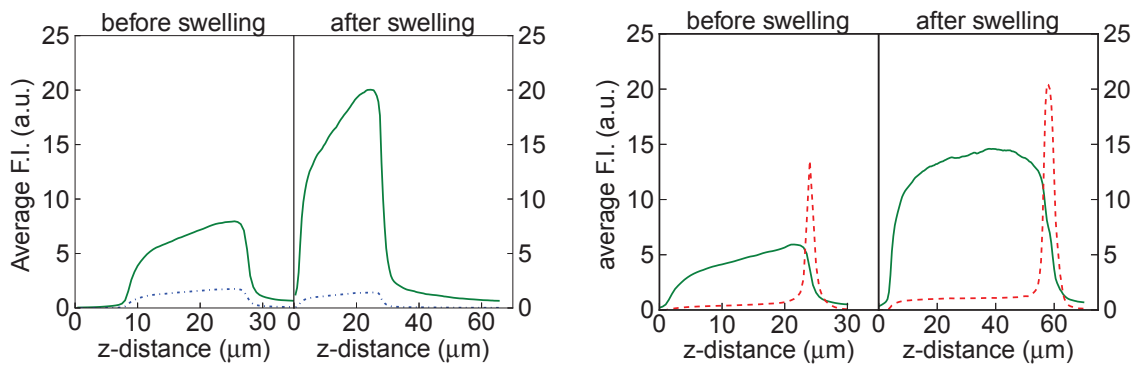


Figure 4.6: CLSM z-profiles of a DTAF-labeled PVA film (*solid line*) and a fluorescent DPPC film (*dashed line*, right panel). Lipids and gel are well separated before and after swelling with PBS buffer solution at room temperature. Residual red fluorescence inside can be observed in the gel (*dash-dotted line*, left panel) and is due to emission bleeding of the DTAF. A z-distance of zero micron corresponds to the bottom of the labeled PVA gel. Bleaching of the DTAF-labeled PVA can be observed deep inside the gel. Hence, confocal scans were performed by starting above the PVA gel.

4.4 Lipid distribution

In order to visualize the spatial distribution of the lipids with respect to PVA in the lipid-PVA films, we measured the relative fluorescence intensities of the rhodamine labeled lipids and the fluorescein-labeled PVA of a $20\ \mu\text{m} \times 20\ \mu\text{m}$ patch as a function of height (z-direction) above the glass substrate.

We first focussed on the lipid distribution before and after gel swelling for DPPC, a lipid that is in a gel state at room temperature, its main transition temperature is $41\ ^\circ\text{C}$. As shown in the right panel of Figure 4.6, the lipid bilayer is localized at the gel surface and does not penetrate the polymer film, independently of the degree of swelling of the gel. Also for lipids in the liquid like state, such as DOPC, the lipid bilayer is located

on top of the gel.

In the original gel-assisted swelling method of Horger et al. [65], it was shown that the lipids completely penetrated the agarose film, which is tens of micrometers thick. The agarose and the lipids thus intimately mix over the full film thickness. Our results show that this is not a requirement to promote giant vesicle growth. Figure 4.7 shows grown GUVs of DOPC localized on top of the swollen PVA gel. Moreover, the reduced mixing of lipids with polymer in PVA gels compared to agarose gels reduces the probability of vesicle contamination by gel residues.

As discussed above, GUVs are formed rapidly from films composed of lipids which are in a fluid state at room temperature. Confocal imaging shows that several layers of vesicles can be observed on the gel surface (see Figure 4.7 and inset B in Figure 4.9). Small vesicles are typically located at the gel surface, while larger ones are further away.

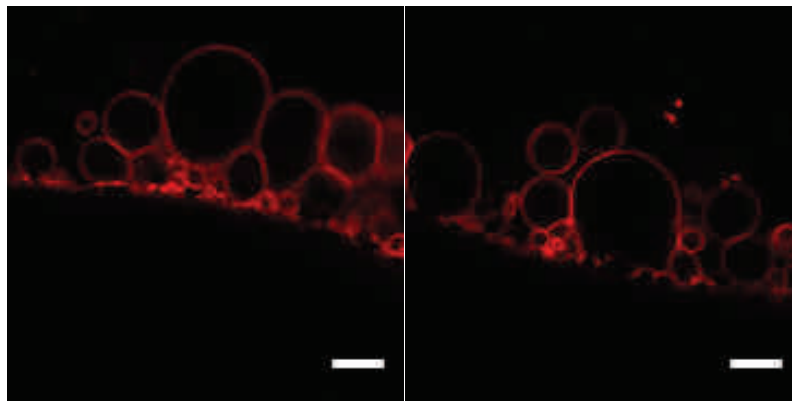


Figure 4.7: CLSM images (XZ plane) of DOPC-GUVs labeled with 0.5 mol% RhodB-PE, grown on unlabeled PVA film. Scale bars 20 μm .

During the growing process, small vesicles often merge into a larger one, that may later detach from the gel. However, while many vesicles detach, many stay on the surface of the PVA film. As the 3D confocal image shows (Figure 4.8), holes in the fluorescently labeled lipid film can be observed directly underneath the vesicles, likely corresponding to the partial consumption of the lipid film in order to build the vesicle above the hole.

After swelling, the PVA surface appears very corrugated with "valleys and mountains". Any XY plane through this interfacial region, as exemplified by Figure 4.9 in inset A, will then display areas inside the gel and areas outside the gel where lipids can be observed. In this geometry the gel interface is almost perpendicular to the confocal section, allowing to precisely screen the GUVs for fluorescent PVA traces and to reconstruct a 3D representation as in Figure 4.8.

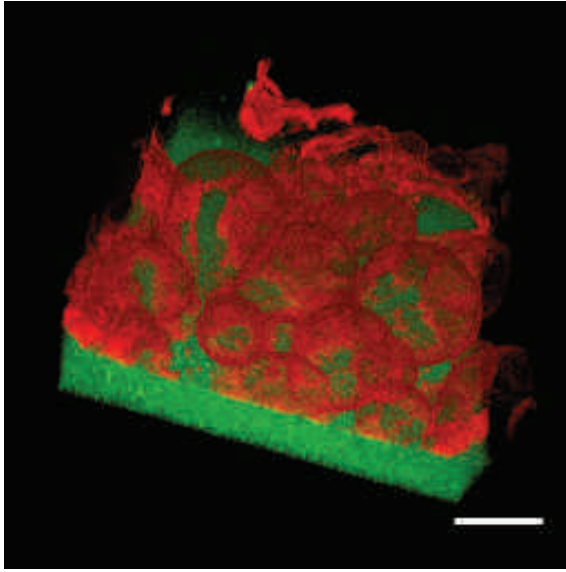


Figure 4.8: 3D reconstruction of a z-stack recorded by CLSM of RhodB-labeled DOPC vesicles grown on a DTAF-labeled PVA gel. Scale bar 20 μm .

Depth profiles of the PVA and lipid fluorescence intensity reveal the heterogeneity of the lipid distribution on the gel film, that can be related to the lipid deposition process or to the swelling of the gel. Figure 4.9 summarizes all the observed cases. The vertical line represents the z-position where the confocal micrograph shown in inset A was recorded. The green channel represents the fluorescently labeled PVA, the red channel the fluorescently labeled lipid. The figure inset I displays for reference a z-profile from the same sample before swelling. Inset II shows gel surface regions after swelling without any traces of lipids, while inset III corresponds to a lipid film still attached to the gel without any vesicles. In some regions GUVs still attached to the gel can be observed, as displayed in inset IV. The last inset V corresponds to the rarest case where a detached vesicle is still in the neighborhood of the gel interface above a membrane. Inset B in Figure 4.9 corresponds to a vertical cross section, which better views the cases III to V.

In summary, our results show thus that GUVs free of polymer contamination grow during gel swelling from a heterogeneous lipid film at the gel surface. Given that the lipid solution spread on a PVA gel does not penetrate into the gel, we tested the effect of lipid/PVA mixing by forcing lipids into the gel. This was achieved by spreading a PVA solution mixed with small multilamellar vesicles. In this case, no unilamellar vesicle formation could be observed upon hydration, thus confirming that gel/lipid mixing is not required for vesicle growth on PVA (compare Figure 4.10).

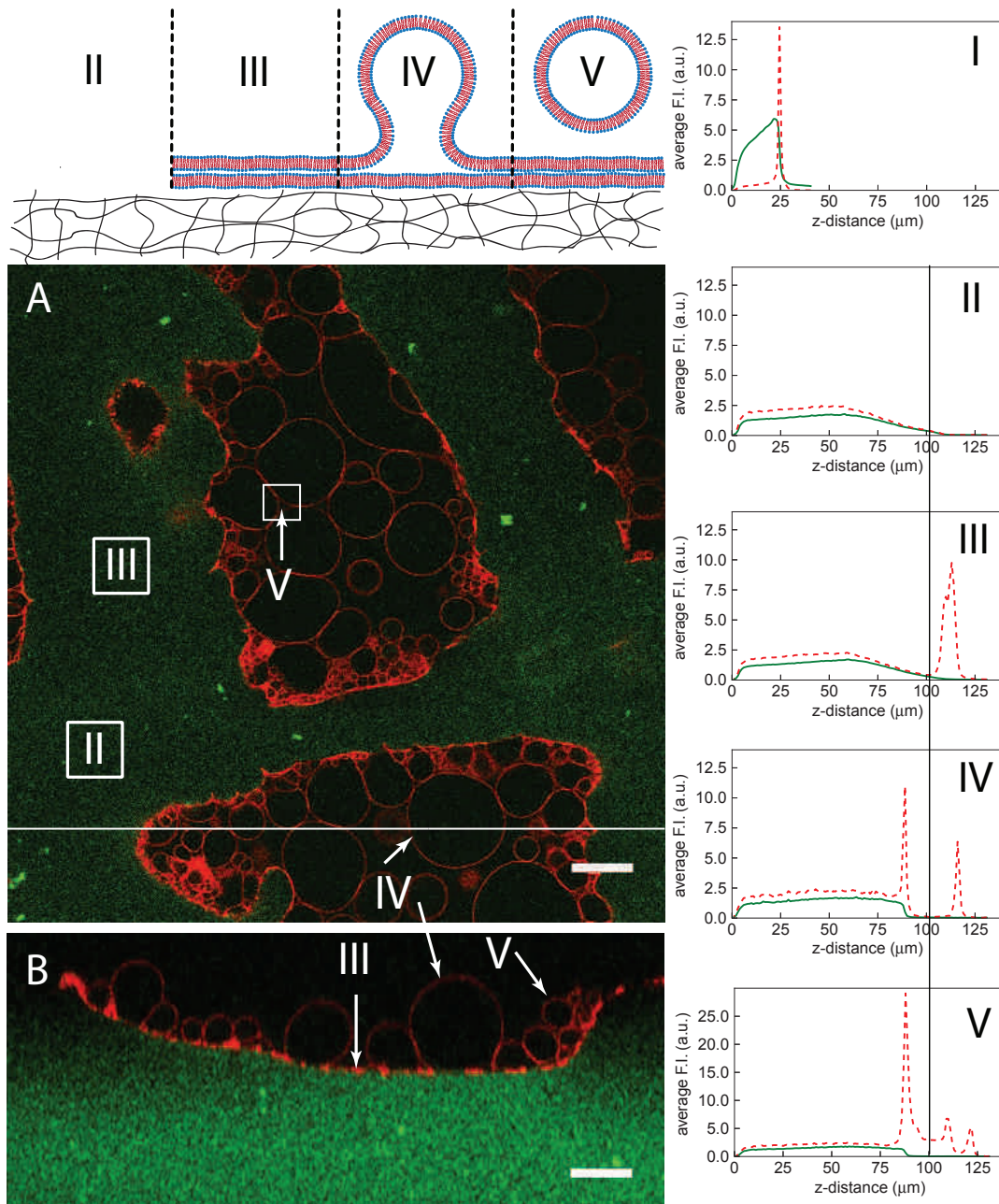


Figure 4.9: Heterogeneity of lipid distribution on a swollen gel interface. Inset A shows the XY section of a DTAF-labeled PVA gel (*green*) and DOPC-GUVs labeled with 0.2 mol% Rhodamine (*red*) recorded with CLSM at a z-position of 31 μm . Inset B is a XZ section at the position of the white line. Graph I is a z-profile of the same sample in the dry state before hydration with buffer solution, other graphs correspond to the different labeled regions of the micrograph which are further sketched in the diagram above. Average intensity of a given z was determined for a 20 μm x 20 μm square and the average intensity variations plotted with z. The scan was performed starting at the top of the sample, a z-distance of zero micron corresponds to the bottom of the labeled PVA gel. Scale bar 20 μm .

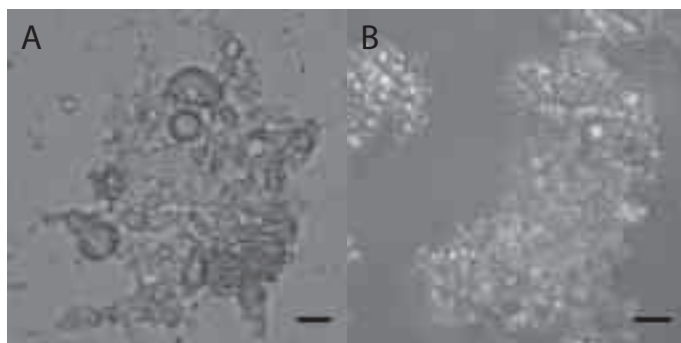


Figure 4.10: (A) Phase contrast image from a swollen precursor of dried mixture of small multilamellar vesicles of DOPC with PVA solution. (B) DIC image; precursor prepared by mixing of small multilamellar vesicles and PVA dissolved in sucrose solution. Swelling buffer: PBS. Scale bars 20 μm .

4.5 GUV formation: dealing with the hard cases

Besides DPPC with two saturated C-16 tails, all other phospholipids used in this work have two C-18 tails with one unsaturation per tail.

We tested a range of head groups, including neutral zwitterionic head groups (DOPC), as well as head groups bearing a negative net charge (DOPG, DOPS) or a positive net charge (DOTAP). Additionally, we tested growing with cardiolipin, a lipid containing four tails and two negatively charged headgroups.

As shown in the preceding section, GUVs can be rapidly formed from the zwitterionic lipid DOPC by PVA-assisted swelling. In this section we will show that the PVA growing method also provides a valuable tool to form vesicles from other types of lipids, which are difficult to form by other film swelling methods. Lipids with charged head groups are a clear challenge for electroformation. Recently, a method to grow charged lipid vesicles under physiological buffer conditions at high frequencies was proposed [81, 82]. However, even under such conditions, a number of difficult issues remain, related to the growth of vesicles from purely charged lipids, to the vesicle yield, and to the detachment of the vesicles from the growing substrate. We have for instance compared the growth of DOPC-GUVs containing DOTAP, a cationic lipid, by electroformation and by PVA swelling. For these lipid mixtures, vesicles are obtained in a high number by electroformation, but they cannot be detached from the ITO substrate. With the PVA swelling method, even 100 % DOTAP vesicles can be formed and transferred, albeit with a smaller yield than in the case of zwitterionic lipids. Figure 4.11 shows a free floating GUV composed from DOTAP grown by PVA swelling. The detachment yield can be improved by gentle sonication.

In some cases, the presence of sucrose in the dry gel improves vesicle formation. Similar results can be obtained by making the PVA gel in a PBS solution, although with somewhat less efficiency of vesicle detachment (compare Figure 4.12).

Figure 4.11: Left image: free floating DOTAP-GUV. Right image: DOTAP vesicles in the growing chamber. Both were formed by PVA swelling at room temperature in PBS. Images were recorded in phase contrast mode. Scale bar 20 μm .

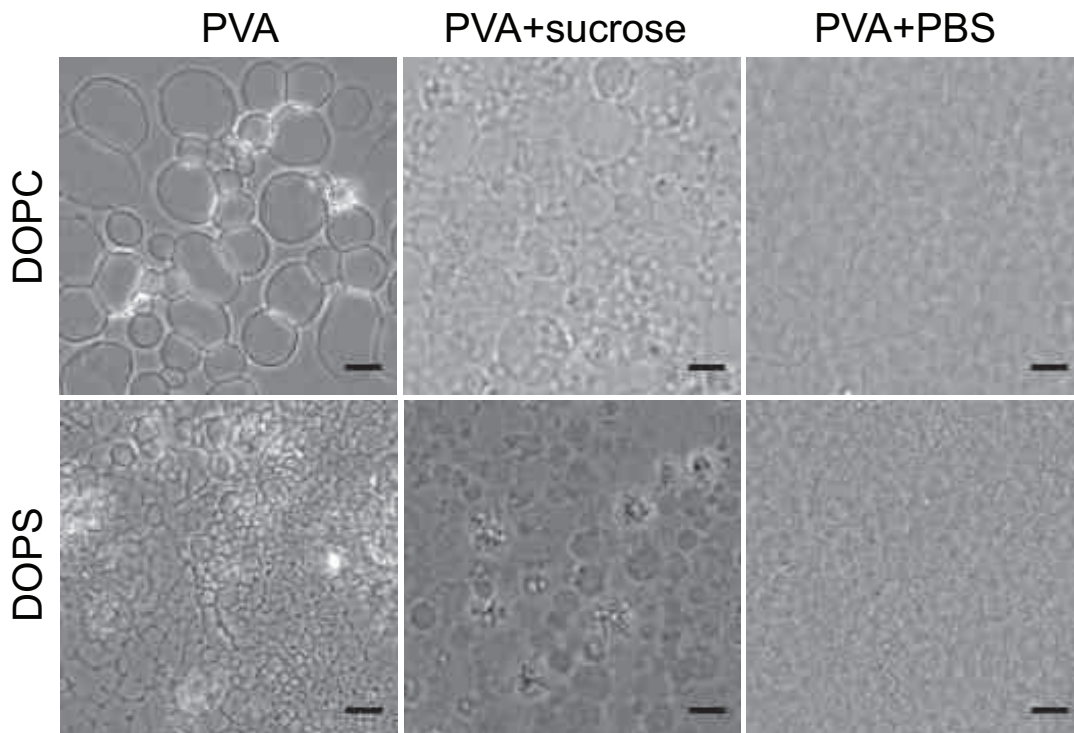
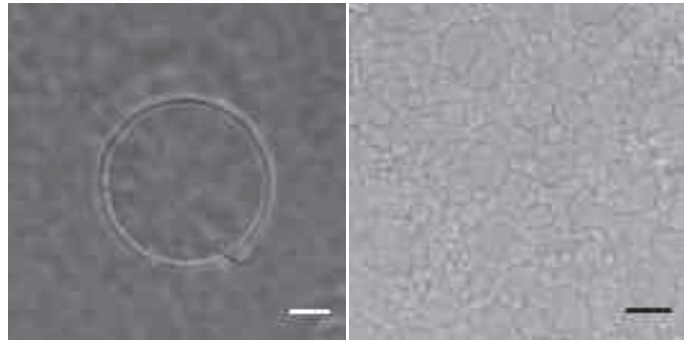


Figure 4.12: Phase contrast images of GUVs formed from DOPC and DOPS by PVA swelling. Left column: growth on pure PVA gel. Middle column: growth on PVA containing sucrose. Right column: growth on PVA containing PBS. Swelling solution: PBS. Scale bars 20 μm .

Examples of other systems grown by the PVA swelling method are displayed in Figure 4.13. Images in the left column show vesicles formed by growing on pure PVA gel, while images in the right column show vesicles grown on a PVA gel containing sucrose.

The figure 4.13 shows GUVs grown from DOPC, DOPG, DOPS and the triblock copolymer PMOXA-PDMS-PMOXA. In all cases, GUVs formed on a PVA gel that contains sucrose detach better during the growing process. Also the formed vesicles are less prone to adhere to each other in the growing chamber.

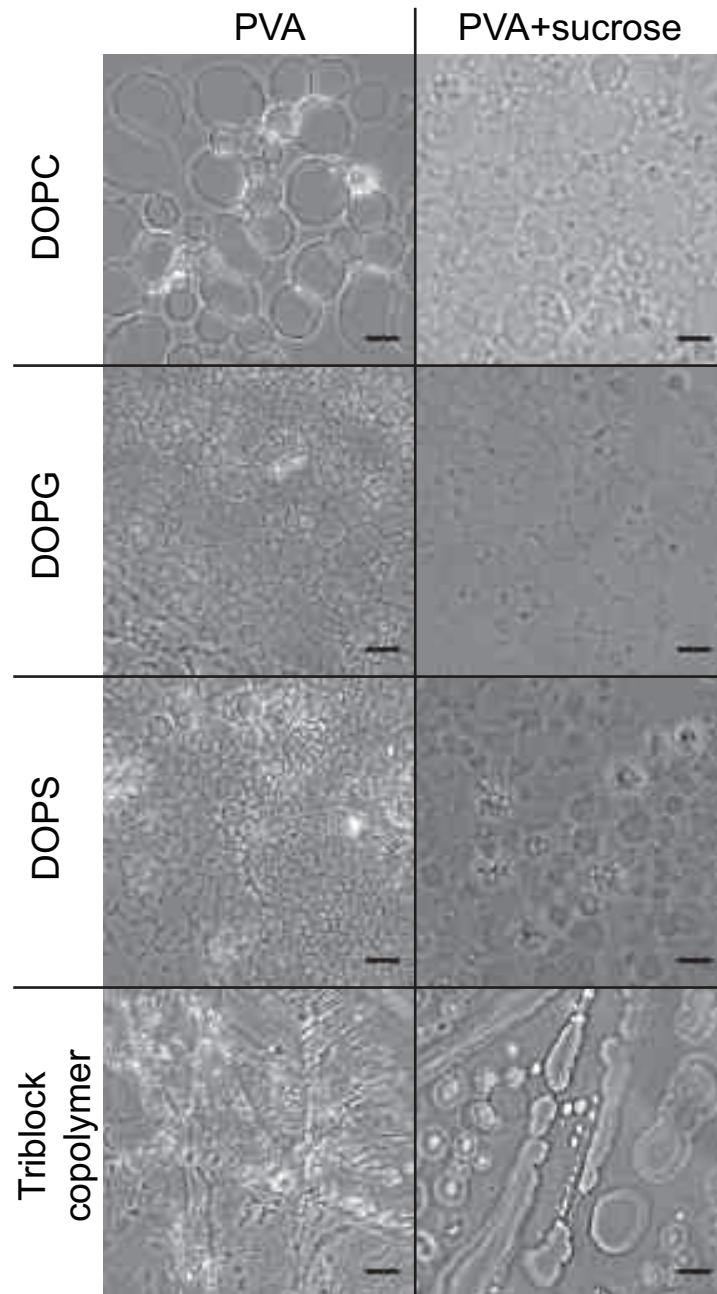


Figure 4.13: Phase contrast images of GUVs formed from different amphiphiles. Left column: growth on pure PVA gel. Right column: growth on a PVA gel containing sucrose. Amphiphiles: DOPC, DOPG, DOPS and triblock copolymer (PMOXA₁₀-PDMS₈₇-PMOXA₁₀). Swelling solution: PBS. Scale bars 20 μm .

Interestingly, in the case of DOPS on pure PVA, tubular vesicles could be observed in the first few seconds of swelling (compare Figure 4.14), that disappear over time to form spherical vesicles instead. None of the other lipid cases showed this behavior. Tubular vesicles were also observed for the triblock copolymer (PMOXA-PDMS-PMOXA) on pure PVA, but here they did not lead to spherical polymersomes, a structure which could only be observed on PVA containing sucrose. Nonetheless the formation of polymersomes yielded in a fewer number of GUVs compared with phospholipids.

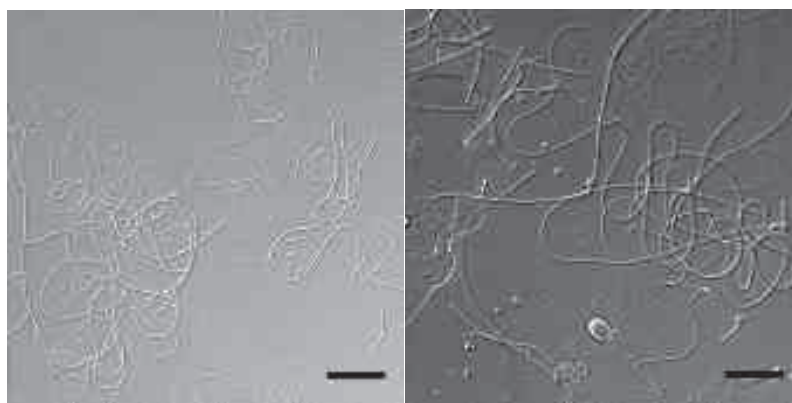
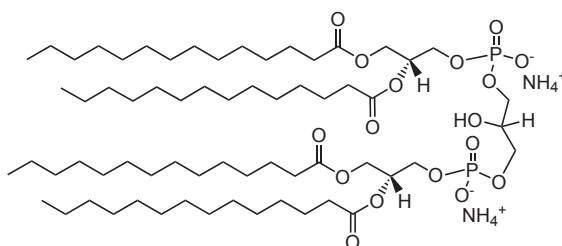


Figure 4.14: DIC images of tubular vesicles of DOPS, formed in the first few seconds on PVA substrate, that disappear over time to form spherical vesicles instead. Swelling solution: PBS. Scale bars 20 μm .

We also investigated lipids with more than one charge per head group. A particularly relevant example is cardiolipin, a lipid containing four lipid tails and two negatively charged headgroups, see Figure 4.15.

Figure 4.15: Chemical structure of the cardiolipin used in this study. This phospholipid possesses four C-14 tails and two negative charges in the phosphate headgroups.



Although GUVs containing up to 50 % cardiolipin in DOPC/cardiolipin mixtures can be grown by electroformation, we find that the structures obtained systematically display defects, similar to those observed by Fedotenko et al. [146], which may be caused by head group degradation from the applied electric field (Figure 4.16 A). The PVA-assisted swelling method allows us to form defect-free GUVs within minutes, even from 100 % cardiolipin (Figure 4.16 B and C).

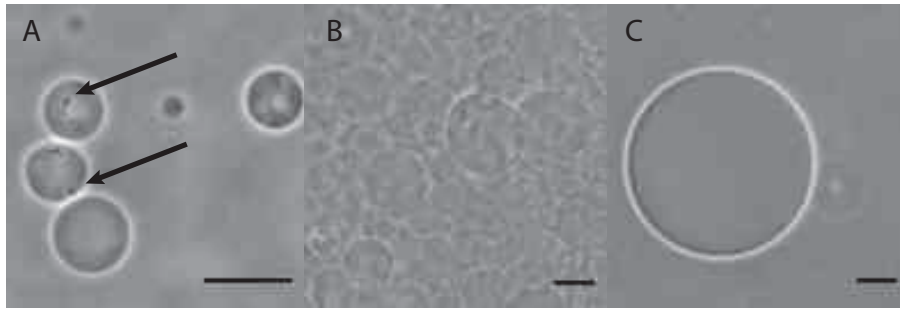


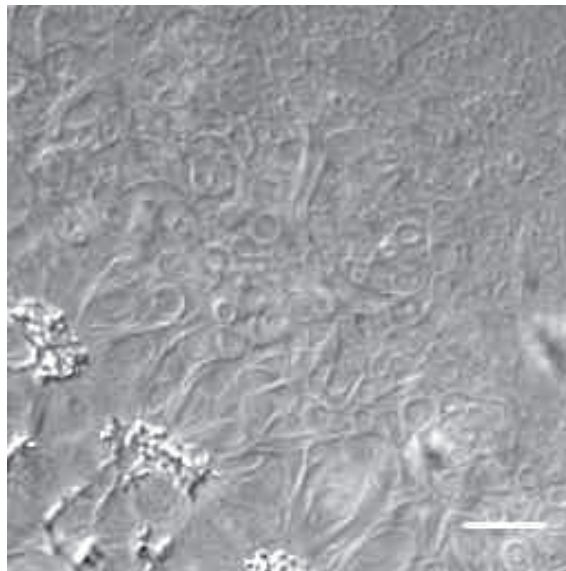
Figure 4.16: (A) Vesicles of 1:1 DOPC/cardioliipin mixtures grown by electroformation. Arrows show vesicle defects. (B) cardioliipin vesicles on the PVA gel after growing. (C) cardioliipin vesicles after dispersion in PBS. Images were recorded in phase contrast mode. Swelling solution: sucrose. Scale bars 20 μm . Experiments were performed by Thais Schmidt.

The PVA swelling method can also be performed at temperatures different from room temperature. For instance, one can obtain DPPC vesicles by swelling with preheated buffer in a heated chamber at 50 $^{\circ}\text{C}$ or DOPC vesicles by swelling in the fridge at 4 $^{\circ}\text{C}$. For high temperatures, the only limitation is the preservation of gel integrity.

Indeed, depending on PVA molecular mass, some of the polymer can dissolve upon heating, thus leading to lower yields and GUV contamination. The PVA used in this work, in the range of 145 kDa, does not dissolve at room temperature but partially dissolves if exposed for more than half an hour at temperatures above 50 $^{\circ}\text{C}$. When lower molecular weight PVA is used, around 16 kDa, partial dissolution is already observed at room temperature. It is also possible to successfully grow GUVs composed from sphingomyelin and cholesterol in a range where this lipid mixture is in the liquid ordered phase, however a complete study of the conditions under which GUVs from domain-forming ternary mixtures can be grown by the gel method is beyond the scope of this thesis.

Tests to improve the temperature-stability of the PVA-gel, thus leading to an even broader range of lipid compositions, involved chemical cross-linking of the PVA gel. For first tests, polyacrylic acid was mixed with PVA, which upon drying in the oven results in cross-linking of the hydroxylic groups of the PVA with the carboxylic group of the polyacrylic acid. Hydration of a DOPC lipid stack on this substrate leads to formation of onion-like multilamellar structures (compare Figure 4.17). Low degree of swelling of the formed copolymer did not lead to the formation of unilamellar vesicles. Hence, the degree of cross-linking, which in turn influences the degree of swelling, has to be carefully balanced to achieve stability without compromising efficiency of GUV formation. Other tests with UV-cross-linkable hyaluronic acid or a small amount of glutaraldehyde seem also to lead to unsatisfactory results.

Figure 4.17: Multilamellar structures of DOPC were observed when a PVA-PAA substrate was used. Images were recorded in DIC mode. Scale bars 20 μm



Careful tuning of the system composition, such as the introduction of a small fraction of PEGylated lipids [55], or better spreading of the precursor film by spin-coating [83], have been reported in the literature to improve the yield of GUVs containing charged head groups and to facilitate detachment from the growing surface. Similar results have been observed in our case for gel-assisted growth.

Although we have not precisely quantified the yield of vesicles swollen on the gel, for charged lipids the number and average size of vesicles is higher in the gel swelling method than in the electroformation method. In both methods i.e. with the electroformation method and with the gel swelling method, a high number of vesicles could be obtained for neutral lipids.

A common problem with charged lipids is that vesicles do not detach easily from the growing surface after formation by simple pipetting of the buffer solution. We found that detachment can be improved by several different strategies. Sonication for 1-2 seconds in a standard ultrasound bath (35 kHz, HF-power 80 W), for instance, detaches a significant number of GUVs, enough for obtaining diluted vesicle samples of typically a couple of hundred GUVs. Also, if a sugar such as sucrose is added to the gel, a larger number of vesicles spontaneously detach during the formation process. This can be due to the extra osmotic pressure from the sugar dissolving from the gel that pushes away the membranes [61].

In summary, we have shown that the PVA swelling method can successfully deal with different classes of lipids which are otherwise difficult to grow, the method being in particular well adapted for charged lipids.

4.6 Encapsulation of proteins

The PVA gel formation method is advantageous for encapsulating many molecular species of biological relevance that are often prone to react at room temperature e.g. cross-linking or degradation due to peroxidation caused by electric fields [88].

This encapsulation experiments and sample preparation were performed in our laboratory within a collaborative project with Feng-Ching Tsai, a PhD-student of Gijsje Koenderink from the AMOLF institute in Amsterdam. We first tested the ability of this method to encapsulate the molecules required to reconstitute a simple biomimetic cytoskeleton inside a GUV. In all these experiments 5 % of DOPC lipid was substituted by PEGylated lipids (PEG-PE), which proved to be beneficial for GUV formation [55]. To encapsulate actin filaments, DOPC-GUVs were grown at 4 °C.

As shown in Figure 4.18 actin filaments were successfully incorporated in vesicles and bundles formed if the swelling solution contained additional cross-linker. Similar actin structures have been shown by swelling on agarose gels [142]. However, in this case the vesicles are contaminated by agarose, which adheres to the membrane.

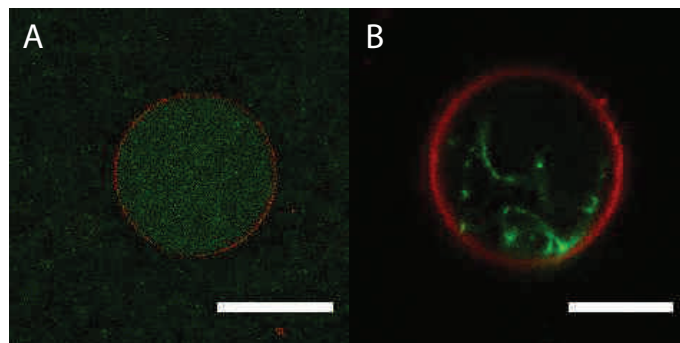


Figure 4.18: CLSM images of DOPC-GUVs grown by PVA swelling at 4 °C from 94.8:0.2:5.0 DOPC/RhodB-PE/PEG-PE mixtures. (A) Encapsulated actin filaments in the interior of the GUV. (B) Actin bundles inside the GUV, formed by adding of streptavidin with an actin/streptavidin ratio of 25:1 as a cross-linker. Scale bars 20 μm .

It is often desirable to control the anchoring of encapsulated molecules to the vesicle membrane. A convenient way to achieve anchoring is to use biotinylated lipids (biotin-PE), which enables anchoring to biotinylated species by neutravidin. We can localize neutravidin specifically on the membrane by combining the PVA swelling method with the inverse-phase precursor method, which allows complexation of lipids with neutravidin. Inverse-phase precursor films were already successfully used for the encapsulation of large hydrophilic molecules during electroformation [85]. As shown in panel B of Figure 4.19, GUVs grown from a precursor film containing neutravidin have a neutravidin functionalized membrane.

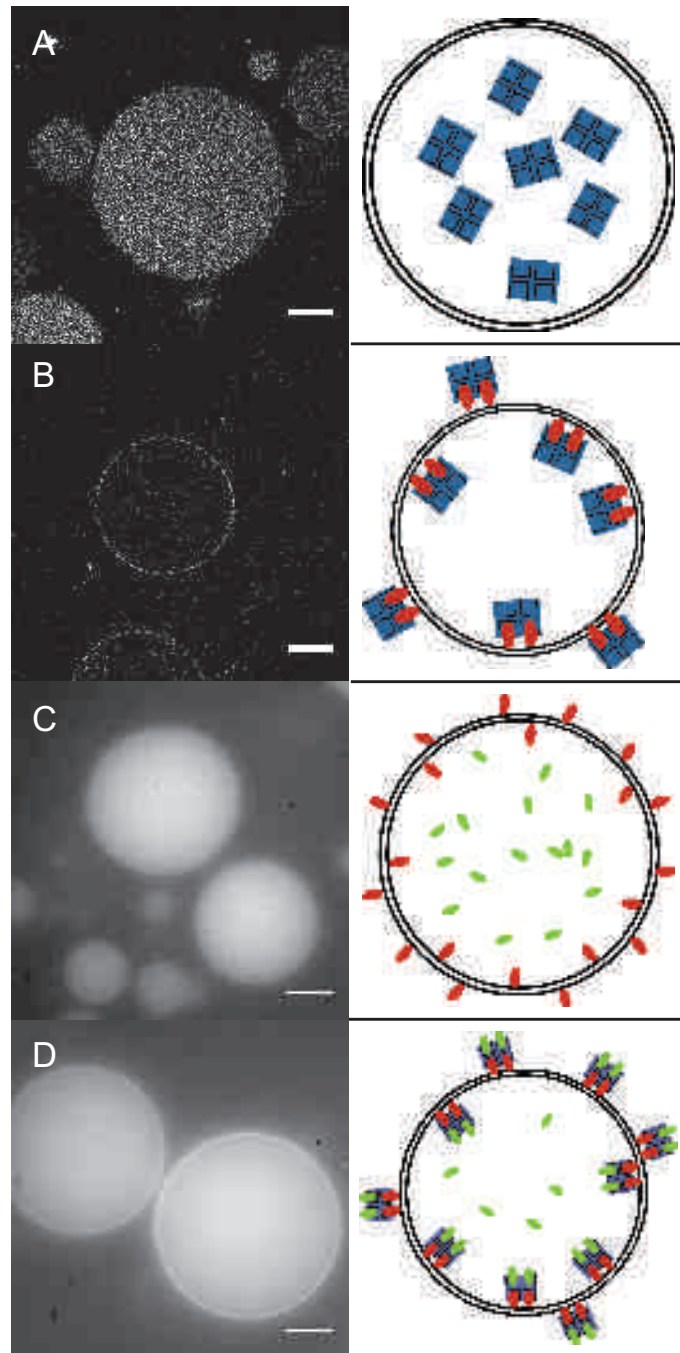


Figure 4.19: CLSM images of DOPC-GUVs grown by a combination of PVA swelling and the inverse-phase precursor method [85] from 94.8:0.2:5.0 DOPC/RhodB-PE/PEG-PE mixtures. (A) In the absence of biotinylated lipids, AF350 labeled neutravidin is homogeneously distributed in the vesicle interior. (B) In the presence of 1 % biotinylated lipids, AF350 labeled neutravidin binds to the membrane. (C) In vesicles swollen in a solution containing 500 nM fluorescently labeled biotin, the biotin is homogeneously distributed inside the vesicle interior in the absence of membrane-bound neutravidin. (D) Vesicles were formed as in (C) but with neutravidin on the membrane surface. The encapsulated biotin-fluorescein binds to the membrane anchored neutravidin, resulting in a bright ring of fluorescent-biotin. The right column displays sketches of the systems in the left images: The membrane is represented by black lines, biotinylated lipids by red rods, fluorescein-biotin by green rods and neutravidin by a blue square. Scale bars 20 μm .

In the absence of biotinylated lipids, the neutravidin is in the vesicle interior, as shown in panel A. The neutravidin is still functional, as shown by encapsulation of fluorescently labeled biotin. When neutravidin is on the membrane, fluorescent biotin forms a bright ring, signifying binding to neutravidin (panel D). In the absence of membrane-bound neutravidin, fluorescent biotin is found throughout the vesicle (panel C).

4.7 A growth scenario

In order to understand how the efficiency of encapsulation of water-soluble (bio)molecules in the vesicles can be optimized, one needs to gain a deeper insight into the mechanisms of vesicle formation during gel swelling. When a film of DOPC is spread from a chloroform solution on a glass slide and subsequently hydrated in an aqueous solution, one can observe the spontaneous formation of bilayer structures with a majority of multilamellar vesicles [147]. The left drawing of Figure 4.20 shows the possible pathways for water penetration into the stacks of preordered phospholipid bilayers on glass.

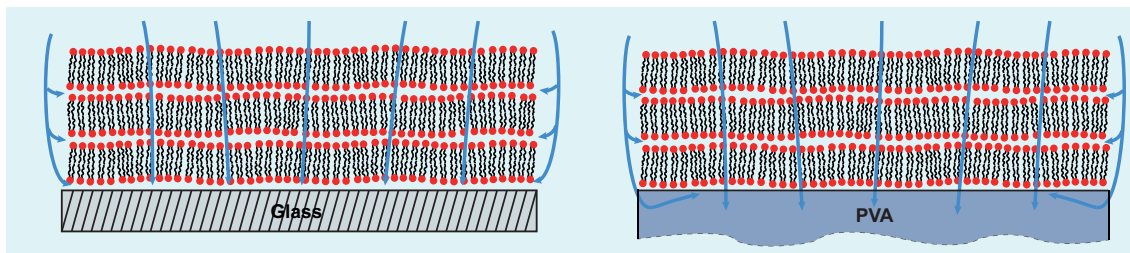


Figure 4.20: Schematic illustration of water penetration pathways through a bilayer stack deposited on glass and PVA gel.

There are two main water transport modes. First, the water can access the inter-lamellar region from the edges and swell the stack, a feature easily observed using differential interference contrast (DIC) microscopy [80]. A second pathway for water transport is by direct membrane permeation, since phospholipid bilayers display a finite water permeability in the order of $160 \mu\text{m s}^{-1}$ [41]. Direct permeation can generate swollen structures of tens of micrometers in a few seconds.

The right drawing of Figure 4.20 shows the pathways of water penetration during swelling of a preordered bilayer stack on the surface of a dry PVA gel. The most prominent difference from the case of swelling on glass is related to water-uptake by the PVA gel: indeed a strong chemical potential gradient exists between the outer solution and the dry gel which drives water across the bilayer stack. As a consequence of gel swelling, the capillary forces driving water at the membrane-gel interface are

modified. This effect is further amplified by gel stretching and by gel surface corrugation, which may increase the number of membrane defects for water access. These different solution transport mechanisms are likely to display different degrees of selectivity with respect to aqueous solutions containing other molecules or nano-particles. We argue that the differences previously observed in encapsulation efficiencies as a function of molecular size and growing methods [63, 65, 142, 148, 149] are due to the respective importance of different water penetration pathways in the final aqueous content of GUVs.

In order to discriminate between the effects of different water penetration pathways on encapsulation efficiency, we performed two comparative experiments. In the first, we formed vesicles by swelling lipids on a PVA gel with a solution containing fluorescein. In the second, we formed vesicles by swelling a PVA gel preloaded with fluorescein with a non-fluorescent solution. The formed vesicles were transferred in glucose as outside buffer and the fluorescence intensity inside the vesicle was measured. Figure 4.21 shows a typical confocal image recorded after transfer in the dilution buffer. We also recorded the fluorescence intensities of fluorescein solutions at different concentrations on a fluorospectrometer to ensure that the experiments were performed in a concentration range of fluorescein, where self-quenching does not occur. Self-quenching of fluorescein occurs above a concentration of $30 \mu\text{mol L}^{-1}$, experiments were performed below a concentration of $2 \mu\text{mol L}^{-1}$ of fluorescein (compare Figure 4.21).

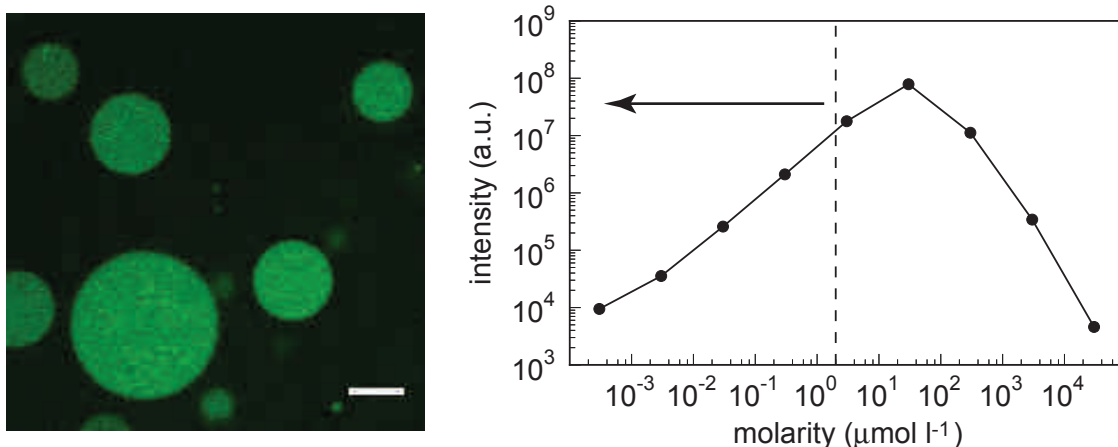


Figure 4.21: Left side: characteristic CLSM image from GUVs swollen with a fluorescein containing solution. Comparable images were also recorded from GUVs swollen on a fluorescein-preloaded PVA gel. Scale bar 20 μm . Right side: Self-quenching effect of fluorescein above a concentration of $30 \mu\text{M}$. Typical experiments were performed with a total fluorophor concentration below $2 \mu\text{M}$, represented by the dashed line.

Figure 4.22 A displays the fluorescence intensity of vesicles grown from a fluorescent solution whose average fluorescence intensity of the swelling solution is indicated by the arrow. The fluorophore content of the vesicles is roughly 50 % of that of the swelling solution, comparable to encapsulation efficiencies reported in the literature [65, 142]. This result suggests that on average roughly half of the water content inside the GUVs is due to solution transport across the membrane, which is impermeable to the fluorophore.

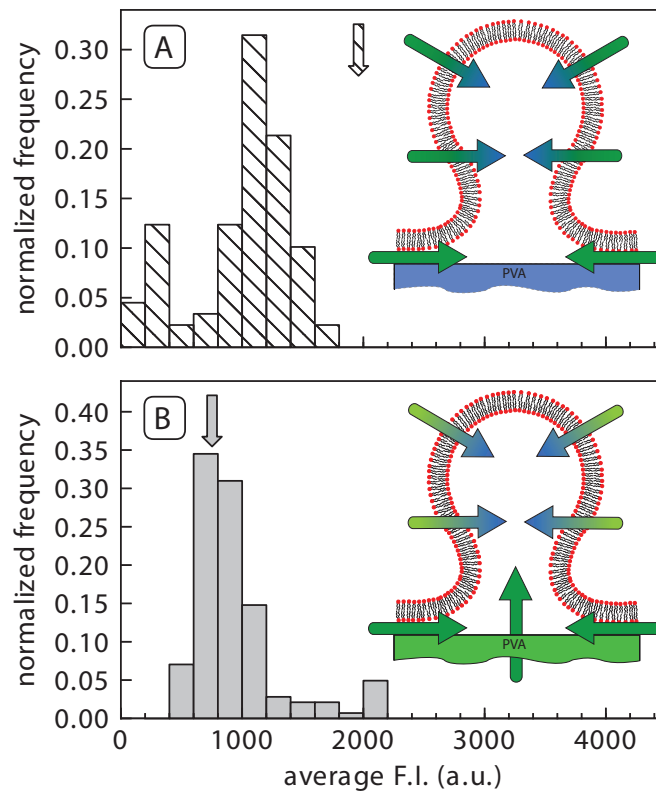


Figure 4.22: CLSM measurements of the average internal fluorescence intensity of GUVs grown on a PVA gel. (A) Vesicles swollen with a solution containing fluorescein. The average solution intensity is denoted by the arrow. (B) Vesicles swollen with a non-fluorescent solution on PVA gel loaded with fluorescein. The arrow indicates the fluorescent intensity of the solution after the fluorophore diffused from the gel. Histograms built from 89 vesicles for (A) and 142 vesicles for (B). Vesicles smaller than 5 μm in diameter were neglected.

Figure 4.22 B shows fluorescence levels from GUVs grown on a fluorophore-loaded gel. The arrow indicates the average fluorescence intensity of the swelling solution after the swelling process took place. Solution volumes used in both experiments were comparable, but the total amount of fluorophore in the second experiment was ca. 2.5 times smaller than in the first one, which corresponds to the ratio of the average fluorescence intensities of the two solutions. As the histogram in figure B

shows, the encapsulation efficiency is higher when the PVA gel is preloaded with fluorophore. As sketched in the inset, we propose that this is due to a direct transport of fluorophore from the gel reservoir to the growing vesicle and not only from side penetration through defects.

Our findings thus suggest that membrane permeability is an important parameter determining vesicle growth by gel swelling. Indeed, the water permeability of DOPC is circa $160 \mu\text{m s}^{-1}$ [41], while the water permeability for typical polymersomes was reported to be of the order of $2.5 \mu\text{m s}^{-1}$ [35]. This is likely an important factor which can explain why the yield of polymersomes grown by swelling is lower than the yield of liposomes. Furthermore, permeability plays a role in the final composition of solutions encapsulated in GUVs, by determining the relative importance of the different possible water penetration pathways.

4.8 Summary: GUV formation on PVA-gel

The following table 4.1 tries to summarize all of the observed and tested cases, which lead to GUVs.

Temperature	Description	Buffer	Modifications
RT	DOPC Cardiolipin 60 % Sphingomyelin/ 35 % Cholesterol	Sucrose	Spin-coating PEGylated lipids
RT	DOPC DOPG DOPS DOTAP PMOXA-PDMS-PMOXA*	PBS	Pure PVA Sucrose in PVA PBS in PVA
4 °C	Actin encapsulation in DOPC-GUVs	I-buffer	Spin-coating PEGylated lipids
RT	Neutravidin encapsulation in DOPC-GUVs	I-buffer	Spin-coating PEGylated lipids
50 °C	DPPC	Sucrose	

Table 4.1: Summary of successfully grown lipid species and experimental conditions for PVA-assisted swelling. *Low yield of GUVs.

Substitution of a pure lipid by fluorescently-labeled and biotinylated lipid in the range of 5 % does not reduce the yield, adding a small amount of pegylated lipids can even increase the yield. Spin-coating of the PVA film or the lipid mixture can further

increase the yield. However, spin-coating increases the amount of lipids needed and adds as well additional preparation time, which can often be avoided.

Success is generally obtained for mixtures composed of two pure lipids with at least 50 % of a lipid that can be successfully grown by this method. In cases of synthetic lipids which were not able to form GUVs in their pure form (see chapter 5), GUVs could be grown with a maximum of 20 % of these lipids by utilizing PVA-assisted swelling.

For all tests, adding salt (PBS) or sugar (sucrose) in the precursor film of the PVA, helped to improve the efficiency of GUV formation. PVA containing sucrose leads typically to the highest amount of formed GUVs.

Note that in all cases, PVA swelling has to be performed above the main transition temperature of the main lipid, in order to be able to form GUVs.

4.9 Conclusions

Gel-assisted formation of giant unilamellar vesicles on PVA allows for an easy and rapid growth of polymer-free GUVs in high yields without the need for special equipment. The process works for many different lipid mixtures, covering a wide range of lipids with one or more head groups of zwitterionic, cationic or anionic nature. Due to the ability of PVA to swell at low temperatures close to the freezing point of water, the method is well adapted for the encapsulation of biomolecules such as actin, which can be encapsulated in monomer form at low temperature and subsequently polymerized by warming the vesicles to room temperature. Importantly, no input of energy is required to form GUVs, which minimizes the risk of degradation of the amphiphiles and of the proteins for membrane embedment or vesicle encapsulation.

Furthermore, we found experimentally that the gel formation process can be combined with inverse-phase precursor films to improve the encapsulation efficiency or localize (bio)molecules specifically to the membrane surface. Our method provides also a natural way to improve encapsulation efficiency of small hydrophilic molecules by pre-dissolving them in the PVA gel.

Our results point to different penetration pathways involved in the swelling of membrane stacks by the aqueous solution. Part of the swelling originates at the defects in the membrane, where water can invade the interlamellar spacing. But a significant amount of water also penetrates by direct permeation across the bilayers. This confirms the importance of bilayer water permeability in the formation of GUVs. For polymersomes too, osmotic imbalance generated by added sucrose improves conditions for vesicle formation.

PVA-assisted formation of GUVs provides a new route to prepare GUVs in a membrane laboratory. Although we have prepared small scale samples, the method has potential for large scale production and can be easily automated. Current work in our group, exploring new lipids and buffer compositions, points to an application range of this method beyond the one reported here.

Artificial lipids

In this chapter we study two new classes of bilayer-forming lipids, for which membrane assembly into GUVs is difficult or impossible with the classic electroformation method. For these lipids, development of the gel-assisted formation method discussed in chapter 4 was essential.

In the first part we investigate the membrane assembly potential of molecules designed and synthesized within the framework of the International Research Training Group (IRTG): “Soft Matter Science - Concepts for the Design of Functional Materials”. Glycolipids were synthesized by Nehrukumar Mathaiyan in the group of Stefan Schiller in Freiburg (Germany). The work presented here is preliminary in nature but conclusive in many aspects. It certainly confirms the potential of these lipids and points to relevant design rules.

In a second part we study amide-bearing phospholipids synthesized in the group of Andreas Zumbuehl in Fribourg (Switzerland). Such lipids display shear sensitivity with important potential applications in drug delivery.

5.1 Synthetic glycolipids

5.1.1 Introduction

Glycolipids, lipids with a carbohydrate residue attached, are found exclusively in the outer (mono)layer of the membranes, generally close to 5 mol%. The exact biological functions of glycolipids are still not clear, but it is suggested that glycolipids help cells to bind to the extracellular matrix. They are also thought to function in cell-recognition processes and might play a role in electrical insulation [14]. Bound carbohydrates

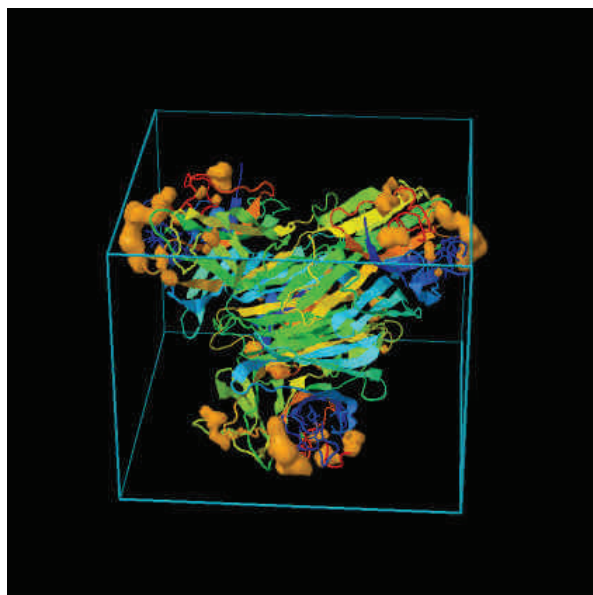


Figure 5.2: 3D model of a concanavalin A tetramer, showing the cavities in orange at the corners of a tetraeder. Image from the RCSB Protein Data Bank: <http://www.rcsb.org/>.

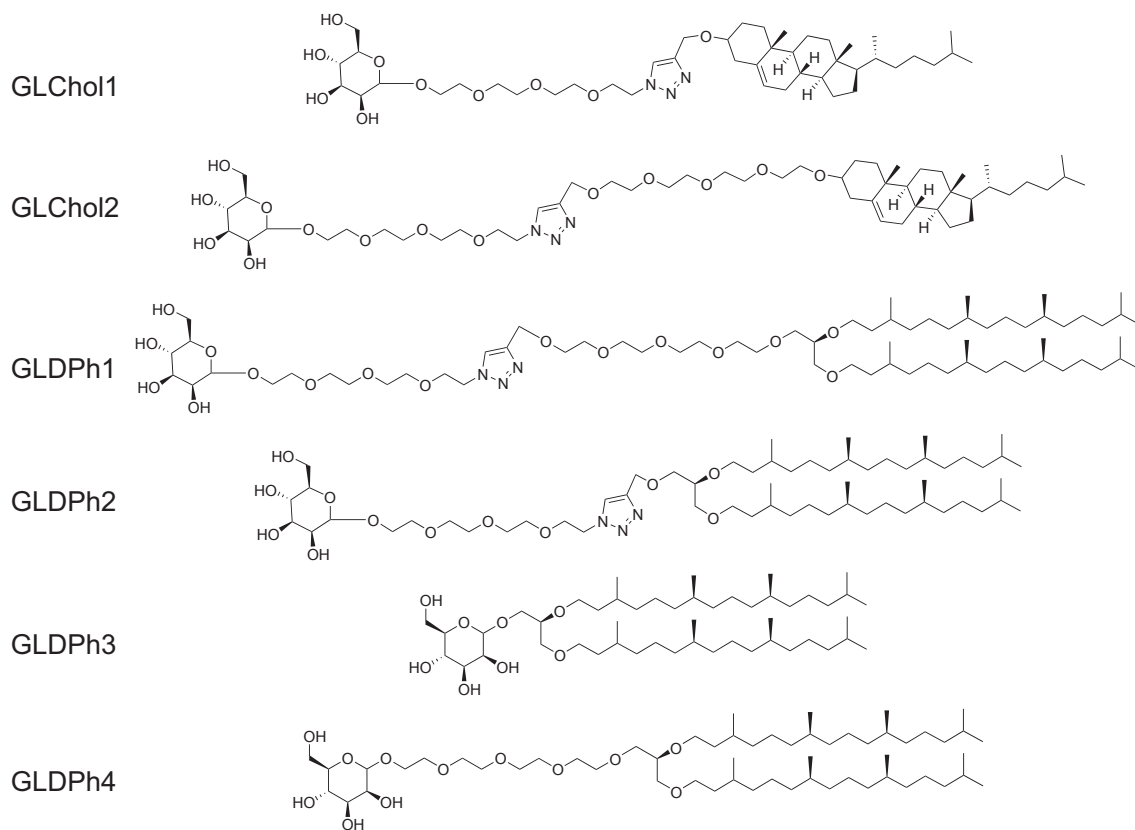


Figure 5.3: Glycolipids synthesized by Nehrukumar Mathaiyan in the group of Stefan Schiller in Freiburg. GLChol1, GLChol2, GLDPh1 and GLDPh2 were synthesized via the same synthetic route, GLDPh3 and GLDPh4 by a different route.

Figure 5.3 shows the glycolipids synthesized by Nehrukumar Mathaiyan in Freiburg. Standard nomenclature of these lipids is too complex and therefore a simplified nomenclature is required. For this manuscript lipids were named by an abbreviation for glycolipids (GL) and then adding an abbreviation for the hydrophobic moiety, Chol for cholesterol and DPh for diphytanoyl, plus a number to distinguish different lipids of the same class. As further discussed in chapter 1 naming of lipid based on the abbreviation of the fatty acid plus an abbreviation for the chemical linker was suggested for new synthetic lipids. Based on these suggestions a nomenclature is proposed in the following way: an abbreviation for the lipid tails as already established, followed by abbreviations for the linker in the order of occurrence starting from the tails and finally a three letter code for the sugar head group. For lipid GLChol1 following this system a suggested name of Chol-TAz-EO₄-Man is obtained, with Chol for cholesterol, TAz for the triazol ring, EO₄ for a tetramer of ethylenoxide and Man for mannose. This system can be applied to all of the lipids leading to unique names. Table 5.1 lists the molecular weights and name suggestions for the synthesized lipids.

Abbreviation	Suggested name	M (g mol ⁻¹)
GLChol1	Chol-TAz-EO ₄ -Man	806.08
GLChol2	Chol-EO ₄ -TAz-EO ₄ -Man	982.29
GLDPh1	DPh-EO ₄ -TAz-EO ₄ -Man	1248.79
GLDPh2	DPh-TAz-EO ₄ -Man	1072.58
GLDPh3	DPh-Man	815.3
GLDPh4	DPh-EO ₄ -Man	991.51

Table 5.1: Glycolipids with a name suggestion and their molecular weights. Abbreviations: cholesterol (chol), triazol (TAz), ethylene oxide tetramer (EO₄) and mannose (Man).

In the next chapter the experimental methods used to investigate these new glycolipids are described.

5.1.2 Experimental methods

In a first step, the ability to form GUVs composed from 100 % of GLDPh1 to GLDPh4 was investigated. Formation of GUVs was performed utilizing PVA-assisted swelling as described in section 2.2.3. Briefly, 200 μL of 5 wt% solution of PVA containing 100 mM sucrose was spread on a glass slide and dried in the oven at 50 °C for 30 min. 10 μL of the lipid solutions (1 mg mL⁻¹ in CHCl₃) of the glycolipids in Figure 5.3 were spread on top of it. After drying for 30 min in the desiccator to completely remove chloroform, GUV formation was initiated by addition of a PBS buffer solution containing 1 mM of Ca²⁺ and Mn²⁺ ions. GUV formation in the formation chamber was observed in Phase Contrast or Differential Interference Contrast.

When growing of GUVs was observed in the formation chamber, GUVs were transferred into an observation chamber containing PBS. To test the accessibility of the mannose heads, FITC labeled ConA was added. Adhesion of the FITC-ConA was observed by confocal microscopy. Typically, 80 μL of the vesicle containing solution was transferred in a chamber containing 300 μL of the PBS buffer. To this solution, 50 μL of a FITC labeled concanavalin solution (2 mg mL^{-1}) was added, leading to a total concentration of $2.3 \mu\text{M}$ ConA homotetramer in the sample.

When successful growth of GUVs made from pure lipid compositions was achieved, GUV mixtures with different amounts of DPhPC were prepared and the experiments repeated. Additionally, GUVs of DPhPC containing approximately 15 mol% cholesterol-containing lipids (GLChol1 and GLChol2) were prepared. As a control experiment, pure DPhPC-GUVs were formed and tested for binding with ConA.

To be able to directly compare different experiments with each other, confocal settings were kept at the same values for all experiments. Table 5.2 lists the used settings.

Gain	100
Laser intensity	1 %
Pinhole size	L
Field zoom	1x (212 μm)
Pixel dwell	5.52 μs

Table 5.2: Confocal microscopy settings for experiments performed with FITC-labeled ConA.

5.1.3 Results

Ability of glycolipids to form pure stable GUVs. Three out of the four glycolipids with two phytanoyl tails formed GUVs with the PVA-assisted swelling method. Only GLDPh2 (for abbreviations compare Table 5.1) did not lead to any GUVs in the formation chamber. Figure 5.4 shows images recorded in the formation chamber.

However, only GLDPh1 formed vesicles that could be successfully transferred into an observation chamber filled with PBS. FITC-labeled ConA was added to test for active mannose head groups. Immediately after addition of FITC-ConA a corona could be observed around the GLDPh1 GUVs. This indicates a successful binding of ConA to the mannose heads of the lipid. With pure DPhPC-GUVs as a control experiment, no corona could be observed (Figure 5.5).

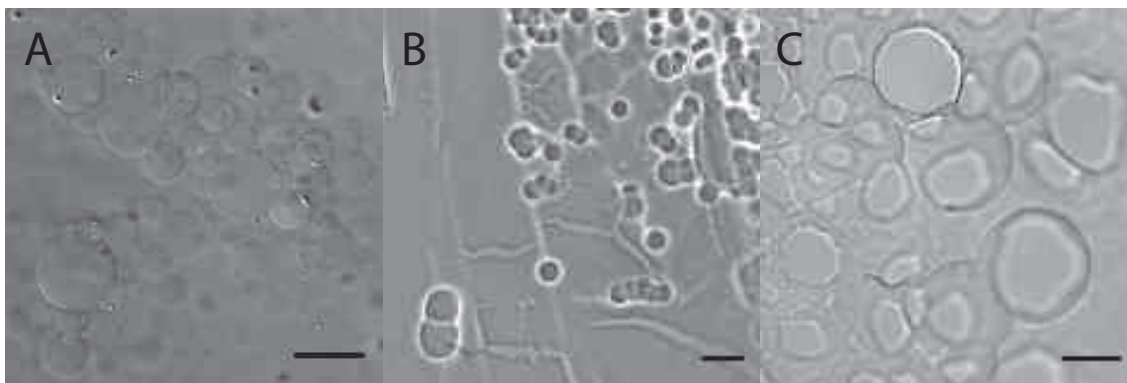
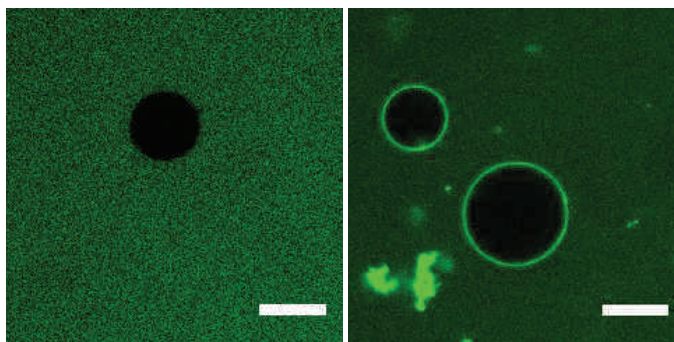


Figure 5.4: GUVs could be observed in the formation chamber for vesicle composed from (A) 100 mol% GLDPh1, (B) 100 mol% GLDPh3 and (C) 100 mol% GLDPh4. Images were recorded in DIC mode (A+C) and phase contrast mode (B). Scale bars 20 μm .

Figure 5.5: Left: Pure DPhPC-GUVs do not show a corona, because ConA only binds specifically to mannose groups. Right: FITC-labeled ConA can bind to pure GLDPh1 GUVs. Scale bars 20 μm .



Glycolipids with cholesterol It was not expected that the cholesterol containing glycolipids GLChol1 and GLChol2 form stable bilayers on their own. Therefore, mixtures containing approximately 15 mol% of these lipids with DPhPC were prepared, see Figure 5.6. In both cases GUVs could successfully be transferred into the observation chamber.

To test the accessibility of the mannose head group, GUVs were dispersed in PBS buffer containing FITC-ConA. In the case of the glycolipid possessing the longest linker (GLChol2) mannose can be bound to the ConA, see Figure 5.7.

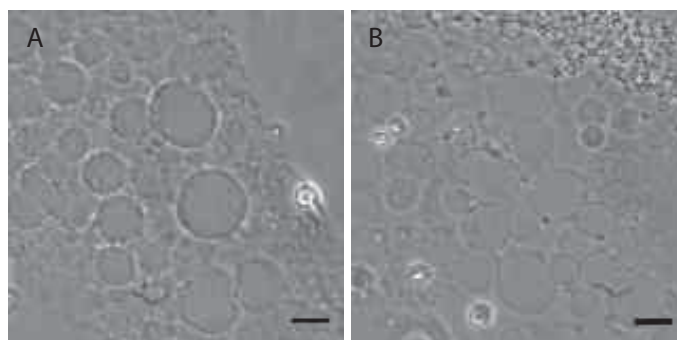


Figure 5.6: (A) GUVs grown from a mixture of DPhPC : GLChol1 = 83.7 : 16.3. (B) GUVs grown from DPhPC : GLChol2 = 85.6 : 14.4. Images were recorded in phase contrast mode. Scale bars 20 μm .

Importance of the linker length. One important feature to investigate is the importance of the length of the linker between the head group (mannose) and the lipid (cholesterol or diphytanoyl). It becomes immediately clear that longer linkers are beneficial.

For instance, for GLDPh2 no GUVs could be observed in the growing chamber, whereas for GLDPh1 numerous GUVs could be obtained and transferred in a high number. For GLDPh3 only small GUVs in the range of 10–20 μm in diameter could be observed, whereas for GLDPh4 vesicles of twice the size could be observed. However, in both cases GUVs composed from 100 % of these lipids seem to be unstable, GUVs could not be successfully transferred into the observation buffer.

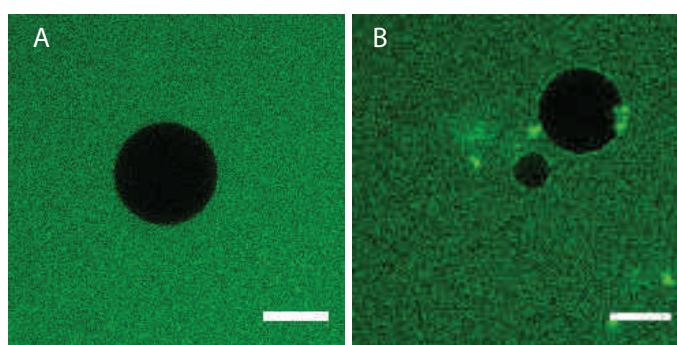


Figure 5.7: (A) GUV containing 16.3 mol% GLChol1. ConA cannot bind to the mannose head group (B) GUVs containing 14.4 mol% GLChol2. Corona formed by binding of FITC-ConA to the mannose head group. Scale bars 20 μm .

As seen in Figure 5.7, FITC-labeled ConA can only bind successful to glycolipids with a long linker (GLChol2).

To summarize, the length of the linker between headgroup and lipid tails seems not

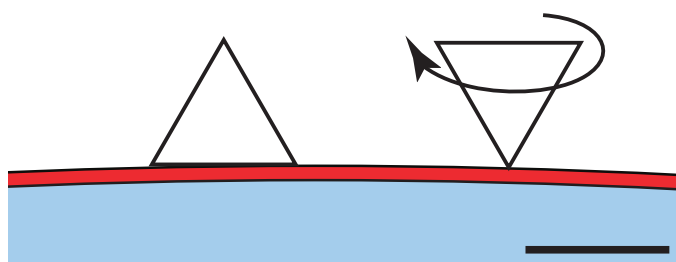
only to be beneficial for forming a stable bilayer, but also crucial for binding of proteins to glycolipids embedded into a membrane.

Binding of ConA with different glycolipid content. The ability to control the amount of glycolipid in the bilayer by tailoring the initial lipid mixture was tested in a last experiment. Upon binding of ConA, higher amounts of glycolipids should lead to higher values for ConA in the corona. GLDPh1 in mixtures with DPhPC was used.

A radial profile was drawn across the GUV and the area under the peak integrated, as already described in chapter 3.1. By relating the integrated area to the concentration of ConA in the buffer, the amount of lipids per ConA sub-unit can be calculated. From our experiments values between 100 and 300 lipids per ConA were obtained.

The dimensions of a ConA protomer (sub-unit) are 4.2 nm x 4.0 nm [153]. As shown in Figure 5.2, the ConA homotetramer, assembled from four ConA protomers, assumes a tetrahedral geometry, with cavities for binding of mannose residues at corners of the tetraeder. If it is assumed that the base of the tetrahedron is a equilateral triangle with a projected area of 28 nm². Assuming a full coverage of the outer membrane by the triangular base of the tetrahedron, ratios of approximately 40 lipids per ConA tetrahedron (homotetramer) are obtained, taking for the headgroup area the one of a phosphocholine (0.75 nm²), compare Figure 5.8.

Figure 5.8: Schematic illustration of possible confirmations of ConA bound to glycolipids inserted in membranes. (Left) ConA is attached to glycolipids in such a way that the triangular base is oriented on the membrane. (Right) ConA is attached at the tip of the tetraeder, able to freely rotate around the tether. Scale bar 8 nm.



As mentioned above, we obtained values between 100 and 300 lipids per ConA sub-unit. This difference can be only explained by the fact that ConA more likely binds to the glycolipids with the tip of the tetraeder and that this tetraeder is able to rotate freely around the tether. In this case an area of around 200 nm² is occupied by rotation of the ConA protein, giving values of around 270 lipids per ConA homotetramer. This corresponds to a mean distance of 16 nm between the ConA tetramers.

Binding to the tip of the ConA tetramer means binding to one ConA sub-unit only, thus

the number of lipids per ConA sub-unit is equal to the number of lipids obtained from our evaluation in the experiments with fluorescent ConA.

Figure 5.9 shows the number of lipids per ConA sub-unit as a function of amount of glycolipids in the prepared GUVs. The green triangle relates to a study on GUVs with 15 mol% of mannose-bearing lipids. This value corresponds to the theoretical value for a rotating tetrahedron, corresponding to a mean distance of 16 nm between the glycolipid that acts as a tether for the ConA homotetramer. With higher amounts of glycolipids, above 25 mol%, the ability to rotate becomes hindered, leading to lower values of lipids per ConA homotetramer and a decreased mean distance of around 10 nm.

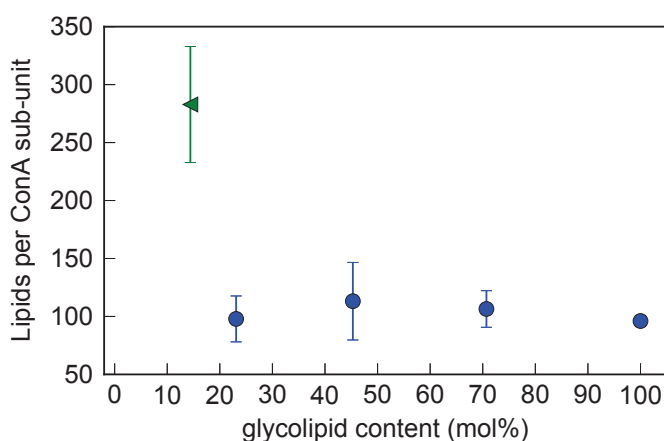


Figure 5.9: Number of lipids per ConA sub-unit with different glycolipid concentrations in the membrane. Blue circles are mixtures of GLDPh1 and DPhPc. The green triangle is obtained for the mixture of GLChol2 with DPhPC.

5.1.4 Conclusions

In this section it was shown that the length of the linker is crucial for both the formation of stable bilayers and the accessibility of the mannose headgroup of glycolipids. One may suggest that the length of the linker has also a big influence on the ability of ConA to rotate around the lipid tether.

These preliminary experiments on glycolipids with a tailored sugar spacer opens many interesting perspectives. The strength of the ConA/sugar interactions can be systematically studied by varying glycolipid fraction on mixed GUVs and ConA concentration.

This would allow not only to study the order and strength of the sugar ConA reaction but also to test for the role of spacer length.

5.2 Amide-bearing phospholipids

5.2.1 Introduction

In nature a nearly endless variety of phospholipids can be found and scientists are only starting to comprehend why this diversity is needed [154]. Nature focused on lipids made from interchangeable parts, if the head groups or fatty acids are exchanged against another one, a lipid with completely different properties can be obtained. This opens a door in the field of lipidomic chemistry, new classes of lipids may be synthesized, which allow new perspectives and unique properties.

In the group of Andreas Zumbuehl in Fribourg, Switzerland, phospholipids containing stable amido fatty acids chains instead of hydrocarbon tails were successfully synthesized [13]. His team was able to synthesize a small library of these so-called 1,3-diamidophospholipids, carrying fatty acid tails in the range of C₁₂ to C₁₈. Table 5.3 lists the properties of these new class of phospholipids. The main transition temperature increases linearly with chain length. The nomenclature of these 1,3-diamidophospholipids has been better described in the introductory chapter 1. This symmetric, artificial 1,3-diamidophospholipids are believed to form faceted vesicles below their transition temperature.

name	tail length	M (g mol ⁻¹)	T _m (°C)
Lad-PC-Lad	C ₁₂	619.05	< 0
Mad-PC-Mad	C ₁₄	674.79	21
Pad-PC-Pad	C ₁₆	691.36	35
Sad-PC-Sad	C ₁₈	750.00	52

Table 5.3: Properties of artificial 1,3-diamidophospholipids, synthesized in the group of Andreas Zumbuehl.

Over the last years, non-spherical vesicles composed from lipids, became of particular interest. There are hints in the literature, that GUVs could form faceted vesicles [155], although this feature is typically only observed for SUV. DPPC, for instance, seem to form non spherical unilamellar vesicles of up to 100 nm in diameter under isoosmotic conditions [156]. However, the high curvature found in SUVs leads to packing disorders that result in spontaneous vesicle fusion into LUVs with more favorable curvature and would therefore again be spherical [157].

For this work, Pad-PC-Pad was chosen to test for the ability to form faceted vesicles. The advantage of utilizing these lipids is that the T_m is slightly higher than room temperature. The T_m is low enough to overcome problems related with formation of

GUVs at higher temperatures, but high enough to work below the T_m of the lipid at room temperature. Figure 5.10 displays the chemical structure of Pad-PC-Pad.

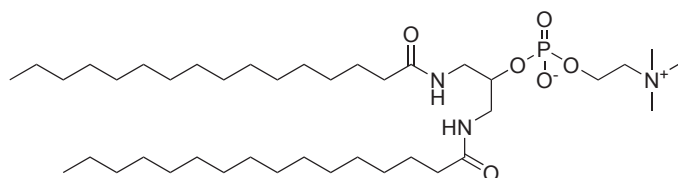


Figure 5.10: Pad-PC-Pad was chosen for this work and giant unilamellar vesicles were formed.

Holme et al. [158] showed that LUVs composed of Pad-PC-Pad are mechanosensitive, they are stable under static conditions but release entrapped carboxyfluorescein as cargo upon application of a shear stress. Nanocontainers that can release drugs locally in areas of high shear stress can be useful in targeted drug delivery. Atherosclerosis, for instance, causes narrowing of arterial blood vessels, accompanied by an increase of shear stress. Indeed, by using a model vascular system, the authors of this paper show that Pad-PC-Pad vesicles may preferentially release drugs in constricted vessels. The non-spherical shape of the liposomes leads to preferential breaking points making them sensitive to increased shear stresses. This might be a promising solution for the treatment or prevention of strokes.

Therefore, in a complementary test, we try to evaluate mechanosensitivity for GUVs composed of Pad-PC-Pad, instead of LUVs, under the optical microscope.

5.2.2 Results

Pad-PC-Pad form GUVs. At first giant unilamellar vesicles of Pad-PC-Pad were formed as described in the Materials & Methods chapter by electroformation. As a fluorescent marker rhod-PE was used at a concentration of 0.5 mol%. GUV-formation was performed in an oven at 45 °C to ensure formation above the transition temperature of the lipid. Prior to recording optical and confocal images, GUV dispersions were cooled down to 25 °C.

At room temperature domains can be observed in GUVs formed by electroformation in confocal and epifluorescence images. However, such a biphasic system of only a single lipid at a specific temperature contradicts thermodynamic principles. By using the PVA-assisted swelling method as a more gentle preparation protocol, GUVs could be prepared without any domains. Figure 5.11 shows a 3D reconstruction of a z-stack recorded by confocal microscopy of Pad-PC-Pad vesicles grown by both methods.

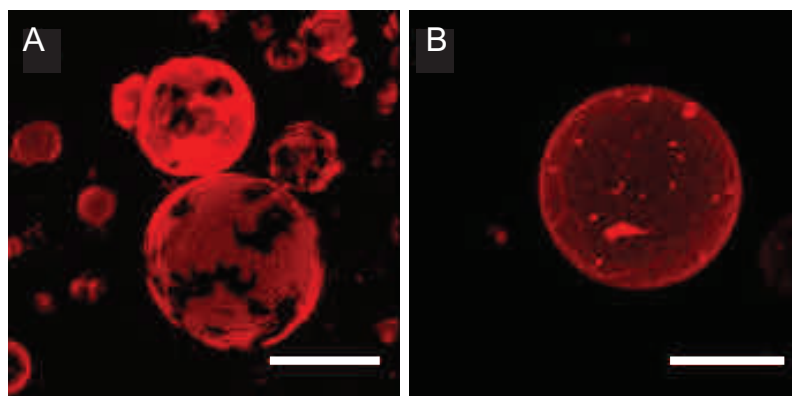


Figure 5.11: 3D reconstruction of a z-stack recorded by CLSM of RhodB-labeled Pad-PC-Pad vesicles grown (A) by electroformation and (B) by PVA-assisted swelling. Scale bars 20 μm .

The observed domains are most likely due to degradation of the lipid during electroformation. By adding a NBD-labeled lipid (emitting green light), which preferably accumulates in the gel-phase and RhodB-labeled lipid, which prefers the liquid phase, we observed that both fluorophores segregate in two different locations in the membrane. This indicates that there are indeed two different lipid phases in coexistence. Figure 5.12 shows from left to right respectively images of the red channel, the green channel and superposition of both channel images obtained by confocal microscopy. Figure 5.13 shows a 3D reconstruction of one recorded confocal z-stack.

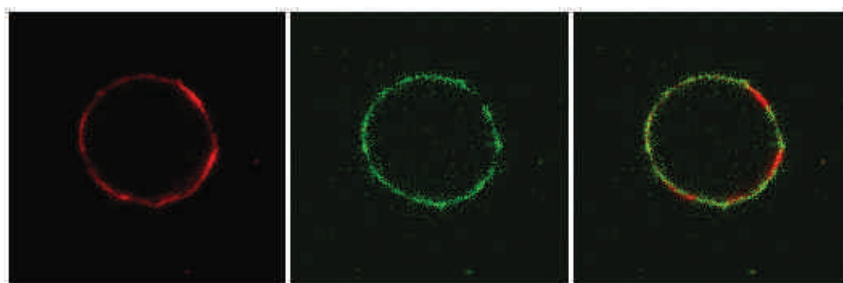


Figure 5.12: Confocal images: (Left) Excitation at 543 nm and emission at 605 ± 75 nm of rhodamine-labeled DOPE. (Middle) Excitation at 488 nm, emission at 515 ± 30 nm of NBD-labeled DPPE. (Right) Merged image of both channels. Vesicle has a size of 18 μm .

Further investigation by thin layer chromatography and mass spectroscopy in Andreas Zumbuehl group confirmed that electroformation of Pad-PC-Pad led to a hydrolysis of the phosphate diester. The product of this hydrolysis is the phosphate monoester Pad-POH-Pad. This degradation of lipids during electroformation with ITO coated glass slides was as well reported for other lipids in the literature [64].

We also tested, if this behavior could be reproduced for the natural phospholipid analog to Pad-PC-Pad, that is DPPC. No such degradation was found.

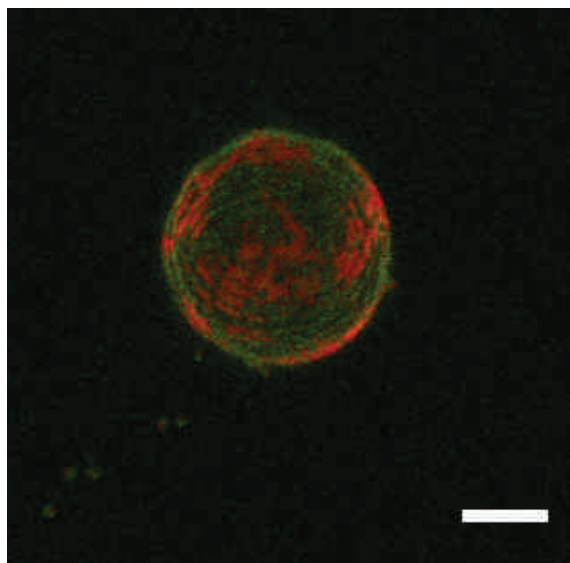


Figure 5.13: 3D reconstruction of a z-stack recorded by CLSM of RhodB- and NBD-labeled Pad-PC-Pad vesicle grown by electroformation. Scale bars 20 μm .

Note that the observed domains are present above and below the transition temperature of Pad-PC-Pad, however smaller domains were observed above the transition temperature.

Faceted vesicles are easily obtained by fast cooling. At room temperature, Pad-PC-Pad is in the gel state (T_m 35 $^{\circ}\text{C}$). Faceted giant vesicles were observed for pure Pad-PC-Pad vesicles as expected below the transition temperature.

However, we noticed that the observation of facets depends on the cooling rate of the obtained GUV solution. The GUVs are prepared at a temperature above the T_m of Pad-PC-Pad, typically around 45 $^{\circ}\text{C}$. Only a rapid cooling, e.g cooling rates above 4 $^{\circ}\text{C min}^{-1}$, leads to apparently faceted vesicles. When the GUVs were cooled down more slowly, with cooling rates below 1 $^{\circ}\text{C min}^{-1}$, no facets were observed and the GUVs looked spherical. Rapid cooling of DPPC-GUVs also yielded to faceted vesicles. This is consistent with the fact reported in the literature more than thirty years ago. SUVs of DPPC are faceted below the gel-liquid phase transition [159], a feature which is less pronounced with increasing vesicle size. Figure 5.14 shows epifluorescence pictures of Pad-PC-Pad and DPPC-GUVs after rapid cooling (A+C) and slow cooling (B+D). It should be mentioned that the observation of facets is limited by the lower resolution of the microscopy techniques, facets smaller than 0.5 μm , can not be observed by optical microscopy.

In all experiments DPPC vesicles were less faceted than Pad-PC-Pad vesicles, showing the improved efficiency of 1,3-diamidophospholipids to form non-spherical vesicles.

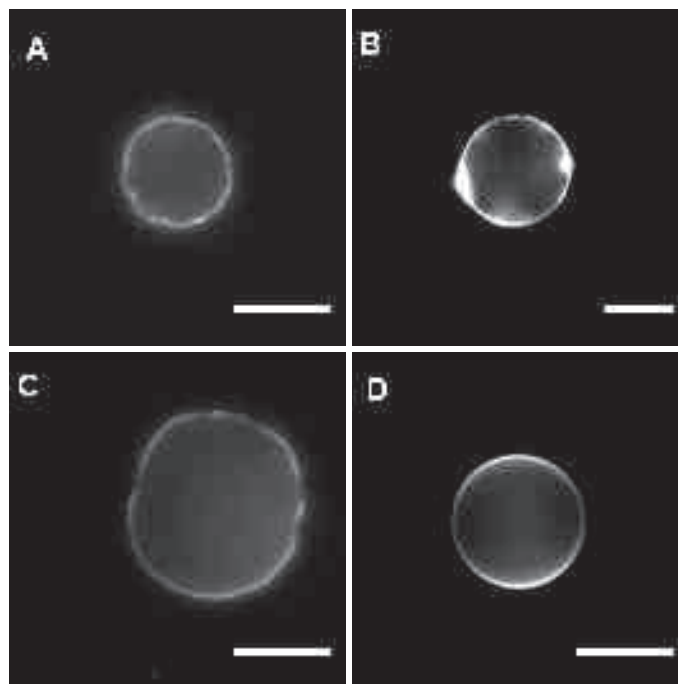


Figure 5.14: The formation of faceted GUVs depends on the cooling rate of the vesicle dispersion once formed: rapid cooling (A) and slow cooling (B) of Pad-PC-Pad and rapid cooling (C) and slow cooling (D) of DPPC. Only rapid cooling leads to faceted vesicles. Scale bars 20 μm .

Andreas Zumbuehl and coworkers proposed that the interplay of the amido groups, the 1,3-substitution pattern and intermolecular hydrogen bonding pattern could promote facet occurrence.

Pad-PC-Pad GUVs are mechanosensitive. LUVs formed from these recently developed 1,3-diamidophospholipids showed a change in membrane permeability, if a shear force is applied on the membrane [158]. We tested this property on GUVs, using the in-house built shearing apparatus (Figure 5.15). It allows the application of an oscillatory shear flow by using the reverse piezoelectric effect. Mechanical stresses were applied with a sphere located at a distance of 300 μm from the GUV. This distance was controlled by the RICM technique. The applied shear was modulated by changing the amplitude of the resonance peak of the piezo crystal. Amplitudes were chosen between 5-7 V. The resonance frequency was set to 5 Hz for all experiments.

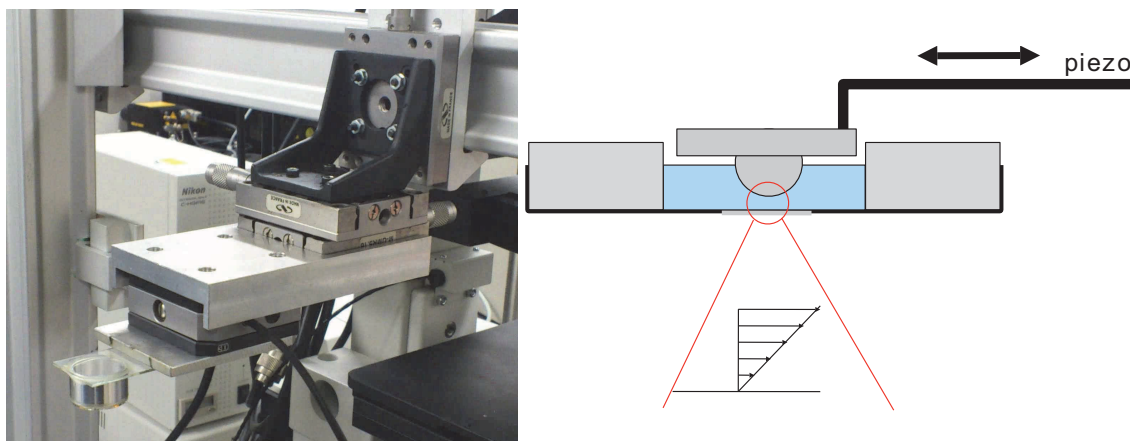


Figure 5.15: Shearing apparatus for shearing of GUVs. An oscillatory shear flow can be applied, which is controlled by shear amplitude and frequency of the piezo crystal.

In a first step we sheared the vesicles formed by electroformation. Upon application of a shear force, we observed that the phase domains start mixing, see Figure 5.16.

Change of membrane permeabilities were determined by dispersing vesicles formed with the gel-assisted swelling method in a carboxyfluorescein solution and applying an oscillatory shear flow. Figure 5.17 shows the evolution of the partition coefficient upon shearing. The starting time (0 min) corresponds to a ΔP of zero. For Pad-PC-Pad and DOPC vesicles the partition coefficient increases over the first 10 minutes. Pad-PC-Pad vesicles show an increased permeability by a factor of two compared to DOPC vesicles.

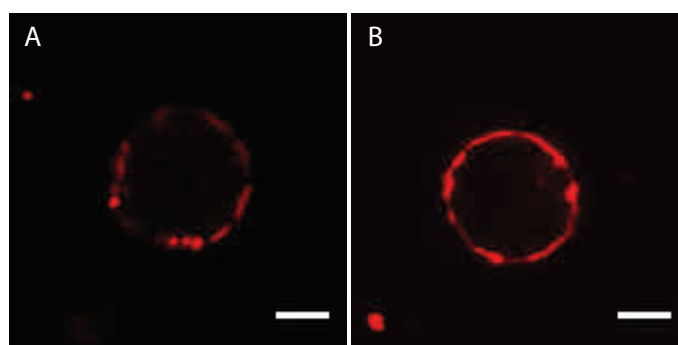
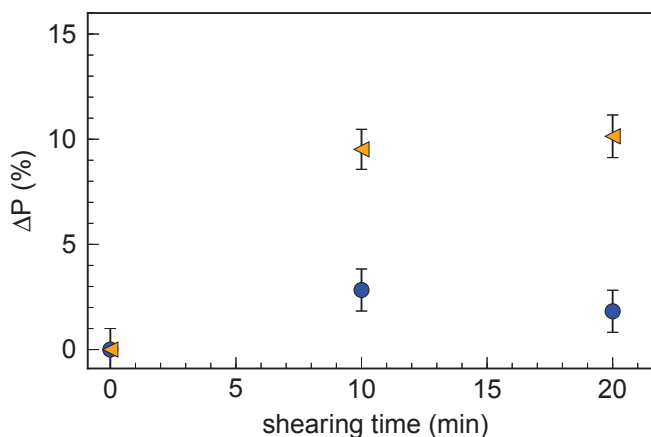


Figure 5.16: (A) GUVs of Pad-PC-Pad formed by electroformation show the typical domains. (B) After shearing for 5 min, domains seem to start mixing. Scale bars 20 μm .

These results show that for the first 10 min of shearing, a probable reorganization of the lipid within the membrane leads to a better permeability of the vesicles. After further shearing for 10 min it seems to stabilize. From our results, it is not clear

whether carboxyfluorescein could still cross the membrane after this time. Shearing for longer than 20 minutes was not performed, as in experiments performed on LUVs a cargo release could be observed within minutes [158].

Figure 5.17: Shearing of GUVs composed of DOPC (blue circles) and GUVs of Pad-PC-Pad (orange triangles) in carboxyfluorescein solution before shearing (0 min) and after shearing for 10 and 20 min. Change of the partition coefficient (ΔP) is monitored with shearing time.



5.2.3 Conclusions

In this section, we show that 1,3-diamidophospholipids, i.e. Pad-PC-Pad form giant unilamellar vesicles. We also demonstrate that it is important to minimize lipid damage by a careful choice of the formation method. Faceted vesicles are obtained from this class of lipids and seem to be mechanosensitive. They show increased membrane permeability upon shearing, allowing drugs to enter vesicles or to be released from them.

Conclusions & Perspectives

In this thesis we studied new model lipid bilayers and their interactions with self-assembling cell penetrating peptides. Motivated by the difficulties that we met at the beginning of our work to make giant unilamellar vesicles containing charged lipids, we developed a new method of giant vesicle growth based on gel-assisted swelling. This new method leads to the efficient and rapid growth of polymer-free giant unilamellar vesicles without the need for special equipment. Numerous lipid mixtures can be used as precursors for giant unilamellar vesicle formation. This method is well adapted for the encapsulation of biomolecules and does not require external input of energy, which minimizes the risk of degradation of involved substances. This was particularly important for the last part of our work, where we investigated new synthetic glycolipids and new amide-bearing phospholipids with shear sensitivity.

Our work on the PVA-assisted swelling method paves the way for many new potential developments. First, the method itself is worth investigating. For instance, it is still unclear, if gel-surface roughness plays a role in the final vesicle size distribution, and correspondingly if gel-surface patterning would be of any help. Also, for practical applications of this method at high temperatures, one needs to develop gel-substrates that do not dissolve at high temperatures. In practice, the PVA polymers that we used, of roughly 150 kDa, dissolve for temperatures above 55 °C. Although, this method allows encapsulation of many molecules of biological relevance, it suffers also from variations of encapsulation efficiencies with molecular size. We noticed also that bilayer stacks of lipids in the gel phase form interesting fracture patterns on the gel surface after gel-swelling, without forming giant vesicles. An interesting side project would be to study the interplay between bilayer phase separation and structure of fracture patterns. This could provide a pathway for the formation of vesicle structures from the liquid domains in phase separated membranes. Finally, this method has potential for large scale production with robot automation, allowing for the screening

of a large spectrum of lipid mixtures.

The collaboration with the group of Professor Chilkoti from Duke University in North Carolina brought us to the field of peptide-assisted translocation of biomedical relevant molecules. Professor Chilkoti original intuition was that the local density of cell penetrating residues can be increased, if the cargo molecules to which they are attached form self-assembled micellar structures. For this purpose his group developed new elastin-based diblock polypeptides that were shown to successfully translocate into living cells above their self-assembling temperature, albeit by yet unknown mechanisms. We studied the fundamental aspects involved in the interactions between zwitterionic lipid bilayers and self-assembling elastin-like polypeptides functionalized with arginine rich residues. We first noticed that cargo attachment to the cell penetrating peptide suppresses the attractive interaction between the peptides and the bilayer, below the self-assembling transition temperature. Above this temperature self-assembly offsets the suppression of attraction by cargo attachment and leads to the accumulation of micellar structures on the membrane.

For cargo-free peptides it was shown that passive translocation across the membrane occurs only for bilayers assembled from mixtures of zwitterionic and anionic lipids with charged lipid fractions above 30 %. Since this is much larger than typical charged lipid fractions in mammalian cells, we believe that translocation of cell penetrating peptides requires energy-driven endocytotic processes. In our experiments, no passive translocation of peptide micelles was observed. It is an important continuation for this study to investigate whether passive translocation of self-assembled micelles would require fractions of charged lipids close to typical plasma membrane content. It would be interesting to test if localized passive translocation can be induced by charge-rich phase separated domains. This could be achieved by working with mixtures of saturated and unsaturated phospholipids and cholesterol, where one of the phospholipids has a charged headgroup.

We benefited during this PhD thesis from the collaborative framework of the International Research Training Group Soft Matter Science and developed a common project with the group of Stefan Schiller in Freiburg. Professor Schiller is interested in developing new synthetic platforms for glycolipids, a special class of lipids bearing sugar heads. Glycolipids are important in many protein-membrane interactions, but the interplay between lipid structure, sugar content and protein nature is poorly known. Nehrukumar Mathaiyan recently synthesized a new family of glycolipids based on diphytanoyl tails and mannose headgroups attached to the tails by different spacers. By using our PVA-assisted method, we were able to demonstrate that some of the glycolipids successfully form giant unilamellar vesicles. By studying the interactions between these GUVs and fluorescently labeled concanavalin A, we could also show

that the sugar spacer is essential for binding to the glycolipids.

This novel family of glycolipids would deserve a complete physical-chemical characterization of membrane formation and binding affinities. For this a systematic study as a function of glycolipid fraction in vesicles and of concanavalin A bulk concentration will be required.

We also studied amide-bearing phosphocholines, which were developed in the group of Andreas Zumbuehl in Fribourg. These 1,3-diamidophospholipids are an important class of lipids for mechanosensitive drug carriers. They are known to form faceted vesicles below the transition temperature of the lipid. We have shown that the classical electroformation method is not suitable for these lipids, thus showing the importance of careful choice of the formation method to minimize lipid damage.

Amide-bearing phospholipids are an interesting class of lipids for targeted drug delivery triggered by mechanical stresses. In order to test these lipids in conditions closer to applications, it would be important to test the ability of these lipids to form stealth mixtures with PEGylated lipids. Our preliminary results also show the feasibility of conducting systematic shear-sensitive release studies with giant unilamellar vesicles under our shear apparatus.

Appendix

List of publications

At the time of writing this manuscript, one article has already been published using results presented in this thesis.

Andreas Weinberger, Feng-Ching Tsai, Gijsje H. Koenderink, Thais F. Schmidt, Rosângela Itrî, Wolfgang Meier, Tatiana Schmatko, Andre Schröder and Carlos Marques, “Gel-assisted Formation of Giant Unilamellar Vesicles”, *Biophysical Journal*, 2013 (105), 154-164.

Additional graphs

In this section also additional graphs not shown in the main text can be found.

Gel-Assisted Formation of Giant Unilamellar Vesicles

Andreas Weinberger,[†] Feng-Ching Tsai,[‡] Gijsje H. Koenderink,[‡] Thais F. Schmidt,[§] Rosângela Itri,[¶] Wolfgang Meier,^{||} Tatiana Schmatko,[†] André Schröder,[†] and Carlos Marques^{†*}

[†]Institut Charles Sadron (UPR22-CNRS), Université de Strasbourg, Strasbourg, France; [‡]Biological Soft Matter Group, FOM Institute AMOLF, Amsterdam, The Netherlands; [§]Universidade Federal do ABC, Santo André, SP, Brazil; [¶]Departamento de Bioquímica, Instituto de Química, Universidade de São Paulo, SP, Brazil; and ^{||}Department of Chemistry, University of Basel, Basel, Switzerland

ABSTRACT Giant unilamellar vesicles or GUVs are systems of choice as biomimetic models of cellular membranes. Although a variety of procedures exist for making single walled vesicles of tens of microns in size, the range of lipid compositions that can be used to grow GUVs by the conventional methods is quite limited, and many of the available methods involve energy input that can damage the lipids or other molecules present in the growing solution for embedment in the membrane or in the vesicle interior. Here, we show that a wide variety of lipids or lipid mixtures can grow into GUVs by swelling lipid precursor films on top of a dried polyvinyl alcohol gel surface in a swelling buffer that can contain diverse biorelevant molecules. Moreover, we show that the encapsulation potential of this method can be enhanced by combining polyvinyl alcohol-mediated growth with inverse-phase methods, which allow (bio)molecule complexation with the lipids.

INTRODUCTION

Cellular membranes, that envelop the cytoplasm of the cell, its nucleus, and its various organelles, are self-assembled lipid bilayers that host also a variety of proteins and other biomolecules. For typical cell sizes on the order of ten micrometers, the lipid membranes span a few thousands of square micrometers, holding on the order of tens of billion lipids. The fact that self-assembly can drive so many individual molecules into a well defined and robust liquid structure of five nanometers thickness has long fascinated researchers in Physics, Chemistry, and Biology, who have studied lipid membrane structure and function.

Lipid bilayers self-assembled from a single or a reduced number of lipid species are often used as biomimetic models of cell membranes. Several membrane structures have become available for biophysical studies on the intrinsic properties of lipid bilayers as well as their interactions with other biomolecules: unilamellar and multilamellar vesicles of different sizes (1), supported bilayers (2) and nanodiscs (3) to only name a few.

Among these model biomembranes, giant unilamellar vesicles (GUVs) have played a prominent role (4). Due to their large dimensions, in the range of typical cell sizes, GUVs can be easily observed and micromanipulated under an optical microscope, thus allowing for the direct observation of relevant biophysical phenomena at a single membrane level (5).

The importance of GUVs has triggered a host of efforts seeking GUV preparation methods that can provide a fast and easy route to form vesicles from a variety of lipid compositions and under different buffer conditions (4). Methods for GUV formation typically involve a lipid bilayer preas-

sembly step by evaporation of a lipid-containing organic solvent at a solid-liquid interface. Depending on the lipid composition, vesicles are sometimes formed spontaneously when the precursor lipid film is simply exposed to a buffer solution. This method is known as gentle hydration (6,7). A disadvantage of this method is that vesicle formation usually requires long timescales on the order of several days. Moreover, it works only with restricted lipid compositions and ionic conditions. Electromagnetic radiation (8) and electrical or mechanical stresses tend to promote the formation of unilamellar vesicles. Indeed, the most widely used vesicle formation method is known as electroformation, where an alternating electrical field is applied across a buffer-filled chamber bounded by conductive slides or crossed by metal wires (9). Electroformation is reasonably fast, taking several hours. However, growing vesicles in physiological buffers or from lipid mixtures containing charged lipids is still a challenging task, despite the recent improvements brought by electroformation at high field frequencies (10,11) or using a flow chamber with exchange of the buffer (12). Another important difficulty of preparation methods based on hydration is that encapsulation of proteins or other (bio)molecules, especially in buffers of physiological ionic strength, is generally inefficient and variable among liposomes. Alternatives are the rapid solvent exchange method (13) or the evaporation method (14). However, the rapid solvent evaporation method requires a large amount, typically one milligram, of lipid per sample.

There is currently broad interest in the use of vesicles as a platform to build either protocells or artificial cells that mimic aspects of bacterial or mammalian cells (15). Examples include the reconstitution of cytoskeletal protein networks (16–19), membrane-protein interactions (20,21), cell adhesion (22), and gene transcription and translation (23). In all these applications, biomolecules need to be

Submitted February 28, 2013, and accepted for publication May 8, 2013.

*Correspondence: marques@unistra.fr

Editor: Claudia Steinem.

© 2013 by the Biophysical Society
0006-3495/13/07/0154/11 \$2.00

<http://dx.doi.org/10.1016/j.bpj.2013.05.024>



encapsulated inside GUVs in physiological buffers. This is still a challenging task due to the high salt levels present in physiological buffers and to the relatively low vesicle formation speed that hinders a precise control of the biological activity of the proteins. Recently several new strategies have been proposed, which were designed to improve preparation speed, encapsulation efficiency, and/or applicability to charged lipids. One class of methods uses water-in-oil emulsion droplets as templates for bilayer vesicles. Bilayers can either be formed by transferring emulsion droplets stabilized by a lipid monolayer through an oil/water interface (24–26) or by forming double emulsion droplets with an oil shell and extracting the oil (27). Biomolecule encapsulation into emulsion droplets is highly efficient and reproducible even at physiological salt conditions. However, the emulsion-based methods generally require advanced equipment such as microfluidic devices. Moreover, traces of the oil phase can often be detected in the self-assembled membrane (4,28). Microfluidic inkjet encapsulation methods also improve biomolecule encapsulation and preparation speed compared to film hydration methods (29,30), but again specialized equipment is needed and residual oil can be left in the membrane.

To minimize damage of the molecules of interest (31), one is restricted so far to film hydration methods. Lipid film hydration methods have a strong potential for further development. It is important for instance to realize that membrane swelling from a preordered bilayer film requires water penetration into the membrane stacks, a process that is partially hindered when the lipids are deposited on glass or other solid substrates. A larger exposure of the preordered lipid films to hydration is achieved in a recently discovered agarose swelling method (32). Here, the organic solution containing the lipids is spread on a thin dried film of agarose, a naturally occurring polysaccharide. Upon addition of the buffer solution, GUVs are rapidly formed at the interface between the swollen agarose gel and the buffer. Vesicle formation is much faster than in classical electroformation or gentle swelling. Moreover, this method works with a wide range of lipid compositions and buffer conditions, and it is possible to efficiently encapsulate various biomolecules (32), including cellular proteins (28). However, the vesicle formation efficiency is reduced because lipids are distributed over the whole gel thickness, which are several micrometers. Furthermore, the agarose gel dissolves partly upon swelling and remnants can be detected in/on the membrane (32).

Here, we report a new, to our knowledge, swelling method inspired by the earlier work on swelling from agarose gels, which provides a facile and fast way to prepare vesicles with a wide range of lipid compositions. Instead of agarose, we use polyvinyl alcohol (PVA) gels. Our hypothesis was that PVA gels can optimize the lipid distribution at the interface between the substrate and the hydrating buffer. Moreover, PVA gels are expected to be much less prone to

dissolution upon swelling at room temperature than other physical hydrophilic gels (33,34). Indeed, we find that vesicles formed by PVA-assisted swelling are not contaminated by polymer. We first demonstrate the efficiency of GUV formation on a PVA gel and study the growth process by inspecting the distribution of lipids before and after growth. Next, we compare growing efficiencies for different ionic and nonionic amphiphiles and show that the method allows us to encapsulate hydrophilic substances in the vesicles. We conclude by proposing a mechanism for vesicle growth.

MATERIALS AND METHODS

Lipids

Lipids were purchased from Avanti Polar Lipids (Alabaster, AL) as a powder and dissolved in chloroform. Lipid solutions were stored at -20°C before use. In addition to 1,2-dipalmitoyl-*sn*-glycero-3-phosphocholine (DPPC) with two saturated C-16 tails, all other phospholipids used in this work have two C-18 tails with one unsaturation per tail (1,2-dioleoyl-*sn*-glycero-). We tested a range of headgroups, including neutral zwitterionic headgroups (-phosphocholine (DOPC)), as well as headgroups bearing a negative net charge (-phosphoglycerol (DOPG), -phosphoserine (DOPS)), or a positive net charge (trimethyl ammonium-propane (DOTAP)). DPPC was used for membranes in the gel state at room temperature, because its main transition temperature is 41°C . All other lipids undergo the fluid-gel transition below 0°C . As a fluorescent marker we used 1,2-dioleoyl-*sn*-glycero-3-phosphoethanolamine-N-(lissamine rhodamine B sulfonyl)(rhodamine-DOPE) in a 0.2 mol % mixture with other lipids. Other lipids used were 1,1',2,2'-tetramyristoyl cardiolipin, 1,2-dipalmitoyl-*sn*-glycero-3-phosphoethanolamine-N-(cap biotinyl) (biotin-PE) and the PEGylated 1,2-dipalmitoyl-*sn*-glycero-3-phosphoethanolamine-N-[methoxy(polyethyleneglycol)-2000].

Proteins

Neutravidin and Alexa Fluor 350-labeled neutravidin were purchased from Invitrogen (Breda, The Netherlands). Streptavidin was purchased from Thermo Scientific (Breda, The Netherlands). Rabbit skeletal muscle G-actin was purified by standard procedures including a gel filtration on a Sephacryl S-200 high-resolution column (GE Healthcare, Munich, Germany) (35) or purchased from Tebu-bio (Heerhugowaard, The Netherlands). Fluorescent actin with a dye/protein molar ratio of 0.6 was prepared by labeling amine groups with AlexaFluor488 carboxylic acid succinimidyl ester (Invitrogen) (36) or purchased from Invitrogen. G-actin labeled with biotin was purchased from Tebu-bio. G-actin was stored at -80°C in G-buffer (2 mM Tris-HCl, 0.2 mM Na_2ATP , 0.2 mM CaCl_2 , 2 mM dithiothreitol (DTT), pH 7.8). Before use, G-actin solutions were thawed, treated with 5 mM DTT to reduce potential oxidized sulfhydryl groups, centrifuged at $120,000 \times g$ for 30 min to remove potential protein aggregates, and finally bath-sonicated for 5 min to disrupt potential actin dimers (37).

PVA

PVA (MW 145000, Merck KGaA, Darmstadt, Germany) was purchased from VWR International (Fontenay-sous-Bois, France). For fluorescent studies, we labeled PVA with [5-(4,6-Dichlorotriazinyl)-aminofluorescein] (DTAF) by elimination of hydrochloride using previously described protocols (38,39). DTAF covalently couples to the alcohol groups of PVA at pH levels above 9. DTAF-labeled PVA was separated from free DTAF by extensive dialysis against MilliQ water using a regenerated cellulose membrane

with a molecular mass cutoff of 4000–6000 Da. The average labeling stoichiometry was determined by spectrophotometric measurements of the light absorbance of the dialyzed PVA-DTAF solution at a wavelength of 495 nm, corresponding to the excitation maximum. The emission maximum of DTAF is at 516 nm. We first determined the extinction coefficient of aqueous solutions of DTAF at different concentrations by recording absorbance spectra between wavelengths of 400 to 800 nm with a scan rate of 600 nm min⁻¹ on a UV/Vis Cary 500 Spectrometer (Fig. S1 in the Supporting Material). These measurements were performed using pH adjusted solutions, because of the pH dependence of the fluorescence properties of fluorescein analogs. We determined an extinction coefficient of 82,900 L mol⁻¹ cm⁻¹ (see inset of Fig. S1), and measured a DTAF concentration of 8.72 10⁻⁵ mol L⁻¹ in the solution of DTAF-labeled PVA. The polymer concentration (determined by drying 1 g of the PVA-DTAF solution) was 2.97 ± 0.07% (w/w). Thus, the degree of labeling was 0.43 mol DTAF per mol PVA chain, or 1.30 10⁻⁴ mol DTAF per mol repeating unit, implying that approximately every second PVA chain bears one fluorescent label. Both labeled and unlabeled polymers can be dissolved when exposed at temperatures higher than 50°C for longer than 30 min.

Other materials

In some experiments we formed polymersomes from the triblock copolymer, PMOXA₁₀-PDMS₈₇-PMOXA₁₀ (MW 8154, PDI 2.2). Its synthesis is described elsewhere (40). All other chemicals were purchased from Sigma Aldrich (St. Louis, MO) and used without further purification unless specified otherwise.

Electroformation method

Electroformation was performed following the method of Angelova et al. (9). Briefly, 10 μL of a lipid solution (1 mg mL⁻¹ in chloroform) were spread on an indium tin oxide (ITO)-coated glass slide. After drying of the lipid film under vacuum for 30 min, a chamber was formed with a second ITO slide and Sigillum wax (Vitrex, Copenhagen, Denmark) as a sealing agent. This chamber was filled with sucrose solution for neutral lipids and with a phosphate buffered saline (PBS) buffer solution (0.01 M phosphate buffer, 0.0027 M KCl and 0.137 M NaCl, pH 7.4) for lipid mixtures containing charged lipids. The osmolarity of the buffer was measured with an osmometer (Osmomat030, Gonotec, Berlin, Germany) and adjusted to 280 mOsm kg⁻¹. An alternating electric field was applied across the chamber for 3–12 h. The amplitude and the frequency of the field were 1 V and 10 Hz for neutral lipids and up to 5 V and 500 Hz for charged lipids. Successful formation was checked by observing the growing chamber by phase contrast microscopy. The obtained GUVs were transferred to an Eppendorf tube, diluted 5 times with PBS solution, and left undisturbed for 15 min before observation. Table S1 summarizes the growing conditions for different lipids.

Gel-assisted GUV formation

A 5% (w/w) solution of PVA was prepared by stirring PVA in water or 280 mM sucrose solution while heating at 90°C. For fluorescent PVA substrates, one part of the DTAF-labeled PVA was mixed with 140 volume parts of unlabeled PVA. To estimate the amount of residual free fluorophore, we immersed PVA-DTAF-coated glass slides, chemically cross-linked with glutaraldehyde, in water for 1 h and measured the absorbance of the solution after adjusting the pH. We found a maximum amount of free fluorophore of 10%, providing an estimate for the uncertainty in fluorescence measurements. PVA-coated substrates were prepared by spreading 100–300 μL of PVA solution on a microscope coverslip (30 mm in diameter, Menzel-Gläser), which was then dried for 30 min in an oven at 50°C. 10–20 μL of lipids dissolved in chloroform (1 mg mL⁻¹) were spread

on the dried PVA film and placed under vacuum for 30 min to evaporate the solvent. Before use, the coverslips were cleaned with UV/Ozone for 15 min to prevent dewetting of the PVA film. A chamber was formed with Vitrex and filled with sucrose for neutral lipids or PBS buffer for charged lipids as described for the electroformation method in the previous section. GUV formation was followed using phase contrast microscopy. When the desired vesicle sizes were reached, typically in <1 h, GUVs were transferred into an Eppendorf tube using a pipette. The solution was diluted 5 times with PBS buffer and left undisturbed for 15 min before use. Table S1 summarizes the growing conditions for different lipids.

Encapsulation of proteins by gel-assisted GUV formation

For encapsulation of proteins a similar protocol was used. Instead of spreading the PVA and lipid solutions (3.75 mg mL⁻¹) by hand, PVA was spin-coated on the coverslips at 1200 rpm for 30 s (DELTA 10 BM, SUSS MicroTec). A typical lipid mixture was composed of 94.8:0.2:5.0 DOPC/RhodB-PE/PEG-PE. In experiments containing biotinylated lipids 1% of DOPC was substituted by biotin-PE. 150 μL of lipid mixture was spin-coated on the dried PVA-coated slide at 1200 rpm for 300 s. We used either open-top formation chambers, assembled by placing a 0.12 mm thick spacer (secure-seal spacer, Invitrogen) on the coated slide, or closed chambers, assembled by placing a 0.5 mm thick spacer (Coverwell, 13 mm in diameter, Invitrogen) and another cover slide on the coated slide. Lipid swelling was initiated by introducing a buffer containing the proteins to be encapsulated (I-buffer). This I-buffer contains all necessary elements for the polymerization of actin (25 mM imidazole-HCl (pH 7.4), 1 mM DTT, 0.1 mM MgATP, 50 mM KCl, 2 mM MgCl₂), 280 mM sucrose for osmotic pressure matching, 0.5% (v/v) glycerol, and an oxygen-scavenging mixture of 2 mM trolox, 2 mM protocatechuic acid, and 0.1 μM protocatechuate 3,4-dioxygenase that minimizes blinking and photobleaching (41). The lipid film was allowed to swell for 45 min, at a temperature of 4°C where actin polymerization is minimized. The GUVs were harvested by pipetting at least 2 chamber volumes of a glucose solution (O-buffer) into the formation chamber, causing the GUVs to flow into the adjacent observation chamber or into an open-top observation chamber assembled by placing a 0.5 mm thicker spacer on a glass slide and closed by a cover slide after GUVs harvest. The glass slides were passivated by a casein solution (2 mg mL⁻¹) to prevent liposome adhesion and rupture. Actin polymerization was initiated by bringing the observation chamber to room temperature. The O-buffer osmolarity was adjusted to be at least 20 mOsm kg⁻¹ higher than the I-buffer osmolarity (Osmomat030, Gonotec GmbH) to prevent bursting of vesicles. The actin concentration in all experiments was 23.8 μM (equivalent to 1 mg/mL), including 20 mol % or 30 mol % of AlexaFluor488-labeled actin and 0.25 mol % of biotinylated actin (1:400 molar ratio to actin). Streptavidin at a 1:25 molar ratio to the total actin concentration was included as a network cross-linker.

Inverse-phase precursor films for gel-assisted encapsulation

We adapted the inverse phase precursor method, which was previously combined with electroformation (42), to prepare lipid films containing biotinylated lipids complexed with neutravidin. By dispersing small water droplets containing hydrophilic moieties in the organic solvent containing the phospholipids, this method enables to prepare vesicles decorated with neutravidin or chitosan on their membrane. If neutravidin is used, it enables specific anchoring of encapsulated molecules to the membrane. An inverse emulsion was prepared from a mixture of lipid in chloroform and buffer solution as described previously (42). Briefly, a volume of 2 μL neutravidin in PBS (48 mg mL⁻¹) was added to 60 μL of a lipid solution as described previously. In control experiments without biotin-PE lipids, pure PBS buffer was added. The mixture was pipetted up and down several times

with a 500 μL glass syringe in a vial until the mixture became opalescent, signifying that inverted micelles have formed. 40 μL of this precursor emulsion was spin-coated on the PVA-coated slide (prepared as described previously) at 100 rpm for 100 s. The slide was then dried under vacuum for 100 min at room temperature. The remaining steps were the same as in the PVA swelling method, except that the lipid swelling time was 90 min instead of 45 min.

Optical microscopy

Vesicle contours were imaged by phase contrast microscopy using an inverted TE 2000 microscope (Nikon, Japan) equipped with a 60 \times WI/1.2 NA Plan Apo DIC objective, 100 \times NA 1.4 Plan Apo objective, or 40 \times Ph2/NA 0.60 Plan Fluor objective. Images were recorded with a digital camera (Hamamatsu EM-CCD, Japan) with a pixel depth of 16 bits. Three-dimensional (3D) fluorescent imaging was performed using confocal laser scanning microscopy (CLSM) with a Nikon C1 scanhead. Images were captured using EZ-C1 software (Nikon, version 3.50). The DTAF-labeled PVA film was excited using an argon-ion laser (Melles-Griot) at 488 nm, whereas rhodamine-labeled lipids were excited using a helium-neon laser (Melles-Griot) at 543 nm. Quantitative analysis of fluorescent intensities in the confocal images was performed using ImageJ, using appropriate rescaling of the acquired signals to the same standard levels. In all measurements the background noise measured from blank samples containing no fluorophores was subtracted.

For dried DTAF-PVA films, some bleaching of the fluorophores was observed when obtaining confocal z-stacks, typical confocal scans were performed by starting above the PVA gel and finishing on the glass surface. Hydration of the films caused an increase of the fluorescence intensity of both the DTAF-PVA and rhodamine lipids. This intensity increase can be explained by the change in refractive indices of the films upon hydration. In solution, the fluorescence of DTAF increases in the presence of PVA, as determined by fluorescence spectrophotometry using a Horiba Jobin Yvon FluoroMax-4 spectrofluorometer (see Fig. S2), a comparable increase is found when DTAF is directly coupled to PVA. Additionally, in the swollen DTAF-PVA films, the fluorescence spectrum of DTAF was broadened compared to free DTAF in solution (*dashed line* in Fig. S2), as measured by CSLM. As a result, some emission bleeding of the green channel into the red channel occurred. We checked that this did not influence the qualitative measurements of the lipid distribution by performing additional scans of labeled GUVs grown on unlabeled PVA (see Fig. S3) and also compared the bleeding profile of labeled PVA with our samples, which is exactly the same up to experimental errors (see Fig. 2 and Fig. S4).

RESULTS AND DISCUSSION

Fully hydrolyzed high-molecular weight PVA was used to form a dry but swellable polymer film on a glass support. A thin film of lipids was then spread on the gel surface and the lipid-gel system was hydrated in an aqueous solution. Within 2 min, numerous unilamellar vesicles can be observed, as shown in Fig. 1. This observation is in stark contrast with hydration of a lipid stack deposited directly on glass, where the majority of bilayer structures correspond to multilamellar vesicles or cylinders and only a minor fraction correspond to unilamellar vesicles. Compared to the standard electroformation method, vesicle formation from PVA-lipid films has the advantage that GUVs are formed much faster, as shown in Fig. 1. Furthermore, the gel-assisted swelling method avoids the risk of lipid degradation, which may occur during electroformation (31,43).

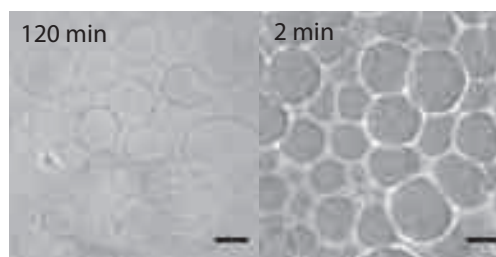


FIGURE 1 Phase contrast images of DOPC-GUVs, obtained by (A) electroformation and by (B) PVA-assisted swelling. Variations in contrast are due to differences in composition of inner and outer solutions. Scale bars 20 μm .

The speed of vesicle formation on swelling PVA gels is comparable to that observed previously on an agarose substrate (32). However, the agarose-growing method leads to encapsulation of some agarose polymer, as well as to polymer decoration of the membrane (28). To test whether PVA is present in the GUVs, we performed confocal microscopy of DOPC GUVs grown on fluorescently labeled PVA films. As shown in Fig. S5, no traces of fluorescent PVA can be found either on the vesicle membranes or inside the vesicles. This visual observation is confirmed by quantitative image analysis; weak fluorescence in the green channel is due to some free DTAF, as discussed in the Materials and Methods section. The absence of vesicle contamination by PVA can be primarily traced to the PVA gel structure, which is much less prone to dissolution upon swelling at room temperature than other physical hydrophilic gels (33,34). Moreover, the lipid distribution in the PVA film prevents contamination of the vesicles by PVA, as discussed below.

Lipid distribution

To visualize the spatial distribution of the lipids with respect to PVA in the lipid-PVA films, we measured the relative fluorescence intensities of the rhodamine-labeled lipids and the fluorescein-labeled PVA of a 20 μm \times 20 μm patch as a function of height (z direction) above the glass substrate. We first focused on the lipid distribution before and after gel swelling for DPPC, a lipid that is in a gel state at room temperature. As shown in Fig. 2, the lipid bilayer is localized at the gel surface and does not penetrate the polymer film, independently of the degree of swelling of the gel.

In the original gel-assisted swelling method of Horger (32), it was shown that the lipids completely penetrated the agarose film, which is tens of micrometers thick. The agarose and the lipids thus intimately mix over the full film thickness. Our results show that this is not a requirement to promote giant vesicle growth (see also Fig. S3). Moreover, the reduced mixing of lipids with polymer in PVA gels compared to agarose gels reduces the probability of vesicle contamination by gel residues.

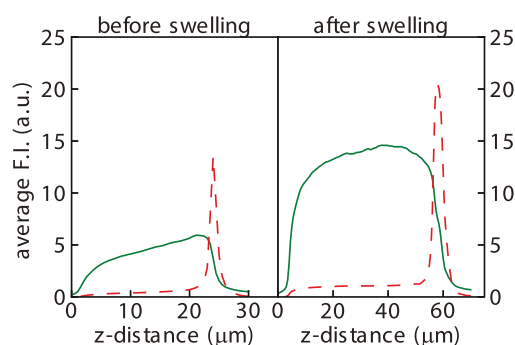


FIGURE 2 CLSM z profiles of a DTAF-labeled PVA film (solid line) and a fluorescent DPPC film (dashed line). Lipids and gel are well separated before and after swelling with PBS buffer solution at room temperature. Residual red fluorescence inside the gel is due to emission bleeding of the DTAF, as explained in Materials and Methods. A z distance of zero microns corresponds to the bottom of the labeled PVA gel.

As discussed previously, GUVs are formed rapidly from films composed of lipids which are in a fluid state at room temperature. Confocal imaging shows that several layers of vesicles can be observed on the gel surface (see Fig. 3 inset B and Fig. S3). Small vesicles are typically located at the gel surface, while larger ones are further away. During the growing process, small vesicles often fuse into a larger one that may later detach from the gel. However, although many vesicles detach, many stay on the surface of the PVA film. As the 3D confocal image shows (Fig. S6), holes in the fluorescently labeled lipid film can be observed directly underneath the vesicles, likely corresponding to the partial consumption of the lipid film to build the vesicle above the hole.

After swelling, the PVA surface appears very corrugated with valleys and mountains. Any XY plane through this interfacial region, as exemplified by Fig. 3 in inset A, will then display areas inside the gel and areas outside the gel where lipid can be observed. In this geometry the gel interface is almost perpendicular to the confocal section, allowing to precisely screen the GUVs for fluorescent PVA traces and to reconstruct a 3D representation as in Fig. S6. Depth profiles of the PVA and lipid fluorescence intensity reveal the heterogeneity of the lipid distribution on the gel film, which can be related to the lipid deposition process or to the swelling of the gel. Fig. 3 summarizes all the observed cases. The vertical line represents the z -position where the confocal micrograph shown in inset A was recorded. The green channel represents the fluorescently labeled PVA, the red channel the fluorescently labeled lipid. The figure inset I displays for reference a z profile from the same sample before swelling. Inset II shows gel surface regions after swelling without any traces of lipids, whereas inset III corresponds to a lipid film still attached to the gel without any vesicles. In some regions GUVs still attached to the gel can be observed, as displayed in inset IV. The last inset V corresponds to the more rare case where a detached vesicle is still

in the neighborhood of the gel interface above a membrane. Inset B in Fig. 3 corresponds to a vertical cross section, which better views the cases III to V.

In summary, our results show that GUVs free of polymer contamination grow during gel swelling from a heterogeneous lipid film at the gel surface. Given that the lipid solution spread on a PVA gel does not penetrate into the gel, we tested the effect of lipid/PVA mixing by forcing lipids into the gel. This was achieved by spreading a PVA solution mixed with small multilamellar vesicles. In this case, no vesicle formation could be observed upon hydration, thus confirming that gel/lipid mixing is not required for vesicle growth on PVA.

GUV formation: dealing with the hard cases

As shown in the preceding section, GUVs can be rapidly formed from the zwitterionic lipid DOPC by PVA-assisted swelling. In this section, we will show that the PVA growing method also provides a valuable tool to form vesicles from other types of lipids, which are difficult to form by other film swelling methods. Lipids with charged headgroups are a clear challenge for electroformation. Recently, a method to grow charged lipid vesicles under physiological buffer conditions at high frequencies was proposed (10,11). However, even under such conditions, a number of difficult issues remain, related to the growth of vesicles from purely charged lipids, to the vesicle yield, and to the detachment of the vesicles from the growing substrate. We have for instance compared the growth of DOPC-GUVs containing DOTAP, a cationic lipid, by electroformation and by PVA swelling. For these lipid mixtures, vesicles are obtained in a high number by electroformation, but they cannot be detached from the ITO substrate. With the PVA swelling method, even 100% DOTAP vesicles can be formed and transferred, albeit with a smaller yield than in the case of zwitterionic lipids. Fig. S7 shows a free floating GUV composed from DOTAP grown by PVA swelling. The detachment yield can be improved by gentle sonication.

Examples of other systems grown by the PVA swelling method are displayed in Fig. 4. Images in the left column show vesicles formed by growing on pure PVA gel, whereas images in the right column show vesicles grown on a PVA gel containing sucrose. In some cases, the presence of sucrose in the dry gel improves vesicle formation. The figure shows GUVs grown from DOPC, DOPG, DOPS, and the triblock copolymer PDMS-PMOXA-PDMS. In all cases, GUVs formed on a PVA gel that contains sucrose detach better during the growing process. Furthermore, the formed vesicles are less prone to adhere to each other in the growing chamber. Similar results can be obtained by making the PVA gel in a PBS solution, although with somewhat less efficiency of vesicle detachment (compare Fig. S8). Interestingly, in the case of DOPS on pure PVA, tubular vesicles could be observed in the first few seconds

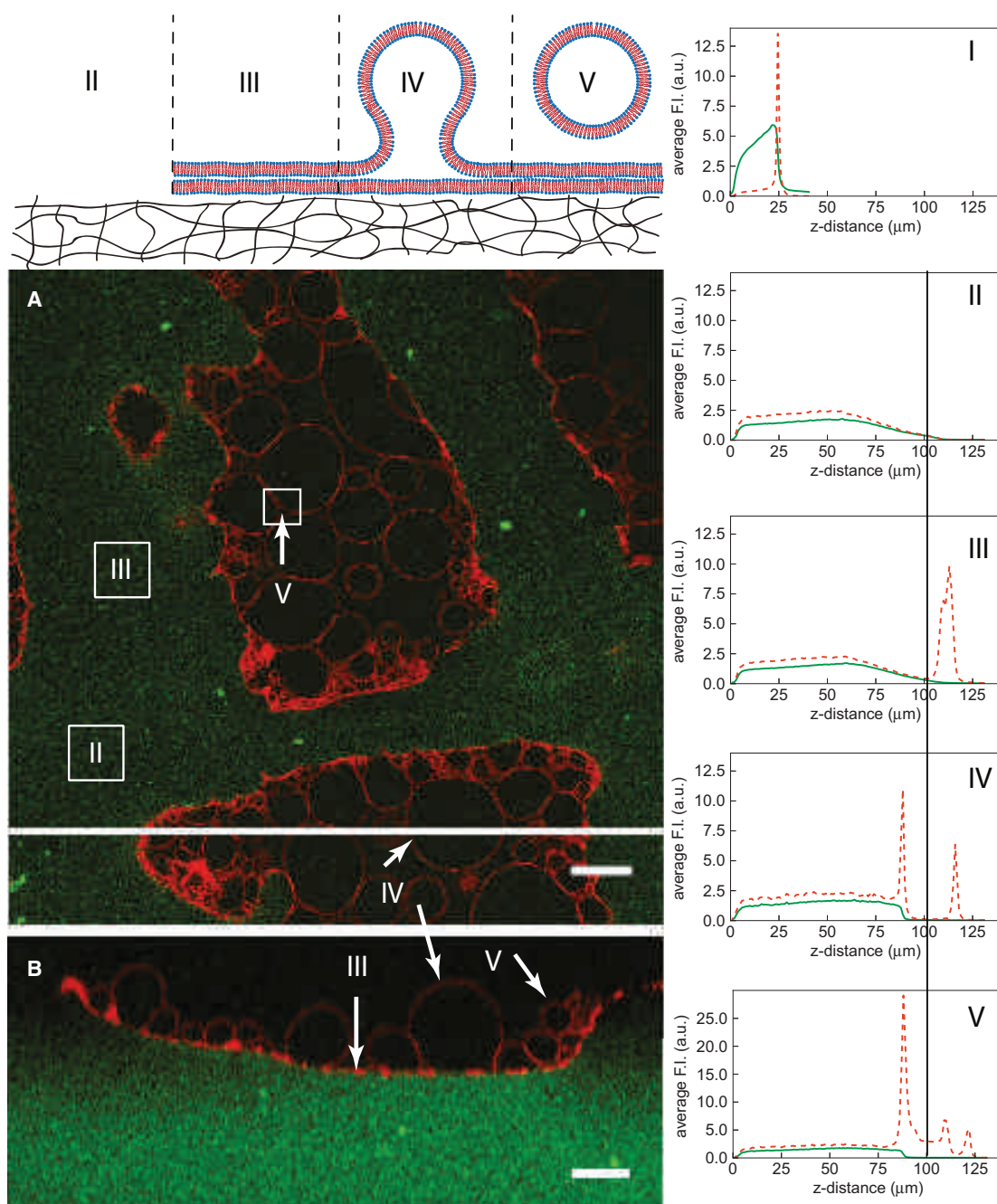


FIGURE 3 Heterogeneity of lipid distribution on a swollen gel interface. Inset *A* shows the XY section of a DTAF-labeled PVA gel (green) and DOPC-GUVs labeled with 0.2 mol % Rhodamine (red) recorded with CLSM at a z -position of 31 μm . Inset *B* is a XZ section at the position of the white line. Graph I is a z profile of the same sample in the dry state before hydration with buffer solution, other graphs correspond to the different labeled regions of the micrograph, which are further sketched in the diagram above. Average intensity of a given z was determined for a $20\ \mu\text{m} \times 20\ \mu\text{m}$ square and the average intensity variations plotted with z . The scan was performed starting at the top of the sample; a z distance of zero microns corresponds to the bottom of the labeled PVA gel. Scale bar 20 μm .

of the swelling, which disappear over time to form spherical vesicles. None of the other lipid cases showed this behavior. Tubular vesicles were also observed for the triblock copolymer (PMOXA-PDMS-PMOXA) on pure PVA, but here they do not lead to spherical polymersomes, a structure that could only be observed on PVA containing sucrose.

Nonetheless, the formation of polymersomes yielded in a fewer number of GUVs compared with phospholipids.

We also investigated lipids with more than one charge per headgroup. A particularly relevant example is cardiolipin, a lipid containing four lipid tails and two negatively charged headgroups. Although GUVs containing up to

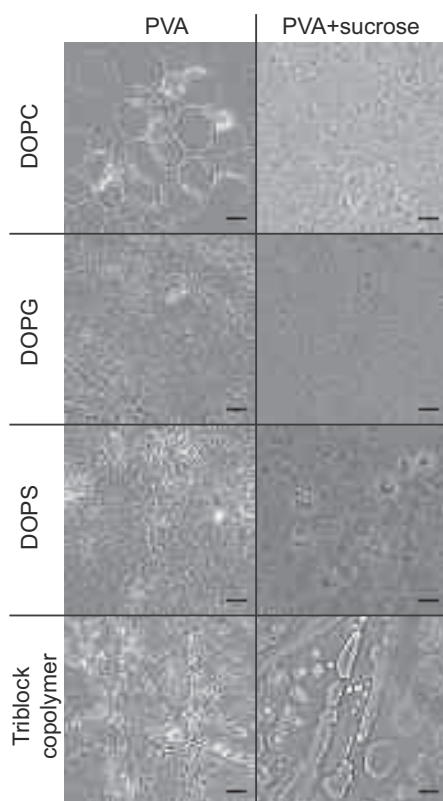


FIGURE 4 Phase contrast images of GUVs formed from different amphiphiles. Left column: growth on pure PVA gel. Right column: growth on a PVA gel containing sucrose. Amphiphiles: DOPC, DOPG, DOPS, and triblock copolymer (PDMS₁₀-PMOXA₈₇-PDMS₁₀). Swelling solution: PBS. Scale bars 20 μ m.

50% cardiolipin in DOPC/cardiolipin mixtures can be grown by electroformation, we find that the structures obtained systematically display defects, similar to those observed by Fedotenko et al. (I. Fedotenko, A. Weinberger, T. Tanasescu, F. Favarger, C. Stefanu, I. Tashi, G. Brezesinski, C. Marques, and A. Zumbuehl, unpublished), which may be caused by headgroup degradation from the applied electric field (Fig. 5 A). The PVA-assisted swelling method allows us to form defect-free GUVs within minutes, even from 100% cardiolipin (Fig. 5, B and C).

The PVA swelling method can also be performed at temperatures different from room temperature. For instance, one can obtain DPPC vesicles by swelling with preheated buffer in a heated chamber at 50°C or DOPC vesicles by swelling in the fridge at 4°C. For high temperatures, the only limitation is the preservation of gel integrity. Indeed, depending on PVA molecular mass, some of the polymer can dissolve upon heating, thus leading to lower yields and GUV contamination. The PVA used in this work, in the range of 145 kDa, does not dissolve at room temperature but partially dissolves if exposed for more than half an hour at temperatures above 50°C. When lower molecular mass PVA is used, around 16 kDa, partial dissolution is already

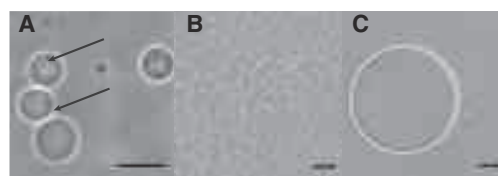


FIGURE 5 (A) Vesicles of 1:1 DOPC/cardiolipin mixtures grown by electroformation. Arrows show vesicle defects. (B) Cardiolipin vesicles on the PVA gel after growing. (C) Cardiolipin vesicles after dispersion in PBS. Images were recorded in phase contrast mode. Swelling solution: sucrose. Scale bars 20 μ m.

observed at room temperature. It is also possible to successfully grow GUVs composed from Sphingomyelin and Cholesterol in a range where this lipid mixture is in the liquid-ordered phase, however a complete study of the conditions under which GUVs from domain-forming ternary mixtures can be grown by the gel method is beyond the scope of this work.

Careful tuning of the system composition, such as the introduction of a small fraction of PEGylated lipids (45), or better spreading of the precursor film by spin-coating (12), have been reported in the literature to improve the yield of GUVs containing charged headgroups and to facilitate detachment from the growing surface. Similar results have been observed in our case for gel-assisted growth.

A common problem with some lipids is that vesicles do not detach easily from the growing surface after formation. We found that detachment can be improved by several different strategies. Sonication for 1–2 s in a standard ultrasound bath, for instance, can better detach the GUVs without breaking them. Furthermore, if a sugar such as sucrose is added to the gel, a larger number of vesicles spontaneously detach during the formation process. This can be due to the extra osmotic pressure from the sugar dissolving from the gel that pushes away the membranes (46).

In summary, we have shown that the PVA swelling method can successfully deal with different classes of lipids, which are otherwise difficult to grow, the method being in particular well adapted for charged lipids.

Encapsulation

The PVA gel formation method is advantageous for encapsulating many molecular species of biological relevance that are often prone to react at room temperature, e.g., cross-linking or degradation due to peroxidation caused by electric fields (43). We first tested the ability of this method to encapsulate the molecules required to reconstitute a simple biomimetic cytoskeleton inside a GUV. As shown in Fig. 6, A and B, actin filaments were successfully incorporated into vesicles and bundles formed if the swelling solution contained additional cross-linker. Similar actin structures have been shown by swelling on agarose gels (28). However, in

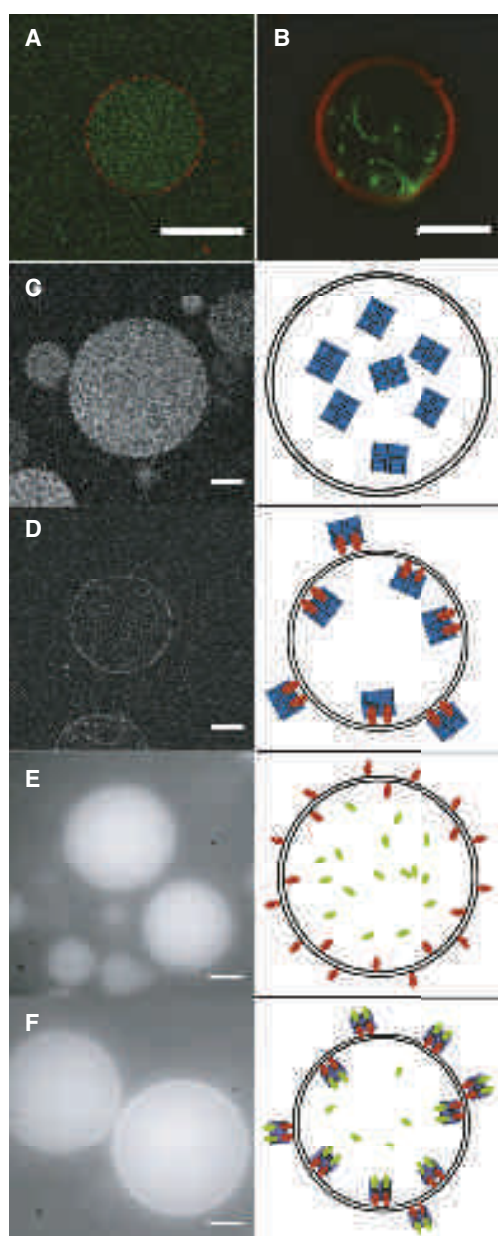


FIGURE 6 CLSM images of DOPC-GUVs grown by (A and B) PVA swelling at 4°C from 94.8:0.2:5.0 DOPC/RhodB-PE/PEG-PE mixtures and (C–F) DOPC-GUVs grown by a combination of PVA swelling and the inverse-phase precursor method (42). (A) Encapsulated actin filaments in the interior of the GUV. (B) Actin bundles inside the GUV, formed by adding of streptavidin with an actin/streptavidin ratio of 25:1 as a cross-linker. (C) In the absence of biotinylated lipids, AlexaFluor350-labeled neutravidin is homogeneously distributed in the vesicle interior. (D) In the presence of 1% biotinylated lipids, AlexaFluor350-labeled neutravidin binds to the membrane. (E) In vesicles swollen in a solution containing 500 nM fluorescently labeled biotin, the biotin is homogeneously distributed inside the vesicle interior in the absence of membrane-bound neutravidin. (F) Vesicles were formed as in (E) but with neutravidin on the membrane surface. The encapsulated biotin-fluorescein binds to the membrane-anchored neutravidin, resulting in a bright ring of fluorescent-biotin. The right column displays sketches of the systems in the left images: The membrane is represented by black lines, biotinylated lipids by red rods, fluorescein-biotin by green rods, and neutravidin by a blue square. Scale bars 20 μm .

this case the vesicles are contaminated by agarose, which adheres to the membrane.

It is often desirable to control the anchoring of encapsulated molecules to the vesicle membrane. A convenient way to achieve anchoring is to use biotinylated lipids, which enables anchoring to biotinylated species by neutravidin. We can localize neutravidin specifically on the membrane by combining the PVA swelling method with the inverse-phase precursor method, which allows complexation of lipids with neutravidin. Inverse-phase precursor films were already successfully used for the encapsulation of large hydrophilic molecules during electroformation (42). As shown in panel D of Fig. 6, GUVs grown from a precursor film containing neutravidin have a neutravidin functionalized membrane. In the absence of biotinylated lipids, the neutravidin is in the vesicle interior, as shown in panel C. The neutravidin is still functional, as shown by encapsulation of fluorescently labeled biotin. When neutravidin is on the membrane, fluorescent biotin forms a bright ring, signifying binding to neutravidin (panel F). In the absence of membrane-bound neutravidin, fluorescent biotin is found throughout the vesicle (panel E).

A growth scenario

To understand how the efficiency of encapsulation of water-soluble (bio)molecules in the vesicles can be optimized, one needs to gain a deeper insight into the mechanisms of vesicle formation during gel swelling. When a film of DOPC is spread from a chloroform solution on a glass slide and subsequently hydrated in an aqueous solution, one can observe the spontaneous formation of bilayer structures with a majority of multilamellar vesicles (47). The left drawing of Fig. 7 shows the possible pathways for water penetration into the stacks of preordered phospholipid bilayers on glass. There are two main water transport modes. First, the water can access the interlamellar region from the edges and swell the stack; a feature easily observed using differential interference contrast microscopy (48). A second pathway for water transport is by direct membrane permeation, because phospholipid bilayers display a finite water permeability in the order of $160 \mu\text{m s}^{-1}$ (49). Direct permeation can generate swollen structures of tens of micrometers in a few seconds.

The right drawing of Fig. 7 shows the pathways of water penetration during swelling of a preordered bilayer stack on the surface of a dry PVA gel. The most prominent difference from the case of swelling on glass is related to water-uptake by the PVA gel: indeed a strong chemical potential gradient exists between the outer solution and the dry gel, which drives water across the bilayer stack. As a consequence of gel swelling, the capillary forces driving water at the membrane-gel interface are modified. This effect is further amplified by gel stretching and by gel surface corrugation, which may increase the number of membrane defects for

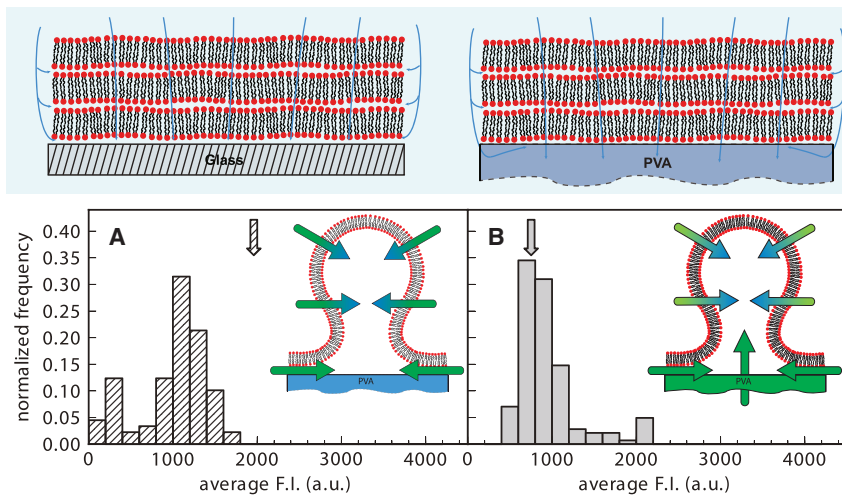


FIGURE 7 Top panel schematically depicts water penetration pathways through a bilayer stack deposited on glass and PVA gel. Lower panel are CLSM measurements of the average internal fluorescence intensity of GUVs grown on a PVA gel. (A) Vesicles swollen with a solution containing fluorescein. The average solution intensity is denoted by the arrow. (B) Vesicles swollen with a nonfluorescent solution on PVA gel loaded with fluorescein. The arrow indicates the fluorescent intensity of the solution after the fluorophore diffused from the gel. Histograms built from 89 vesicles for (A) and 142 vesicles for (B). Vesicles smaller than $5 \mu\text{m}$ were neglected.

water access. These different solution transport mechanisms are likely to display different degrees of selectivity with respect to aqueous solutions containing other molecules or nanoparticles. We argue that the differences previously observed in encapsulation efficiencies as a function of molecular size and growing methods (28,32,50–52) are due to the respective importance of different water penetration pathways in the final aqueous content of GUVs.

To discriminate between the effects of different water penetration pathways on encapsulation efficiency, we performed two comparative experiments. In the first, we formed vesicles by swelling lipids on a PVA gel with a solution containing fluorescein. In the second, we formed vesicles by swelling a PVA gel preloaded with fluorescein with a nonfluorescent solution. Fig. 7 A displays the fluorescence intensity of vesicles grown from a fluorescent solution whose average fluorescence intensity is indicated by the arrow. The fluorophore content of the vesicles is roughly 50% of that of the swelling solution, comparable to encapsulation efficiencies reported in the literature (28,32). This result suggests that on average roughly half of the water content inside the GUVs is due to solution transport across the membrane, which is impermeable to the fluorophore. Fig. 7 B shows fluorescence levels from GUVs grown on a fluorophore-loaded gel. The arrow indicates the average fluorescence intensity of the swelling solution after the swelling process took place. Solution volumes used in both experiments were comparable, but the total amount of fluorophore in the second experiment was ~ 2.5 times smaller than in the first one, which corresponds to the ratio of the average fluorescence intensities of the two solutions. As the histogram in Fig. 7 B shows, the encapsulation efficiency are higher when the PVA gel is preloaded with fluorophore. As sketched in the inset, we propose that this is due to a direct transport of fluorophore from the gel reservoir to the growing vesicle and not only from side penetration through defects.

Our findings thus suggest that membrane permeability is an important parameter determining vesicle growth by gel swelling. Indeed, the water permeability of DOPC is circa $160 \mu\text{m s}^{-1}$ (49), whereas the water permeability for typical polymersomes was reported to be the order of $2.5 \mu\text{m s}^{-1}$ (53). This is likely an important factor, which can explain why the yield of polymersomes grown by swelling is lower than the yield of liposomes. Furthermore, permeability plays a role in the final composition of solutions encapsulated in GUVs, by determining the relative importance of the different possible water penetration pathways.

CONCLUSIONS

Gel-assisted formation of GUVs on PVA allows for an easy and rapid growth of polymer-free GUVs in high yields without the need for special equipment. The process works for many different lipid mixtures, covering a wide range of lipids with one or more headgroups of zwitterionic, cationic or anionic nature. Due to the ability of PVA to swell at low temperatures close to the freezing point of water, the method is well adapted for the encapsulation of biomolecules such as actin, which can be encapsulated in monomer form at low temperature and subsequently polymerized by warming the vesicles to room temperature. Importantly, no input of energy is required to form GUVs, which minimizes the risk of degradation of the amphiphiles and of the proteins for membrane embedment or vesicle encapsulation.

Furthermore, we found experimentally that the gel formation process can be combined with inverse-phase precursor films to improve the encapsulation efficiency or localize (bio)molecules specifically to the membrane surface. Our method provides also a natural way to improve encapsulation efficiency of small hydrophilic molecules by predisolving them in the PVA gel.

Our results point to different penetration pathways for the aqueous solution that swells the membrane stacks. Part of

the swelling originates at the defects in the membrane, where water can invade the interlamellar spacing. However, a significant amount of water also penetrates by direct permeation across the bilayers. This confirms the importance of bilayer permeability for water in the formation of GUVs. For polymersomes too, osmotic imbalance generated by added sucrose improves conditions for vesicle formation.

PVA-assisted formation of GUVs provides a new route to prepare GUVs in a membrane laboratory. Although we have prepared small-scale samples, the method has potential for large-scale production and can be easily automated. Current work in our group, exploring new lipids and buffer compositions, points to an application range of this method beyond the one reported here.

SUPPORTING MATERIAL

Supporting Material for the paper “Gel-assisted formation of Giant Unilamellar Vesicles,” containing eight figures and one table are available at [http://www.biophysj.org/biophysj/supplemental/S0006-3495\(13\)00580-8](http://www.biophysj.org/biophysj/supplemental/S0006-3495(13)00580-8).

The authors thank S. Z. Omar and I. Moroz for valuable input.

This work was performed in the framework of the International Research Training Group (IRTG) Soft Matter Science and Foundation for Fundamental Research on Matter (FOM). A.W. thanks the Région Alsace for grant support, F.-C.T. and G.H.K. the Netherlands Organisation for Scientific Research (NWO), and W.M. the Swiss National Science Foundation and NCCR Nano Sciences for funding the work leading to the paper.

REFERENCES

- Lasic, D. 1993. Liposomes: from physics to applications. Elsevier Science.
- Tanaka, M., and E. Sackmann. 2005. Polymer-supported membranes as models of the cell surface. *Nature*. 437:656–663.
- Bayburt, T. H., and S. G. Sligar. 2003. Self-assembly of single integral membrane proteins into soluble nanoscale phospholipid bilayers. *Protein Sci.* 12:2476–2481.
- Walde, P., K. Cosentino, ..., P. Stano. 2010. Giant vesicles: preparations and applications. *ChemBioChem*. 11:848–865.
- Dimova, R., S. Aranda, ..., R. Lipowsky. 2006. A practical guide to giant vesicles. Probing the membrane nanoregime via optical microscopy. *J. Phys. Condens. Matter*. 18:S1151–S1176.
- Reeves, J. P., and R. M. Dowben. 1969. Formation and properties of thin-walled phospholipid vesicles. *J. Cell. Physiol.* 73:49–60.
- Akashi, K., H. Miyata, ..., K. Kinoshita, Jr. 1996. Preparation of giant liposomes in physiological conditions and their characterization under an optical microscope. *Biophys. J.* 71:3242–3250.
- Billerit, C., G. Jeffries, ..., A. Jesorka. 2012. Formation of giant unilamellar vesicles from spin-coated lipid films by localized IR heating. *Soft Matter*. 8:10823–10826.
- Angelova, M. I., and D. S. Dimitrov. 1986. Liposome electroformation. *Faraday Discuss.* 81:303–311.
- Montes, L.-R., A. Alonso, ..., L. A. Bagatolli. 2007. Giant unilamellar vesicles electroformed from native membranes and organic lipid mixtures under physiological conditions. *Biophys. J.* 93:3548–3554.
- Pott, T., H. Bouvrais, and P. Méléard. 2008. Giant unilamellar vesicle formation under physiologically relevant conditions. *Chem. Phys. Lipids*. 154:115–119.
- Estes, D. J., and M. Mayer. 2005. Giant liposomes in physiological buffer using electroformation in a flow chamber. *Biochim. Biophys. Acta*. 1712:152–160.
- Buboltz, J. T., and G. W. Feigenson. 1999. A novel strategy for the preparation of liposomes: rapid solvent exchange. *Biochim. Biophys. Acta*. 1417:232–245.
- Moscho, A., O. Orwar, ..., R. N. Zare. 1996. Rapid preparation of giant unilamellar vesicles. *Proc. Natl. Acad. Sci. USA*. 93:11443–11447.
- Noireaux, V., Y. T. Maeda, and A. Libchaber. 2011. Development of an artificial cell, from self-organization to computation and self-reproduction. *Proc. Natl. Acad. Sci. USA*. 108:3473–3480.
- Tagiguchi, K., A. Yamada, ..., K. Yoshikawa. 2009. Chapter 3 - Construction of cell-sized liposomes encapsulating actin and actin-cross-linking proteins. *Methods Enzymol.* 464:31–53.
- Shaklee, P. M., S. Semrau, ..., T. Schmidt. 2010. Protein incorporation in giant lipid vesicles under physiological conditions. *ChemBioChem*. 11:175–179.
- Merkle, D., N. Kahya, and P. Schwill. 2008. Reconstitution and anchoring of cytoskeleton inside giant unilamellar vesicles. *ChemBioChem*. 9:2673–2681.
- Osawa, M., D. E. Anderson, and H. P. Erickson. 2008. Reconstitution of contractile FtsZ rings in liposomes. *Science*. 320:792–794.
- Walde, P., and S. Ichikawa. 2001. Enzymes inside lipid vesicles: preparation, reactivity and applications. *Biomol. Eng.* 18:143–177.
- Sunami, T., K. Sato, ..., T. Yomo. 2006. Femtoliter compartment in liposomes for in vitro selection of proteins. *Anal. Biochem.* 357:128–136.
- Fenz, S. F., and K. Sengupta. 2012. Giant vesicles as cell models. *Integr. Biol. (Camb)*. 4:982–995.
- Noireaux, V., and A. Libchaber. 2004. A vesicle bioreactor as a step toward an artificial cell assembly. *Proc. Natl. Acad. Sci. USA*. 101:17669–17674.
- Pautot, S., B. Frisken, and D. Weitz. 2003. Production of unilamellar vesicles using an inverted emulsion. *Langmuir*. 19:2870–2879.
- Abkarian, M., E. Loiseau, and G. Massiera. 2011. Continuous droplet interface crossing encapsulation (cDICE) for high throughput monodisperse vesicle design. *Soft Matter*. 7:4610–4614.
- Pontani, L.-L., J. van der Gucht, ..., C. Sykes. 2009. Reconstitution of an actin cortex inside a liposome. *Biophys. J.* 96:192–198.
- Shum, H. C., D. Lee, ..., D. A. Weitz. 2008. Double emulsion templated monodisperse phospholipid vesicles. *Langmuir*. 24:7651–7653.
- Tsai, F.-C., B. Stuhmann, and G. H. Koenderink. 2011. Encapsulation of active cytoskeletal protein networks in cell-sized liposomes. *Langmuir*. 27:10061–10071.
- Stachowiak, J. C., D. L. Richmond, ..., D. A. Fletcher. 2008. Unilamellar vesicle formation and encapsulation by microfluidic jetting. *Proc. Natl. Acad. Sci. USA*. 105:4697–4702.
- Ota, S., S. Yoshizawa, and S. Takeuchi. 2009. Microfluidic formation of monodisperse, cell-sized, and unilamellar vesicles. *Angew. Chem. Int. Ed. Engl.* 48:6533–6537.
- Zhou, Y., C. K. Berry, ..., R. M. Raphael. 2007. Peroxidation of polyunsaturated phosphatidyl-choline lipids during electroformation. *Biomaterials*. 28:1298–1306.
- Horger, K. S., D. J. Estes, ..., M. Mayer. 2009. Films of agarose enable rapid formation of giant liposomes in solutions of physiologic ionic strength. *J. Am. Chem. Soc.* 131:1810–1819.
- Hassan, C., and N. Peppas. 2000. Structure and applications of poly(vinyl alcohol) hydrogels produced by conventional cross-linking or by freezing/thawing methods. *J. Adv. Polymer. Sci.* 153:37–65.
- Peppas, N., J. Hilt, ..., R. Langer. 2006. Hydrogels in biology and medicine: from molecular principles to bionanotechnology. *Adv. Mater.* 18:1345–1360.
- Pardee, J. D., and J. A. Spudich. 1982. Purification of muscle actin. *Methods Enzymol.* 85: Pt B:164–181.

36. Gentry, B. S., S. van der Meulen, ..., G. H. Koenderink. 2012. Multiple actin binding domains of Ena/VASP proteins determine actin network stiffening. *Eur. Biophys. J.* 41:979–990.
37. Carlier, M. F., D. Pantaloni, and E. D. Korn. 1985. Polymerization of ADP-actin and ATP-actin under sonication and characteristics of the ATP-actin equilibrium polymer. *J. Biol. Chem.* 260:6565–6571.
38. Dai, W., and T. A. Barbari. 2000. Characterization of mesh size asymmetry in hydrogel membranes using confocal microscopy. *J. Membr. Sci.* 171:45–58.
39. Wu, L., and C. S. Brazel. 2008. Modifying the release of proxiphylline from PVA hydrogels using surface crosslinking. *Int. J. Pharm.* 349:144–151.
40. Nardin, C., T. Hirt, ..., W. Meier. 2000. Polymerized ABA triblock copolymer vesicles. *Langmuir*. 16:1035–1041.
41. Aitken, C. E., R. A. Marshall, and J. D. Puglisi. 2008. An oxygen scavenging system for improvement of dye stability in single-molecule fluorescence experiments. *Biophys. J.* 94:1826–1835.
42. Mertins, O., N. P. da Silveira, ..., C. M. Marques. 2009. Electroformation of giant vesicles from an inverse phase precursor. *Biophys. J.* 96:2719–2726.
43. Ayuyan, A. G., and F. S. Cohen. 2006. Lipid peroxides promote large rafts: effects of excitation of probes in fluorescence microscopy and electrochemical reactions during vesicle formation. *Biophys. J.* 91:2172–2183.
44. Reference deleted in proof.
45. Yamashita, Y., M. Oka, ..., M. Yamazaki. 2002. A new method for the preparation of giant liposomes in high salt concentrations and growth of protein microcrystals in them. *Biochim. Biophys. Acta.* 1561:129–134.
46. Tsumoto, K., H. Matsuo, ..., T. Yoshimura. 2009. Efficient formation of giant liposomes through the gentle hydration of phosphatidylcholine films doped with sugar. *Colloids Surf. B Biointerfaces.* 68:98–105.
47. Hope, M., M. Bally, ..., P. Cullis. 1986. Generation of multilamellar and unilamellar phospholipid vesicles. *Chem. Phys. Lipids.* 40:89–107.
48. Rodriguez, N., F. Pincet, and S. Cribier. 2005. Giant vesicles formed by gentle hydration and electroformation: a comparison by fluorescence microscopy. *Colloids Surf. B Biointerfaces.* 42:125–130.
49. Mathai, J. C., S. Tristram-Nagle, ..., M. L. Zeidel. 2008. Structural determinants of water permeability through the lipid membrane. *J. Gen. Physiol.* 131:69–76.
50. Dominak, L. M., and C. D. Keating. 2007. Polymer encapsulation within giant lipid vesicles. *Langmuir*. 23:7148–7154.
51. Dominak, L. M., and C. D. Keating. 2008. Macromolecular crowding improves polymer encapsulation within giant lipid vesicles. *Langmuir*. 24:13565–13571.
52. Dominak, L. M., D. M. Omiatek, ..., C. D. Keating. 2010. Polymeric crowding agents improve passive biomacromolecule encapsulation in lipid vesicles. *Langmuir*. 26:13195–13200.
53. Discher, B. M., Y. Y. Won, ..., D. A. Hammer. 1999. Polymersomes: tough vesicles made from diblock copolymers. *Science*. 284:1143–1146.

Additional graphs

In this section additional graphs not shown in the main text can be found.

Quenching of BODIPY labeled ELP_{BC}

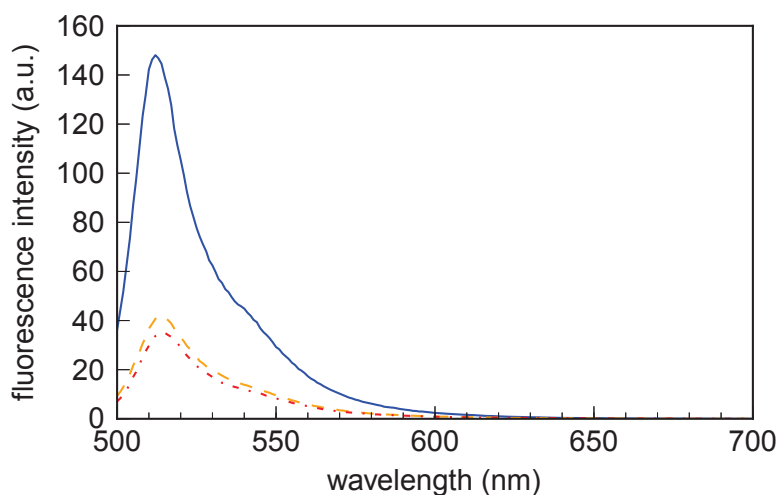


Figure A.1: Spectrum of a 54 % BODIPY-labeled non-functionalized ELP_{BC} solution in the unimer state at 25 °C (blue solid line) recorded on a fluorospectrometer. A total self-quenching of around 70 % is observed at 40 °C (orange dashed line) and 42 °C (red dashed dotted line).

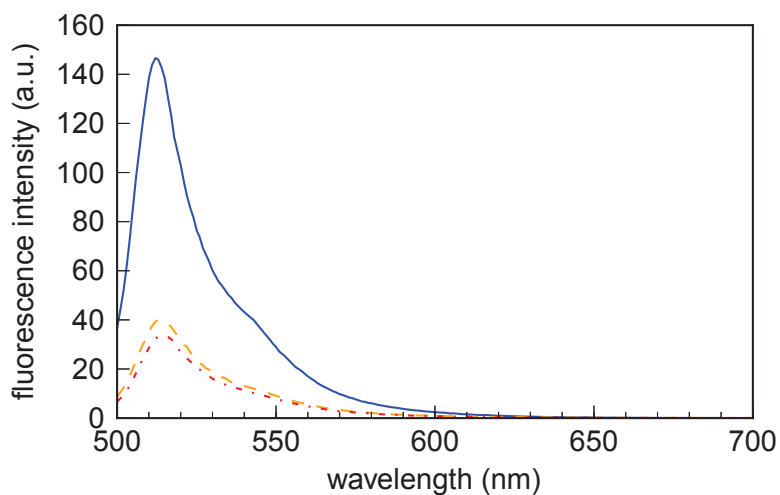


Figure A.2: Spectrum of a 54 % BODIPY-labeled TAT-functionalized ELP_{BC} solution in the unimer state at 25 °C (blue solid line) recorded on a fluorospectrometer. A total self-quenching of around 70 % is observed at 40 °C (orange dashed line) and 42 °C (red dashed dotted line).

Quartz crystal microbalance with dissipation

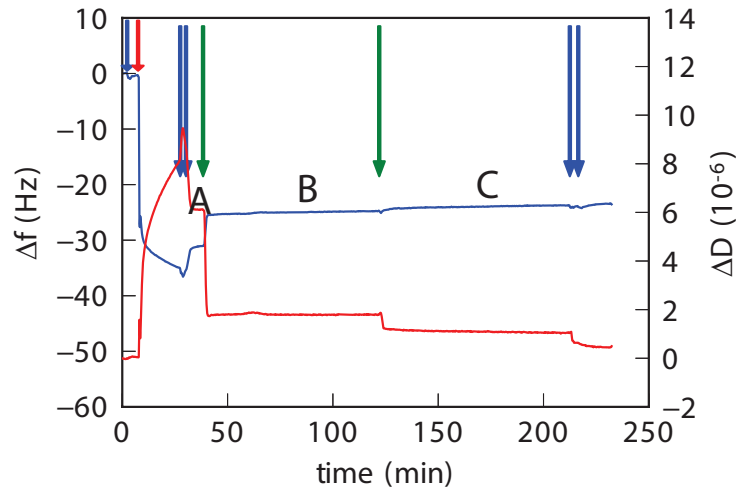


Figure A.3: Frequency shift and dissipation recorded by QCM-D for non-functionalized ELP_{BC} . Plot shows the 7th overtone. Blue arrows indicate washing the cell with pure PBS buffer. The red arrow shows the injection of the SUVs to form a supported bilayer. The green arrows indicate injection of ELPs. Point A is the stable supported bilayer after washing with PBS. B and C are the incubation of the supported bilayer with ELPs.

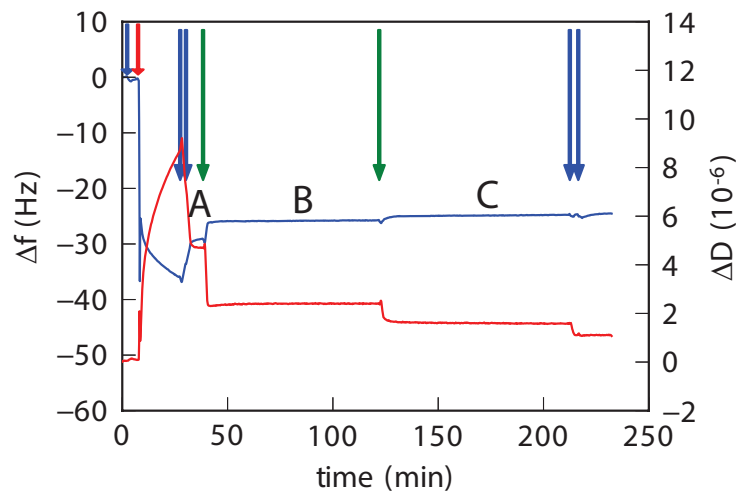


Figure A.4: Frequency shift and dissipation recorded by QCM-D for TAT-functionalized ELP_{BC} . Plot shows the 7th overtone. Blue arrows indicate washing the cell with pure PBS buffer. The red arrow shows the injection of the SUVs to form a supported bilayer. The green arrows indicate injection of ELPs. Point A is the stable supported bilayer after washing with PBS. B and C are the incubation of the supported bilayer with ELPs.

Isothermal titration calorimetry

Graphs show the dilution of ELP_{BC} in PBS.

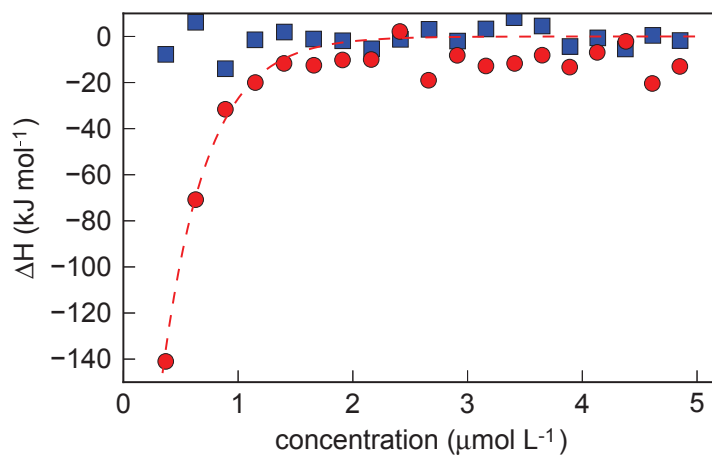


Figure A.5: ITC curves obtained for dilution non-functionalized ELP_{BC} solutions with PBS. Red circles signify the dilution of a micellar solution at 37 °C. Blue squares show dilution of a solution containing control-ELP_{BC} unimers at 25 °C.

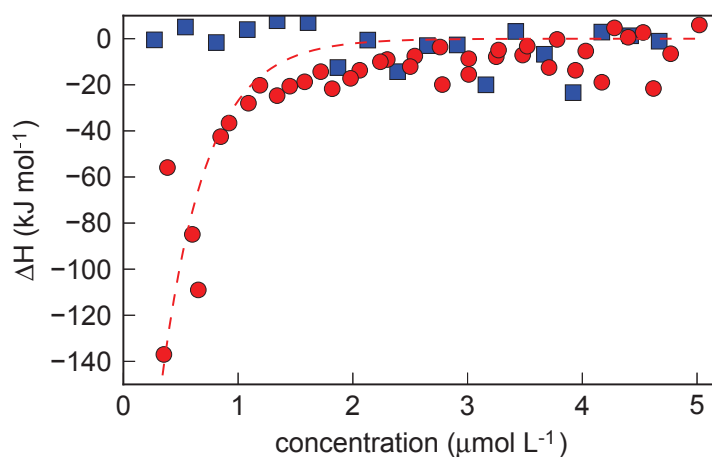


Figure A.6: ITC curves obtained for dilution TAT-functionalized ELP_{BC} solutions with PBS. Red circles signify the dilution of a micellar solution at 37 °C. Blue squares show dilution of a solution containing TAT-ELP_{BC} unimers at 25 °C.

Bibliography

- [1] Singer, S. J., G. L. Nicolson, et al., 1972. The fluid mosaic model of the structure of cell membranes. *Science* 175:720–731.
- [2] Simons, K., E. Ikonen, et al., 1997. Functional rafts in cell membranes. *Nature* 387:569.
- [3] Accessed on June,1 2013. http://php.med.unsw.edu.au/cellbiology/index.php?title=Cell_Membranes_and_Compartments.
- [4] Mulder, M., 1996. Basic Principles of Membrane Technology Second Edition. Kluwer Academic Pub.
- [5] Hamley, I. W., 2008. Introduction to soft matter: synthetic and biological self-assembling materials. Wiley.
- [6] Israelachvili, J. N., 1992. Intermolecular and surface forces. Academic press.
- [7] Massignani, M., H. Lomas, and G. Battaglia, 2010. Polymersomes: a synthetic biological approach to encapsulation and delivery. *In Modern Techniques for Nano-and Microreactors/-reactions*, Springer, 115–154.
- [8] Kita-Tokarczyk, K., and W. Meier, 2008. Biomimetic block copolymer membranes. *CHIMIA International Journal for Chemistry* 62:820–825.
- [9] Discher, D. E., and F. Ahmed, 2006. Polymersomes. *Annual Review of Biomedical Engineering* 8:323–341.
- [10] Van Meer, G., D. R. Voelker, and G. W. Feigenson, 2008. Membrane lipids: where they are and how they behave. *Nature Reviews. Molecular Cell Biology* 9:112–124.
- [11] Fahy, E., S. Subramaniam, R. C. Murphy, M. Nishijima, C. R. Raetz, T. Shimizu, F. Spener, G. van Meer, M. J. Wakelam, and E. A. Dennis, 2009. Update of the

- LIPID MAPS comprehensive classification system for lipids. *Journal of Lipid Research* 50:S9–S14.
- [12] on Biochemical Nomenclature, I.-I. C., 1977. The nomenclature of lipids (Recommendations 1976). *Lipids* 12:455–468.
- [13] Fedotenko, I. A., P.-L. Zaffalon, F. Favarger, and A. Zumbuehl, 2010. The synthesis of 1, 3-diamidophospholipids. *Tetrahedron Letters* 51:5382–5384.
- [14] Alberts, B., A. Johnson, J. Lewis, M. Raff, K. Roberts, and P. Walter, 1994. *Molecular Biology of the Cell*. Third edition., volume 1. Garland Science, New York.
- [15] Sackmann, E., 1995. Biological membranes architecture and function. *Handbook of biological physics* 1:1–63.
- [16] Virtanen, J. A., K. H. Cheng, and P. Somerharju, 1998. Phospholipid composition of the mammalian red cell membrane can be rationalized by a superlattice model. *Proceedings of the National Academy of Sciences* 95:4964–4969.
- [17] Dodge, J. T., and G. B. Phillips, 1967. Composition of phospholipids and of phospholipid fatty acids and aldehydes in human red cells. *Journal of Lipid Research* 8:667–675.
- [18] Evans, D. F., and H. Wennerström, 1999. *The colloidal domain: where physics, chemistry, and biology meet*. Wiley-vch New York.
- [19] Kaganer, V. M., H. Möhwald, and P. Dutta, 1999. Structure and phase transitions in Langmuir monolayers. *Rev. Mod. Phys.* 71:779–819.
- [20] Moghaddam, B., M. H. Ali, J. Wilkhu, D. J. Kirby, A. R. Mohammed, Q. Zheng, and Y. Perrie, 2011. The application of monolayer studies in the understanding of liposomal formulations. *International Journal of Pharmaceutics* 417:235–244.
- [21] Jähnig, F., 1996. What is the surface tension of a lipid bilayer membrane? *Biophysical Journal* 71:1348.
- [22] Richter, R. P., and A. R. Brisson, 2005. Following the formation of supported lipid bilayers on mica: a study combining AFM, QCM-D, and ellipsometry. *Biophysical Journal* 88:3422–3433.
- [23] Murray, D. H., L. K. Tamm, and V. Kiessling, 2009. Supported double membranes. *Journal of Structural Biology* 168:183–189.

- [24] Malaquin, L., T. Charitat, and J. Daillant, 2010. Supported bilayers: Combined specular and diffuse X-ray scattering. *The European Physical Journal E* 31:285–301.
- [25] Hemmerle, A., L. Malaquin, T. Charitat, S. Lecuyer, G. Fragneto, and J. Daillant, 2012. Controlling interactions in supported bilayers from weak electrostatic repulsion to high osmotic pressure. *Proceedings of the National Academy of Sciences* 109:19938–19942.
- [26] Bangham, A., M. Standish, and J. Watkins, 1965. Diffusion of univalent ions across the lamellae of swollen phospholipids. *Journal of Molecular Biology* 13:238–IN27.
- [27] Lasic, D. D., 1988. The mechanism of vesicle formation. *Biochemical Journal* 256:1.
- [28] Walde, P., K. Cosentino, H. Engel, and P. Stano, 2010. Giant vesicles: preparations and applications. *ChemBiochem* 11:848–865.
- [29] Torchilin, V. P., 2005. Recent advances with liposomes as pharmaceutical carriers. *Nature Reviews Drug Discovery* 4:145–160.
- [30] Gregoriadis, G., 2008. Liposome research in drug delivery: The early days. *Journal of Drug Targeting* 16:520–524.
- [31] Klibanov, A. L., K. Maruyama, V. P. Torchilin, and L. Huang, 1990. Amphipathic polyethyleneglycols effectively prolong the circulation time of liposomes. *FEBS Letters* 268:235–237.
- [32] Lasic, D. D., and D. Needham, 1995. The "Stealth" liposome: a prototypical biomaterial. *Chemical Reviews* 95:2601–2628.
- [33] Sadzuka, Y., I. Sugiyama, T. Tsuruda, and T. Sonobe, 2006. Characterization and cytotoxicity of mixed polyethyleneglycol modified liposomes containing doxorubicin. *International Journal of Pharmaceutics* 312:83–89.
- [34] Photos, P. J., L. Bacakova, B. Discher, F. S. Bates, and D. E. Discher, 2003. Polymer vesicles in vivo: correlations with PEG molecular weight. *Journal of Controlled Release* 90:323–334.
- [35] Discher, B. M., Y. Y. Won, D. S. Ege, J. C. Lee, F. S. Bates, D. E. Discher, and D. A. Hammer, 1999. Polymersomes: tough vesicles made from diblock copolymers. *Science* 284:1143–1146.
- [36] Egli, S., M. G. Nussbaumer, V. Balasubramanian, M. Chami, N. Bruns, C. Paliyan, and W. Meier, 2011. Biocompatible functionalization of polymersome sur-

- faces: a new approach to surface immobilization and cell targeting using polymersomes. *Journal of the American Chemical Society* 133:4476–4483.
- [37] Ahmed, F., and D. E. Discher, 2004. Self-porating polymersomes of PEG–PLA and PEG–PCL: hydrolysis-triggered controlled release vesicles. *Journal of Controlled Release* 96:37–53.
- [38] Srinivas, G., D. E. Discher, and M. L. Klein, 2004. Self-assembly and properties of diblock copolymers by coarse-grain molecular dynamics. *Nature Materials* 3:638–644.
- [39] Lee, J. C.-M., M. Santore, F. S. Bates, and D. E. Discher, 2002. From membranes to melts, rouse to reptation: diffusion in polymersome versus lipid bilayers. *Macromolecules* 35:323–326.
- [40] Dimova, R., U. Seifert, B. Pouligny, S. Förster, and H.-G. Döbereiner, 2002. Hyperviscous diblock copolymer vesicles. *The European Physical Journal E* 7:241–250.
- [41] Mathai, J. C., S. Tristram-Nagle, J. F. Nagle, and M. L. Zeidel, 2008. Structural determinants of water permeability through the lipid membrane. *Journal of General Physiology* 131:69–76.
- [42] Jansen, M., and A. Blume, 1995. A comparative study of diffusive and osmotic water permeation across bilayers composed of phospholipids with different head groups and fatty acyl chains. *Biophysical Journal* 68:997–1008.
- [43] Lawaczeck, R., 1979. On the permeability of water molecules across vesicular lipid bilayers. *The Journal of Membrane Biology* 51:229–261.
- [44] Heimburg, T., 2008. Thermal biophysics of membranes, volume 1. Wiley-Vch.
- [45] Olbrich, K., W. Rawicz, D. Needham, and E. Evans, 2000. Water permeability and mechanical strength of polyunsaturated lipid bilayers. *Biophysical Journal* 79:321.
- [46] Lande, M. B., J. M. Donovan, and M. L. Zeidel, 1995. The relationship between membrane fluidity and permeabilities to water, solutes, ammonia, and protons. *The Journal of general physiology* 106:67–84.
- [47] Huster, D., A. J. Jin, K. Arnold, and K. Gawrisch, 1997. Water permeability of polyunsaturated lipid membranes measured by ^{17}O NMR. *Biophysical journal* 73:855–864.
- [48] Paula, S., A. Volkov, A. Van Hoek, T. Haines, and D. W. Deamer, 1996. Permeation of protons, potassium ions, and small polar molecules through phos-

- pholipid bilayers as a function of membrane thickness. *Biophysical Journal* 70:339–348.
- [49] Lodish, H., A. Berk, S. L. Zipursky, P. Matsudaira, D. Baltimore, and J. Darnell, 2000. *Molecular cell biology*. W. H. Freeman, 4th edition.
- [50] Corvera, E., O. Mouritsen, M. Singer, and M. Zuckermann, 1992. The permeability and the effect of acyl-chain length for phospholipid bilayers containing cholesterol: theory and experiment. *Biochimica et Biophysica Acta (BBA)-Biomembranes* 1107:261–270.
- [51] Mouritsen, O. G., 2005. *Life-as a matter of fat: the emerging science of lipidomics*. Springer.
- [52] Fenz, S. F., and K. Sengupta, 2012. Giant vesicles as cell models. *Integrative Biology* 4:982–995.
- [53] Dimova, R., S. Aranda, N. Bezlyepkina, V. Nikolov, K. A. Riske, and R. Lipowsky, 2006. A practical guide to giant vesicles. Probing the membrane nanoregime via optical microscopy. *J Phys Condens Matter* 18:S1151–S1176.
- [54] Noireaux, V., and A. Libchaber, 2004. A vesicle bioreactor as a step toward an artificial cell assembly. *Proceedings of the National Academy of Sciences of the United States of America* 101:17669–17674.
- [55] Yamashita, Y., M. Oka, T. Tanaka, and M. Yamazaki, 2002. A new method for the preparation of giant liposomes in high salt concentrations and growth of protein microcrystals in them. *Biochimica et Biophysica Acta* 1561:129–134.
- [56] Reeves, J. P., and R. M. Dowben, 1969. Formation and properties of thin-walled phospholipid vesicles. *Journal of Cellular Physiology* 73:49–60.
- [57] Hishida, M., H. Seto, N. Yamada, and K. Yoshikawa, 2008. Hydration process of multi-stacked phospholipid bilayers to form giant vesicles. *Chemical Physics Letters* 455:297–302.
- [58] Shimanouchi, T., H. Umakoshi, and R. Kuboi, 2009. Kinetic study on giant vesicle formation with electroformation method. *Langmuir* 25:4835–4840.
- [59] Akashi, K.-i., H. Miyata, H. Itoh, and K. Kinoshita Jr, 1998. Formation of giant liposomes promoted by divalent cations: critical role of electrostatic repulsion. *Biophysical Journal* 74:2973–2982.
- [60] Akashi, K., H. Miyata, H. Itoh, and K. Kinoshita, Jr, 1996. Preparation of giant liposomes in physiological conditions and their characterization under an optical microscope. *Biophysical Journal* 71:3242–3250.

- [61] Tsumoto, K., H. Matsuo, M. Tomita, and T. Yoshimura, 2009. Efficient formation of giant liposomes through the gentle hydration of phosphatidylcholine films doped with sugar. *Colloids Surf B Biointerfaces* 68:98–105.
- [62] Howse, J. R., R. A. Jones, G. Battaglia, R. E. Ducker, G. J. Leggett, and A. J. Ryan, 2009. Templated formation of giant polymer vesicles with controlled size distributions. *Nature Materials* 8:507–511.
- [63] Dominak, L. M., and C. D. Keating, 2008. Macromolecular crowding improves polymer encapsulation within giant lipid vesicles. *Langmuir* 24:13565–13571.
- [64] Morales-Pennington, N. F., J. Wu, E. R. Farkas, S. L. Goh, T. M. Konyakhina, J. Y. Zheng, W. W. Webb, and G. W. Feigenson, 2010. GUV preparation and imaging: Minimizing artifacts. *Biochimica et Biophysica Acta (BBA)-Biomembranes* 1798:1324–1332.
- [65] Horger, K. S., D. J. Estes, R. Capone, and M. Mayer, 2009. Films of agarose enable rapid formation of giant liposomes in solutions of physiologic ionic strength. *Journal of the American Chemical Society* 131:1810–1819.
- [66] Moscho, A., O. Orwar, D. T. Chiu, B. P. Modi, and R. N. Zare, 1996. Rapid preparation of giant unilamellar vesicles. *Proceedings of the National Academy of Sciences of the United States of America* 93:11443–11447.
- [67] Pautot, S., B. Frisken, and D. Weitz, 2003. Production of unilamellar vesicles using an inverted emulsion. *Langmuir* 19:2870–2879.
- [68] Mabrouk, E., D. Cuvelier, F. Brochard-Wyart, P. Nassoy, and M.-H. Li, 2009. Bursting of sensitive polymersomes induced by curling. *Proceedings of the National Academy of Sciences* 106:7294–7298.
- [69] Pautot, S., B. J. Frisken, and D. Weitz, 2003. Engineering asymmetric vesicles. *Proceedings of the National Academy of Sciences* 100:10718–10721.
- [70] Funakoshi, K., H. Suzuki, and S. Takeuchi, 2007. Formation of giant lipid vesiclelike compartments from a planar lipid membrane by a pulsed jet flow. *Journal of the American Chemical Society* 129:12608–12609.
- [71] Stachowiak, J. C., D. L. Richmond, T. H. Li, A. P. Liu, S. H. Parekh, and D. A. Fletcher, 2008. Unilamellar vesicle formation and encapsulation by microfluidic jetting. *Proceedings of the National Academy of Sciences of the United States of America* 105:4697–4702.
- [72] Abkarian, M., E. Loiseau, and G. Massiera, 2011. Continuous droplet inter-

- face crossing encapsulation (cDICE) for high throughput monodisperse vesicle design. *Soft Matter* 7:4610–4614.
- [73] Shum, H., D. Lee, I. Yoon, T. Kodger, and D. Weitz, 2008. Double emulsion templated monodisperse phospholipid vesicles. *Langmuir* 24:7651–7653.
- [74] Papahadjopoulos, D., and J. Watkins, 1967. Phospholipid model membranes. II. Permeability properties of hydrated liquid crystals. *Biochimica et Biophysica Acta (BBA)-Biomembranes* 135:639–652.
- [75] Pick, U., 1981. Liposomes with a large trapping capacity prepared by freezing and thawing of sonicated phospholipid mixtures. *Archives of Biochemistry and Biophysics* 212:186–194.
- [76] Hope, M., M. Bally, G. Webb, and P. Cullis, 1985. Production of large unilamellar vesicles by a rapid extrusion procedure. Characterization of size distribution, trapped volume and ability to maintain a membrane potential. *Biochim Biophys Acta* 812:55–65.
- [77] Angelova, M. I., and D. S. Dimitrov, 1986. Liposome electroformation. *Faraday Discussions* 81:303–311.
- [78] Angelova, M., and D. Dimitrov, 1988. A mechanism of liposome electroformation. *In Trends in colloid and interface science II*, Springer, 59–67.
- [79] Kralj-Iglič, V., G. Gomišček, J. Majhenc, V. Arrigler, and S. Svetina, 2001. Myelin-like protrusions of giant phospholipid vesicles prepared by electroformation. *Colloids and Surfaces A: Physicochemical and Engineering Aspects* 181:315–318.
- [80] Rodriguez, N., F. Pincet, and S. Cribier, 2005. Giant vesicles formed by gentle hydration and electroformation: a comparison by fluorescence microscopy. *Colloids Surf B Biointerfaces* 42:125–130.
- [81] Montes, L.-R., A. Alonso, F. M. Goñi, and L. A. Bagatolli, 2007. Giant unilamellar vesicles electroformed from native membranes and organic lipid mixtures under physiological conditions. *Biophysical Journal* 93:3548–3554.
- [82] Pott, T., H. Bouvrais, and P. Méléard, 2008. Giant unilamellar vesicle formation under physiologically relevant conditions. *Chemistry and Physics of Lipids* 154:115–119.
- [83] Estes, D. J., and M. Mayer, 2005. Giant liposomes in physiological buffer using electroformation in a flow chamber. *Biochimica et Biophysica Acta* 1712:152–160.

- [84] Estes, D. J., and M. Mayer, 2005. Electroformation of giant liposomes from spin-coated films of lipids. *Colloids Surf B Biointerfaces* 42:115–123.
- [85] Mertins, O., N. P. da Silveira, A. R. Pohlmann, A. P. Schröder, and C. M. Marques, 2009. Electroformation of giant vesicles from an inverse phase precursor. *Biophysical Journal* 96:2719–2726.
- [86] Okumura, Y., H. Zhang, T. Sugiyama, and Y. Iwata, 2007. Electroformation of giant vesicles on a non-electroconductive substrate. *Journal of the American Chemical Society* 129:1490–1491.
- [87] Zhou, Y., C. K. Berry, P. A. Storer, and R. M. Raphael, 2007. Peroxidation of polyunsaturated phosphatidyl-choline lipids during electroformation. *Biomaterials* 28:1298–1306.
- [88] Ayuyan, A. G., and F. S. Cohen, 2006. Lipid peroxides promote large rafts: effects of excitation of probes in fluorescence microscopy and electrochemical reactions during vesicle formation. *Biophysical Journal* 91:2172–2183.
- [89] Billerit, C., G. Jeffries, O. Orwar, and A. Jesorka, 2012. Formation of giant unilamellar vesicles from spin-coated lipid films by localized IR heating. *Soft Matter* 8:10823–10826.
- [90] Nardin, C., T. Hirt, J. Leukel, and W. Meier, 2000. Polymerized ABA triblock copolymer vesicles. *Langmuir* 16:1035–1041.
- [91] Pardee, J. D., and J. A. Spudich, 1982. Purification of muscle actin. *Methods in Enzymology* 85 Pt B:164–181.
- [92] Gentry, B., S. van der Meulen, P. Noguera, B. Alonso-Latorre, J. Plastino, and G. Koenderink, 2012. Multiple actin binding domains of Ena/VASP proteins determine actin network stiffening. *Eur. Biophysics J.* 1–12.
- [93] Carlier, M. F., D. Pantaloni, and E. D. Korn, 1985. Polymerization of ADP-actin and ATP-actin under sonication and characteristics of the ATP-actin equilibrium polymer. *Journal of Biological Chemistry* 260:6565–6571.
- [94] Dai, W., and T. Barbari, 2000. Characterization of mesh size asymmetry in hydrogel membranes using confocal microscopy. *Journal of Membrane Science* 171:45–58.
- [95] Wu, L., and C. S. Brazel, 2008. Modifying the release of proxiphylline from PVA hydrogels using surface crosslinking. *International Journal of Pharmaceutics* 349:144–151.

- [96] Meyer, D. E., and A. Chilkoti, 2002. Genetically encoded synthesis of protein-based polymers with precisely specified molecular weight and sequence by recursive directional ligation: examples from the elastin-like polypeptide system. *Biomacromolecules* 3:357–367.
- [97] McDaniel, J. R., J. A. Mackay, F. G. Quiroz, and A. Chilkoti, 2010. Recursive directional ligation by plasmid reconstruction allows rapid and seamless cloning of oligomeric genes. *Biomacromolecules* 11:944–952.
- [98] Meyer, D. E., and A. Chilkoti, 1999. Purification of recombinant proteins by fusion with thermally-responsive polypeptides. *Nat. Biotechnol.* 17:1112–1115.
- [99] Frisken, B., C. Asman, and P. Patty, 2000. Studies of vesicle extrusion. *Langmuir* 16:928–933.
- [100] Aitken, C. E., R. A. Marshall, and J. D. Puglisi, 2008. An oxygen scavenging system for improvement of dye stability in single-molecule fluorescence experiments. *Biophysical Journal* 94:1826–1835.
- [101] Lettinga, M. P., and S. Egelhaaf, 2011. Light Microscopy. In Lecture Notes of 42nd IFF Spring School "Macromolecular Systems in Soft and Living Matter", Forschungszentrum Jülich.
- [102] Pécréaux, J., H.-G. Döbereiner, J. Prost, J.-F. Joanny, and P. Bassereau, 2004. Refined contour analysis of giant unilamellar vesicles. *The European Physical Journal E* 13:277–290.
- [103] Lide, D. R., and T. J. Bruno, 2003. CRC handbook of chemistry and physics. CRC Press.
- [104] Curtis, A., 1964. The mechanism of adhesion of cells to glass A study by interference reflection microscopy. *The Journal of cell biology* 20:199–215.
- [105] Rädler, J., and E. Sackmann, 1993. Imaging optical thicknesses and separation distances of phospholipid vesicles at solid surfaces. *Journal de Physique II* 3:727–748.
- [106] Limozin, L., and K. Sengupta, 2009. Quantitative reflection interference contrast microscopy (RICM) in soft matter and cell adhesion. *ChemPhysChem* 10:2752–2768.
- [107] Höök, F., M. Rodahl, P. Brzezinski, and B. Kasemo, 1998. Energy dissipation kinetics for protein and antibody-antigen adsorption under shear oscillation on a quartz crystal microbalance. *Langmuir* 14:729–734.

- [108] Sauerbrey, G., 1959. Verwendung von Schwingquarzen zur Wägung dünner Schichten und zur Mikrowägung. *Zeitschrift für Physik* 155:206–222.
- [109] Keller, C., and B. Kasemo, 1998. Surface specific kinetics of lipid vesicle adsorption measured with a quartz crystal microbalance. *Biophysical journal* 75:1397–1402.
- [110] Billot, V., 2005. Deux approches de l'interaction entre membranes et supra-molécules: effets de polymères et de cyclodextrines. Ph.D. thesis, Université Luis Pasteur Strasbourg 1.
- [111] Lamaze, C., and S. L. Schmid, 1995. The emergence of clathrin-independent pinocytic pathways. *Current opinion in cell biology* 7:573–580.
- [112] Macewan, S. R., and A. Chilkoti, 2012. Digital switching of local arginine density in a genetically encoded self-assembled polypeptide nanoparticle controls cellular uptake. *Nano Lett.* 12:3322–8.
- [113] Green, M., and P. M. Loewenstein, 1988. Autonomous functional domains of chemically synthesized human immunodeficiency virus tat< i> trans</i>-activator protein. *Cell* 55:1179–1188.
- [114] Frankel, A. D., and C. O. Pabo, 1988. Cellular uptake of the tat protein from human immunodeficiency virus. *Cell* 55:1189–1193.
- [115] Richard, J. P., K. Melikov, E. Vives, C. Ramos, B. Verbeure, M. J. Gait, L. V. Chernomordik, and B. Lebleu, 2003. Cell-penetrating peptides A reevaluation of the mechanism of cellular uptake. *Journal of Biological Chemistry* 278:585–590.
- [116] Ter-Avetisyan, G., G. Tünnemann, D. Nowak, M. Nitschke, A. Herrmann, M. Drab, and M. C. Cardoso, 2009. Cell entry of arginine-rich peptides is independent of endocytosis. *Journal of Biological Chemistry* 284:3370–3378.
- [117] Madani, F., S. Lindberg, Ü. Langel, S. Futaki, and A. Gräslund, 2011. Mechanisms of cellular uptake of cell-penetrating peptides. *Journal of Biophysics* 2011.
- [118] Duchardt, F., M. Fotin-Mleczek, H. Schwarz, R. Fischer, and R. Brock, 2007. A Comprehensive Model for the Cellular Uptake of Cationic Cell-penetrating Peptides. *Traffic* 8:848–866.
- [119] Ziegler, A., 2008. Thermodynamic studies and binding mechanisms of cell-penetrating peptides with lipids and glycosaminoglycans. *Advanced drug delivery reviews* 60:580–597.

- [120] Miyaji, Y., S. Walter, L. Chen, A. Kurihara, T. Ishizuka, M. Saito, K. Kawai, and O. Okazaki, 2011. Distribution of KAI-9803, a novel δ -protein kinase C inhibitor, after intravenous administration to rats. *Drug Metabolism and Disposition* 39:1946–1953.
- [121] MacEwan, S. R., and A. Chilkoti, 2010. Elastin-like polypeptides: Biomedical applications of tunable biopolymers. *Peptide Science* 94:60–77.
- [122] Wender, P. A., D. J. Mitchell, K. Pattabiraman, E. T. Pelkey, L. Steinman, and J. B. Rothbard, 2000. The design, synthesis, and evaluation of molecules that enable or enhance cellular uptake: peptoid molecular transporters. *Proceedings of the National Academy of Sciences* 97:13003–13008.
- [123] Fischer, R., M. Fotin-Mleczek, H. Hufnagel, and R. Brock, 2005. Break on through to the Other Side – Biophysics and Cell Biology Shed Light on Cell-Penetrating Peptides. *ChemBioChem* 6:2126–2142.
- [124] Fleer, G., C. Stuart, and J. Scheutjens, 1993. *Polymers at interfaces*. London [etc.]: Chapman & Hall.
- [125] Richter, R., A. Mukhopadhyay, and A. Brisson, 2003. Pathways of lipid vesicle deposition on solid surfaces: a combined QCM-D and AFM study. *Biophysical Journal* 85:3035–3047.
- [126] Ciobanasu, C., J. P. Siebrasse, and U. Kubitscheck, 2010. Cell-penetrating HIV1 TAT peptides can generate pores in model membranes. *Biophysical Journal* 99:153–162.
- [127] Thorén, P. E., D. Persson, E. K. Esbjörner, M. Goksör, P. Lincoln, and B. Nordén, 2004. Membrane binding and translocation of cell-penetrating peptides. *Biochemistry* 43:3471–3489.
- [128] Säälük, P., A. Niinep, J. Pae, M. Hansen, D. Lubenets, Ü. Langel, and M. Pooga, 2011. Penetration without cells: membrane translocation of cell-penetrating peptides in the model giant plasma membrane vesicles. *Journal of Controlled Release* 153:117–125.
- [129] Melikov, K., and L. Chernomordik, 2005. Arginine-rich cell penetrating peptides: from endosomal uptake to nuclear delivery. *Cellular and Molecular Life Sciences CMLS* 62:2739–2749.
- [130] Herce, H., A. Garcia, J. Litt, R. Kane, P. Martin, N. Enrique, A. Rebolledo, and V. Milesi, 2009. Arginine-rich peptides destabilize the plasma membrane, con-

- sistent with a pore formation translocation mechanism of cell-penetrating peptides. *Biophysical journal* 97:1917–1925.
- [131] Hitz, T., R. Iten, J. Gardiner, K. Namoto, P. Walde, and D. Seebach, 2006. Interaction of α - and β -oligoarginine-acids and amides with anionic lipid vesicles: a mechanistic and thermodynamic study. *Biochemistry* 45:5817–5829.
- [132] Ziegler, A., X. Li Blatter, A. Seelig, and J. Seelig, 2003. Protein transduction domains of HIV-1 and SIV TAT interact with charged lipid vesicles. Binding mechanism and thermodynamic analysis. *Biochemistry* 42:9185–9194.
- [133] Ciobanasu, C., E. Harms, G. T'unnemann, M. C. Cardoso, and U. Kubitscheck, 2009. Cell-penetrating HIV1 TAT peptides float on model lipid bilayers. *Biochemistry* 48:4728–4737.
- [134] Noireaux, V., Y. Maeda, and A. Libchaber, 2011. Development of an artificial cell, from self-organization to computation and self-reproduction. *Proceedings of the National Academy of Sciences* 108:3473–3480.
- [135] Takiguchi, K., A. Yamada, M. Negishi, M. Honda, Y. Tanaka-Takiguchi, and K. Yoshikawa, 2009. Chapter 3 - Construction of cell-sized liposomes encapsulating actin and actin-cross-linking proteins. *Methods in Enzymology* 464:31–53.
- [136] Shaklee, P. M., S. Semrau, M. Malkus, S. Kubick, M. Dogterom, and T. Schmidt, 2010. Protein incorporation in giant lipid vesicles under physiological conditions. *ChemBiochem* 11:175–179.
- [137] Merkle, D., N. Kahya, and P. Schwille, 2008. Reconstitution and anchoring of cytoskeleton inside giant unilamellar vesicles. *ChemBiochem* 9:2673–2681.
- [138] Osawa, M., D. E. Anderson, and H. P. Erickson, 2008. Reconstitution of contractile FtsZ rings in liposomes. *Science* 320:792–794.
- [139] Walde, P., and S. Ichikawa, 2001. Enzymes inside lipid vesicles: preparation, reactivity and applications. *Biomolecular Engineering* 18:143–177.
- [140] Sunami, T., K. Sato, T. Matsuura, K. Tsukada, I. Urabe, and T. Yomo, 2006. Femtoliter compartment in liposomes for in vitro selection of proteins. *Analytical Biochemistry* 357:128–136.
- [141] Pontani, L.-L., J. van der Gucht, G. Salbreux, J. Heuvingh, J.-F. Joanny, and C. Sykes, 2009. Reconstitution of an actin cortex inside a liposome. *Biophysical Journal* 96:192–198.

- [142] Tsai, F.-C., B. Stuhmann, and G. H. Koenderink, 2011. Encapsulation of active cytoskeletal protein networks in cell-sized liposomes. *Langmuir* 27:10061–10071.
- [143] Ota, S., S. Yoshizawa, and S. Takeuchi, 2009. Microfluidic formation of monodisperse, cell-sized, and unilamellar vesicles. *Angewandte Chemie. International Edition in English* 48:6533–6537.
- [144] Hassan, C., and N. Peppas, 2000. Structure and applications of poly (vinyl alcohol) hydrogels produced by conventional crosslinking or by freezing/thawing methods. *Biopolymers· PVA Hydrogels, Anionic Polymerisation Nanocomposites* 37–65.
- [145] Peppas, N., J. Hilt, A. Khademhosseini, and R. Langer, 2006. Hydrogels in biology and medicine: from molecular principles to bionanotechnology. *Advanced Materials* 18:1345–1360.
- [146] Fedotenko, I. A., A. Weinberger, R. Tanasescu, F. Favarger, C. Stefaniu, I. Takashi, G. Brezesinski, C. Marques, and A. Zumbuehl, In Submission. Vesicle Origami using 1,3-Diamidophospholipids. *Langmuir* .
- [147] Hope, M., M. Bally, L. Mayer, A. Janoff, and P. Cullis, 1986. Generation of multilamellar and unilamellar phospholipid vesicles. *Chem Phys Lipids* 40:89–107.
- [148] Dominak, L. M., and C. D. Keating, 2007. Polymer encapsulation within giant lipid vesicles. *Langmuir* 23:7148–7154.
- [149] Dominak, L. M., D. M. Omiattek, E. L. Gundermann, M. L. Heien, and C. D. Keating, 2010. Polymeric crowding agents improve passive biomacromolecule encapsulation in lipid vesicles. *Langmuir* 26:13195–13200.
- [150] Redwood, W., F. Pfeiffer, J. Weisbach, and T. Thompson, 1971. Physical properties of bilayer membranes formed from a synthetic saturated phospholipid in n-decane. *Biochimica et Biophysica Acta (BBA)-Biomembranes* 233:1–6.
- [151] Lindsey, H., N. Petersen, and S. I. Chan, 1979. Physicochemical characterization of 1,2-diphytanoyl-sn-glycero-3-phosphocholine in model membrane systems. *Biochimica et Biophysica Acta (BBA)-Biomembranes* 555:147–167.
- [152] Veatch, S. L., and S. L. Keller, 2003. Separation of liquid phases in giant vesicles of ternary mixtures of phospholipids and cholesterol. *Biophysical journal* 85:3074–3083.
- [153] Becker, J. W., G. Reeke, J. L. Wang, B. A. Cunningham, and G. M. Edelman,

1975. The covalent and three-dimensional structure of concanavalin A. III. Structure of the monomer and its interactions with metals and saccharides. *Journal of Biological Chemistry* 250:1513–1524.
- [154] Dowhan, W., 1997. Molecular basis for membrane phospholipid diversity: why are there so many lipids? *Annual review of biochemistry* 66:199–232.
- [155] Sackmann, E., 1994. Membrane bending energy concept of vesicle- and cell-shapes and shape-transitions. *FEBS letters* 346:3–16.
- [156] Lichtenberg, D., E. Freire, C. Schmidt, Y. Barenholz, P. Felgner, and T. Thompson, 1981. Effect of surface curvature on stability, thermodynamic behavior, and osmotic activity of dipalmitoylphosphatidylcholine single lamellar vesicles. *Biochemistry* 20:3462–3467.
- [157] Lichtenberg, D., and C. Schmidt, 1981. Molecular packing and stability in the gel phase of curved phosphatidylcholine vesicles. *Lipids* 16:555–557.
- [158] Holme, M. N., I. A. Fedotenko, D. Abegg, J. Althaus, L. Babel, F. Favarger, R. Reiter, R. Tanasescu, P.-L. Zaffalon, A. Ziegler, et al., 2012. Shear-stress sensitive lenticular vesicles for targeted drug delivery. *Nature Nanotechnology* 7:536–543.
- [159] Blaurock, A., and R. Gamble, 1979. Small phosphatidylcholine vesicles appear to be faceted below the thermal phase transition. *The Journal of Membrane Biology* 50:187–204.



Andreas WEINBERGER

Systèmes Modèles de membranes et Potentiel de Pénétration de Polypeptides

Résumé

Les vésicules géantes unilamellaires (GUV) permettent d'étudier efficacement les interactions entre les lipides et les peptides. Dans ce manuscrit, il a été montré que les interactions attractives lipides-peptides sont supprimées par l'attachement de polypeptides de type élastine (ELP) sur des peptides riches en arginine et peuvent être modulées par l'auto-assemblage en micelles ainsi que par le nombre de groupements arginine dans la séquence des peptides capables de pénétrer les cellules. De plus, une nouvelle méthode pour former des GUV à partir de systèmes complexes en seulement quelques minutes a été développée. Cette méthode est basée sur le gonflement d'un film de PVA sous une bicouche lipidique. Elle supprime la dégradation des molécules pendant la formation des GUV de lipides synthétiques, tels que des glycolipides et des phospholipides portant des groupements amides, où les méthodes traditionnelles ne réussissent pas à produire des vésicules non endommagées.

Vésicules géantes unilamellaires, bicouche lipidique, gonflement, PVA, polypeptides, glycolipides, phospholipides

Résumé en anglais

Giant Unilamellar Vesicles (GUVs) are a valuable tool to study lipid bilayer-biomolecule interactions in simplified cell-like model systems. In this work, a new method to efficiently form GUVs within minutes from more complex systems was developed. This method is based on swelling of a PVA-film under a lipid bilayer and minimizes damage of involved molecules during GUV formation. It also opens up many interesting perspectives for the formation of GUVs composed from new classes of synthetic lipids, such as glycolipids and amide-bearing phospholipids, where the traditional methods fail to efficiently produce "undamaged" vesicles. GUVs were also used for studying lipid-peptide interactions of a new class of elastin-like polypeptides functionalized with arginine-rich residues. It is shown that attractive interactions between lipids and peptides are suppressed by cargo-attachment and can be tuned by self-assembly into micelles and the arginine-amount of the cell penetrating residue.

Giant Unilamellar Vesicles, lipid membranes, PVA-assisted swelling, spontaneous swelling, arginine-rich polypeptides, cargo-delivery, glycolipids, amide-bearing phospholipids